The Neurodegenerative Disease Autosomal Recessive Spastic Ataxia of Charlevoix-Saguenay (ARSACS): Cellular Defects Due To Loss of Sacsin Function

Emma Jane Duncan

Thesis submitted to Queen Mary University of London for the degree of Doctor of Philosophy (PhD)

Centre for Endocrinology
William Harvey Research Institute
Barts and the London School of Medicine and Dentistry
Queen Mary University of London

STATEMENT OF ORIGINALITY

I, Emma Jane Duncan, confirm that the research included within this thesis is my own work or that where it has been carried out in collaboration with, or supported by others, that this is duly acknowledged below and my contribution indicated. Previously published material is also acknowledged below.

I attest that I have exercised reasonable care to ensure that the work is original, and does not to the best of my knowledge break any UK law, infringe any third party's copyright or other Intellectual Property Right, or contain any confidential material.

I accept that the College has the right to use plagiarism detection software to check the electronic version of the thesis.

I confirm that this thesis has not been previously submitted for the award of a degree by this or any other university.

Signature:

Date: 20th April 2016

ABSTRACT

Sacsin, which is mutated in the neurodegenerative disease Autosomal Recessive Spastic Ataxia of Charlevoix-Saguenay (ARSACS), is a 520 kDa modular protein with regions of homology to molecular chaperones and domains linking to the ubiquitin proteasome system. This suggests a role in proteostasis.

Previously, sacsin has been shown to partially localise with mitochondria, and loss of sacsin results in elongated and dysfunctional mitochondria. Moreover, alterations in neurofilaments have recently been reported in a mouse model of ARSACS. Despite these findings, pathophysiological mechanisms of ARSACS are poorly understood.

The aim of this thesis was to elucidate the cellular role of sacsin by determining how loss of its function leads to the observed mitochondrial and intermediate filament defects. This hoped to shed light on the mechanism of disease in ARSACS.

The results indicate that the mitochondrial elongation seen in ARSACS is likely due to reduced mitochondrial localisation of the essential fission factor DRP1. This may be mediated by loss of function of a complex involving sacsin and dynactin-6, a subunit of the dynein-dynactin motor complex, which has previously been shown to be required for DRP1 mitochondrial recruitment. DRP1-mediated mitochondrial fission is necessary for mitochondrial quality control; hence a disruption to mitochondrial quality control is likely to occur in sacsin deficient cells, which may explain the mitochondrial dysfunction in ARSACS.

Furthermore, sacsin null cells display a dramatic collapse and perinuclear bundling of the vimentin intermediate filament network. This is coupled with the displacement of cellular organelles, particularly mitochondria, early endosomes and the Golgi, which accumulate at the periphery of the vimentin bundle. These are characteristic features of aggresome formation, indicating an aggregation of misfolded protein, which occurs due to disrupted proteostasis. Further supporting this, the proteostasis components ubiquitin, HSP70, LAMP2 and p62 are recruited to the perinuclear vimentin bundles.

In summary, the findings of this thesis indicate a role for sacsin in mitochondrial and protein quality control, the dysfunction of which is likely to be particularly detrimental in neurons. Mitochondrial dysfunction along with protein misfolding and aggregation are implicated in many neurodegenerative diseases, and ARSACS is no exception.

ACKNOWLEDGEMENTS

First and foremost, I would like to express my appreciation and gratitude to my supervisor Professor Paul Chapple for his guidance, support, and valuable time. It has been a privilege to work on such an interesting and fruitful project.

The work of this thesis would not have been possible without the generous funding from the Ataxia Charlevoix-Saguenay Foundation and the Medical Research Council, to whom I am most grateful. In particular, I would like to thank the founders of the Ataxia Charlevoix-Saguenay Foundation, Jean Groleau and Sonia Gobeil, for an inspirational visit to Montreal.

I would like to thank my second supervisor Dr Louise Metherell and my panel of advisors Dr Gregory Michael and Professor Andrew Tinker for their valuable time and useful suggestions.

I would also like to thank members of the Chapple group, Dr Teisha Bradshaw, Dr Suran Nethisinghe, Dr Sam O'Toole and Lisa Romano for their encouragement, friendship and support. I am grateful to have been part of such a great team!

I would like to thank Professor Carol Shoulders for providing me with the opportunity to start a career in research and for continuing to be a great mentor throughout my PhD.

My thanks also go to Professor Mike Cheetham, Professor Alison Hardcastle and members of the UCL Institute of Ophthalmology for their useful advice throughout my project.

Thanks to my colleagues in the Centre for Endocrinology, both past and present, for creating such an enjoyable place to work and for sharing their expertise. In particular, I am thankful to Tozen Ozkan who made doing my PhD all the more pleasurable with her wonderful friendship and kindness.

Thank you to my boyfriend, Luke Williams for his support, encouragement and patience throughout my PhD. He kept me smiling through the tough bits!

Finally, thank you to my friends and family for their continued support and encouragement throughout my education, especially my parents Jeanette and Andrew Duncan, to whom I dedicate this thesis. I hope that I have made them proud.

CONTENTS

LIST OF FIGURES

LIST OF TABLES

LIST OF ABBREVIATIONS

ACTN4	α-actinin-4
AD	Alzheimer's disease
ADOA	Autosomal dominant optic atrophy
ADP	Adenosine diphosphate
ALP	Autophagy-lysosome pathway
ALS	Amyotrophic lateral sclerosis
ARCA	Autosomal recessive cerebellar ataxia
ARSACS	Autosomal recessive spastic ataxia of Charlevoix-Saguenay
AT	Ataxia telangiectasia
ATG	Autophagy-related
ATP	Adenosine triphosphate
ATPase	Adenosine triphosphatase
ATP6ap2	ATP6 associated protein 2
ATXN3	Ataxin 3
ADOA	Autosomal dominant optic atrophy
Aβ	β-amyloid
BSA	Bovine serum albumin
CAD	Coronay artery disease
CaMK1α	Calcium/calmodulin-dependent kinase 1α
CaN	Calcineurin
CAPs	Cytoskeletal associated proteins
CAP-Gly	Glycine-rich cytoskeleton-associated protein
Ca2+	Calcium ion
CCCP	Carbonyl cyanide m-chlorophenylhydrazone
CDK5	Cyclin-dependent kinase 5
cDNA	Complementary DNA
CFTR	Cystic Fibrosis Transmembrane Conductance Regulator
CHIP	C-terminus of HSP70 interacting protein
CMA	Chaperone mediated autophagy
CMT	Charcot-Marie-Tooth
CNS	Central nervous system
Co-IP	Co-immunoprecipitation

COPS5	COP9 subunit 5
CO_2	Carbon dioxide
C-terminus	Carboxy-terminus
DAPI	4',6-diamidino-2-phenylindole dihydrochloride
DCTN6	Dynactin-6
dH_20	Deionised water
DIC	Dynein intermediate chain
DMEM	Dulbecco's Minimum Eagle Medium
DMSO	Dimethyl sulfoxide
DNA	Deoxyribonucleic acid
dNTP	Deoxynucleotide
DPBS	Dulbecco’s phosphate buffered saline
DRG	Dorsal root ganglion
DRP1	Dynamin related protein 1
DSP	Dithiobis[succinimidylpropionate]
DUB	Deubiquitinating enzyme
E.coli	*Escherichia coli*
ECACC	European Collection of Cell Culture
EDTA	Ethylenediaminetetraacetic acid
EEA1	Early endosome antigen 1
EGTA	Ethylene glycol tetraacetic acid
ER	Endoplasmic reticulum
ERAD	ER-associated degradation
EV	Empty vector
FBS	Foetal bovine serum
Fis1	Mitochondrial fission protein 1
FP	Fluorescent polarisation
FRAP	Fluorescence recovery after photobleaching
FRDA	Friedreich ataxia
g	Standard acceleration due to gravity
GAN	Giant axonal neuropathy
GAPDH	Glyceraldehyde 3-phosphate dehydrogenase
gDNA	Genomic DNA
GED	GTPase effector domain

GFAP	Glial fibrillary acidic protein
GFP	Green fluorescent protein
GTP	Guanosine triphosphate
HD	Huntington's disease
HDAC6	Histone deacetylase 6
HDF	Human dermal fibroblasts
HEK293	Human embryonic kidney 293 cells
HEPES	4-(2-hydroxyethyl)-1-piperazineethanesulfonic acid
HEPN	Higher eukaryote and prokaryote nucleotide binding
HIP	HSP70 interacting protein
HOP	HSP70 and HSP90 organising protein
HPA	Health Protection Agency
HPD	Histidine-proline-glutamate
HSF1	Heat shock factor 1
HSP	Heat shock protein
HSR	Heat shock response
HuH-7	Human hepatoma cell line 7
IB	Immunoblotting
IC	Immunocytochemistry
IF	Intermediate filaments
IFT	Intraflagellar transport
IGF	Insulin growth factor
IMM	Inner mitochondrial membrane
IP	Immunoprecipitation
iPSC	Induced pluripotent stem cells
IPTG	Isopropyl β-D-1-thiogalactopyranoside
kDa	kiloDalton
LAMP2	Lysosome-associated membrane protein-2
LB	Luria broth
LSD	Lysosome storage disease
MAPL	Mitochondria-anchored protein ligase
MEFs	Mouse embryonic fibroblasts
MFF	Mitochondrial fission factor
MFN1	Mitofusin 1

MFN2	Mitofusin 2
MiD49/51	Mitochondrial dynamics proteins of 49 and 51 kDa
MJD	Machado-Joseph disease
MOPS	3-(N-morpholino)propanesulfonic acid
MPP	Mitochondrial processing peptidase
MRI	Magnetic resonance imaging
mRNA	messenger RNA
MSS	Marinesco-Sjögren syndrome
mtDNA	mitochondrial DNA
MTOC	Microtubule organising centre
mTOR	Mammalian target of rapamycin
NEFs	Nucleotide exchange factors
NFs	Neurofilaments
NFH	Neurofilament heavy chain
NFL	Neurofilament light chain
NFM	Neurofilament medium chain
NFT	Neurofibrillary tangles
NGS	Normal goat serum
NHDF	Normal human dermal fibroblasts
nm	Nanometers
nM	Nanomoles
NO	Nitric oxide
npNFH	Non-phosphorylated neurofilament heavy chain
N-terminus	amino-terminus
O_2	Oxygen
OMIM	Online mendelian inheritance in man
OMM	Outer mitochondrial membrane
OPA1	Optic atrophy 1
OCT	Optical coherence tomography
PARL	Presenilins-associated rhomboid-like protein
PBST	Phosphate buffered saline with Tween20
PCR	Polymerase chain reaction
PD	Parkinson's disease
Pen/Strep	Penicillin/streptomycin

PICK1	Protein interacting with C kinase 1
PINK-1	PTEN-induced kinase 1
PKA	Protein kinase A
PolyQ	Polyglutamine
PS1	Preslin 1
Rad23A	Radiation-sensitive mutant 23
RNFL	Retinal nerve-fibre layer
RIPA	Radio-Immunoprecipitation assay
RNA	Ribonucleic acid
RNAi	RNA interference
RNAase	Ribonuclease
ROS	Reactive oxygen species
rpm	Revolutions per minute
RT	Reverse transcription
RT-qPCR	Reverse transcription-quantitative polymerase chain reaction
SACS	Sacsin
SCA	Spinocerebellar ataxias
SCRM	Scrambled
SD	Standard deviation
SDS	Sodium dodecyl sulphate
SDS-PAGE	Sodium dodecyl sulphate polyacrylamide gel electrophoresis
SEM	Standard error of mean
SENP	Sentrin-specific protease
Ser	Serine
sHSP	Small heat shock protein
siRNA	Small interfering RNA
SOC	Super optimal broth with catabolite repression
SRR	Sacsin repeating region
SR-SIM	Super resolution structured illumination microscopy
SUMO	Small ubiquitin-like modifier
TAE	Tris-acetate-EDTA buffer
Taq	*Thermus aquaticus*
TBST	Tris buffered saline with Tween20
TMRM	Tetra methylrhodamine methyl ester

TOM20	Translocase of outer mitochondrial membrane 20
TPR	Tetratricopeptide repeat
Ub	Ubiquitin
UbA	Ubiquitin-associated
UbL	Ubiquitin-like
UIM	Ubiquitin-interaction motif
UPR	Unfolded protein response
UPS	Ubiquitin-proteasome system
UV	Ultraviolet
V-ATPase	Vacuolar-type adenosine triphosphatase
VDCCs	Voltage-dependent calcium channels
WT	Wild type
X-Gal	5-bromo-4-chloro-3-indolyl- beta-D-galactopyranoside
XPCB	Xeroderma pigmentosum complementation group C binding
Y2H	Yeast two-hybrid
ΔΨm	Mitochondrial membrane potential
2-ME	2-Mercaptoethan
3D	Three dimensional

CHAPTER 1: INTRODUCTION

1.1. Cerebellar Ataxias

Within the brain, the cerebellum plays an important role in motor control. It does not initiate movement, but coordinates and regulates motor activity. The cerebellum is divided into three distinct layers: the fibre-rich molecular layer, the Purkinje cell layer, and the inner granular layer, which has high concentrations of granule cells. Lesions of the cerebellum or spinal cord result in disorders known as ataxias. Ataxias are characterised by loss of gross muscle control, leading to posture and gait disturbances, uncoordinated movement and unsteadiness. Other features may include dysarthria (motor speech disorder), dysphagia (difficulty swallowing), vertigo, and diplopia (double vision (Perlman, 2004)).

Ataxias can be inherited or sporadic, and are also caused by external forces or agents such as injury, drugs or alcohol (Manto and Marmolino, 2009). Purkinje cell degeneration is frequently observed (Crossman and Neary, 2004), along with atrophy of the cerebellum, which can be seen on magnetic resonance imaging (MRI) of patients (Fogel and Perlman, 2007; Palau and Espinas, 2006; Viau and Boulanger, 2004).

Hereditary ataxias are usually divided into four main categories based on their mode of inheritance: autosomal dominant, autosomal recessive, X-linked and mitochondrial (Fogel and Perlman, 2007). The autosomal dominant ataxias, also known as spinocerebellar ataxias (SCAs), typically have adult onset (Schols et al., 2004) and more than 35 have been described (Jayadev and Bird 2013, Soong and Paulson, 2007). The most common subtypes are SCA 1, 2, 3, 6, and 7, all of which are nucleotide repeat expansion disorders. The autosomal recessive ataxias manifest mostly in children and young adults (Anheim et al., 2012b) and are typically associated with loss-of-function protein mutations. More than 20 have been described to date (Embirucu et al., 2009; Jayadev and Bird, 2013), and the most common of these are discussed in section 1.2.

1.2. Autosomal Recessive Cerebellar Ataxias

Autosomal recessive cerebellar ataxias (ARCAs) represent a heterogeneous and complex group of inherited neurodegenerative diseases. They are generally associated with peripheral sensorimotor neuropathy and also tend to have involvement outside the nervous system (Di Donato et al., 2001; van de Warrenburg et al., 2002). The major ARCAs can be divided into three groups: (1) Friedreich's ataxia and phenotypically related disorders, (2) Friedreich's ataxia phenotype with cerebellar atrophy, and (3) early-onset ataxia with cerebellar atrophy (Table 1.1 (Fogel and Perlman, 2007)). In the latter group, Autosomal Recessive Spastic Ataxia of Charlevoix-Saguenay (ARSACS) is the main focus of this PhD.

Table 1.1. Autosomal Recessive Cerebellar Ataxias

	Defective gene/protein	Proposed protein function
Friedreich's ataxia-like		
Friedreich's ataxia	Frataxin (FXN)	Mitochondrial iron metabolism
Ataxia with vitamin E deficiency	α-tocopherol transfer protein (TTPA)	Vitamin E homeostasis
Abetalipoproteinaemia	Microsomal triglyceride transfer protein (MTP)	Lipoprotein metabolism
Refsum's disease	Phytanoyl-CoA hydroxylase (PHYH) Peroxin 7 (PEX7)	Fatty-acid oxidation Peroxisomal protein importation
Friedreich's ataxia-like with cerebellar atrophy		
Late-onset Tay-Sachs disease	B-hexosaminidase A (HEXA)	Glycosphingolipid metabolism
Cerebrotendinous xanthomatosis	Sterol 27-hydroxylase (CYP27)	Bile-acid synthesis
DNA polymerase γ disorders	DNA polymerase γ (POLG)	Mitochondrial DNA repair and replication
Spinocerebellar ataxia with axonal neuropathy	Tyrosyl-DNA phosphodiesterase 1 (TDP1)	DNA repair
Early-onset ataxia with cerebellar atrophy		
Ataxia telangiectasia	Ataxia telangiectasia-mutated (ATM)	DNA damage response
Ataxia telangiectasia-like disorder	Meiotic recombination 11 (MRE11)	DNA damage response
Ataxia with oculomotor apraxia, type 1	Aprataxin (APTX)	DNA repair, possibly RNA processing
Ataxia with oculomotor apraxia, type 2	Senataxin (SETX)	Possibly DNA repair, DNA transcription, or RNA processing
Autosomal recessive spastic ataxia of Charlevoix-Saguenay	Sacsin (SACS)	Possibly protein folding
Infantile-onset spinocerebellar ataxia	Twinkle, twinky (C10orf2)	DNA replication
Cayman ataxia	Caytaxin (ATCAY)	Possibly neurotransmitter metabolism
Marinesco-Sjogren's syndrome	BiP-associated protein (SIL1)	Possibly protein folding

Table adapted from (Fogel and Perlman, 2007)

ARCAs are heterogeneous within and between disorders with respect to the age of onset, the severity of disease progression, and the frequency of extra-cerebellar and systemic signs (Anheim et al., 2012b). Even mutations in the same gene can lead to distinct phenotypes. For example, Friedreich's ataxia may manifest as early-onset (Anheim et al., 2012a), late-onset (Schols et al., 1997), or very late-onset (Berciano et al., 2005) disease (before 10 years, after 25 years, and after 40 years of age, respectively).

1.2.1. Friedreich's ataxia

Friedreich's ataxia (OMIM: 229300) is the most common ARCA in North America and Europe, with a prevalence of approximately 1 in 30,000-50,000 in most populations and a carrier frequency of approximately 1 in 85 in white Caucasians (Cossee et al., 1997; Pandolfo, 1999; Schols et al., 1997). Age of onset is typically before 25 years and characteristic features include progressive gait and limb ataxia, dysarthria, loss of vibration and proprioceptive sense, areflexia (absence of reflexes), abnormal eye movements, cardiomyopathy, diabetes mellitus, scoliosis (abnormal curvature of the spine to the sides), and pes cavus (high-arched foot) (Alper and Narayanan, 2003; Delatycki et al., 2000; Harding, 1981).

The disease is caused by a triplet Guanine-Adenine-Adenine (GAA) expansion within the first intron of the frataxin gene (*FXN*) on chromosome 9q13 in 98% of patients (Campuzano et al., 1996). There is an inverse correlation between both the age of onset and severity of the disease with the size of the GAA repeat expansions, which range from 70-90 repeats to over 1000 (normal size of the GAA tract in unaffected individuals is less than 40). Point mutations can also cause the disorder in 2-4% of patients (Pandolfo, 1999; Pandolfo, 2001; Schols et al., 1997).

The frataxin protein is associated with the inner mitochondrial membrane and cristae, and contains a N-terminal mitochondrial targeting sequence, which is encoded by the first 20 amino acids (Campuzano et al., 1997). Loss of frataxin impairs mitochondrial iron handling and respiratory chain function and contributes to increased oxidative stress and cellular damage (Bradley et al., 2000; Cavadini et al., 2002; Lodi et al., 1999). Neuron-specific and striated-muscle-specific knockout mice have ataxia, proprioceptive loss, cardiac hypertrophy and a deficiency in respiratory-chain complexes (Puccio et al., 2001).

1.2.2. Ataxia telangiectasia

Ataxia telangiectasia (AT, OMIM: 208900), also known as Louis–Bar syndrome, is the second most common ARCA, with a prevalence of 1 in 40,000-100,000 people worldwide (Swift et al., 1986) and age of onset is early childhood, typically before 5 years. It is a multi-systemic disorder characterised by neurodegeneration with progressive cerebellar ataxia and oculomotor dysfunction (Chun and Gatti, 2004; Hoche et al., 2012; Sedgwick, 1991), elevated serum alpha-fetoprotein levels, chromosome instability, immunodeficiency and a predisposition to cancer. Telangiectases, small clusters of enlarged blood vessels in the eyes and on the surface of the skin, are also characteristic of this condition. Brain imaging and post-mortem analysis reveals atrophy and degeneration of the cerebellar cortex, with loss of Purkinje and granule cells (Verhagen et al., 2012).

The disease is caused by mutations in *ATM* on chromosome 11q22-23, which encodes a constitutively expressed Serine/Threonine protein kinase involved in the control of cell division and DNA repair (Mavrou et al., 2008; Savitsky et al., 1995). Over 400 *ATM* mutations have been identified, with about 85% of mutations resulting in premature protein truncation. Most patients have compound heterozygous mutations (Hall, 2005). ATM phosphorylates several proteins that play key roles in DNA damage response pathways. In the brain, the ATM kinase may also be involved in vesicle traffic to the Golgi (Cara et al., 2016; Li et al., 2009). Loss of function of *ATM* leads to oxidative stress and cell apoptosis, particularly of Purkinje cells in the cerebellum (Chen et al., 2003b; Takao et al., 2000).

1.2.3. Marinesco-Sjogren's syndrome

Marinesco-Sjogren syndrome (MSS, OMIM: 248800) was identified as the fourth most common form of ARCA (Anheim et al., 2010). Characteristic features include cerebellar atrophy due to loss of Purkinje and granule cells (Mahloudji et al., 1972; Todorov, 1965), congenital cataracts, progressive muscle weakness due to myopathy, and delayed psychomotor development (Lagier-Tourenne et al., 2003; Sjogren, 1950). Additional features include short stature, hypergonadotrophic hypogonadism, and skeletal deformities. The disease is caused by homozygous or compound heterozygous mutations in *SIL1* on chromosome 5q31, which lead to premature termination of translation or abnormal splicing of the transcript, resulting in loss of SIL1 function

(Anttonen et al., 2005; Senderek et al., 2005). *SIL1* is ubiquitously expressed and encodes a nucleotide exchange factor for the heat-shock protein 70 (HSP70) family molecular chaperone BiP (also known as GRP78 and HSPA5), which functions in the endoplasmic reticulum (ER) lumen (Chung et al., 2002; Tyson and Stirling, 2000). SIL1 regulates the ATPase cycle of GRP78 and hence, may be involved in protein translocation into the ER, protein folding and degradation, and responses to cell stress (Hendershot, 2004).

1.3. Autosomal Recessive Spastic Ataxia of Charlevoix-Saguenay (ARSACS)

ARSACS (OMIM: 270550) is a rare complex hereditary neurological disease originally described in a founder population in the Charlevoix and Saguenay-Lac Saint Jean regions of North-Eastern Québec in Canada, in 1978, where the carrier frequency is estimated to be 1 in 22 (Bouchard et al., 1978; Bouchard et al., 1998; De Braekeleer et al., 1993). ARSACS patients have now been identified worldwide, with cases in Europe, North Africa, Turkey, Japan and Brazil (Bouhlal et al., 2011; Pyle et al., 2012). Along with Freidreich's ataxia, AT and MSS, ARSACS is one of the more common types of ARCA worldwide (Bouhlal et al., 2011; Synofzik et al., 2013; Vermeer et al., 2008). Disease onset is typically in early childhood, but may also be later in life, particularly in patients outside of Québec (Pyle et al., 2012). The disease has frequently been confused with cerebral palsy and secondary spastic diplegia.

1.3.1. Clinical Features

Bouchard *et al.* first reported the clinical features of ARSACS in 1978, with most patients showing a typical triad of slowly progressive, early-onset cerebellar ataxia, lower limb spasticity and peripheral neuropathy (Synofzik et al., 2013). Lower limb spasticity is evident between the ages of 12-24 months when patients begin to walk, although this may develop later, but rarely after the age of 12 (Bouhlal et al., 2011). However, the classical triad is not present in all ARSACS patients. Patients more recently identified outside of Canada display considerable phenotypic heterogeneity, so that now neither spasticity nor ataxia can be regarded as obligate features of the condition (Synofzik et al., 2013). For example, several ARSACS siblings were misdiagnosed with Charcot-Marie-Tooth (CMT) disease due to the absence of cerebellar ataxia and lower limb spasticity (Pyle et al., 2012; Synofzik et al., 2013).

ARSACS patients with an absence of peripheral neuropathy have also been identified (Synofzik et al., 2013). Age of onset may be later in patients outside of Canada, for example, out of a series of 17 Belgian patients, 29% had onset of symptoms at or after age 20, with one as late as 40 years of age (Baets et al., 2010).

Retinal changes are an additional characteristic phenotype, not seen in other ataxias. These retinal changes were originally described as hypermyelination of retinal nerve fibres (Bouchard et al., 1998; Richter et al., 2004), however more recently this has been suggested to be a thickening of the retinal nerve-fibre layer (RNFL) rather than hypermyelination (Nethisinghe et al., 2011; Pilliod et al., 2015). In support of this, a 29-year old British male patient had a RNFL thickness above the 95th percentile, as determined by optical coherence tomography (OCT) (Nethisinghe et al., 2011). It has been suggested that more ARSACS patients have their RNFL thickness assessed using OCT, as this retinal phenotype could be useful in diagnosis. Despite the presence of thickened RNFL, optic nerve and retinal function are not generally affected, with normal acuity, fields and colour vision (Bouchard, 1991).

Other disease characteristics include dysarthria, which is reported in all ARSACS patients worldwide, with slurring of speech in childhood, which becomes explosive in adulthood (Bouhlal et al., 2011), nystagmus (involuntary eye movement), amyotrophy (muscle wasting), and finger and foot deformities, which are due to distal muscle weakness and atrophy (Haga et al., 2012; Li, 2013; Tzoulis et al., 2013).

Pathological features of ARSACS include atrophy of the upper cerebellar vermis (Bouhlal et al., 2011; Martin et al., 2007; Pilliod et al., 2015), and absence of Purkinje cells post mortem (Bouchard, 1991; Bouchard, 2000). Spinal cord and linear T2 hypointensities are also commonly found in the basis pontis (Bouchard et al., 1998; Martin et al., 2007; Sanchez et al., 2015). Québec patients are wheelchair-bound on average by age 41, and their life expectancy is shortened to a mean age of 51 (Bouchard, 1991; Dupre et al., 2006). There is no available therapy for ARSACS and treatment is provided to control symptoms.

1.3.2. Causative Gene and Mutations

SACS (OMIM: 604490) was identified as the causative gene for ARSACS in 2000 and has been mapped to chromosome 13q12.12 (Engert et al., 2000). The gene was initially thought to be encoded by a single gigantic exon spanning 12,794bp with a 11,487bp

open reading frame (Engert et al., 2000), but since then 8 further coding exons and a tenth non-coding exon have been identified upstream of this, forming a 13,737bp open reading frame (Figure 1.1A, (Ouyang et al., 2006; Parfitt et al., 2009; Vermeer et al., 2008). To date, over 120 pathogenic mutations in *SACS* have been identified worldwide (Table 1.2), which consist of missense, nonsense, frameshift and splice-site mutations, the most of which are located in the giant exon 10 (Kamada et al., 2008; Ouyang et al., 2006; Takado et al., 2007; Thiffault et al., 2013; Vermeer et al., 2008). The majority of cases of ARSACS in Québec are caused by two founder mutations: a single nucleotide deletion (c.8844delT) and a nonsense mutation (c.7504C>T (Engert et al., 2000; Engert et al., 1999; Richter et al., 1999)).

Table 1.2. *SACS* mutations in ARSACS patients

Mutation	Amino Acid Change	Protein Domain	Origin	Reference
216delT	C72fs*76		Belgium	(Baets et al., 2010)
237insAfs*	S80Ifs*98		Canada	(Thiffault et al., 2013)
414 C >G	Y138*	R1: sr1	Japan	(Shimazaki et al., 2012)
482delA	N161-fs*175	R1: sr1	Japan	(Kamada et al., 2008)
502 G> T	D168Y	R1: sr1	Netherlands	(Vermeer et al., 2008)
600_604+1delA ACAGG	I200M-fs*214	R1: sr1	Italy	(Terracciano et al., 2009)
602 C >A	T201K	R1: sr1	Belgium	(Baets et al., 2010)
814 C > T	R272C	R1: sr1	Canada	(Guernsey et al., 2010)
815 G > A	R272H	R1: sr1	Italy	(Dibilio et al., 2013)
826 C > T	R276C	R1: sr1	Italy	(Prodi et al., 2012)
922 C > T	L308F	R1: sr1	Japan	(Takado et al., 2007)
961 C > T	R321*	R1: sr1	Netherlands	(Vermeer et al., 2008)
1184_1193delG TAACAGTGT	C395W-fs*407	R1	Japan	(Ouyang et al., 2006)
1190insAfs*	S397Kfs*405	R1	Canada	(Thiffault et al., 2013)
1228_1229delT T	S409fs*2	R1: sr2	Italy	(Prodi et al., 2012)
1373 C > T	T458I	R1: sr2	Germany	(Synofzik et al., 2007)
1420 C > T	R474C	R1: sr2	Italy	(Romano et al., 2013)
1475 G> A	W492*	R1: sr2	Netherlands	(Vermeer et al., 2008)

1597 C > T	P536L	R1: sr2	France	(Anheim et al., 2010)
1647_1658del	L549_552del	R1: sr2	Germany	(Synofzik et al., 2007)
1667 T > C	L556P	R1: sr2	Morocco	(Baets et al., 2010)
2063delT	V687-fs*713	R1: srX	Japan	(Ouyang et al., 2006)
2076delG	T692T fs*713	R1: srX	UK	(Pyle et al., 2012)
2094-2A > G		R1: srX	Netherlands	(Vermeer et al., 2008)
2115_2116insC	R707Kfs*6	R1: srX	India	(Faruq et al., 2014)
2182 C >T	R728*	R1: srX	Netherlands	(Vermeer et al., 2008)
2185+7748_9836 del12kb	G729_W3278del	R1: srX	Italy	(Prodi et al., 2012)
2387del	L796Yfs*13	R1: srX	Germany	(Synofzik et al., 2007)
2405 T > C	L802P	R1: srX	Japan	(Kamada et al., 2008)
2439_2440delAT	V815Gfs*4	R1: srX	Tunisia	(Hammer et al., 2013)
2881 C > T c11634ins A	R961*K3878 fs*13	R1: srX	Italy	(Prodi et al., 2012)
2971 T > C	C991R	R1: srX	Belgium	(Baets et al., 2010)
2983 G > T	V995F	R1: srX	Germany	(Synofzik et al., 2007)
3161 T > C	F1054S	R1: srX	Japan	(Shimazaki et al., 2005)
3328insA	I1110-fs*1111	R1: srX	Tunisia	(El Euch-Fayache et al., 2003)
3421_3422insAC	L1141-fs*1150	R1: srX	Belgium	(Baets et al., 2010)
3491 T > A	M1164K		Belgium	(Ouyang et al., 2006)
3585 delT	I1195-fs*1206		Tunisia	(El Euch-Fayache et al., 2003)
3769 G > T	G1257*	R1: sr3	Japan	(Shimazaki et al., 2012)
3904 C > T	P1302S	R1: sr3	Spain	(Sanchez et al., 2015)
3965-3966delAC	G1322Vfs*1343	R1: sr3	UK	(Pyle et al., 2012)
4033 T > C	Q1345*	R1: sr3	Japan	(Okawa et al., 2006)
4033insC	Q1345-fs*1349	R1: sr3	Italy	(Criscuolo et al., 2004)
4060 C > T	Q1354*	R1: sr3	Italy	(Prodi et al., 2012)
4108 C > T	Q1370*	R1: sr3	Italy	(Grieco et al., 2004)
4145_4146insA	H1382Qfs*2		Italy	(Prodi et al., 2012)

4195 T > C	C1398R		Turkey	(Richter et al., 2004)
4205 A > T	D1402V		Canada	(Thiffault et al., 2013)
4593dupA	S1531fs*9	R2: sr1	Italy	(Prodi et al., 2012)
4724 G > C	R1575P	R2: sr1	Serbia	(Baets et al., 2010)
4744 G > A	D1582N	R2: sr1	Canada	(Thiffault et al., 2013)
4760 T > G	H1587R	R2: sr1	Belgium	(Baets et al., 2010)
4775_4776insA	I1592fs*1	R2: sr1	Italy	(Prodi et al., 2012)
4954 C > T	Q16652*	R2: sr1	Germany	(Synofzik et al., 2007)
4957 G> T	E1653*	R2: sr1	Netherlands	(Vermeer et al., 2008)
4882_4886 delCAGTT/insA GAAGC	Q1628*	R2: sr1	Algeria	(H'mida-Ben Brahim et al., 2011)
5125 C >T	E1709*	R2: sr1	Netherlands	(Vermeer et al., 2008)
5143 A>T	K1715*	R2: sr1	Netherlands	(Vermeer et al., 2008)
5151dupA	S1718fs*173 6	R2: sr1	UK	(Stevens et al., 2013)
5201_5202delA G	E1734G-fs*1736	R2: sr1	Japan	(Yamamoto et al., 2005)
5263-4delAA	K1755Vfs*1 775	R2	Japan	(Shimazaki et al., 2012)
5544dupA	V1849Sfs*48	R2: sr2	Germany	(Synofzik et al., 2007)
5629 C > T	R1877*	R2: sr2	Italy	(Anesi et al., 2011)
5719 C >T	R1907*	R2: sr2	Italy	(Prodi et al., 2012)
5836 T > C	W1946R	R2: sr2	Tunisia	(El Euch-Fayache et al., 2003)
5948 C > T	S1983F	R2	UK	(Stevens et al., 2013)
5988-9delT	fs*1999	R2	Japan	(Shimazaki et al., 2007)
6006delA	R2002fs*201 3	R2	Netherlands	(Vermeer et al., 2008)
6093_6095delT TC	S2032del	R2	Serbia	(Baets et al., 2010)
6172delT	S2058Lfs*20 76	R2	Japan	(Yamamoto et al., 2005)
6355C > T	R2119*	R2	Japan	(Hara et al., 2007)
6352delT	F2131fs*214 4	R2	UK	(Stevens et al., 2013)
6409 C > T	Q2137*	R2	Algeria	(H'mida-Ben Brahim et al., 2011)

6890 T>G	L2297W	R2: sr3	Norway	(Tzoulis et al., 2013)
6835insA	E2280Rfs*2291	R2: sr3	Italy	(Grieco et al., 2004)
7121 T > C	L2374S	R2: sr3	Italy	(Terracciano et al., 2009)
7250_7254del	T2417-fs*2429	R2: sr3	Italy	(Grieco et al., 2004)
7255_7259	E2418fs*10	R2: sr3	Italy	(Prodi et al., 2012)
7277 G > C	R2426P	R2: sr3	Germany	(Synofzik et al., 2007)
7279 C > T	R2426*	R2: sr3	Belgium	(Baets et al., 2010)
7374delT	L2458Lfs*2474		Belgium	(Baets et al., 2010)
7372_7376delCTTAT	L2458-fs*2463		Algeria	(H'mida-Ben Brahim et al., 2011)
7504 C > T	R2502*		Canada	(Engert et al., 2000)
7613 C > T	A2558V	R3: sr1	France	(Anheim et al., 2010)
8107 C > T	R2703C	R3: sr1	Spain	(Criscuolo et al., 2005)
8339 T > G	F2780C	R3	UK	
8393 C > A	P2798Q	R3	Morocco	(Baets et al., 2010)
8401-8403del	E2801del	R3	Netherlands	(Vermeer et al., 2008)
8584 A > T	K2862*	R3: sr2	Germany	(Synofzik et al., 2007)
8793delA	K2931-fs*2952	R3: sr2	Japan	(Hara et al., 2005)
8844delT	K2948-fs*2952	R3: sr2	Canada	(Engert et al., 2000)
8920_8923dup	Y2975Ffs*29	R3	Germany	(Synofzik et al., 2007)
9305_9306 insT	L3102Ffs*	R3: srX	Germany	(Synofzik et al., 2007)
9497_9498delTT	F3166*	R3: srX	Canada	(Thiffault et al., 2013)
9508C>T	R3170*	R3: srX	Canada	(Thiffault et al., 2013)
9742 T > C	W3248R	R3: srX	Japan	(Ogawa et al., 2004)
9911_9912del	L3304fs	R3: srX	Netherlands	(Vermeer et al., 2008)
10034 T > C	V3345A	R3: srX	Italy	(Prodi et al., 2012)
10290 C > G	Y3430*	R3: srX	Algeria	(H'mida-Ben Brahim et al., 2011)
10298delC	T3433-fs*3458	R3: srX	Turkey	(Richter et al., 2004)
10442 T > C	L3481P	R3: srX	Netherlands	(Vermeer et al., 2008)

10517 T > C	F3506S	R3: srX	Belgium	(Breckpot et al., 2008)
10906 C > T	R3636Q	R3: srX	Belgium	(Baets et al., 2010)
10906 C > T	R3636*	R3: srX	Netherlands	(Vermeer et al., 2008)
10954 C > A	R3652T	R3: srX	Belgium	(Baets et al., 2010)
10958 T > C	F3653S	R3: srX	Belgium	(Baets et al., 2010)
11012_11013delAA	Q3671Rfs*23	XPCB	Italy	(Masciullo et al., 2012)
11104 A > G	T3702A	XPCB	Italy	(Gregianin et al., 2013)
11234_11235delTT	L3745-fs*3746	XPCB	Belgium	(Baets et al., 2010)
11242del688	3748fs3756*	XPCB	Canada	(Thiffault et al., 2013)
11265_11266delAT	I3755-fs*3762	XPCB	Hungary	(Baets et al., 2010)
11361-2insT	R3788Sfs*3820	R3: sr3	Japan	(Shimazaki et al., 2012)
11375 C > T	R3792*	R3: sr3	Tunisia	(Bouhlal et al., 2011)
11542_11544del	I3848del	R3: sr3	Germany	(Synofzik et al., 2007)
11598delC	G3866fs*3	R3: sr3	Italy	(Masciullo et al., 2012)
11624 G > A	R3875H	R3: sr3	Germany	(Synofzik et al., 2007)
11675 C > G	S3892*	R3: sr3	UK	
11707 C > T	R3903*		Canada	(Guernsey et al., 2010)
11803 C > T	Q3935*		China	(Liu et al., 2016)
11829-32AGTT	L3943-fs*3958		Turkey	(Richter et al., 2004)
11984_11986dupTGT	L3995dup		Germany	(Synofzik et al., 2007)
12020 C>T	S4007F		Japan	(Miyatake et al., 2012)
12160 C >T	Q4054*		Netherlands	(Vermeer et al., 2008)
12220 G > C	A4074P		Tunisia	(El Euch-Fayache et al., 2003)
12232 C > T	R4078		Italy	(Prodi et al., 2012)
12416 T > C	L4139S		UK	
12428_12429insA	Y4143*		Italy	(Prodi et al., 2012)
12603 C > A	Y4201*		Germany	(Synofzik et al., 2007)
12847_12850delAGAG	Q4284-fs*4305		Tunisia	(Bouhlal et al., 2009)

12851_12854del AGAG	E4284-fs*4307		Algeria	(H'mida-Ben Brahim et al., 2011)
12973 C > T	R4325*	J-domain	Japan	(Yamamoto et al., 2005)
12982 delA	K4327fs*7	J-domain	Italy	(Prodi et al., 2012)
12991 C > T	R4331W	J-domain	Italy	(Prodi et al., 2012)
12992 G > A	R4331Q	J-domain	Netherlands	(Vermeer et al., 2008)
13027 G > A	E4343K	J-domain	Belgium	(Baets et al., 2010)
13048 G >T	E4350	J-domain	UK	(Pyle et al., 2013)
13056 delT	F4352Lfs*11	J-domain	Germany	(Synofzik et al., 2007)
13132 C > T	R4378*	J-domain	Italy	(Anesi et al., 2011)
13237 T > C	Q4413*		UK	(Terracciano et al., 2010)
13352 T > C	L4451P		Norway	(Tzoulis et al., 2013)
13389 G > T	D4464Y	HEPN	Tunisia	(Bouhlal et al., 2011)
13523 A > C	K4508T	HEPN	Belgium	(Baets et al., 2010)
13538 G > A	S4513N	HEPN	Germany	(Synofzik et al., 2007)
13645 A > G	N4549D	HEPN	Turkey	(Richter et al., 2004)
Del 0.7Mb 13q12.12			UK	(Pyle et al., 2013)
Del 1.33Mb 13q12.12			China	(Liu et al., 2016)

Amino acid changes refer to full length sacsin (4579 amino acids, ENSP00000371729). Amino acid change to an * indicates a truncated protein, fs indicates a frameshift and del indicates a deletion. For the protein domains, R1: repeat region 1, R2: repeat region 2, R3: repeat region 3, sr1: subrepeat 1, sr2: subrepeat 2, sr3: subrepeat 3, srX: subrepeat X (Figure 1.1B).

There is no current evidence for a genotype-phenotype correlation in ARSACS. Patients with mutations in coding exon 7 are clinically identical to those with mutations in coding exon 9 (Takado et al., 2007). Also, in two unrelated Tunisian families with the same mutation (12220G>C) only one had skeletal deformities and the age of onset was different between the two families (Bouhlal et al., 2011). Possible explanations for these differences may be that an additional mutation is present in another gene in one of the families, or environmental factors are influencing phenotype.

1.3.3. Sacsin (DNAJC29)

SACS encodes the protein sacsin, a modular protein of 4579 amino acids (520 kDa), one of the largest known proteins in the human genome. From N- to C-terminus, sacsin is composed of a ubiquitin-like (UbL) domain that binds to the proteasome (Parfitt et al., 2009), three large sacsin repeat region (SRR) supra-domains, which contain regions of homology to HSP90 (Anderson et al., 2010; Romano et al., 2013), a xeroderma pigmentosum complementation group C (XPC)-binding domain that binds to the UBE3A ubiquitin protein ligase (Kamionka and Feigon, 2004), a DNAJ domain that binds and stimulates HSP70 (Parfitt et al., 2009), and a higher eukaryotes and prokaryotes nucleotide (HEPN)-binding domain that mediates sacsin dimerisation (Figure 1.1B, (Girard et al., 2012; Grynberg et al., 2003)). The nature of these domains suggests a role for sacsin in protein quality control. This is discussed further in section 1.6.

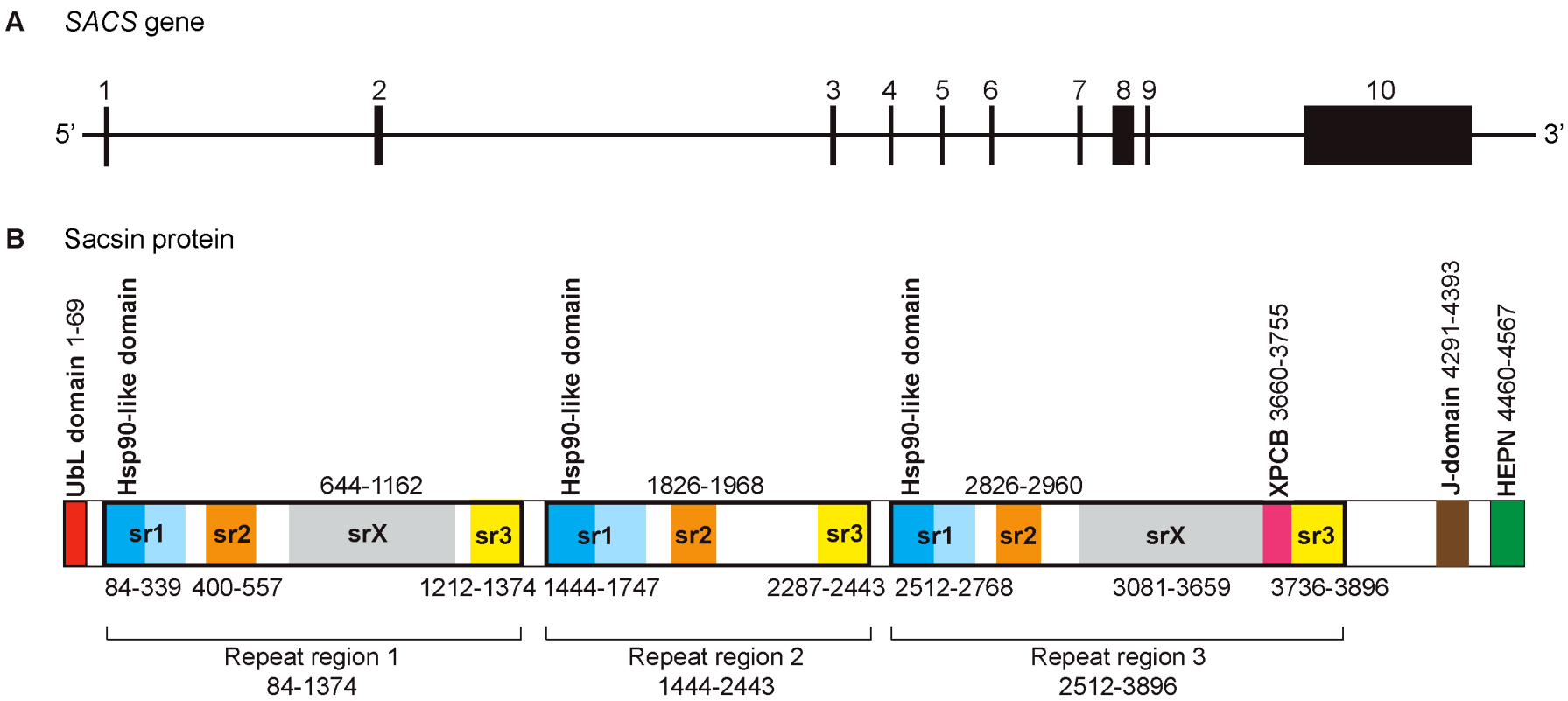

Figure 1.1. Schematic of *SACS* gene and protein domain structure. (A) Schematic of *SACS* intron-exon structure. The *SACS* coding sequence includes 10 exons shown as black rectangles numbered from 1–10, which are seperated by introns (black line). siRNAs targeting exons 7, 8 and 10 were used to achieve *SACS* knockdown in this thesis. **(B)** Schematic of sacsin domain structure. Amino acid residues are indicated by numbers. Repeating regions consist of sr1: subrepeat 1 (blue), sr2: subrepeat 2 (orange), sr3: subrepeat 3 (yellow), srX: subrepeat X (grey). Exon 10 encodes over three quarters of the C-terminal portion of the protein, with upstream exons (2-9) encoding the N-terminal quarter. Further details of the domain architecture are in section 1.6.

1.3.4. Sacsin Expression and Localisation

The gene encoding sacsin is found in all vertebrate genomes sequenced so far (Engert et al., 2000; Parfitt et al., 2009; Romano et al., 2013). Human sacsin shares ~99% to ~93% amino acid identity with that of other mammals (orangutan, mouse, rat, horse, dog), ~84% similarity with birds (chicken, zebra finch), 83% similarity with reptiles (anole lizard), and ~70% to ~68% similarity with fish (zebrafish, tetraodon, fugu, stickleback and medaka). Moreover, all vertebrate sacsin orthologues have the same structural architecture (Romano et al., 2013).

Human sacsin is expressed in many tissues, with high levels of messager RNA (mRNA) and protein in large neurons, particularly cerebellar Purkinje cells (Parfitt et al., 2009). Expression patterns are similar in other mammals and fish (Engert et al., 2000; Parfitt et al., 2009; Romano et al., 2013).

The subcellular localisation of sacsin is cytoplasmic with a significant mitochondrial component in SH-SY5Y neuroblastoma cells (Parfitt et al., 2009). Colocalisation of sacsin with mitochondrial markers was also shown in the soma, dendrites and axons of cultured hippocampal neurons, as well as in COS-7 and HeLa cells (Girard et al., 2012). Analyses of the sacsin protein sequence did not reveal the presence of a mitochondrial leader sequence (Parfitt et al., 2009), suggesting that sacsin's mitochondrial localisation is at or near the cytoplasmic face of the mitochondria.

1.3.5. Sacsin knockout mouse model

Sacs knockout (*Sacs*$^{-/-}$) mice have been generated to study the pathophysiological basis of ARSACS. Behavioural analysis conducted over a one-year period demonstrated that *Sacs*$^{-/-}$ mice develop a grossly abnormal gait with progressive motor, cerebellar, and peripheral nerve dysfunctions (Lariviere et al., 2015). Specifically, assessment of general motor coordination using the rotorod test showed that *Sacs*$^{-/-}$ mice had significantly poorer performance compared to controls, with the most significant differences occurring at 90 days (Lariviere et al., 2015). This is accompanied by an early onset, progressive loss of cerebellar Purkinje cells followed by spinal motor neuron loss and peripheral neuropathy (Lariviere et al., 2015). Thus, the sacsin knockout mouse model recapitulates many of the clinical and pathological features found in ARSACS patients.

In addition, neurons from *Sacs*$^{-/-}$ mice display both mitochondrial and neurofilament defects (Girard et al., 2012; Lariviere et al., 2015). These are discussed further in sections 1.9.6 and 1.11.1, respectively.

1.4. Protein Homeostasis (Proteostasis)

A key molecular pathogenic mechanism in many neurodegenerative diseases, including ataxias, is a disruption to protein quality control mechanisms. This can be a consequence of protein misfolding and lead to the accumulation of protein aggregates that are particularly detrimental to neurons.

1.4.1. Protein folding

The folding of a protein into its native three-dimensional (3D) structure determines the function of the protein. Proteins are constantly under threat of unfolding due to cellular stresses, such as heat shock, nutrient or oxygen deprivation, or local tissue inflammation. Under conditions of stress, proteins denature due to disruption of the bonding interactions responsible for secondary and tertiary structure of proteins, meaning they become unfolded. Protein misfolding can also occur as a result of missense mutations, high levels of protein expression, abberant post-translational modifications, or a shortage of necessary co-factors or components of multimeric complexes (Del Monte and Agnetti, 2014; Goldberg, 2003). Unfolded or partially folded proteins may expose hydrophobic amino acids, which are normally buried in the core of correctly folded proteins, and these may have undesirable interactions with other molecules (Vabulas et al., 2010). This in turn can lead to aggregation of proteins. Protein aggregates are defined by their insolubility in aqueous or detergent solvents, aberrant subcellular or extracellular localisation and non-native secondary structure (Fink 1998). The risk of misfolding and aggregation *in vivo* is enhanced due to the cellular environment being crowded at the molecular level, with a typical mammalian cell having a total protein concentration of ~300 mg per ml (Ellis, 2001; Zhou et al., 2008b).

The cellular protein quality control machinery has evolved to cope with misfolded and unfolded proteins by refolding or degrading misfolded proteins. These processes that

maintain normal cellular function contribute to what is termed proteostasis. The mechanisms are described in detail below.

1.4.2. Mechanisms of Proteostasis

In the cytoplasm, there are four main lines of defence against unfolded or misfolded proteins (Figure 1.2): (1) protein folding and refolding by molecular chaperones (Bukau and Horwich, 1998; Hartl and Hayer-Hartl, 2002), (2) proteasome dependent degradation (Alberti et al., 2002; Chapple et al., 2004; Connell et al., 2001), (3) autophagy-lysosome mediated degradation (Cuervo, 2004), (4) chaperone-mediated autophagy (CMA, (Kaushik and Cuervo, 2012; Massey et al., 2004)).

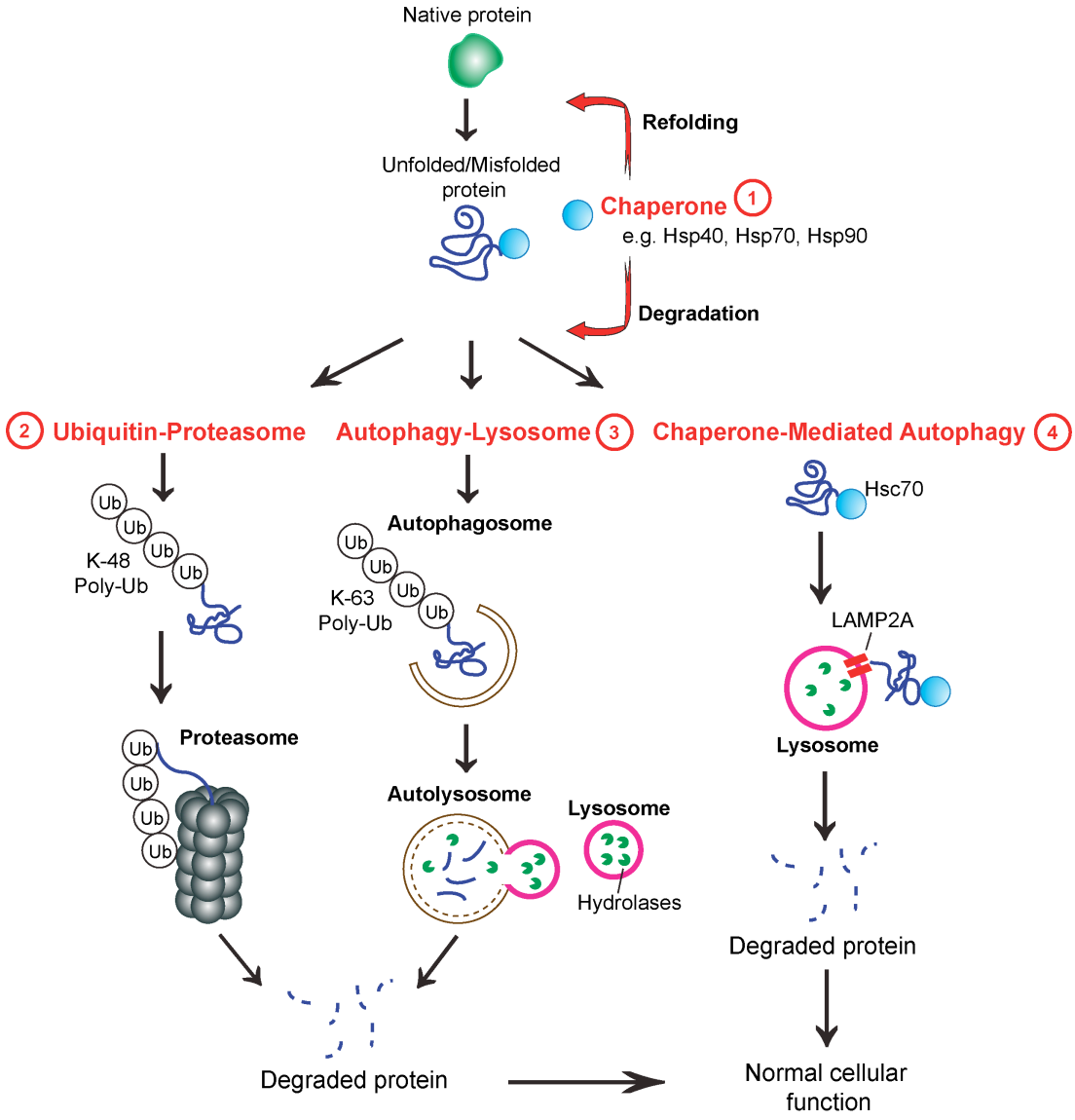

Figure 1.2. Schematic of the cellular protein quality control mechanisms. The chaperone, ubiquitin-proteasome, and autophagy-lysosome systems function simultaneously to maintain intracellular protein homeostasis. **(1)** Molecular chaperones represent the first line of defence in ensuring the correct folding and refolding of proteins. When a native folding state cannot be achieved, chaperones direct the misfolded protein for degradation by **(2)** the ubiquitin-proteasome or **(3)** autophagy-lysosome pathways. Proteins that are destined for proteasome-mediated degradation are tagged with a polyubiquitination chain at lysine residue K48, whereas proteins destined for autophagy are tagged with a polyubiquitination chain at lysine residue K63. The autophagy process involves the sequestration of misfolded proteins into a double-membrane structure called an autophagosome. The autophagosome then fuses with a lysosome to form autolysosomes, within which the proteins and/or organelles are degraded by acidic lysosomal hydrolases. **(4)** Chaperone-mediated autophagy (CMA) is a selective autophagy pathway. HSC70 chaperones target misfolded proteins to the lysosome where they bind to the receptor lysosome-associated membrane protein 2A (LAMP2A), to be translocated into the lysosome for degradation.

1.4.3. Molecular Chaperones

Molecular chaperones, along with their associated co-chaperones, represent the first line of defence against aberrant protein accumulation *in vivo*. Unlike other proteins, molecular chaperones are more resistant to becoming denatured under conditions of stress, as they are more hydrophobic and have enhanced secondary protein structure. They prevent protein aggregation by recognising and binding to the exposed hydrophobic amino acids of unfolded proteins (Hartl and Hayer-Hartl, 2002). They also enhance the efficiency of *de novo* protein folding, and promote refolding of proteins that have become misfolded due to cellular stress (Bukau and Horwich, 1998; Hartl and Hayer-Hartl, 2002). In addition, they assist protein translocation across membranes, protein-protein interactions (Kampinga et al., 2009; Meimaridou et al., 2011; Muchowski and Wacker, 2005), proteasome dependent degradation (Alberti et al., 2002; Chapple et al., 2004; Connell et al., 2001), and inclusion formation and lysosome-mediated autophagy (Cuervo, 2004).

1.4.3.1. *Heat Shock Proteins*

Many molecular chaperones are induced by cellular stresses, such as an increase in temperature (heat shock), infection, inflammation, starvation and hypoxia. These proteins are classified as heat shock proteins (HSPs, also known as stress proteins). They make up a group of structurally unrelated protein families, including HSPA (HSP70), HSPB (small HSPs), HSPC (HSP90), HSPD/E (HSP60/HSP10), HSPH (HSP110), and DNAJ (HSP40). They play key roles in proteostasis by promoting protein folding through binding to substrates to keep them in a state competent for either refolding or degradation. They are crucial for recovery from stress-induced protein damage and are synthesised at greatly increased levels under stress conditions. Most HSPs have a constitutively expressed member that plays a housekeeping role, and a stress-induced member is expressed under cellular stress conditions (Turturici et al., 2011). Heat shock transcription factor 1 (HSF1) is responsible for transcriptional activation of HSPs (Bukau et al., 2006; Hartl and Hayer-Hartl, 2002) by binding to heat shock elements (HSEs) in the promoter of HSPs (Morimoto and Santoro, 1998). HSP90 plays a key role in the regulation of HSF1, and hence in the transcriptional activation or deactivation of HSPs (Ali et al., 1998; Nadeau et al., 1993; Nair et al., 1996).

1.4.3.2. *HSP70/HSPA and HSP40/DNAJ chaperone system*

HSP70 proteins are central components of the molecular chaperone network and their function is facilitated by HSP40 proteins and other co-chaperones. The HSP70/HSP40 chaperone system is known as DnaK/DnaJ in bacteria (Bardwell and Craig, 1984; Craig et al., 1979; McKenzie et al., 1975; Saito and Uchida, 1977). The human genome encodes 13 different HSP70 proteins, the majority of which localise to the cytosol or nucleus (Table 1.3).

Table 1.3. HSPA (HSP70) members

HSPA	Gene and Protein name	Alternative names	Molecular mass (kDa)	Subcellular localisation
1	HSPA1A	HSP70-1; HSP72; HSPA1	70.0	Cytosol, nucelus
2	HSPA1B	HSP70-2	70.0	Cytosol, nucelus
3	HSPA1L	hum70t; hum70t; Hsp-hom	70.4	Cytosol, nucelus
4	HSPA2	Heat-shock 70kD protein-2	70.0	Cytosol, nucelus
5	HSPA5	BIP; GRP78; MIF2	71.0	ER
6	HSPA6	Heat shock 70kD protein 6 (HSP70B′)	71.0	Cytosol, nucelus
7	HSPA7	Heat shock 70kD protein 7	ND	Cytosol, nucelus
8	HSPA8	HSC70; HSC71; HSP71; HSP73	70.9	Cytosol, nucelus
9	HSPA9	GRP75; HSPA9B; MOT; MOT2; PBP74; mot-2	73.7	Mitochondria
10	HSPA12A	FLJ13874; KIAA0417	141.0	ND
11	HSPA12B	RP23-32L15.1; 2700081N06Rik	75.7	ND
12	HSPA13	Stch	51.9	ER
13	HSPA14	HSP70-4; HSP70L1; MGC131990	54.8	Cytosol, nucelus

Taken from (Hageman et al., 2011; Kampinga et al., 2009). ND: not determined.

Typically, HSP70 proteins are composed of two major functional domains, an N-terminal ATPase domain of 45 kDa and a C-terminal substrate-binding domain of 25 kDa, which are separated by a linker domain (Figure 1.3). Cooperation between these

domains is required for HSP70-mediated protein folding (Turturici et al., 2011). Additionally, a C-terminal EEVD sequence motif plays an important role in co-chaperone binding (Figure 1.3 (Turturici et al., 2011)). The HSP70s are functionally diverse, yet have high sequence identity within and across species (Hageman, 2008). The constitutively active member of the HSP70 protein family in eukaryotes is HSPA8, also known as HSC70, which is ubiquitously expressed and considered an essential "housekeeping" HSP70 member (Kampinga et al., 2009; Meimaridou et al., 2011).

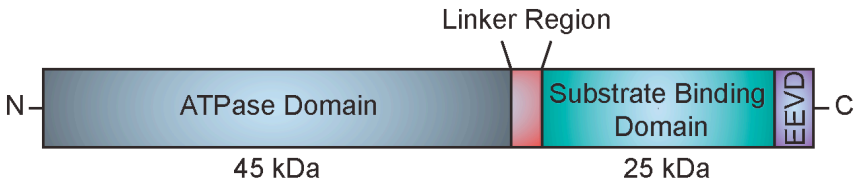

Figure 1.3. Schematic representation of the HSP70 protein domains.

The binding and release of substrates to HSP70 is regulated by its adenosine triphosphatase (ATPase) activity. In an ATP-bound state, the substrate binding pocket of HSP70 is in an open conformation, resulting in a low affinity and fast exchange rate for its substrates (Hartl and Hayer-Hartl, 2002). Upon the hydrolysis of ATP to ADP, which is accelerated by DNAJ/HSP40 proteins (Bukau and Horwich, 1998), a conformational change to HSP70 occurs. Specifically, the α-helical lid of the substrate binding domain of HSP70 closes, leading to tight binding of the substrate (Hartl et al., 2011; Shiber and Ravid, 2014). Thus, this ADP-bound state results in a high affinity and low exchange rate for its substrates (Hartl and Hayer-Hartl, 2002). Nucleotide exchange factors (NEFs), such as BAG1 or HSPBP1, then bind to HSP70, catalysing the disassociation of ADP. Re-association of ATP then induces the opening of the α-helical lid, thereby enabling substrate release (Hartl et al., 2011; Shiber and Ravid, 2014).

Over 50 DNAJ/HSP40-encoding genes have been identified in the human genome, with their encoded proteins ranging in molecular weight from 18-520 kDa (Hageman et al., 2011; Kampinga and Craig, 2010). The 520 kDa DNAJ protein is sacsin (DNAJC29). DNAJ proteins have a highly conserved J-domain over ~70 amino acids. There are four α-helices in the J-domain, and a His, Pro and Asp tripeptide (HPD) motif between the

two main helices (helix II and helix III) is crucial for J-domain function (Kelley, 1998; Tsai and Douglas, 1996; Walsh et al., 2004). Mutations in the HPD tripeptide affect the ability of the J-domain protein to bind to a HSP70 partner and stimulate its ATPase activity.

There are three distinct subgroups of DNAJ proteins, based on the presence of certain structural motifs: Type I/DNAJA, which have an N-terminal J-domain followed by a glycine/phenylalanine (G/F) -rich region and a cysteine-rich region stabilised by two zinc ions; Type II/DNAJB, which have the N-terminal J-domain and the G/F-rich region only; and Type III/DNAJC, which have the J-domain only, located anywhere within the protein (Cheetham and Caplan, 1998; Hageman et al., 2011). The presence of a J-domain within the protein defines it as a DNAJ family member.

Outside of the conserved J-domain, DNAJ proteins have high sequence and structural divergence, which determines their specific functions (Kampinga and Craig, 2010). All DNAJ proteins that have been studied so far accelerate the ATPase activity of HSP70 proteins. Overstimulation of ATPase activity by DNAJ results in failed capture of clients, hence the stoichiometry of HSP70 protein to DNAJ protein in the cell is critical. Usually HSP70 levels within a cell are higher than DNAJs (Kampinga and Craig, 2010). *In vitro*, stimulation of client protein folding is most efficient when HSP70 concentrations are 10-20 times higher than DNAJ protein (Diamant and Goloubinoff, 1998). However, there are usually a higher number of different DNAJ proteins in a cellular compartment compared to HSP70 proteins. For example, mammals have one type of HSP70 in mitochondria and one type in the endoplasmic reticulum, while these organelles have 4 and 6 DNAJ proteins, respectively. Hence, HSP70 proteins interact with multiple DNAJ proteins (Craig et al., 2006; Hageman and Kampinga, 2009).

The ability of DNAJ proteins to recruit HSP70 to specific cellular locations is important for functional diversity, for example, the DNAJ homolog auxilin, which is expressed in neurons, is required for HSC70 to uncoat clathrin from clathrin-coated vesicles (Barouch et al., 1994). Also, the ribosome associated J-protein DNAJC2 recruits HSC70 to the ribosome to act on nascent polypeptides (Hundley et al., 2005). Additionally, DNAJC5, which encodes cysteine string protein α (CSPα), recruits HSC70, along with the small glutamine-rich tetratricopeptide repeat-containing protein (SGT), to form a functional chaperone complex on synaptic vesicles (Tobaben et al.,

2001; Zhang et al., 2012). CSPα directly binds folded dynamin 1 and promotes its oligomerisation, thereby facilitating synaptic vesicle endocytosis (Zhang et al., 2012).

To date, mutations in seven DNAJ proteins have been linked to distinct diseases in humans (Table 1.4, (Koutras and Braun, 2014)).

Table 1.4. DNAJ mutations and resulting human diseases

Gene	Protein	Disease	Reference
DNAJB2	HSJ1	Distal Motor Neuropathy	(Blumen et al., 2012)
DNAJB6	MRJ	Limb-girdle Muscular Dystrophy Type 1D	(Harms et al., 2012; Sarparanta et al., 2012)
DNAJC5	CSPα	Adult-onset Neuronal Ceroid Lipofuscinosis	(Benitez et al., 2011; Noskova et al., 2011)
DNAJC6	Auxilin	Childhood Parkinsonism	(Edvardson et al., 2012)
DNAJC13	RME-8	Parkinsons Disease	(Vilarino-Guell et al., 2014)
DNAJC19	TIM14	Ataxia Dilated Cardiomyopathy	(Davey et al., 2006; Ojala et al., 2012)
DNAJC29	Sacsin	Autosomal Recessive Spastic Ataxia of Charlevoix-Saguenay	(Bouchard et al., 1978; Engert et al., 2000)

HSJ1: Homo sapiens DnaJ 1, MRJ: mammalian relative of DnaJ, CSPα: Cysteine string protein alpha, RME-8: receptor-mediated endocytosis 8, TIM14: translocase of the inner membrane 14

1.4.3.3. *HSP90/HSPC*

The HSP90 protein family has members localised to most organelles of eukaryotic cells (Taipale et al., 2010). The majority of eukaryotic genomes encode organelle-specific isoforms, including ER (GRP94) and mitochondrial forms (TRAP1, (Pearl and Prodromou, 2006). Under normal cellular conditions, HSP90 is highly abundant in the cytoplasm, constituting 1-2% of total protein levels (Borkovich et al., 1989). Under cellular stress, some HSP90 translocates to the nucleus, most likely by co-transport with client proteins, as HSP90 does not contain a nuclear localisation sequence (Taipale et

al., 2010). In a similar way to HSP70, the HSP90 client binding-release cycle is dependent on ATP hydrolysis and is facilitated by co-chaperones (Taipale et al., 2010).

Constitutively expressed and inducible forms of cytosolic HSP90 exist. Inducible transcription is controlled by heat shock factor 1 (HSF1). Under normal conditions, HSF1 is a client of HSP90 and is held in an inactive complex with HSP90 and HSP70. Under cellular stress, HSF1 is released to allow transcriptional activation of inducible HSP90. Thus, HSP90 has an important role in regulating its own transcription (Nadeau et al., 1993). HSP90 can also be regulated by post-translational modifications such as acetylation, phosphorylation and nitrosylation (Taipale et al., 2010).

Structurally, HSP90 is a homodimer consisting of three domains, the N-terminus, middle and C-terminus. The 25 kDa N-terminal domain is involved in nucleotide binding. This is connected to a middle domain by a charged linker (Hainzl et al., 2009; Tsutsumi et al., 2009). Mutations in the linker region impair client activation and prevent regulation by certain co-chaperones (Hainzl et al., 2009). The middle domain is thought to be required for client recognition. A 12 kDa C-terminal domain is involved in dimerisation of HSP90 (Ali et al., 2006; Minami et al., 1994). Five C-terminal residues make up the MEEVD motif (Met-Glu-Glu-Val-Asp), which is a highly conserved tetratricopeptide repeat (TPR) domain-binding site that mediates interaction with over 20 co-chaperones (Taipale et al., 2010; Young et al., 1998), such as HOP and CHIP, *via* their TPR domains.

Members of the different chaperone families, HSP40, HSP70 and HSP90, function together in proteostasis networks, with co-chaperones mediating interaction between them. For example, the multiple TPR domains in the co-chaperone HSP70-HSP90-organising protein (HOP) mediate interactions between HSP70 and HSP90. HOP also modulates the ATPase activity of both HSP70 and HSP90, thus facilitating client transfer between the two, allowing client maturation. HSP90 ATPase activity can be inhibited by co-chaperones, for example HOP, CDC37 and p23 (Prodromou et al., 1999; Siligardi et al., 2002), or can be enhanced by co-chaperones, such as AHA1 and CPR6 (McLaughlin et al., 2002; Panaretou et al., 2002).

Two main classes of HSP90 clients are protein kinases, such as CDK4 and ERBB2, and nuclear steroid receptors, such as glucocorticoid receptor and progesterone receptor. Additional client proteins include transcription factors, such as AHR, HIF1A, HIF2A

and HIF3A, telomerase reverse transcriptase (TERT, (Holt et al., 1999)) and endothelial nitric oxide synthase (eNOS, (Garcia-Cardena et al., 1998)). More recently, the intermediate filament protein vimentin was identified to be a client protein of HSP90 (Zhang et al., 2006). HSP90 protects vimentin from apoptotic cleavage (Zhang et al., 2006).

HSP90 generally assists in the maturation of client proteins, but it can also promote protein degradation, for example it is essential for the degradation of the von Hippel-Lindau (VHL) tumor suppressor protein (McClellan et al., 2005). The E3 ubiquitin ligase, C terminus of HSP70-interacting protein (CHIP), interacts with the C-terminus of both HSP90 and HSP70 through its TPR domain. CHIP knockdown in cultured cells stabilises some HSP90 clients, and CHIP overexpression promotes their degradation (Xu et al., 2002).

1.4.4. Protein Degradation

When a native protein folding state cannot be achieved, molecular chaperones direct misfolded proteins for degradation. This is important to prevent disruption to other cellular processes, for amino acid recycling, and for the regulation of individual protein levels. The ubiquitin-proteasome system (UPS) and autophagy-lysosome pathways (ALP) are the two main routes of protein and organelle clearance in eukaryotic cells (Figure 1.2). The proteasome predominately degrades short-lived nuclear and cytosolic proteins (Ciechanover, 2006), as well as misfolded proteins from the ER, whereas autophagy is responsible mainly for the degradation of long-lived proteins and organelles (Henell et al., 1987; Mizushima et al., 2008).

Autophagy refers to the degradation of cytosolic components in lysosomes, regardless of the mechanism by which the cargo is delivered to lysosomes. In most mammalian cells, the deliver occurs by three different ways that distinguish the subtypes of autophagy: macroautophagy, microautophagy and chaperone-mediated autophagy (CMA). All three subtypes coexist in cells, and alterations in both macroautophagy and CMA have been associated with neurodegenerative disorders (Cuervo et al., 2010). Macroautophagy is the main type of autophagy and this is discussed in more detail below.

The signal for targeting proteins for degradation *via* macroautophagy or the UPS is polyubiquitination, which is the covalent attachment of a chain of four or more

ubiquitin molecules to a substrate protein at a lysine residue (Hershko and Ciechanover, 1998). Ubiquitin itself has seven lysines (e.g. K48 and K63) and linkage of other ubiquitin molecules to these lysines then forms the polyubiquitin chain. Ubiquitination of proteins involves an E1-E2-E3 ubiquitin enzyme cascade (Figure 1.4). E1 (ubiquitin-activating enzyme) hydrolyses ATP and forms a thioester-linked conjugate between itself and ubiquitin, E2 (ubiquitin-conjugating enzyme) receives ubiquitin from E1 and forms a similar thioster bond with ubiquitin, and E3 (ubiquitin ligase) binds both E2 and the substrate, and transfers the ubiquitin to the substrate (Figure 1.4).

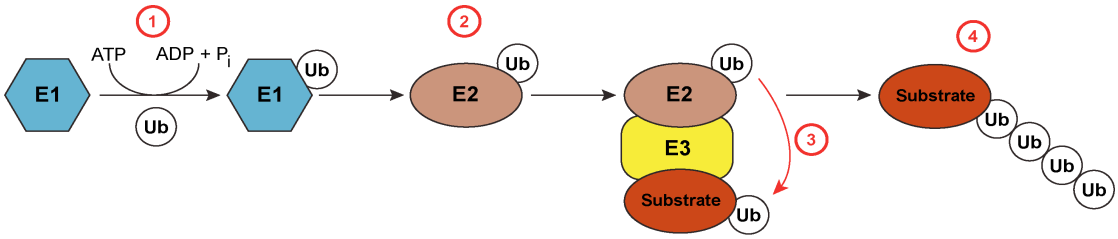

Figure 1.4. Schematic of the ubiquitination pathway. (1) An E1 ubiquitin-activating enzyme charges a single ubiquitin (Ub) molecule via ATP hydrolysis, before (2) transferring the ubiquitin to an E2 ubiquitin-conjugating enzyme. (3) An E3 ubiqutin-ligase then transfers the ubiquitin to the substrate protein, and (4) the ubiquitin chain is extended by E3 ligases.

Polyubiquitin chains, linked by lysines at residue 48 (K48-linked polyubiquitination), are the signal for proteasomal degradation. The K48-linked ubiquitinated proteins are recognised and degraded by the 26S proteasome, which is a complex structure comprising two regulatory 19S subunits and a 20S catalytic core subunit (Navon and Ciechanover, 2009). The targeted protein travels through a channel in the 26S proteasome and is enzymatically degraded. During degradation, ubiquitin is removed from the proteins by deubiquitinating enzymes and recycled (Bhattacharyya et al., 2014; Finley, 2009; Navon and Ciechanover, 2009).

Polyubiquitin chains, linked by lysines at residue 63 (K63-linked polyubiquitination), target proteins for macroautophagy (Tan et al., 2008), particularly larger protein complexes, organelles and protein aggregates, which are too large to pass through the narrow pore of the proteasome (Mizushima et al., 2008; Yorimitsu and Klionsky, 2005). p62/SQSTM1 binds to K63-ubiquitin linked proteins, *via* its ubiquitin-associated (UbA)

domain, targeting them for autophagic degradation (Long et al., 2008; Pankiv et al., 2007). The proteins or protein aggregates are engulfed within a double-membrane, which is proposed to form from the fusion of vesicles from a variety of membrane sources, including plasma membrane-derived endosomal intermediates (Ravikumar et al., 2010), the ER (Hayashi-Nishino et al., 2009; Yla-Anttila et al., 2009), the Golgi (van der Vaart and Reggiori, 2010; Yen et al., 2010), and mitochondria (Hailey et al., 2010). This forms the autophagosome (Figure 1.5). Fifteen autophagy-related (ATG) proteins mediate the formation of the autophagosome, including the initiation of autophagy, and the expansion and closure of autophagosomal membranes (Mizushima et al., 2011). Mature autophagosomes are trafficked by dynein motors along microtubules, in a retrograde manner, to the perinuclear region where they fuse with lysosomes (autolysosomes) to degrade their contents by acidic lysosomal hydrolases (Figure 1.5 (Knaevelsrud and Simonsen, 2010)).

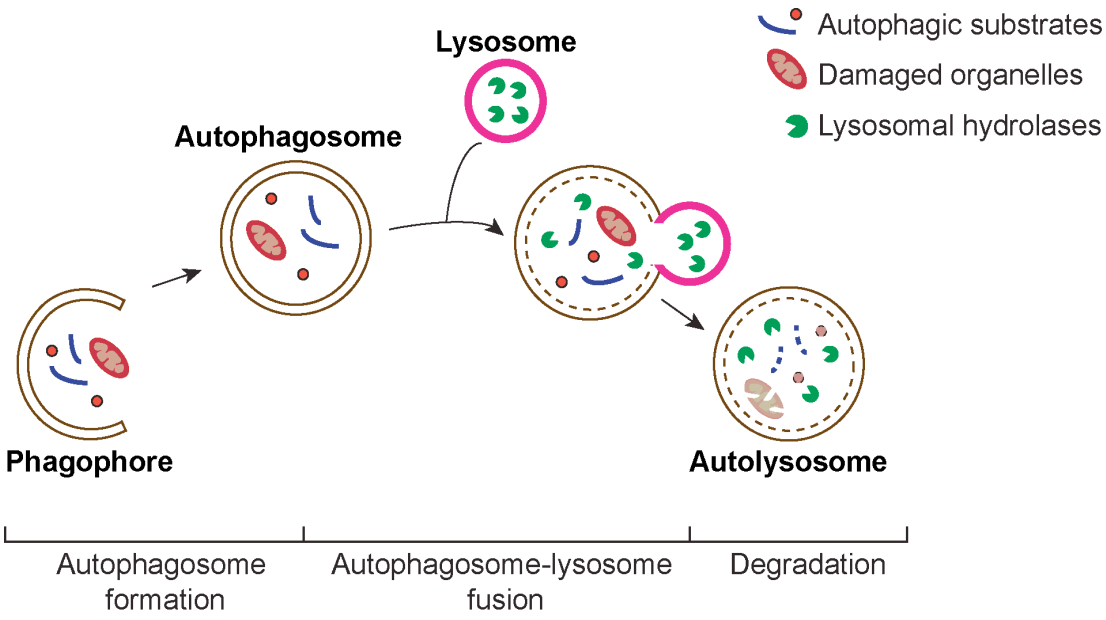

Figure 1.5. Schematic of macroautophagy. Following the induction of autophagy, autophagic substrates and/or damaged organelles are engulfed by an isolation membrane known as a phagophore. This elongates to form an autophagosome, which has a double membrane. Autophagosomes fuse with lysosomes (autolysosome) to degrade their contents by the action of lysosomal hydrolases. Adapted from (Ao et al., 2014).

Polyglutamine-expansion proteins, such as mutant huntingtin and ataxin-3, and mutant forms of α-synuclein and tau, are strongly dependent on macroautophagy for their clearance (Iwata et al., 2005b; Qin et al., 2003; Webb et al., 2003).

Dysfunction of macroautophagy prevents efficient nutrient recycling, enhances susceptibility to apoptosis (Boya et al., 2005), and leads to the formation of ubiquitinated inclusions (Rideout et al., 2004). Dynein-dynactin function is also important for autophagosome-lysosome fusion, and autophagic clearance is impaired by loss of dynein-dynactin function (Ravikumar et al., 2005). Mutations in the dynactin subunit $p150^{Glued}$ lead to protein aggregation and a motor neuron disease (Levy et al., 2006).

1.4.4.1. *Chaperone-mediated autophagy (CMA)*

CMA is a selective autophagy pathway for cytosolic protein clearance directly through lysosomes, without being trafficked *via* autophagosomes (Figure 1.2). This pathway is independent of ubiquitin, as substrates do not require ubiquitination prior to degradation. It involves the recognition of a targeting motif on substrates, Lys-Phe-Glu-Arg-Gln (KFERQ, (Dice, 1990; Massey et al., 2004)). This motif is present in around 30% of cytosolic proteins (Wing et al., 1991) and is recognised by the HSC70 chaperone. HSC70 targets substrates to the lysosomal membrane where they bind to the receptor lysosome-associated membrane protein 2A (LAMP2A), to be translocated in to the lysosome for degradation. Wild-type α-synuclein, which contains a KFERQ-like motif (VKKDQ, (Liu et al., 2009)), has been shown to be selectively translocated into lysosomes for degradation by the CMA pathway (Cuervo et al., 2004). Mutation of the sequence VKKDQ by replacing DQ with AA prevents α-synuclein from binding to LAMP2A, which leads to dramatically reduced translocation of α-synuclein into the lysosomal lumen (Cuervo et al., 2004).

1.4.4.2 *Mitophagy*

Several types of cargo-specific autophagy have been reported and widely studied, including mitophagy, which selectively removes dysfunctional or excessive mitochondria. In functional mitochondria that are able to maintain their mitochondrial membrane potential, phosphatase and tensin homologue-induced putative kinase 1 (PINK1) is imported *via* the translocase of the outer membrane (TOM) complex and the

translocase of the inner membrane (TIM23) complex. It is then cleaved by mitochondrial processing peptide (MPP) and presenilins-associated rhomboid-like protein (PARL) in the inner membrane before being translocated back to the cytoplasm for degradation by the proteasome (Becker et al., 2012; Greene et al., 2012; Jin et al., 2010). However, in the absence of a mitochondrial membrane potential, PINK1 accumulates on the mitochondrial outer membrane where it recruits the E3-ubiquitin ligase parkin (Geisler et al., 2010; Matsuda et al., 2010; Vives-Bauza et al., 2010), resulting in the targeting of mitochondria for degradation by mitophagy. Interruptions in the normal mechanisms of mitophagy have been implicated in the pathogenesis of neurodegenerative diseases. For example, mutations in the genes encoding PINK1 or parkin lead to defects in mitophagy and are the leading cause of recessive parkinsonism (Kitada et al., 1998; Michiorri et al., 2010; Valente et al., 2004).

1.5. Disrupted proteostasis in neurodegeneration

When the lines of defence against misfolded proteins fail or become overwhelmed, misfolded proteins can form aggregates. These protein aggregates are transported on microtubules, in a retrograde manner, to the microtubule organising centre (MTOC) where they accumulate and may form inclusion bodies or aggresomes (Garcia-Mata et al., 1999; Johnston et al., 1998; Kopito, 2000).

Neurons are particularly vulnerable to the toxicity of misfolded proteins. This is believed to be, in part, because they are post-mitotic cells so are unable to dilute misfolded or aggregated proteins through cell division (Muchowski and Wacker, 2005). Consequently, many neurodegenerative disorders are characterised by the presence of inclusion bodies. For example, Alzheimer's disease is characterised by the presence of extracellular amyloid plaques, which consist of aggregated β-amyloid peptide, and intracellular neurofibrillary tangles, containing aggregated, hyperphosphorylated tau protein (Glenner and Wong, 1984; Grundke-Iqbal et al., 1986). Similarly, sporadic Parkinson's disease features intracellular inclusions known as Lewy bodies, which contain aggregated α-synuclein (Spillantini et al., 1997). Huntington's disease has the presence of intranuclear inclusions of aggregated huntingtin protein, which contain polyglutamine (polyQ) expansion (DiFiglia et al., 1997). This is similar to what occurs in other polyQ disorders, such as spinocerebellar ataxias (SCAs), which are all caused

by expansions in the CAG tract of the affected gene, leading to polyQ expansion, misfolding and inclusion body formation (Bates, 1996; Trottier et al., 1995).

Interestingly, most of these disease-specific inclusions contain proteins that are ubiquitinated, along with other proteostasis components, such as molecular chaperones and components of the proteasome (Muchowski and Wacker, 2005; Ross and Poirier, 2004; Sherman and Goldberg, 2001). This suggests that the accumulated proteins with abnormal conformation have been detected by the protein quality control system, but due to inefficent or impaired clearance, they remain within cells and are sequestered to inclusions.

Mutations in certain proteins that are involved in UPS and ALP function are known to lead to neurodegenerative diseases. Many of these proteins contain domains that mediate interactions with polyubiquitinated proteins or the proteasome, such as an ubiquitin-like domain (UbL), ubiquitin-associated domain (UbA), or ubiquitin-interacting motifs (UIM, (Grabbe and Dikic 2009, Su and Lau 2009)). An example is parkin, which contains an N-terminal UbL-domain and is involved in transferring ubiquitin to substrates, targeting them for degradation *via* the UPS or ALP (Shimura et al., 2000). Interestingly, wild-type parkin is found in Lewy bodies in sporadic PD (Schlossmacher et al., 2002).

1.5.1. HSP70 and HSP40 as modulators of neurodegeneration

Molecular chaperones are particularly associated with protein aggregates (Barral et al., 2004; Johnston et al., 1998; Verhoef et al., 2002). For example, HSP70 is found in nuclear inclusions of mutant huntingtin (Muchowski et al., 2000; Wyttenbach et al., 2000) and in Lewy bodies (Lee and Lee, 2002), and the DNAJ/HSP40 protein DNAJB6 is associated with Lewy bodies (Durrenberger et al., 2009).

Recent studies have demonstrated that activation of the heat shock response (HSR), and in particular elevation of HSP70 levels, inhibits aggregate formation and prevents cell toxicity in several models of neurodegeneration. For example, HSP70 overexpression reduced α-synuclein accumulation and toxicity in mouse and *Drosophila* models of Parkinson Disease (Auluck et al., 2002; Klucken et al., 2004). Also, in a model of Alzheimer's disease, HSP70 overexpression rescued primary neuronal cultures from the toxic effects of intracellular β-amyloid (Aβ) accumulation (Magrane et al., 2004). The ability of HSP70 to reduce the severity of polyQ-mediated degeneration has also been

demonstrated in mouse models. For example, when a spinocerebellar ataxia type 1 (SCA1) transgenic mouse was crossed with a hemizygous mouse overexpressing HSP70 at around 10-fold normal levels, behavioural and neuropathological symptoms improved (Cummings et al., 2001).

HSP40 proteins also have a neuroprotective role. In a cellular model of spinocerebellar ataxia type 1 (SCA1), overexpression of the HSP40 protein HDJ2 (DNAJA1) caused a significant decrease in the incidence of ataxin-1 inclusions (Cummings et al., 1998). Additionally, the overexpression of either HDJ1 (DNAJB1) or HDJ2 (DNAJA1) in a cell model of spinocerebellar ataxia type 3 (SCA3)/Machado-Joseph disease (MJD) suppressed the aggregation and toxicity of polyQ-expanded full-length or truncated mutant ataxin-3 (Chai et al., 1999). HSP40 proteins that are enriched in neuronal tissues or have a neuronal specific expression profile may be particularly relevant in neurodegenerative diseases. For example, HSJ1a (DNAJB2a) has been shown to increase ubiquitylation and reduce the incidence of polyQ protein aggregation in cellular and *in vivo* models of polyQ and protein misfolding diseases (Gao et al., 2011; Howarth et al., 2007; Novoselov et al., 2013; Westhoff et al., 2005). Therefore, HSP70 and its co-chaperones appear to have a protective effect against misfolded proteins.

1.6. Sacsin Domains

Sacsin contains multiple domains that suggest a role in proteostasis. If this is the case, then like many other neurodegenerative diseases, disrupted proteostasis may also be a molecular pathogenic mechanism in ARSACS.

1.6.1 Sacsin Repeating Region (SRR)

Sacsin consists of three repeated regions, known as the sacsin-repeating region (SRR, (Anderson et al., 2010; Romano et al., 2013)). These repeating regions are much larger than originally described (Anderson et al., 2010; Engert et al., 2000), with each repeated region being ≥1100 amino acids, covering ~84% of the protein sequence, and this repeated architecture is conserved in all vertebrate sacsins (Romano et al., 2013). The three repeated regions have a low overall similarity (16-18%), but they contain discrete sub-repeats based on there degree of local similarity, the first of which is homologous to the HATPase_c (Histidine kinase-like ATPases; SMART acc. no. SM00387) domain of HSP90 (Figure 1.1. (Anderson et al., 2010; Romano et al., 2013)).

Anderson *et al* (2010) demonstrated, by biochemical characterisation, that the first SRR has ATPase activity. A disease causing mutation (D168Y) within the first sub-repeat region, homologous to HSP90, abolished the full proteins ability to hydrolyse ATP (Anderson et al., 2010). From this, it was suggested that ATPase activity is a requirement for sacsin function, as this mutation lead to essentially the same clinical phenotype as nonsense mutations close to the N-terminus of the protein that result in truncations of the protein (Anderson et al., 2010). In HSP90, the middle domain contains an arginine residue that accepts phosphate after ATP hydrolysis (Pearl and Prodromou, 2006). This arginine is conserved in each of the second sub-repeats and a mutation occurring in one of these conserved arginines, namely c.1420C>T (p.R474C), leads to a severe clinical phenotype (Romano et al., 2013).

The functional nature of the sub-repeating regions is also implicated by the observation that sacsin pathogenic missense mutations are found to be over-represented in the SRRs, and particularly in conserved positions (Romano et al., 2013). Previously, HSP90 and the HDJ2 HSP40/DNAJ protein have been implicated to function together in folding pathways, for example in the maturation of the glucocorticoid receptor (Kimura et al., 1995).

1.6.2. J-domain

J-domains are the defining feature of the DNAJ/HSP40 family of HSP70 co-chaperones. A region of over 30 residues near the C-terminus of sacsin (Figure 1.1) shares ~60% identity to the J-domain of HSP40 proteins and is highly conserved (Parfitt et al., 2009), suggesting a role with the HSP70 chaperone machinery. Sacsins J-domain is similar to that of other DNAJ proteins, for example DNAJB6, which is an HSP40 homolog that has been associated with several neurodegenerative disorders, such as Parkinson's disease (Durrenberger et al., 2009) and Huntington disease (Chuang et al., 2002; Gillis et al., 2013). The sacsin J-domain was found to be able to function with the bacterial HSP70, DnaK, by an *in vivo* complementation assay (Parfitt et al., 2009). Also, a recombinant version of the J-domain from mouse sacsin increased the ATPase activity of HSP70 (Anderson et al., 2010). This confirmed that sacsin is a type III HSP40 protein and it is thus also known as DNAJC29 (Kampinga et al., 2009). Other type III HSP40 proteins are known to recruit HSP70s for specialised roles (examples in section 1.4.3.2).

The sacsin J-domain contains the highly conserved histidine-proline-aspartic acid (HPD) motif, which is important for HSP70 interaction (Parfitt et al., 2009). A histidine-to-glutamine substitution within the HPD motif disrupts the ability of J-domains to functionally interact with HSP70 (Hennessy et al., 2005). To date, the only identified ARSACS-causing mutation in the sacsin J-domain is the heterozygous missense mutation R4331Q. The Dutch family with this *SACS* mutation are compound heterozygotes (K1715*/R4331Q (Vermeer et al., 2008)). The arginine occupies a position critical for J-domain function and this mutation is predicted to be intolerant and probably leads to loss of function of the protein (Vermeer et al., 2008). However, the R4331Q mutation alone did not affect the ability of the sacsin J-domain to rescue the function of mutant bacterial DnaJ with non-functional J-domain (Parfitt et al., 2009). Vermeer *et al*., (2008) suggest that both mutations (K1715*/R4331Q) may need to be present to affect the function of sacsin's J-domain. However, this is unlikely as these two mutations are located far from each other and the result may be different when inserting this mutant sacsin J-domain into a non-functional human DNAJ. The K1715* mutation resides within the second SRR, and Li (2013) suggests that the function of the sacsin J-domain may require its interaction with the SRR, whose ATPase activity may contribute to J-domain's recruitment and stimulation of HSP70 (Li, 2013).

1.6.3. HEPN domain

At the C-terminus of sacsin is a higher eukaryotes and prokaryotes nucleotide-binding (HEPN) domain. This was first described by Grynberg *et al*. (2003) and has been shown to bind to various nucleotides, such as ATP, ADP, and GTP, but does not exhibit any GTPase or ATPase activity (Kozlov et al., 2011). Crystal structure of the human sacsin-HEPN domain revealed that it exists as a dimer, which interacts with nucleotides electrostatically *via* a large positively charged cavity at the dimer interface (Kozlov et al., 2011). An ARSACS patient mutation, N4549D, at the dimer interface was shown to hinder protein folding and dimerisation of the domain, which is likely responsible for its loss of function (Kozlov et al., 2011). HEPN domains are widely distributed in eubacteria and archaea but are restricted to animals in eukaryotes (Grynberg et al., 2003). In humans, the HEPN domain occurs only in the protein sacsin.

Very recently, it has been confirmed that the HEPN domain of sacsin binds nucleotides with low micromolar affinities using fluorescence polarisation (FP) assays (Li et al.,

2015b). This is consistent with the HEPN domain contributing to the functional activity of sacsin by binding to nucleotides.

It has been suggested that the close proximity of the sacsin J-domain and HEPN domain could be important for the hypothesised function of sacsin as a co-chaperone. The HEPN domain may increase the local concentration of ATP to promote nucleotide exchange onto HSP70 (Kozlov et al., 2011).

1.6.4. UBL-domain, XPCB domain, and UIM domain

The ubiquitin-proteasome pathway of protein degradation is a major mechanism for maintenance of cellular protein levels. Proteins containing UbL and UbA domains are implicated in proteasomal degradation through associations with proteins destined for degradation and with subunits of the proteasome (Su and Lau, 2009). The N-terminus of sacsin contains a UbL domain (Figure 1.1), which shares 43% homology to the RAD23A UbL domain over 65 residues (Parfitt et al., 2009), and has been shown by co-immunoprecipitation to interact with the 20S proteasomal alpha subunit C8 (Parfitt et al., 2009).

Towards the C-terminus is the Xeroderma pigmentosum complementation group C binding (XPCB) domain (Figure 1.1), which shares 35% homology with the hHR23 XPCB domain (Kamionka and Feigon, 2004). Interestingly, the hHR23 protein also contains a UbL domain which, similar to sacsin, interacts with the 19S regulatory subunit of the 26S proteasome (Mueller and Feigon, 2002). The sacsin-XPCB domain was recently identified as a potential binding domain for the E3 ubiquitin ligase UBE3A, which is non-functional in the neurodevelopmental disorder Angelman's syndrome (Greer et al., 2010). In *Ube3A* knockout mice levels of ubiquitinated sacsin were severely reduced, suggesting Ube3A is responsible for ubiquitinating sacsin (Jana, 2012). Bioinformatic analyses also potentially identified two ubiquitin-interaction motifs (UIM) in sacsin, located either side of the XPCB domain (Parfitt, 2011). UIMs interact with ubiquitin itself.

The presence of the UbL domain and XPCB domain, and possible UIM motifs, all point towards a function for sacsin in a ubiquitin-mediated degradation pathway. This, along with the presence of the J-domain and HSP90 like chaperone domains, suggests that sacsin plays a role in proteostasis. Interestingly, other proteins that function in the ubiquitin-proteasome pathway are linked to ataxias, for example, ataxin-3 contains a

UIM and functions as a deubiquitination enzyme (Burnett et al., 2003).

1.7. Mitochondrial Dynamics

Mitochondrial disruption is another key molecular pathogenic mechanism implicated in neurodegenerative disorders (Chen and Chan, 2009; Knott and Bossy-Wetzel, 2008; Liesa et al., 2009) and in particular, cerebellar ataxias, such as SCA3 (Laco et al., 2012; Ramos et al., 2015) and ataxia telangiectasia (Eaton et al., 2007; Valentin-Vega et al., 2012).

Mitochondria are highly dynamic; double-membrane bound organelles that contain their own genome and protein synthesis machinery. They migrate throughout the cell, and constantly fuse and divide, changing the length, shape, size and number of mitochondria. This is crucial to regulate many cellular processes (Chan, 2006) and is termed mitochondrial dynamics (Bereiter-Hahn, 1990; Bereiter-Hahn and Voth, 1994).

Mitochondrial division, or fission, produces numerous mitochondrial fragments, and is important to distribute the organelles inside the cell (Collins et al., 2002). Fission is also required to sequester damaged mitochondrial fragments, which become engulfed by autophagosomes and are degraded through mitophagy (Lee et al., 2010; Tanaka et al., 2010). Mitochondrial fusion generates interconnected mitochondria, enabling the exchange of contents between mitochondria, such as the sharing of mitochondrial DNA (mtDNA), dissipation of energy through transmission of a membrane potential (Skulachev, 2001; Westermann, 2010b), and transport of solutes, metabolites, and proteins (Twig et al., 2008).

At steady state, the frequencies of fusion and fission events are balanced (Nunnari et al., 1997); however when this balance is perturbed, dramatic changes in mitochondrial morphology occur. A high fusion-to-fission ratio leads to few mitochondria, which are long and highly interconnected (Bleazard et al., 1999; Chen et al., 2003a; Smirnova et al., 2001). Conversely, a low fusion-to-fission rate leads to numerous small mitochondria that have a spherical or rod like morphology.

Mitochondria accumulate in sites of high-energy demand or where calcium buffering is required; hence certain cell types, such as neurons, are especially dependent on having the correct balance between mitochondrial fission and fusion. In the cerebellum, mitochondrial fission generates mitochondria of the correct size for transport along

dendritic processes of Purkinje neurons, to meet significant energy demands at locations distant from the cell body (Bereiter-Hahn, 2014; Chen et al., 2007).

Mitochondrial fission and fusion are controlled by four large dynamin-related GTPases. These effectors of mitochondrial dynamics are conserved from yeast to mammals. Outer mitochondrial membrane (OMM) fusion is controlled by mitofusin 1 (MFN1) and mitofusin 2 (MFN2, (Chen et al., 2003a; Santel and Fuller, 2001)), inner mitochondrial membrane (IMM) fusion by optic atrophy protein 1 (OPA1, (Alexander et al., 2000; Delettre et al., 2000)), and mitochondrial fission by dynamin-related protein 1 (DRP1, Figure 1.6 (Pitts et al., 1999; Smirnova et al., 1998)).

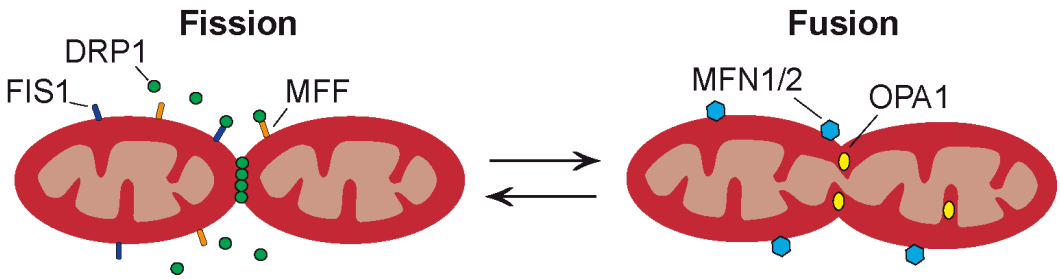

Figure 1.6. Schematic representation of mitochondrial fission and fusion. Mitochondria dynamically alter their morphology through fission (left) and fusion (right) to maintain cellular homeostasis. For mitochondrial fission to occur, DRP1 is recruited from the cytosol to the OMM. FIS1 and MFF are located on the OMM and are adapter proteins for DRP1. For mitochondrial fusion to occur, MFN1 and MFN2 are located on the OMM to coordinate fusion of the outer membrane of adjacent mitochondria, and OPA1 is located on the IMM to coordinate inner membrane fusion. MFF: mitochondrial fission factor, FIS1: fission protein-1.

1.7.1. Mitochondrial Fusion

The first known mediator of mitochondrial fusion, fuzzy onions (FZO), was discovered in 1997 in *Drosophila*, and is an OMM GTPase required for the fusion of mitochondria during spermatogenesis (Hales and Fuller, 1997). FZO is the first identified member of the mitofusin family of proteins found in yeast (Fzo1, (Hermann et al., 1998; Rapaport et al., 1998), worms (Kanazawa et al., 2008), and mammals (Santel and Fuller, 2001). The mammalian homologues are mitofusins MFN1 and MFN2, which form homo-oligomeric and hetero-oligomeric complexes that tether and possibly fuse OMMs of mitochondria (Chen et al., 2003a; Koshiba et al., 2004). MFN1 and MFN2 are anchored

to the OMM and have a large N-terminal GTPase domain and a C-terminal domain containing a heptad repeat region, both of which are exposed to the cytosol. Mutations in the GTPase domain or the heptad repeat region, which forms coiled-coil structures, prevent mitochondrial fusion (Chen et al., 2003a; Santel et al., 2003). Mutations in *MFN2* cause Charcot-Marie-Tooth disease type 2A (CMT2A), with patients having a loss of peripheral nerve function (Lawson et al., 2005; Zuchner et al., 2004). The majority of mutations identified in MFN2 cluster in or near the GTPase domain of the protein. Mitochondria in the sural nerve of two patients with CMT2A showed structural aberrations in their outer and inner membranes and mitochondrial dysfunction (Verhoeven et al., 2006). Due to the ability of MFN1 and MFN2 to form hetero-oligomeric complexes, MFN1 can partially compensate for loss of functional MFN2. For example, in mouse embryonic fibroblasts (MEFs), expression of Mfn2 mutants that cause CMT2A leads to lack of mitochondrial fusion activity. This phenotype can be partially rescued when wild-type Mfn1 is co-expressed due to the formation of heterotypic complexes (Chen et al., 2003a). It has been suggested that tissues with low MFN1 expression are vulnerable in patients with CMT2A and that methods to increase MFN1 expression in the peripheral nervous system may be beneficial.

Mice lacking Mfn2 show highly specific degeneration of Purkinje neurons in the cerebellum, leading to cerebellar ataxia (Chen et al., 2007). These mutant Purkinje cells have fragmented mitochondria that fail to distribute effectively along dendrites, and show loss of respiratory activity.

OPA1 is essential for IMM fusion in mammals, the yeast orthologue being Mgm1 (Meeusen et al., 2006). *OPA1* is present in eight isoforms that are generated by alternative splicing and alternative processing at two cleavage sites located between the N-terminal transmembrane domain and the first heptad repeat. Heterozygous mutations in *OPA1* cause autosomal dominant optic atrophy (ADOA), the most common form of optic neuropathy (Alexander et al., 2000; Delettre et al., 2000). Over 100 *OPA1* mutations have been identified, most commonly occurring in the GTPase domain of the protein (Ferre et al., 2005). Fibroblasts depleted of OPA1 have fragmented mitochondria, defects in respiration, mitochondria with aberrant cristae structure and increased susceptibility to apoptosis (Cipolat et al., 2004; Olichon et al., 2003). However, defects in diseased tissue from ADOA patients seem to be less severe, with

patients having aggregated, fragmented, or normal mitochondria (Delettre et al., 2000; Olichon et al., 2003).

A lack of mitochondrial fusion results in a reduction in the exchange of contents between mitochondria and thus, reduced exchange of mtDNA-encoded electron transport proteins. This in-turn leads to defects in oxidative phosphorylation (Chen and Chan, 2010).

1.7.2. Mitochondrial Fission

The dynamin-related protein DRP1, or Dnm1 in yeast, is an ~80 kDa soluble, cytosolic protein containing an N-terminal GTPase domain, a middle domain necessary for oligomerisation and a C-terminal GTPase effector domain (GED) that is involved in self-assembly (Westermann, 2010a). In addition, humans have an alternatively spliced brain-specific isoform of DRP1 with an insertion between the middle domain and the GED, known as the variable domain. This contains post-translational modification sites (Chen et al., 2000; Smirnova et al., 1998; Wilson et al., 2013). The role of DRP1 in mitochondrial fission is thought to be similar to that of the GTPase dynamin in scission of clathrin-coated endocytic vesicles (Hoppins et al., 2007; Praefcke and McMahon, 2004). Dynamin oligomerises and self-assembles around endocytic vesicles, which stimulates its GTPase activity and mediates scission of vesicles from the plasma membrane.

Mitochondrial fission requires the recruitment of DRP1 from the cytosol to the OMM. DRP1 exists in the cytosol as small oligomers (dimers and tetramers), which are thought to self-assemble into large multimeric structures at the OMM, wrapping around the mitochondrial membrane forming ring-like structures, which constrict and sever the mitochondrion (Figure 1.7, (Seo et al., 2010; Shaw and Nunnari, 2002; Smirnova et al., 2001; Yoon et al., 2001b)). Recent data suggests that DRP1 exists in a dynamic, dimer-oligomer equilibrium in solution (Macdonald et al., 2014). The minimal functional assembly subunit of DRP1 on the mitochondrial membrane for fission to occur is thought to be a dimer, and not a tetramer, as previously suggested (Macdonald et al., 2014).

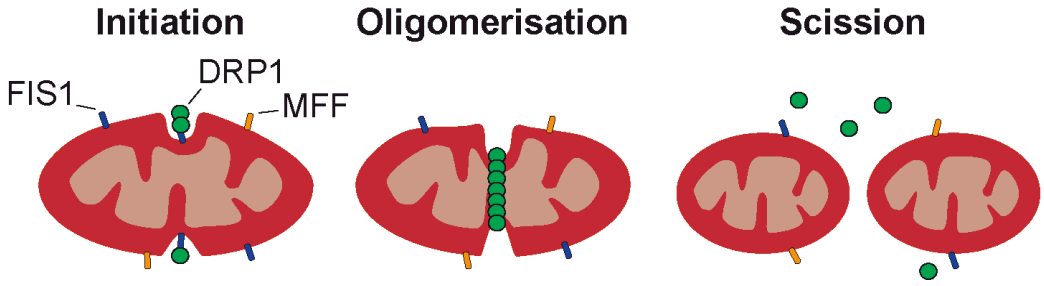

Figure 1.7. Schematic of mitochondrial fission through oligomerisation of DRP1 on the outer mitochondrial membrane. DRP1 (green) self-oligomerises and assembles around the OMM, constricting and severing the mitochondrion. Fis1 and Mff are involved in recruitment of DRP1 from the cytosol to the OMM in mammalian cells.

DRP1 localisation to mitochondria can be seen as punctate spots on mitochondrial tubules at prospective sites of fission (Labrousse et al., 1999; Smirnova et al., 2001), and often at the ends of mitochondria where fission has occurred. This can be seen by time-lapse imaging of GFP-tagged DRP1 showing that mitochondrial tubules divide at sites where these DRP1 punctate structures are found (Benard and Karbowski, 2009; Smirnova et al., 2001), although not all mitochondrial-associated DRP1 sites undergo division. Electron microscopy studies reveal that DRP1 oligomers on the mitochondrial membrane have an approximate diameter of 100-150 nm (Macdonald et al., 2014).

Cells deficient for DRP1 contain highly interconnected mitochondria due to ongoing fusion in the absence of fission (Otsuga et al., 1998; Smirnova et al., 1998). In addition, *Drp1* knockout in mice leads to embryonic lethality (Ishihara et al., 2009; Wakabayashi et al., 2009). A lethal, dominant-negative mutation in the middle domain of DRP1 (A395D) was reported in a neonate with microcephaly, abnormal brain development, optic atrophy and hypoplasia. In addition, mitochondrial elongation was seen in the cells of this patient (Waterham et al., 2007). Functional analysis revealed that this A395D mutation impaired higher order assembly, GTPase activity and mitochondrial localisation of DRP1 (Chang et al., 2010). Another dominant-negative mutation, K38A, located in the GTP-binding domain, impedes fission and leads to elongated mitochondria (Smirnova et al., 2001; Smirnova et al., 1998).

The mitochondrial fission machinery is best understood in yeast. Dnm1 is recruited to the mitochondrial membrane by the proteins mitochondrial fission 1 (Fis1), mitochondrial division protein 1 (Mdv1) and Caf4. Fis1 is an 18kDa mitochondrial

integral outer membrane protein that is essential for fission (Fekkes et al., 2000; Mozdy et al., 2000; Tieu and Nunnari, 2000). Fis1 binds indirectly to Dnm1 through the molecular adaptors, Mdv1 or Caf4 (Griffin et al., 2005). Mdv1 and Caf4 both contain an N-terminal domain that dimerises and binds to Fis1 and a C-terminal domain containing WD40 repeats that binds to Dnm1 (Cerveny and Jensen, 2003; Griffin et al., 2005). Loss of Fis1 leads to failed recruitment of Dnm1 from the cytosol to the mitochondrial membrane and hence, results in a severe mitochondrial fission defect (Fekkes et al., 2000; Mozdy et al., 2000). In humans, less is known about the recruitment of DRP1 from the cytosol onto mitochondria. Fis1 exists in mammalian cells, but no homologues of Mdv1 or Caf4 are currently known. Currently, the four strongest candidates for DRP1 recruitment in mammalian cells are FIS1, MFF, MiD49 and MiD51 (Chan, 2012).

1.7.2.1. *FIS1*

Human FIS1 may be involved in recruiting DRP1 to mitochondria, although the evidence is conflicting. FIS1 localises throughout the OMM in contrast to the punctate localisation of DRP1 (Lee et al., 2004; Otera et al., 2010). Early studies found that overexpression of *FIS1* in mammalian cells resulted in fragmentation of mitochondria (Stojanovski et al., 2004; Yoon et al., 2001b; Yu et al., 2005), and loss of *FIS1* resulted in elongation of mitochondria (Koch et al., 2005; Stojanovski et al., 2004; Yoon et al., 2001b). However, FIS1 inhibition does not affect recruitment of DRP1 to mitochondria (Lee et al., 2004) and a more recent study failed to show an effect of *FIS1* knockdown on mitochondrial morphology in HeLa cells (Otera et al., 2010). Also, targeted deletion of *FIS1* from human carcinoma HCT116 cells does not disrupt mitochondrial morphology or DRP1 recruitment to mitochondria (Otera et al., 2010). It may be possible that FIS1 is involved in mitochondrial fission only in specific cell types.

1.7.2.2. *MFF*

Mitochondrial fission factor (MFF) is a C-tail anchored protein on the OMM, which is conserved in metazoans but does not exist in yeast. It was identified in a small interfering RNA (siRNA) screen for *Drosophila* genes whose knockdown resulted in mitochondrial elongation (Gandre-Babbe and van der Bliek, 2008). A mammalian MFF homologue exists, and similarly, knockdown reduces DRP1 recruitment to

mitochondria, leading to mitochondrial elongation (Otera et al., 2010). In contrast, *MFF* overexpression induces mitochondrial fragmentation, concomitant with increased DRP1 recruitment to mitochondria (Otera et al., 2010). Additionally, immunoprecipitation experiments have shown MFF and DRP1 to transiently associate with each other (Lee et al., 2004; Otera et al., 2010), and MFF co-localises with DRP1 foci on the OMM (Otera et al., 2010). Currently, MFF is the best established receptor for DRP1.

1.7.2.3. *MiD49 and MiD51*

Mitochondrial dynamics protein of 49kDa (MiD49) and mitochondrial dynamics protein of 51kDa (MiD51, also known as mitochondrial elongation factor 1 (MIEF1)) are located on the OMM. Overexpression of MiD49 or MiD51 in mammalian cells results in mitochondrial elongation and collapse of the network. However, unexpectedly, this also leads to increased recruitment of DRP1 to the mitochondria (Palmer et al., 2011; Zhao et al., 2011). The suggested explanation for this is that although excessive MiD production results in increased DRP1 recruitment, the recruited DRP1 is not active, thereby resulting in a fission defect (Palmer et al., 2011; Zhao et al., 2011). Moreover, co-immunoprecipitation and yeast two-hybrid experiments show an interaction between DRP1 and these two proteins (Palmer et al., 2011).

MID knockdown studies are less clear and show conflicting results. In one study, MID49 or MID51 knockdown had no effect on mitochondrial morphology, but double knockdown of both resulted in elongated mitochondria (Palmer et al., 2011). Another study found that knockdown of MID51 resulted in mitochondrial fragmentation (Zhao et al., 2011). It seems that the MID proteins are important regulators of DRP1 function, but more studies are required to understand their precise roles.

1.7.3. DRP1 post-translational modifications

Overexpression of wild-type DRP1 does not lead to mitochondrial fragmentation. This suggests that a change in levels does not directly alter mitochondrial fission, and it is activation of DRP1 that is required for mitochondrial fission. Implicated mechanisms for activation of DRP1 include the post-translational modifications: phosphorylation, *S*-nitrosylation, ubiquitination, and sumoylation. These may influence mitochondrial

translocation of DRP1, higher order assembly or GTPase activity (Otera and Mihara, 2011).

1.7.3.1. *Phosphorylation of DRP1*

Several protein kinases have been identified that phosphorylate different DRP1 serine residues, for example, cyclin B dependent kinase (CDK1, (Taguchi et al., 2007)), cyclic AMP-dependent protein kinase (PKA, (Chang and Blackstone, 2007)), and calcium/calmodulin-dependent kinase 1α (CaMK1α, (Han et al., 2008)). Calcineurin (CaN), a calcium-dependent phosphatase, dephosphorylates DRP1 (Han et al., 2008).

Two main phosphorylation sites in DRP1 are at serine residues 616 and 637 (Ser616 and Ser637), which are conserved residues in the GTPase effector domain (GED, or variable domain, (Chang and Blackstone, 2007; Cribbs and Strack, 2007; Slupe et al., 2013; Taguchi et al., 2007)). CDK1 phosphorylates DRP1 at Ser616 (Ser635 in rat) during mitosis, promoting fission to facilitate the proper distribution and segregation of mitochondria into daughter cells (Taguchi et al., 2007). However, this modification does not directly affect GTPase activity (Taguchi et al., 2007). Other kinases, including ERK1/2 (Yu et al., 2011) and PKCδ (Qi et al., 2011), also phosphorylate DRP1 at Ser616, which enhances DRP1 activity under high glucose or oxidative stress conditions, respectively, leading to mitochondrial fragmentation. Also, CDK5 was recently identified to phosphorylate DRP1 at Ser616, which induces mitochondrial fragmentation by the mobilisation of DRP1 to mitochondria from microtubules (Cho et al., 2014; Strack et al., 2013).

Reversible phosphorylation of DRP1 occurs at Ser637 (also noted as residue 617 or 656 depending on the DRP1 transcript and species of origin). Two different protein kinases, PKA and CaMK1α, phosphorylate DRP1 at Ser637. However, contradictory results are reported for the effect of these two kinases on mitochondrial dynamics. PKA phosphorylation inhibits mitochondrial fission by preventing an interaction between the GTPase and GED domains of DRP1, leading to reduced GTPase activity and eventually mitochondrial recruitment of DRP1 (Chang and Blackstone, 2007; Cribbs and Strack, 2007). Conversely, CaMK1α–dependent phosphorylation of DRP1 at Ser637 leads to translocation of DRP1 to mitochondria and increased mitochondrial fission in response to calcium influx through voltage-dependent calcium channels (VDCCs, (Chang and Blackstone, 2010; Han et al., 2008; Otera et al., 2013)).

Calcineurin (CaN) dephosphorylates DRP1 at Ser637, which activates DRP1 and stimulates translocation to mitochondria, leading to increased mitochondrial fission (Cereghetti et al., 2008; Cribbs and Strack, 2007). Calcineurin is activated by calcium; hence a rise in intracellular calcium levels would lead to increased dephosphorylation of DRP1 at Ser637 and increased mitochondrial fission (Cereghetti et al., 2008). Similar to the transcription factor, nuclear factor of activated T cells (NFAT, (Martinez-Martinez et al., 2006; Rodriguez et al., 2009)); a conserved LXVP motif within DRP1 was recently identified to mediate the interaction with CaN (Slupe et al., 2013). Disrupting the CaN-DRP1 signalling axis blocks the translocation of DRP1 to mitochondria, leading to mitochondrial elongation (Cereghetti et al., 2008; Slupe et al., 2013). It seems that intracellular calcium levels are important for the phosphorylation status of DRP1, and hence control of mitochondrial dynamics.

1.7.3.2. *S-Nitrosylation of DRP1*

S-nitrosylation is a redox-related modification of thiols (such as cysteine residues) by nitric oxide (NO). A study suggested that NO produced in response to β-amyloid protein, a key mediator of Alzheimer's disease, triggers excessive mitochondrial fission, followed by synaptic loss and neuronal damage, in part *via S*-nitrosylation of DRP1 at Cys644 within the GED domain (Cho et al., 2009), which enhances the GTPase activity of DRP1 and oligomer formation. A Cys644Ala mutation prevented *S*-nitrosylation of DRP1, blocking the neurotoxicity (Cho et al., 2009).

1.7.3.3. *Sumoylation of DRP1*

Post-translational modification of DRP1 also occurs by the covalent attachment of small ubiquitin-like modifier (SUMO) proteins (Harder et al., 2004), termed sumoylation, which like phosphorylation, seems likely to occur within the variable domain of DRP1 (Guo et al., 2013a). Sumoylation often alters subcellular localisation of proteins or protects them from ubiquitin-mediated destruction. There are four human SUMO isoforms (SUMO1-4), which are conjugated to lysine residues in target proteins, such as DRP1, via an E1 complex (SAE1/SAE2), a single E2 (Ubc9), and various E3 ligases (Wilkinson and Henley, 2010). DRP1 was shown to interact with Ubc9 and conjugation competent forms of SUMO1, -2, and -3, demonstrating that DRP1 is a direct target of sumoylation (Figueroa-Romero et al., 2009).

Mitochondrial-anchored protein ligase (MAPL) is a mitochondrion-anchored SUMO E3 ligase that attaches SUMO to DRP1, stabilising the mitochondrial pool of DRP1 and stimulating mitochondrial fission (Braschi et al., 2009; Harder et al., 2004). SUMO proteins are removed from substrates by the sentrin-specific protease (SENP) family of isopeptidases. There are six SENPs in mammals, with SENP3 and SENP5 involved in removing SUMO from DRP1 (Guo et al., 2013a; Zunino et al., 2007). The dynamic balance between Ubc9-mediated SUMO conjugation and SENP-mediated SUMO removal determines the sumoylation state of proteins. SENP3 and SENP5-mediated desumoylation of DRP1 facilitates DRP1 localisation at mitochondria, formation of functional oligomers, and increased fission (Guo et al., 2013a; Zunino et al., 2007). Following SENP3 knockdown, DRP1 localisation at the mitochondria was reduced in HeLa cells, as determined by immunocytochemistry. Conversely, SENP3 overexpression promoted mitochondrial localisation of DRP1 (Guo et al., 2013a). This indicates that enhanced DRP1 sumoylation, facilitated by reduced levels of SENP3, reduces mitochondrial localisation of DRP1.

1.7.3.4. *Ubiquitination of DRP1*

The mitochondrial E3 ubiquitin ligase MARCH5, also known as MITOL, is essential for mitochondrial fission (Karbowski et al., 2007). Loss of MARCH5 by gene knockdown or overexpression of a MARCH5 mutant lacking ubiquitin ligase activity both induce accumulation of DRP1 on OMM, yet they lead to the opposite effect of mitochondrial elongation (Karbowski et al., 2007) or fragmentation (Nakamura et al., 2006; Yonashiro et al., 2006), respectively. These contradictory results are due to the multiple effects of MARCH5 in promoting MFN2-mediated mitochondrial fusion, while also ubiquitinating DRP1 and promoting degradation (Nakamura et al., 2006).

Parkin is an E3 ubiquitin ligase, which has an essential role in removing damaged mitochondria from the cell *via* mitophagy (Narendra et al., 2008; Pallanck, 2010; Youle and Narendra, 2011). Parkin ubiquitinates DRP1, targeting it for degradation by the proteasome (Wang et al., 2011). Loss of Parkin or overexpression of a pathogenic mutant inhibits the ubiquitination and degradation of DRP1, leading to increased DRP1 levels and aberrant mitochondrial fragmentation (Wang et al., 2011).

1.7.4. Dynamin and DRP1

Much of what is attributed to DRP1's mechanism of action in mitochondrial fission parallels that of dynamin in endocytic vesicle scission. Dynamin is also regulated through post-translation modifications, such as sumoylation (Mishra et al., 2004), phosphorylation (Ahn et al., 2002; Shajahan et al., 2004) and *S*-nitrosylation (Kang-Decker et al., 2007; Wang et al., 2006). For example, the GED domain of dynamin interacts with SUMO-1, UBC9, and PIAS-1, all of which are members of the sumoylation machinery (Mishra et al., 2004). SUMO-1 and UBC9 were shown to inhibit the oligomerisation of dynamin, and their expression in mammalian cells down-regulated the dynamin-mediated endocytosis of transferrin (Mishra et al., 2004). Also, phosphorylation of dynamin by the non-receptor protein tyrosine kinase c-Src induces its self-assembly and increases its GTPase activity (Ahn et al., 2002; Shajahan et al., 2004). Nitric oxide (NO) has also been shown to activate dynamin GTPase activity through *S*-nitrosylation, promoting dynamin self-assembly and endocytosis (Kang-Decker et al., 2007; Wang et al., 2006). Hence, novel findings on the regulation and function of dynamin may also be relevant to DRP1.

The GTP-bound form of dynamin specifically binds to HSC70 and its DNAJ co-chaperone auxilin (Newmyer et al., 2003), which remove the clathrin coat from endocytic vesicles that have budded from the plasma membrane (Schlossman et al., 1984, Ungewickell et al., 1995, Greener et al., 2000). Two domains within auxilin were identified that interact with dynamin, and these domains inhibit endocytosis when overexpressed in HeLa cells (Newmyer et al., 2003). Like auxilin, sacsin may be a co-chaperone, interacting with DRP1 and a HSP70 protein *via* its J-domain, to perform a specific function in mitochondrial dynamics.

1.8. Mitochondrial Transport

Mitochondria travel from the cell body to regions of the cell where they are required to deliver ATP and other metabolites, and then return. This is most strikingly seen in highly elongated cells such as neurons, where mitochondria travel to the synaptic terminals of axons and dendrites where the demand for energy is high.

Mitochondrial transport in mammalian cells is largely microtubule based, *via* kinesin and dynein motors (Hollenbeck and Saxton, 2005), although it also occurs *via* the actin cytoskeleton, through myosins (Ligon and Steward, 2000; Morris and Hollenbeck, 1995). Anterograde microtubule-based movement is driven by three kinesin motor proteins, KIF1Bβ, KIF5 and KLP-6 (Nangaku et al., 1994; Tanaka et al., 1998), which interact with mitochondria through the Milton/TRAK family of proteins, which in-turn interact with the outer mitochondrial membrane Ras GTPases Miro1 and Miro2 (Brickley and Stephenson, 2011; Glater et al., 2006; Macaskill et al., 2009; Reis et al., 2009). Loss of this Miro-dependent pathway in neurons results in depletion of mitochondria from dendrites and axons, resulting in neurotransmission defects (Guo et al., 2005).

Miro is necessary for basal mitochondrial transport as well as acting as a calcium responsive switch for mitochondrial transport. Through Miro, increases in cytosolic calcium lead to mitochondrial transport arrest and this is recovered following a return to basal cytosolic calcium levels (Macaskill et al., 2009; Saotome et al., 2008; Wang and Schwarz, 2009). In addition, Miro mediates mitochondrial fission in response to elevated cytosolic calcium, and mitochondrial elongation when calcium levels are low (Saotome et al., 2008).

Retrograde movement of mitochondria along microtubules is driven by the dynein-dynactin complex. Interestingly, this complex has been shown to play a role in regulating mitochondrial morphology by controlling the recruitment of the fission factor DRP1 to the outer mitochondrial membrane (Varadi et al., 2004). Functional disruption of this complex results in perinuclear, elongated mitochondria (Varadi et al., 2004). No specific mitochondrial adapter proteins have been identified for dynein-dynactin.

1.8.1. Dynein-Dynactin complex

Dynein is the cytoplasmic motor protein that drives retrograde transport of vesicles and organelles along microtubules; that is from the periphery towards the nucleus, to their subcellular locations (Schnapp and Reese, 1989). Dynein function *in vivo* depends on dynactin; a multi-subunit complex which binds and activates dynein, driving the retrograde movement (Eckley et al., 1999; Gill et al., 1991; Schroer and Sheetz, 1991). There are nine subunits of the dynactin complex, which are arranged into distinct sub-complexes (Figure 1.8, Table 1.5).

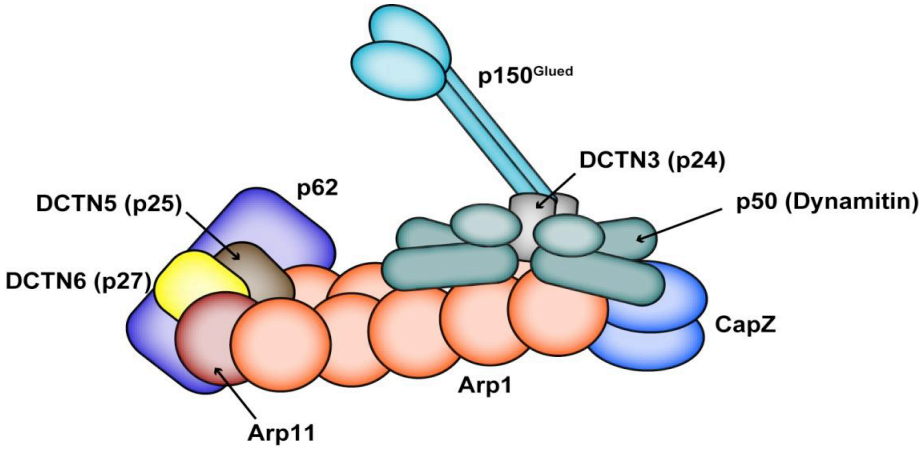

Figure 1.8. Schematic representation of the dynactin complex. Figure taken from **(**Parfitt, 2011).

The Arp1 rod is the core of the dynactin complex and this is capped at one end by the actin-binding protein, CapZ α/β, and at the other end by four subunits, Arp11, p62, p27, and p25 (pointed-end complex). This sub-complex is involved in cargo binding. The projecting arm, which contains the $p150^{Glued}$, dynamitin, and p24 subunits, binds microtubules and dynein (Figure 1.8, (Eckley et al., 1999; Schafer et al., 1994)). Together, the dynactin subunits have a predicted molecular mass of 1.2 MDa (Schroer, 2004).

Table 1.5. Dynactin subunits

Subunit	Gene Name
The Arp1 rod	
Arp1	*ACTR1A*
Arp11	*ACTR10*
CapZ	*CAPZA1*
p62	*DCTN4*
p25	*DCTN5*
p27	*DCTN6*
The projecting arm	
p150^{Glued}	*DCTN1*
Dynamitin (p50)	*DCTN2*
p24/22	*DCTN3*

Dynactin is ubiquitously expressed in vertebrates and typically exhibits small punctae, corresponding to microtubule plus ends (Levy et al., 2006; Valetti et al., 1999), which are distributed throughout the cell (Gill et al., 1991; Paschal et al., 1993).

The dynein-dynactin complex is required for mitosis, particularly nuclear envelope breakdown and spindle formation (Echeverri et al., 1996; Schroer, 2004), and in protein degradation *via* autophagy and aggresome formation (Johnston et al., 2002; Kimura et al., 2008). Other cellular roles suggested are in retrograde signalling from the axon to the cell body in neurons, in neurofilament transport, and in neuronal migration (Schroer, 2004). Dynactin has also been shown to interact with the anterograde microtubule-based motor, kinesin II (Deacon et al., 2003), and *in vitro* studies suggest that dynactin contributes to the anterograde movement of kinesin II (Berezuk and Shroer 2007).

The pointed-end complex, which comprises Arp11, p62, p27, and p25, binds neither dynein nor microtubules, and its p62, p27, and p25 subunits are not present in yeast, indicating that they are not required for dynactin's most fundamental role as a dynein activator (Schroer, 2004). Yeh *et al* (2012) demonstrated that the pointed-end complex dissociates into two heterodimers, p62/Arp11 and p27/p25. Depletion of each subunit using RNA interference (RNAi) showed that Arp11 and p62 were essential for dynactin stability and they allow dynactin to bind the nuclear envelope prior to mitosis,

contributing to dynein recruitment and nuclear envelope breakdown. On the other hand, p27 and p25 were not essential for dynactin stability, but were required for binding of dynactin and recruitment of dynein to early and recycling endosomes for their movement (Yeh et al., 2012; Zhang et al., 2011).

Disruption of dynein-dynactin function has been causally linked to multiple neurodegenerative diseases (Perlson et al., 2010). For example, mutations in $p150^{Glued}$ cause amyotrophic lateral sclerosis (ALS, (Munch et al., 2004)).

Overexpression of dynamitin (p50) in HeLa cells results in redistribution of mitochondria from the cell periphery towards the nucleus and the formation of long, interconnected mitochondria (Varadi et al., 2004). This suggests a disruption in the balance between mitochondrial fission and fusion and is associated with a large decrease in localisation of DRP1 at the outer mitochondrial membrane. Dynamitin and $p150^{Glued}$ were also shown to interact with DRP1 by co-immunoprecipitation (co-IP (Varadi et al., 2004)).

1.8.1.1. *Dynactin-6/p27 subunit*

Interestingly, the dynactin-6 subunit, also known as p27, of the dynein-dynactin complex was found to interact with sacsin by a yeast-two-hybrid (Y2H) screen using residues 1-649 of sacsin as bait (Parfitt, 2011). Dynactin-6 (*DCTN6*) encodes a protein product of 190 amino acids with a molecular weight of 25 kDa (Eckley et al., 1999). The exact molecular function of *DCTN6* is still unknown. However, the mouse homolog of *DCTN6*, which shares extensive sequence homology with the human protein, has been suggested to be involved in mitochondrial biogenesis (Murdock et al., 1999).

Since *DCTN6* exists as a heterodimer with *DCTN5*, siRNA-mediated depletion of one also leads to depletion of the other. Conversely, expression of siRNA-resistant *DCTN6* results in recovery of both *DCTN6* and *DCTN5* (Yeh et al., 2012).

DCTN5 and *DCTN6* are also reported to exist in a freely soluble pool in cells, so are available to provide functions outside of dynactin and may serve as adapter proteins that target dynactin to more subcellular structures (Schroer, 2004).

Interestingly, like DRP1, DCTN6 is phosphorylated by CDK1 at the conserved consensus site Thr186, which generates a binding site for the mitotic kinase, polo kinase 1 (PLK1, (Yeh et al., 2013)). This phosphorylation of DCTN6 occurs during mitosis

and depletion of DCNT6 leads to accelerated mitotic progression. The crystal structure of *DCTN6* reveals an unusual left-handed parallel β-helix (LβH) domain and the CDK1 phosphorylation site is in an unstructured C-terminal segment (Yeh et al., 2013).

1.9. Mitochondrial Dysfunction and Neurodegeneration

The central nervous system (CNS) is dependent on efficient mitochondrial function, since brain tissue has a high energy demand. Mutations in mitochondrial DNA (mtDNA), defects in mitochondrial dynamics, generation and presence of reactive oxygen species (ROS), and environmental factors, contribute to loss of mitochondrial energy production, which in turn may lead to neurodegenerative diseases (Filosto et al., 2011). Previously, functional defects in mitochondria were considered to be downstream effects of neurodegenerative disease. However, in recent years it has been realised that impaired mitochondrial function is an important factor in the onset and progression of neurodegenerative diseases. Remarkably, more than one-third of the genes linked to neurodegeneration so far are associated with mitochondrial function (Schon and Przedborski, 2011).

Interestingly, neurons have high expression levels of proteins involved in mitochondrial dynamics (Li et al., 2004). *In vitro*, expression of the dominant-negative DRP1 mutant K38A in rat hippocampal neurons, which leads to mitochondrial elongation, reduces the number of dendritic spines (Figure 1.9C, (Li et al., 2004)). Also, neuronal mitochondria lacking functional DRP1 tend to aggregate in the soma (Ishihara et al., 2009; Li et al., 2004), Figure 1.9C). These observations show the importance of mitochondrial fission for neuronal morphogenesis and mitochondrial trafficking to neuron synaptic terminals.

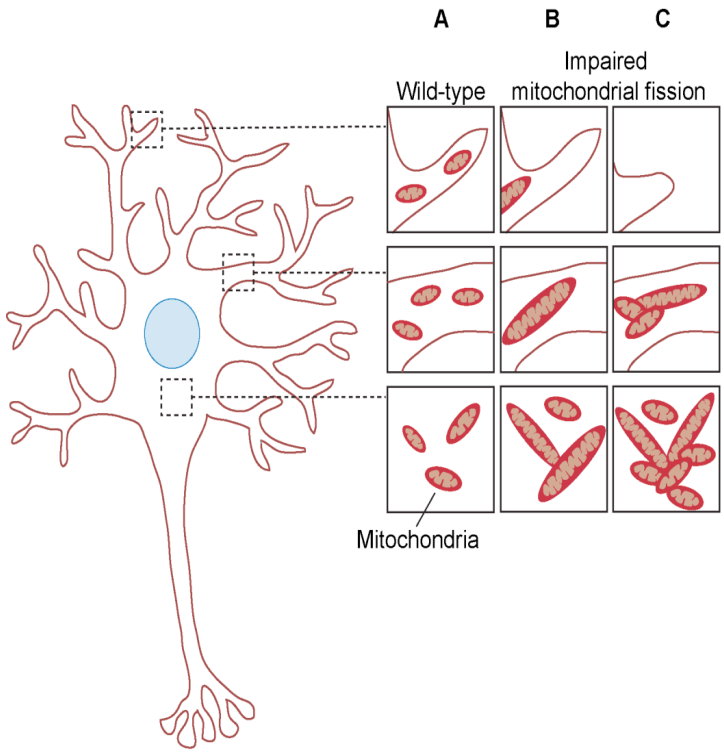

Figure 1.9. Schematic representation of the defects in mitochondrial dynamics that lead to abnormal mitochondrial distribution in neurons. (A) Wild-type mitochondria are evenly distributed in the cell body, dendritic and axonal termini. **(B)** Absence of mitochondrial fission can lead to elongated mitochondria that branch out into the neurites and are they are protected from mitophagy, hence an accumulation of abnormal mitochondria (Cheung et al., 2007; Costa et al., 2010; Dagda et al., 2009). **(C)** Others have found elongated mitochondria to be coupled with impaired mitochondrial trafficking. Mitochondria aggregate within the perinucleur region, which is accompanied by decreased numbers of neurites and synapses (Ishihara et al., 2009; Li et al., 2004).

Impaired mitochondrial dynamics is an important factor in the pathogenesis of many neurodegenerative diseases, some of which are discussed below.

1.9.1. Alzheimer's Disease

Alzheimer's disease (AD) is a late-onset neurodegenerative disease characterised by progressive decline in cognitive functions and memory. Recently, evidence indicates that impaired mitochondrial dynamics may be an important component in the pathogenesis of AD. Studies of AD patient brains report abnormal expression levels of the mitochondrial fission and fusion proteins DRP1, OPA1, MFN1 and MFN2 (Manczak et al., 2011; Wang et al., 2009b). In addition, neurons overexpressing APP or

exposed to toxic Aβ peptides display abnormal levels of mitochondrial fission and fusion proteins and a perinuclear aggregation of mitochondria (Barsoum et al., 2006; Manczak et al., 2011; Wang et al., 2009b; Wang et al., 2008). Furthermore, a study in Aβ transgenic AD mice showed increased mitochondrial fragmentation (Calkins and Reddy, 2011).

Tau is a microtubule-associated protein, abundantly present in the central nervous system and is predominantly expressed in neuronal axons (Brandt et al., 2005). Its physiological role is to stabilise the microtubule network. In AD, tau is hyperphosphorylated and loses its capability to bind with microtubules, which destabilizes the microtubule network and disturbs the transport of vesicles and organelles, such as mitochondria (Ebneth et al., 1998; Kopeikina et al., 2011; Roy et al., 2005). Stable overexpression of the pathogenic tau mutation P301L in SH-SY5Y neuroblastoma cells leads to perinuclear aggregation of mitochondria due to impaired mitochondrial transport and motility, which is accompanied by a reduced rate of mitochondrial fission and fusion (Schulz et al., 2012).

Expression of human tau carrying the R406W mutation in *Drosophila* leads to elongated mitochondria in the neurons of brains from the flies. This is accompanied by reduced localisation of DRP1 at mitochondria. It is suggested that hyperphosphorylation of tau leads to excess stabilisation of the actin cytoskeleton, which in-turn inhibits the association of DRP1 with mitochondria (DuBoff et al., 2012).

DRP1 has also been shown to interact with Aβ and hyperphosphorylated tau in brain specimens from AD patients. This increases the GTPase activity of DRP1, leading to excessive mitochondrial fragmentation, along with mitochondrial and synaptic deficiencies, possibly leading to neuronal damage and cognitive decline (Manczak and Reddy, 2012).

Specific post-translational DRP1 modifications have also been implicated in AD. For example, increased levels of DRP1 phosphorylation at Ser616 and *S*-nitrosylation, which both promote mitochondrial fission, were found in AD patient brains (Wang et al., 2009b).

1.9.2. Parkinson's Disease

Parkinson's disease (PD) is the second most common neurodegenerative disease and is characterised by progressive loss of dopaminergic neurons in the substantia nigra pars compacta and the formation of intraneuronal inclusions known as Lewy bodies (Fearnley and Lees, 1991). PD symptoms include resting tremor, rigidity, bradykinesia and unsteady gait. Mitochondrial dysfunction has long being regarded as a primary cause in the pathogenesis of PD, and more specifically, dysregulation of mitochondrial dynamics has more recently been linked to the pathogenesis of PD (Chaturvedi and Beal, 2013; Santos and Cardoso, 2012; Van Laar and Berman, 2013). Around 10% of all cases of PD are associated with mutations in different *PARK* genes, such as *PARK2,* which encodes Parkin, and PTEN-induced kinase 1 (*PINK1*), which play important roles in the removal of damaged mitochondrial organelles *via* mitophagy (Dodson and Guo, 2007; Narendra et al., 2008; Narendra et al., 2010). DRP1 has been identified as one of the targets of the E3 ubiquitin ligase, Parkin (Wang et al., 2011).

PINK1 is found in both the inner and outer mitochondrial membranes (Jin et al., 2010; Silvestri et al., 2005; Zhou et al., 2008a). Mitochondrial PINK1 is present in two forms, long and short, with the long form (PINK1-L, 64 kDa) cleaved to the short form (PINK1-S, 52 kDa) within the mitochondrial inner membrane by presenilin-associated rhomboid-like protein (PARL), an intramembrane protease (Deas et al., 2011; Jin et al., 2010). PD patient fibroblasts are reported to contain fragmented mitochondria (Exner et al., 2007), and knockdown of *PINK1* in HeLa cells and SH-SY5Y neuroblastoma cells also causes mitochondrial fragmentation, which can be reversed by over-expression of Parkin (Dagda et al., 2009; Exner et al., 2007). PINK1 has also been shown to form a complex with Milton and Miro (Weihofen et al., 2009), suggesting a role in mitochondrial transport.

1.9.3. Huntington's Disease

Huntingdon's disease (HD) is an autosomal dominant progressive neurodegenerative disease characterised by involuntary movements, psychiatric disturbances and cognitive decline. It is caused by an intragenic CAG-triplet expansion within the huntingtin (*HTT*) gene on chromosome 4 leading to an abnormal stretch of polyglutamine residues, which determines age of onset and disease severity. Patients have progressive neuronal loss affecting particular striatal GABAergic spiny neurons, as well as atrophy and gliosis of

the basal ganglia, cortex, and hippocampus. Abnormal mitochondrial dynamics have also been associated with this disease (Bossy-Wetzel et al., 2008). Studies in HD patient lymphoblasts and in primary striatal neurons isolated from HD mouse models revealed fragmented mitochondria (Guo et al., 2013b; Quintanilla et al., 2013). Likewise, mitochondria in HeLa cells overexpressing mutant *HTT* with a 74 glutamine repeat (Htt74Q) show fragmentation, reduced fusion, reduced ATP levels and increased cell death (Wang et al., 2009a). Additionally, HD patient cells have increased activity of calcineurin, which dephosphorylates DRP1 and increases its translocation to mitochondria, leading to mitochondrial fragmentation (Costa et al., 2010). Overexpression of *OPA1*, a dominant-negative DRP1 mutant K38A, or a dominant-negative calcineurin mutant, can rescue the mitochondrial fragmentation (Costa et al., 2010). Cellular models of HD, aswell as striatal and cortical specimens from HD patients, were also shown to have higher mRNA and protein expression levels of DRP1 and FIS1, whereas OPA1, MFN1 and MFN2 fusion proteins are decreased (Cartelli et al., 2010; Kim et al., 2010a; Shirendeb et al., 2011).

In transfected primary rat cortical neurons, mutant, but not wild type *Htt* blocked mitochondrial movement (Chang et al., 2006). Also, expression of mutant *Htt* in transgenic mice impaired trafficking of vesicles and mitochondria (Trushina et al., 2004). Mutant *Htt* was found to bind DRP1 and increase its mitochondrial fission activity (Song et al., 2011).

1.9.4. Hereditary Optic Atrophy

Autosomal dominant optic atrophy (ADOA) is characterised by loss of retinal ganglion cells (RGCs) leading to optic atrophy. A subset of ADOA is caused by *OPA1* mutations (Alexander et al., 2000; Delettre et al., 2000). Patients have a slow progressive loss of bilateral visual function, with onset typically within the first two decades of life. Symptoms include a decrease in visual acuity, colour vision deficiency, and visual field defects (Hoyt, 1980; Kline and Glaser, 1979).

ADOA patient dermal fibroblasts have an inhibition of mitochondrial fusion in about 50% of cells, accompanied by a significant impairment in mitochondrial ATP synthesis (Zanna et al., 2008). In addition, RNAi experiments show that loss of *OPA1* leads to excessive fragmentation of the mitochondrial network and increased cell apoptosis (Cipolat et al., 2004; Lee et al., 2004; Olichon et al., 2003).

1.9.5. Charcot-Marie-Tooth Neuropathy (CMT)

Charcot-Marie-Tooth Disease type 2A (CMT2A) is an autosomal dominant peripheral neuropathy characterised by axonal degeneration and is caused by mutations in the mitochondrial fusion protein MFN2 (Zuchner et al., 2004). Other types of CMT disease affect Schwann cells, resulting in demyelination of peripheral nerves. However, CMT2A affects the axons of the longest sensory and motor peripheral nerves, with a subset showing additional degeneration in the optic nerve (Zuchner and Vance, 2005). It is not known why mutations in *MFN2*, which is ubiquitously expressed, lead to such a highly cell type-specific defect.

Expression of *MFN2* mutants in cultured dorsal root ganglion (DRG) neurons led to disruption of mitochondrial transport in axons. Cellular ATP levels, mitochondrial potential, and respiratory chain function were unaltered (Baloh et al., 2007). Given that the peripheral sensory and motor axons are the longest in the body, they are likely to be particularly sensitive to mitochondrial transport defects, hence this could be the reason for the cell type-specific defect. MFN2 mutant zebrafish were also shown to have perturbed axonal mitochondrial transport. Phenotypically this resulted in progressive motor dysfunction and pathological alterations to the neuro-muscular junction (Chapman et al., 2013).

1.9.6. Mitochondrial dysfunction in ARSACS

Since sacsin is localised at mitochondria, the effect of loss of sacsin on mitochondrial morphology and function has been investigated. Using three-dimensional confocal reconstructions along with fluorescence recovery after photobleaching (FRAP) studies in SH-SY5Y cells, siRNA-mediated sacsin knockdown was shown to lead to a more interconnected mitochondrial network (Girard et al., 2012). Similarly, fibroblasts from ARSACS patients display a hyperfused mitochondrial phenotype indicated by the presence of balloon-like or bulbed mitochondria (Blumkin et al., 2015; Girard et al., 2012; Pilliod et al., 2015). This mitochondrial phenotype parallels that seen in models of DRP1 knockdown (Estaquier and Arnoult, 2007; Lee et al., 2004) or when mutant forms of DRP1 are overexpressed (Frank et al., 2001; Smirnova et al., 1998). This suggests that loss of sacsin function leads to a disruption in normal mitochondrial dynamics. Furthermore, a decrease in mitochondrial fission seems more likely than enhanced fusion due to the identification of a putative interaction between a

heterologously expressed N-terminal portion of sacsin (amino acids 1-1368) and DRP1 by co-immunoprecipitation (Girard et al., 2012), along with co-localisation of the proteins seen by confocal microscopy (Girard et al., 2012).

More recently, motor neurons cultured from *Sacs*$^{-/-}$ knockout mice also show an elongation of mitochondria, along with a significant reduction in mitochondrial motility (Lariviere et al., 2015). It has been hypothesised that larger, unusually shaped mitochondria cannot distribute into the narrow dendrites to reach synapses and instead accumulate in the soma and proximal dendrites (Girard et al., 2012). This leads to striking alterations in the organisation of dendritic fields in the cerebellum of *Sacs*$^{-/-}$ mice, which precedes Purkinje cell death (Girard et al., 2012). Additionally, cultured rat hippocampal neurons transduced with lentivirus encoding shRNA targeting sacsin show an accumulation of mitochondria in the soma and proximal dendrites (Girard et al., 2012). Neurons are very sensitive to changes that disturb mitochondria because of their high metabolic activity and significant energy demand at locations distant from the cell body. Moreover, sacsin knockdown cells and neurons from *Sacs*$^{-/-}$ mice have a loss of mitochondrial membrane potential, which is generated by oxidative phosphorylation, thereby indicating a loss in mitochondrial function (Girard et al., 2012). In line with this, a very recent study has shown that ARSACS patient fibroblasts have reduced mitochondrial respiration and increased reactive oxygen species, which indicates mitochondrial dysfunction and oxidative stress due to loss of sacsin (Criscuolo et al., 2015). Likewise, our group has demonstrated functional impairment of oxidative phosphorylation in ARSACS patient fibroblasts and in SH-SY5Y neuroblastoma cells transfected with siRNA targeting *SACS* (Bradshaw et al., 2016). Along with this, reduced transcript levels of genes involved in oxidative phosphorylation and increased transcript levels of oxidative stress genes were observed in sacsin deficient cells (Bradshaw et al., 2016).

1.10. Intermediate Filaments

Cytoskeletal dysfunction has also been identified as a key feature of several neurodegenerative diseases, including AD, tauopathies and polyQ disorders (Gunawardena and Goldstein, 2005; McMurray, 2000).

The mammalian cytoskeleton is composed of three interconnected filaments: microtubules (25 nm in diameter), actin microfilaments (7-10 nm in diameter), and intermediate filaments (10-12 nm in diameter), which together control the shape and mechanics of eukaryotic cells. Neurons are particularly dependent on the cytoskeleton to deliver proteins synthesised in the cell body to the axons and nerve terminals.

Intermediate filaments (IF) are found in nearly all eukaryotic cells, although different cell types possess different types of IF protein (Table 1.6). In epidermal cells and the axons of neurons, they are at least 10 times more abundant than microfilaments or microtubules. IFs are very stable structures that are assembled from one or more proteins encoded by a large multigene family of >70 members (Herrmann et al., 2009). There are six types of IF proteins, which are classified by gene structure and sequence homology (Table 1.6). All IF proteins have a common domain structure: a central α-helical core flanked by globular N- and C-terminal domains, but they vary greatly in molecular weight and sequence.

Table 1.6. Intermediate filament proteins in mammals

Intermediate filament protein	Molecular Weight (kDa)	Tissue Distribution
Type I		
Acidic keratins	40 - 57	Epithelia
Type II		
Basic keratins	53 - 67	Epithelia
Type III		
Desmin	53	Muscle
Glial fibrillary acidic protein (GFAP)	50	Glial cells and astrocytes
Peripherin	57	Peripheral and central neurons
Vimentin	57	Mesenchyme
Type IV		
α-Internexin	66	Developing central nervous system
Neurofilament - Light	68	Mature neurons
Neurofilament - Medium	145	Mature neurons
Neurofilament - Heavy	200	Mature neurons
Type V		
Nuclear lamins	67 - 70	Nucleus of all cells
Type VI		
Nestin	240	Developing central and peripheral nervous system

IF proteins are differentially expressed throughout the development of the nervous system. Undifferentiated cells express vimentin, a type III IF protein (Bignami et al., 1982; Cochard and Paulin, 1984), whereas at later developmental stages, neuroblasts express nestin, α-internexin, and peripherin (Kaplan et al., 1990; Parysek and Goldman, 1987; Portier et al., 1983). Upon differentiation into neurons, the neurofilament proteins become expressed (Carden et al., 1987; Nixon and Shea, 1992; Shaw and Weber, 1982).

1.10.1. Neurofilaments (NFs)

NFs constitute the major IF proteins in adult neurons, and they are a heteropolymer, composed of the three type IV proteins, NF-L, NF-M, and NF-H. NFs are synthesised in the perikaryon, before being assembled into filaments and actively transported along microtubules in axons by the kinesin and dynein motors, where they move at a net slow velocity of 0.2-1 mm/day (Lariviere and Julien, 2004). Hence, IFs are dependent on an intact microtubule network for extension throughout the cell. They are responsible for the radial growth of large myelinated axons and thus determine axonal diameter, which in turn is directly related to the speed of impulse conduction. Hence, disruption in the assembly of NFs results in hypotrophy of myelinated axons and a reduction in the velocity of nerve conduction (Kriz et al., 2000; Zhu et al., 1997).

NFs within the perikaryon and proximal segments of axons and dendrites are normally hypophosphorylated, while NFs in axons are heavily phosphorylated (Carden et al., 1987; Lee and Johnston, 1997).

1.10.2. Intermediate filaments and mitochondria

There is growing evidence indicating a contribution of IFs to the tethering of mitochondria (Anesti and Scorrano, 2006; Milner et al., 2000; Tang et al., 2008). This has been shown in muscle cells (Milner et al., 2000; Stone et al., 2007), nerve cells (Straube-West et al., 1996; Wagner et al., 2003), and fibroblasts (Mose-Larsen et al., 1982; Summerhayes et al., 1983). There is also evidence that vimentin and NFL-H bind directly to mitochondria *in vitro* and that mitochondrial function requires IFs (Milner et al., 2000; Tao et al., 2009; Tolstonog et al., 2005; Wagner et al., 2003). A recent study demonstrated that mitochondria associate with the non-α-helical N-terminal domain of vimentin and that this binding inhibits their motility (Nekrasova et al., 2011). In cultured fibroblasts, mitochondria are distributed throughout the perinuclear region and they are frequently orientated parallel to vimentin IFs.

Mitochondria can also associate with IFs through interactions with the cytolinker, plectin (Reipert et al., 1999; Rezniczek et al., 2003; Winter et al., 2008). Plectin-1b acts as a direct linker between vimentin IFs and the mitochondrial network, with loss of plectin-1b resulting in mitochondrial elongation (Winter et al., 2008).

Disruptions to the IF network have also been shown to disrupt the morphology, distribution and functions of mitochondria. For example, mutations in the small heat shock protein, αB-crystallin, which lead to desmin aggregation in desmin-related myopathies (Vicart et al., 1998), also lead to alterations in mitochondrial organisation and function. Specifically, a reduced maximum rate of oxygen consumption and a compromised inner membrane potential ensue (Maloyan et al., 2005). Furthermore, mutations in desmin itself lead to changes in the distribution and function of mitochondria in skeletal muscles and the heart (Capetanaki, 2002; Milner et al., 2000). Similarly, morphological and functional changes in mitochondria have been reported in vimentin-null fibroblasts (Tolstonog et al., 2001), and mutations in the NF-L gene, which cause Charcot-Marie-Tooth neuropathy type 2E (CMT2E), result in the clustering of mitochondria in the cell bodies of neurons (Brownlees et al., 2002). Collectively, this highlights the importance of the normal localisation and function of IFs for the normal distribution and function of mitochondria.

1.11. Intermediate Filament Abnormalities and Neurodegeneration

Abnormal accumulations and disorganisation of IFs has been observed in many neurodegenerative disorders such as ALS, CMT2E, AD and PD (Al-Chalabi and Miller, 2003; Forno et al., 1986; Perrot and Eyer, 2009). This may be due to factors such as deregulation of IF protein synthesis, defective axonal transport, abnormal phosphorylation and proteolysis. In ALS, abnormal accumulations of phosphorylated NF proteins are present in the perikaryon of affected neurons, swollen axons and spheroids (Manetto et al., 1988; Schmidt et al., 1987). In addition, the IF protein peripherin is present in ubiquitinated inclusions in motor neurons from ALS patients (He and Hays, 2004).

Mutations in genes encoding neurofilament proteins have also been linked to neurodegenerative diseases. Codon deletions or insertions in the lysine-serine-proline (KSP) phosphorylation motif of NF-H have been reported in a small number of sporadic cases of ALS (Al-Chalabi et al., 1999; Figlewicz et al., 1994; Tomkins et al., 1998). In addition, mutations in the NF-L gene have been reported in many cases of CMT2E (De Jonghe et al., 2001; Georgiou et al., 2002; Jordanova et al., 2003; Mersiyanova et al., 2000). This directly implicates disruption of the IF cytoskeleton in the molecular pathogenesis of some neurodegenerative diseases.

Insoluble neurofibrillary tangles (NFTs) are a predominant feature in the pyramidal cells of the hippocampus and in the cerebral cortex of those with AD. Hyperphosphorylated tau, a microtubule-associated protein, was identified as a core protein in NFTs, and more recently, NF-L, NF-M, and NF-H have also been shown to be integral components of NFTs (Rudrabhatla et al., 2011).

1.11.1. Intermediate filament abnormalities in ARSACS

Morphological and functional changes in mitochondria have been widely reported in different ARSACS disease models (Criscuolo et al., 2015; Girard et al., 2012; Lariviere et al., 2015; Pilliod et al., 2015). More recently, *Sacs*$^{-/-}$ knockout mice were shown to display early abnormal accumulations of non-phosphorylated neurofilament (NF) bundles, specifically the heavy molecular weight subunit (NFH), in the somatodendritic regions of vulnerable neuronal populations, a phenotype also observed in an ARSACS brain (Lariviere et al., 2015). Motor neurons cultured from *Sacs*$^{-/-}$ embryos also exhibit a similar NF rearrangement.

So like many other neurodegenerative diseases, both mitochondrial and cytoskeletal defects have been reported in ARSACS, and this is not suprising since mitochondria rely on microtubules (Anesti and Scorrano, 2006; Hollenbeck and Saxton, 2005; Karbowski et al., 2001) intermediate filaments (Chernoivanenko et al., 2015; Milner et al., 2000; Nekrasova et al., 2011) and actin (Boldogh and Pon, 2006; Hatch et al., 2014; Li et al., 2015a) for their normal morphology, motility and distribution. Also, since sacsin contains domains linking to proteostasis pathways, such as a DNAJ domain and HSP90-like domains, loss of its function may affect proteostasis. Thus, like other neurodegenerative diseases, a combination of proteostasis, mitochondrial and cytoskeletal defects likely contribute to the pathophysiological basis of ARSACS, and these are the factors under investigation in this thesis.

1.12. Aims and Objectives

This thesis aims to elucidate the cellular role of sacsin by determining how loss of its function leads to impaired mitochondrial dynamics and function, along with defects in the intermediate filament cytoskeleton. This may shed light on the mechanism of disease in ARSACS and potentially other neurodegenerative or ataxia-related diseases.

Chapter 3 aimed to delineate the mechanisms leading to an elongated and hyperfused mitochondrial network in cells lacking sacsin. Putative interactions have previously been identified between sacsin and both the mitochondrial fission protein DRP1 (Girard et al., 2012), and DCTN6, a component of the dynein-dynactin motor complex (Parfitt, 2011). Interestingly, the dynein-dynactin complex has been identified to have a role in translocation of DRP1 to mitochondria (Varadi et al., 2004). This led to the hypothesis that sacsin and DCTN6 may function together in the recruitment of DRP1 to mitochondria. To test this hypothesis, interactions between sacsin, DRP1 and DCTN6 were further investigated using co-immunoprecipitation (co-IP). Following this, the effect of either sacsin or DCTN6 siRNA knockdown on DRP1 mitochondrial localisation was examined using confocal microscopy and image analysis to quantify the incidence of DRP1 foci associated with mitochondria. The measurements were performed under basal conditions and after mitochondrial fission had been induced by treatment with a mitochondrial uncoupler. Furthermore, it was hypothesised that loss of sacsin may lead to a reduction in DRP1 complex formation. This was examined through the chemical cross-linking of proteins, followed by immunoblotting for DRP1 under non-reducing conditions.

Chapter 4 addresses the intermediate filament defect observed in ARSACS. The organisation of the intermediate filament network (vimentin) in ARSACS patient fibroblasts and sacsin knockdown cells was analysed by confocal microscopy and image analysis. Since the intermediate filament network is important for the localisation and organisation of other cellular structures, including actin and microtubules, the Golgi complex, endosomes, and mitochondria, the distribution of these organelles was also characterised.

Leading on from this, the impact of loss of sacsin on the dynamic assembly of the vimentin network was assessed by fluorescence recovery after photobleaching (FRAP). This involved the transient transfection of SH-SY5Y cells with vimentin-targeted GFP, in combination with either *SCRM* or *SACS* siRNA.

Moreover, the subcellular localisation of sacsin was further defined using super resolution microscopy and image analysis, along with cellular fractionation studies.

Chapter 5 investigates the possibility that, similar to other neurodegenerative diseases, the intermediate filament defects observed in ARSACS may be the result of disrupted proteostasis. The expression and localisation of key proteostasis components, namely ubiquitin, HSP70, HSP90, p62 and LAMP2, were analysed by confocal microscopy and image analysis, along with biochemical approaches. Evidence for an accumulation of misfolded proteins in cells with loss of sacsin would support a role for sacsin in proteostasis and would provide a novel factor contributing to disease pathogenesis in ARSACS.

Conclusions and details of potential future directions are detailed in Chapter 6. The findings indicate a role for sacsin in maintaining mitochondrial and protein quality control. Impairment of this may contribute to the neurotoxicity and Purkinje cell loss in ARSACS.

CHAPTER 2: MATERIALS AND METHODS

2.1. Cell Culture

2.1.1. Cell lines and Maintenance

The neuroblastoma-derived cell line SH-SY5Y (Biedler et al., 1978) was purchased from the European Collection of Authenticated Cell Cultures (ECACC) at the Health Protection Agency (HPA; Salisbury, UK). Cells were grown in 50% Dulbecco's Minimum Eagle Medium (DMEM)/50% F12 (Sigma, Poole, UK) supplemented with 10% (v/v) heat-inactivated foetal bovine serum (FBS; Life Technologies, Paisley, UK) and 50U/ml penicillin and 50µg/ml streptomycin (Pen/Strep; Life Technologies, Paisley, UK; final concentration in media 1% (v/v)).

ARSACS patient dermal fibroblasts were a gift from Dr Sascha Vermeer (Radboud University, Nijmegen, Netherlands) and Dr Paola Giunti (UCL Institute of Neurology, London). The cells were collected as part of a project approved by the Medical Ethics Committee of the Radboud University (CMO-nr 2014/155), and Giunti has ethical approval for dermal fibroblast collection through a European integrated project on spinocerebellar ataxias (REC Ref - 04/Q0505/21). Written informed consent to participate in this study was obtained from all patients.

Control human dermal fibroblasts were purchased from PromoCell (Heidelberg, Germany) or were kindly provided by Dr Tristan McKay (Biomedical Sciences, St George's, University of London), or Dr Sascha Vermeer (Radboud University, Nijmegen, Netherlands). Control and ARSACS patient fibroblasts used in this work were not closely age matched but were all between passage 3 and 8. Cells were grown in DMEM supplemented with 10% (v/v) heat-inactivated FBS and 50U/ml penicillin and 50µg/ml streptomycin (Pen/Strep; final concentration in media 1% (v/v)). Cells were kept in a constant humidified atmosphere of 5% CO_2 at 37ºC.

2.1.2. Subculturing

All reagents were warmed to 37ºC before use. Media was removed from the culture flask or dish and cells washed with DPBS (Dulbecco's Phosphate Buffered Saline). Trypsin-EDTA (0.5g/l trypsin, 0.2g/l Ethylenediaminetetraacetic acid; Life Technologies, Paisley, UK) was used to detach the cells for 2-5 minutes, and then inactivated by adding media containing 10% (v/v) FBS. The cell suspension was

centrifuged at 125*g* for 5 minutes and the supernatant was removed. The cell pellet was then re-suspended in fresh media and cells were re-plated as required.

2.1.3. Freezing down cells

Cells were grown until confluent, then trypsinised and transferred to a 15ml Falcon tube. From here on, Falcon tubes were spun using a Sorvall legend RT centrifuge with a four-piece swinging bucket rotor (75006445). Falcon tubes were centrifuged at 125*g* for 5 minutes and the media removed. The cell pellet was then re-suspended in a freezing solution containing 90% FBS and 10% (v/v) DMSO (Dimethyl Sulphoxide, Sigma, Poole, UK), and cooled at a maximum of 1^{o}C/min to -80ºC in 1ml cyrotubes. The tubes were transferred to liquid nitrogen for long-term storage. When necessary, the cells were revived from frozen by quickly thawing in a 37ºC water bath. The 1ml aliquot was transferred to a 15ml Falcon tube and centifuged at 125*g* for 5 minutes. The supernatant was removed and the cells were resuspended in 10ml of complete medium and plated into a new flask. Flasks were incubated in a 5% CO_2, 37ºC incubator and the growth media was changed the following day.

2.1.4. Cell counting

Cells were washed with DPBS and trypsinised to detach the cells as if sub-culturing, before transferring them to a 15ml Falcon tube. 10µl of cell suspension was combined with 10µl of trypan blue (to identify dead cells) and pipetted into either end of a haemocytometer. Cells were counted, using a hand tally counter, in all four red corners of one grid (Figure 2.1) using a Leica DMIL light microscope with 10x objective, ignoring dead cells stained with trypan blue. The concentration of cells and volume of the suspension needed to acquire the desired cell density were determined using the following calculations:

Number of cells counted/number red corners counted = number of cells/100ml
Multiply by 2 to adjust for 1:2 trypan blue dilution
x 10^4 = Number of cells/ml (y)
Number of cells required/y = volume of cell suspension to seed (ml)

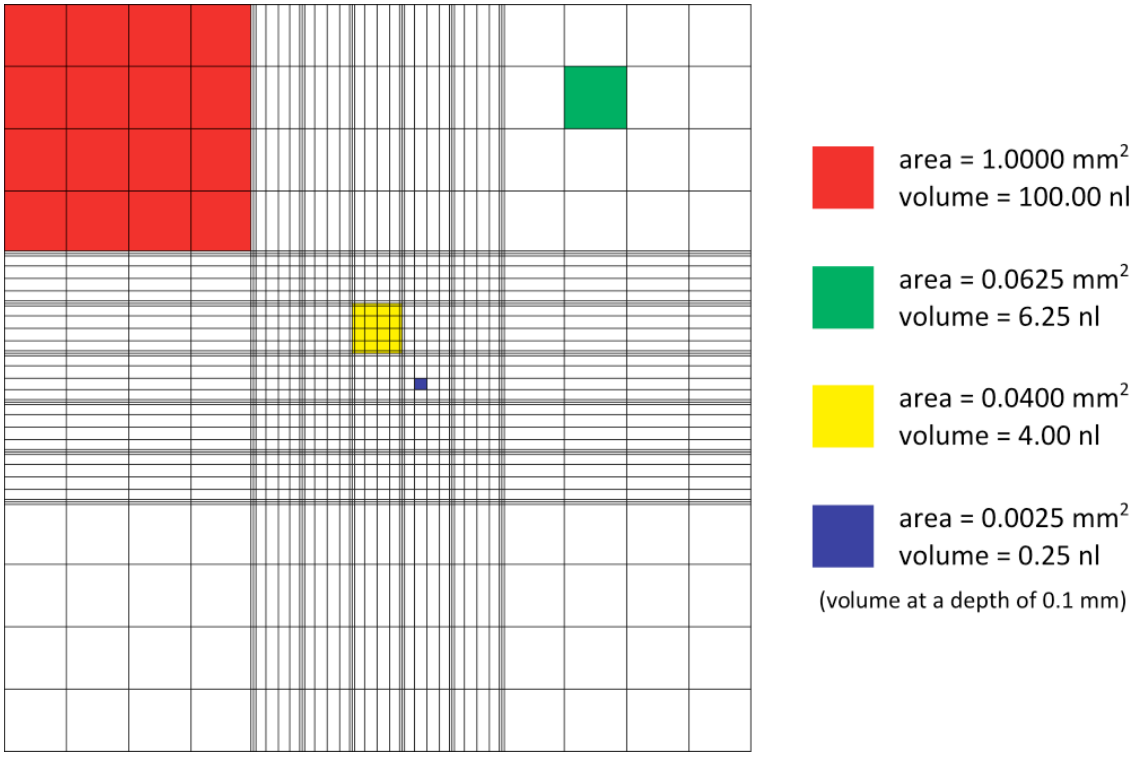

Figure 2.1. Schematic of haemocytometer grid

The calculated volume of cells was transferred to each well, and media was added to cover cells.

2.2. Transient Transfections

2.2.1. Lipofectamine and Plus Reagent

Cells were seeded either in 8 well chamber slides (Nunc, VWR, Leicester, UK), 12 well plates, 6 well plates, 10cm dishes, or 25cm^3 (T25) cell culture flasks (VWR, Leicester, UK) until 60-70% confluent. Cells for live imaging were seeded in 35mm glass-bottomed cell culture dishes (Mat-Tek, Ashland, MA, USA). Cells were transfected with plasmid DNA and/or small interfering RNA (siRNA) using the Lipofectamine and Plus reagent system (Life Technologies, Paisley, UK) as follows:

For an 8 well chamber slide, 100ng of DNA was incubated at room temperature with 1µl Plus reagent in 12.5µl serum free media (Opti-MEM; Life Technologies, Paisley, UK) for 20 minutes. 1µl Lipofectamine and 100µl Opti-MEM were added to the mixture and incubated for 15 minutes. Cells were washed twice with serum free media

before the transfection mixture was added to the cells. Transfection reagents were scaled up or down depending on the culture vessel (Table 2.1). After incubation for 3 hours at 37ºC, an equal volume of 2x serum media containing 20% FBS/2% PenStrep was added to cells, followed by further incubation at 37ºC for 24-48 hours. Cells were then processed for immunocytochemistry or immunoblot analysis.

Table 2.1. Transfection using lipofectamine and plus reagent

Culture vessel	Opti-MEM	Plus reagent	DNA	Opti-MEM	Lipofectamine
8-well slide	12.5 µl	1 µl	100ng	100 µl	1 µl
Mat-Tek dish	100 µl	4 µl	1µg	400 µl	4 µl
12-well plate	50 µl	2 µl	500ng	200 µl	2 µl
6-well plate	100 µl	4 µl	1µg	700 µl	4 µl
T25 flask	250 µl	10 µl	2µg	1.5ml	10 µl

Volumes shown are for a single well for each vessel indicated.

2.2.2. Lipofectamine 3000

Cells were seeded either in 12 well plates, 6 well plates, or 10cm dishes (VWR, Leicester, UK) until 70-90% confluent. Cells for live imaging were seeded in 35mm glass-bottomed cell culture dishes (Mat-Tek, Ashland, MA, USA). Cells were transfected with plasmid DNA and/or siRNA using the Lipofectamine 3000 system (Life Technologies, Paisley, UK) as follows:

For a standard 12 well plate, 500ng of DNA and/or 20pmol siRNA was diluted in 50µl serum free media (Opti-MEM) at room temperature. In a separate Eppendorf tube, 2µl Lipofectamine 3000 was diluted in 50µl Opti-MEM. The diluted DNA was added to the diluted Lipofectamine 3000 reagent (1:1 ratio), mixed by pipetting, and incubated for 5 minutes at room temperature. The DNA-lipid complexes were then added to the cells in 1ml of growth medium. Transfection reagents were scaled up or down depending on the culture vessel (Table 2.2). Cells were incubated for 48 hours at 37ºC before visualising and processing them for immunocytochemistry or immunoblot analysis.

Table 2.2. Transfection using lipofectamine 3000

Culture vessel	Opti-MEM	DNA	siRNA	Opti-MEM	Lipofectamine 3000	Vol. Growth Medium
Mat-Tek dish	125 µl	1.5 µg	50 pmol	125 µl	5 µl	2 ml
12-well plate	50 µl	500 ng	20 pmol	50 µl	2 µl	1 ml
6-well plate	125 µl	1.5 µg	50 pmol	125 µl	5 µl	2 ml
10 cm dish	500 µl	10 µg	350 pmol	500 µl	30 µl	10 ml

Volumes shown are for a single well for each vessel indicated.

For transfection of siRNA, three custom *SACS* siRNAs to exons 7, 8 and 10, and two *DCTN6* siRNAs to exons 3 and 6 were previously validated by our group (Ambion, Life Technologies, Paisley, UK, Table 2.3). The three *SACS* siRNAs were combined to make a stock solution of 20µM concentration. The same was done for the two *DCTN6* siRNAs. The final concentration of siRNA in each transfection was 20nM.

Table 2.3. siRNA sequences

Primer name	Sequence (5' - 3')
SACS exon 7 - sense	GGAUGAUCCUCUGAAGGUC
SACS exon 7 - antisense	GACCUUCAGAGGAUCAUCC
SACS exon 8 - sense	GCGGCCGAAUUCUAUAAAG
SACS exon 8 - antisense	CUUUAUAGAAUUCGGCCGC
SACS exon 10 - sense	CGUAAGAUUUCUAGAUGAC
SACS exon 10 - antisense	GUCAUCUAGAAAUCUUACG
DCTN6 exon 3 - sense	GCCCUUAUCAUAAAUGCUU
DCTN6 exon 3 - antisense	AAGCAUUUAUGAUAAGGGC
DCTN6 exon 6 - sense	GGCAGAAAUGUAAUAUUGA
DCTN6 exon 6 - antisense	UCAAUAUUACAUUUCUGCC

2.3. RNA Extraction

RNA was extracted and purified from cells using an RNeasy mini kit (Qiagen). Cells were washed with cold PBS and lysed directly from plates using 350µl buffer RLT (lysis buffer) containing 10µl/ml of 2-mercaptoethanol (2-ME, Sigma), a reducing agent. Cells were homogenised by passing the lysate ten times through a 23G needle. To each 350µl lysate, one volume of 70% (v/v) ethanol was mixed in by pipetting, and the solution was transferred to an RNeasy spin column over a 2 ml collection tube. From here on, 1.5/2ml Eppendorfs were spun using a Sorvall legend micro 17 centrifuge with a 24 x 1.5/2ml rotor (Thermo scientific). Lysates were centrifuged at 13000*g* for 30 seconds through the column. The flow-through was discarded and the column washed with 700µl buffer RW1. Flow-through was discarded again, and the column washed with 500µl buffer RPE by centrifuging at 13000*g* for 30 seconds. This step was repeated with a centrifugation time of 2 minutes. The column was then transferred to a clean collection tube and centrifuged at 13000*g* for 1 minute to dry the membrane. The column was placed in a 1.5ml Eppendorf and RNA was eluted with 30µl RNase-free water by centrifugation at 13000*g* for 1 minute. The RNA yield was quantified using the Nanodrop ND-1000 spectrophotometer, measuring absorbance at 260 nm. Purity of RNA was determined by the OD260/OD280 ratio, which should be approximately 2.0 for RNA. A lower ratio can signify protein or phenol contamination.

2.4. cDNA Synthesis

Complementary DNA (cDNA) was produced using the QuantiTect reverse transcription kit (Qiagen). First a reaction was carried out to remove genomic DNA (gDNA). 1µg of RNA was mixed with 7x gDNA wipeout buffer and RNase-free water to a final volume of 14µl. This was incubated at 42ºC for 2 minutes, then immediately placed on ice. Reverse transcription was subsequently carried out by creating a master mix, as detailed in table 2.4.

Table 2.4. Reverse-transcription reaction components

Component	Volume/reaction	Final Concentration
Quantiscript reverse transcriptase	1µl	
Quantiscript RT buffer, 5x[1]	4µl	1x
RT primer mix	1µl	
gDNA elimination reaction	14µl	
Total volume	**20µl**	

[1]Contains Mg^{2+} and dNTPs.

This was incubated for 15 minutes at 42ºC, followed by a 3-minute incubation at 95ºC to inactivate the reverse transcriptase. cDNA was then stored at -20ºC or used in real-time PCR reactions. cDNA was amplified with GAPDH primers (Table 2.7) to identify successful reverse transcription, which should reveal a PCR product of approximately 200 base pairs. Presence of a higher molecular weight band would suggest gDNA contamination.

2.5. Polymerase Chain Reaction (PCR)

PCR was used to amplify specific regions of genes of interest. A series of temperature steps are repeated: Denaturation of DNA at 94ºC to separate the double helix, annealing at 50-60ºC to bind sequence specific primers to the template strand, and elongation of complementary strands by DNA polymerase in a 5' to 3' direction at 72ºC. Newly synthesised DNA is used as a template in subsequent cycles, leading to exponential amplification.

cDNA was incubated with DNA polymerase from *Thermus aquaticus* (Taq), primers to the gene of interest (sequences given in table 2.7) and dNTPs to allow amplification (Table 2.5).

Table 2.5. Standard PCR Mastermix

Reagents	50µl reaction	Final Concentration at 1x
10x Standard *Taq* buffer[1,2]	5µl	1x
dNTPs (10mM)	1µl	0.2mM
Forward primer (10µM)	1µl	0.2mM
Reverse primer (10µM)	1µl	0.2mM
dH_20	40.75µl	To final volume 50µl
Taq polymerase (5000U/ml)[1]	0.25µl	
cDNA	1 µl	0.5-1ng/µl

[1] New England BioLabs. [2]10mM Tris-HCl, 50mM KCl, 1.5mM $MgCl_2$, pH8.3.

Mastermix (49µl) and DNA (1µl) were mixed in a PCR tube to a total volume of 50µl. PCR reactions were carried out on a G-storm GS1 thermocycler (G-storm, somerset, UK) and the PCR thermocycle was programmed as indicated in table 2.6. PCR products were separated by agarose gel electrophoresis.

Table 2.6. PCR cycling conditions

Phase	Time	Temperature
Initial denaturation	5 min	94ºC
Denaturation*	30 secs	94ºC
Anneal*[1]	30 secs	~55ºC
Extension*	1min/kb	72ºC
	10 min	72ºC
Cooling	∞	4ºC

*Repeated 30 cycles. [1] Annealing temperature depends on melting temperature of specific primers.

Table 2.7. Primer sequences

Primer name	Sequence (5' - 3')
GAPDH-F	TGCACCACCAACTGCTTAG
GAPDH-R	GGATGCAGGGATGATGTTC
SACS exon 6-7 - F	ACAACAACGCGGTTTTCACC
SACS exon 6-7 - R	GCCTGATTCATGTGGGCCAA
SACS exon 8-9 - F	TTTAAAGGAAGCTGCCCAAA
SACS exon 8-9 - R	CCAAACCATCTTAAGCCATCA
DCTN6-F	GGATCCCATGGCGGAGAAGACTCAAAAGAGT
DCTN6-R	GGATCCGTTCTTTACTGGAGTTGAGCTT
T7 sequencing primer	TAATACGACTCACTATAGGG
SP6 Sequencing primer	ATTTAGGTGACACTATAG

2.6. Agarose Gel Electrophoresis

Amplified DNA samples were loaded into the wells of an agarose gel and an electrical field was applied. Negatively charged DNA molecules migrate through the gel towards the anode. The speed of migration depends on the size of PCR products, with larger molecules migrating more slowly as they incur more resistance passing through the agarose. The size of a PCR product is estimated by comparison to a DNA ladder containing fragments of known sizes, run in an adjacent lane.

To prepare a 1% w/v agarose gel, 1g of agarose was dissolved in 100ml of 1x TAE buffer by heating in a microwave for 3 minutes. After cooling slightly, 10µl of Gel Red (10,000x; Life Technologies, Paisley, UK) was added to the solution before pouring into a gel casting frame with a comb inserted and left to solidify for around 40 minutes. The gel was then placed in an electrophoresis tank containing 1x TAE buffer. 6x loading dye containing bromophenol blue (Promega) was added to samples at a 1:6 dilution to track DNA migration during electrophoresis. GeneRuler DNA ladder mix (Thermo Scientific) was used as a DNA size marker. The gel was run at 100 volts for around 40 minutes and DNA bands were visualised under a UV-light using a Kodak Electrophoresis and Documentation analysis system UV transilluminator (Uvitec, Cambridge, UK).

2.7. Gel Extraction

To purify DNA from an agarose gel, the bands were visualised under UV light, cut out with a clean blade and transferred to a 1.5ml Eppendorf. The QIAquick gel extraction kit (Qiagen, Manchester, UK) was used as described. The weight of the gel slice was determined, and 3 volumes of Buffer QG were added to 1 volume of the gel. The mixture was incubated at 50ºC for 10 minutes to dissolve the gel, vortexing intermittently. One gel volume of 100% isopropanol was added and mixed to precipitate the DNA. The sample was then transferred to the QIAquick column and centrifuged for 1 minute at 13000*g* to bind the DNA to the silica membrane. Through-flow was discarded and the column was washed with 500µl Buffer QG and centrifuged for 1 minute to remove further agarose. Through-flow was removed and another wash step followed. 750 µl Buffer PE was applied to the column and centrifuged for 1 minute to remove salt. Through-flow was discarded and the column was centrifuged for an additional minute to remove traces of Buffer PE. The column was placed in a clean

collection tube, and DNA was eluted with 25µl nuclease free water, centrifuging for 1 minute at 13000*g*. DNA concentration in ng/ml was determined using a Nanodrop ND-1000, measuring absorbance at 260 nanometers (nm). The purity of the DNA was determined by calculating the ratio of absorbance at 260 nm and 280 nm. A ratio of ~1.8 was considered to be pure DNA. Samples were stored at -20ºC.

2.8. Cloning

2.8.1. Generation of Dynactin-6 vectors

Dynactin-6 (DCTN6) vectors were created by recombinant DNA cloning. The DCTN6 sequence was amplified by PCR from an adult human brain cDNA library using the following primers, containing *Bam*HI restriction sites (bold):

F: **GGATCC**CATGGCGGAGAAGACTCAAAAGAGT
R: **GGATCC**CGTTCTTTACTGGAGTTGAGCTT

An aliquot of the amplified product was analysed on an agarose gel to verify that the reaction produced the desired product of 583bp, which was subsequently gel-purified (as section 2.7). This product was then ligated into a pGEMT-Easy vector (Promega, Southampton, UK) with blue-white selection indicating insertion. Restriction digest using *Bam*HI restriction enzyme (NEB, Hitchen, UK) confirmed the insertion of the correct region (as section 2.8.2).

The DCTN6 constructs were subcloned into the p3xFLAG-CMV-14 vector (Sigma, Poole, UK) and the pEGFP-N3 vector (Clontech, Oxford, UK) to generate FLAG-tagged and GFP-tagged dynactin-6 constructs, respectively (Figure 2.2). Restriction digest using *BseRI* and *Xba1* restriction enzymes (NEB, Hitchen, UK) confirmed in-frame insertion of DCTN6 into the vectors (as section 2.8.2).

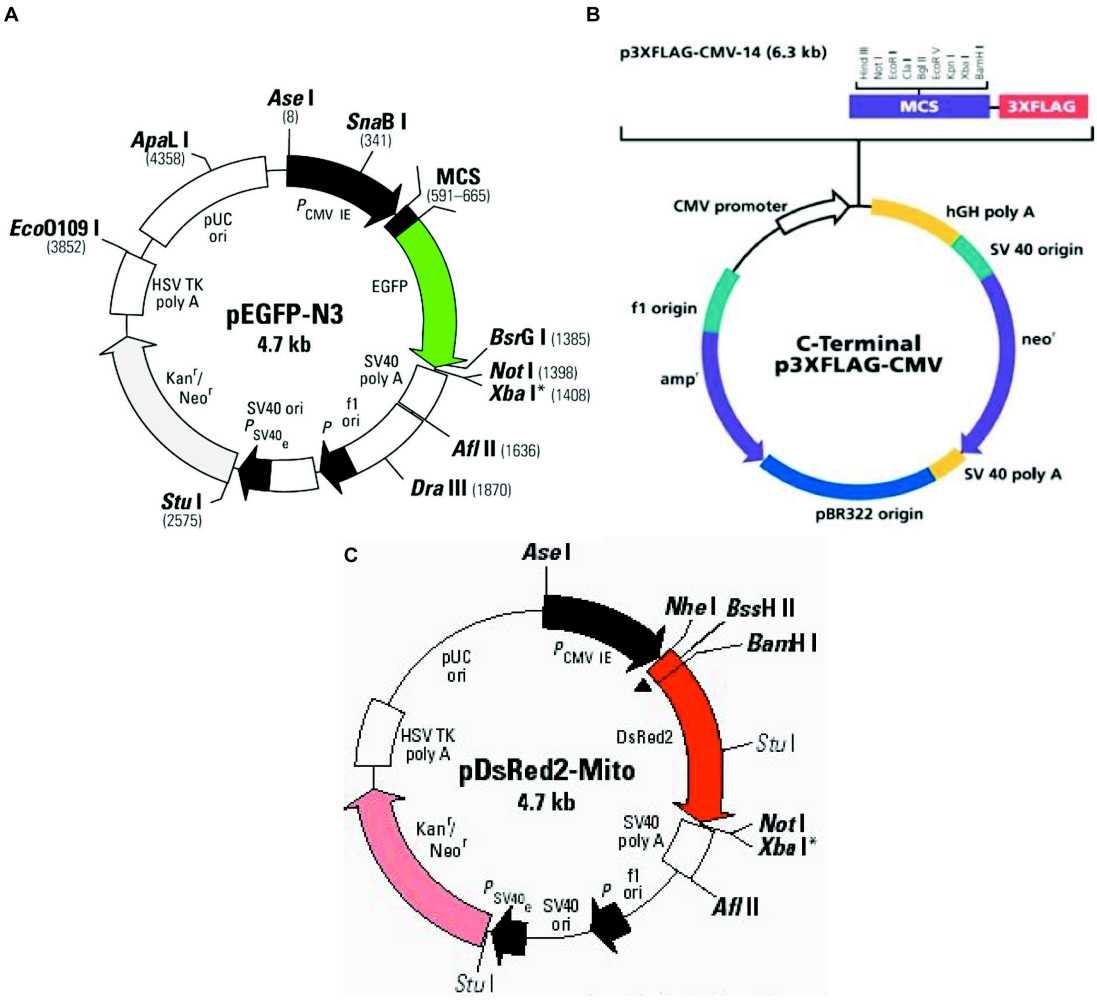

Figure 2.2. Constructs used in this thesis. (A) Vector map of pEGFP-N3, into which dynactin-6 was cloned into the *BamHI* site within the multiple cloning site (MCS). **(B)** Vector map of p3xFLAG-CMV-14, into which dynactin-6 was cloned into the *BamHI* site within the MCS. **(C)** Vector map of pDsRed2-Mito, which contains a mitochondrial targeting sequence from subunit VIII of human cytochrome c oxidase.

2.8.2. Restriction Digest

Restriction enzymes were used to digest inserts and vectors in order to prepare insert sticky ends (3'- or 5'-overhangs of 1 to 4 nucleotides) and linearise vectors before ligation. Restriction digests were also used at the end of the cloning process to screen transformed colonies for release of an insert. Those with the correct size insert after digestion were sent for Sanger sequencing to confirm the insert was in-frame with the correct orientation.

DNA was digested using appropriate restriction enzymes for 2 hours, in a 10µl reaction for checking insert release, and a 30µl reaction for digesting inserts and vectors before ligation, as indicated in table 2.8.

Table 2.8. Restriction digest reaction mix

	Screening colonies for insert	**Preparing insert and vector for ligation**
Vector DNA	100ng	1µg
Enzyme (NEB Biolabs)	1µl	1µl
NEBuffer 1-4 (10x)	1µl	3µl
BSA (100x)	0.1µl	0.3µl
ddH_20 to total volume of	10µl	30µl

Digested products were analysed by gel electrophoresis. If preparing DNA for ligation, an additional step was required before gel electrophoresis. Reaction mixes containing linearised vectors were treated with Alkaline Phosphatase, Calf Intestinal (CIAP; Promega) to dephosphorylate the 5' end, preventing religation of the empty vector. 1µl CIAP was added to restriction digest reactions and incubated for 30 minutes at 37ºC, followed by heating at 65ºC for 10 minutes to deactivate the enzyme. After gel electrophoresis, digested inserts and vectors were gel extracted and purified for ligation.

2.8.3. Ligation

The concentration of PCR product (insert) required for ligation was calculated using the following equation:

(ng vector x kb insert/kb vector) x insert: vector ratio = ng insert

Various insert to vector ratios were used to increase the likelihood of successful ligation. Ligation reaction mixes were prepared as in table 2.9.

Table 2.9. Ligation reaction mixes

	Sample reaction	Positive control	No insert control
2x Rapid Ligation Buffer	5 µl	5 µl	5 µl
Vector	1 µl	1 µl	1 µl
PCR product	1 µl	-	-
Control insert DNA	-	2 µl	-
T4 DNA ligase (3 Weiss units/ µl)	1 µl	1 µl	1 µl
Deionised water	2 µl	1 µl	3 µl
Final volume	10 µl	10 µl	10 µl

A Promega control insert DNA was used as a positive control to give an indication of the number of colonies to expect after transformation. A negative background control was used to assess background due to re-ligation of linear vectors, which should produce few colonies after transformation. Tubes were briefly centrifuged, and reactions were incubated overnight at 4ºC on slushy ice.

2.8.4. Preparation of LB agar plates

10g of Luria broth (LB) and 7.5g of agar were dissolved in 500ml of deionised water, autoclaved to sterilise, and cooled to around 37ºC. Once cooled, antibiotic was added to the solution at a concentration of 100µg/ml for ampicillin or 30µg/ml for kanamycin, and poured into 10cm^2 plates under sterile conditions. Plates were left to set at room temperature, and then stored at 4ºC.

For plates being used to grow competent cells transformed with pGEMT-Easy vectors, 50mg/ml X-Gal (5-bromo-4-chloro-3-indolyl-beta-D-galactopyranoside; Promega) and 200mg/ml of IPTG (Isopropyl β-D-1-thiogalactopyranoside; Promega) were pipetted onto plates and spread using a sterile Pasteur pipette. Plates were left to set at room temperature.

The pGEMT-Easy vector contains a portion of the LacZ gene within the multiple cloning site, which encodes the N-terminal fragment of β-galactosidase. This metabolises X-Gal to produce a blue product. IPTG triggers the transcription of *LacZ*. Thus, competent cells transformed with an empty pGEMT-Easy vector will turn blue. However, when a DNA fragment is inserted into the multiple cloning site of the pGEMT-Easy vector, the LacZ gene is disrupted, preventing β-galactosidase activity, so there will be no action upon X-gal and the cells will not turn blue. This blue-white screening identifies colonies containing the DNA insert.

2.8.5. Transformation

JM109 *E.coli* highly competent cells (>10^8 cfu/µl; Promega) were defrosted on ice until just thawed, mixed by gently flicking the tube, and 50µl transferred to a 1.5ml Eppendorf along with the 10ul ligation reaction. Tubes were mixed by gentle flicking and incubated on ice for 20 minutes. The competent cells were then heat-shocked at 42ºC for 50 seconds in a water bath, then immediately returned to ice for 2 minutes. This allows DNA to enter the cell membrane. 950µl of room temperature S.O.C medium (Life Technologies, Paisley, UK) was added to cells transformed with the ligation reactions, then incubated for 1.5 hours at 37ºC with shaking at 150rpm. 100µl of transformation culture was spread onto pre-prepared LB agar plates containing the appropriate antibiotic with a sterilised glass rod. The remaining 900µl was centrifuged at 1000*g* for 10 minutes to pellet cells, which were then re-suspended in 200µl S.O.C medium to concentrate the remaining cells. 100µl was spread onto a second LB agar plate for each ligation. Plates were incubated overnight at 37ºC to allow colony formation.

In a sterile environment, individual colonies were picked using a sterile pipette tip, and transferred to a 50ml Falcon tube containing 10ml LB with the appropriate antibiotic. For pGEMT-Easy cloning, white colonies were selected and blue colonies were disregarded. Cells were grown for 16 hours at 37ºC with shaking at 300rpm, and then centrifuged at 4000rpm for 20 minutes at room temperature to pellet cells. Supernatent was discarded and plasmid DNA was extracted and purified according to section 2.8.6.

2.8.6. Plasmid Purification

Plasmid DNA was extracted and purified using a QIAprep Spin Miniprep Kit (Qiagen, UK). Pelleted bacterial cells were resuspended in 250µl of cold buffer P1 by vortexing and transferred to a 1.5ml Eppendorf, ensuring no cell clumps were visible. Cells were lysed by adding 250µl of alkaline buffer P2 and inverting the tubes to mix. 350µl of acidic neutralisation buffer N3 was added to tubes and mixed by inversion. Samples were then centrifuged for 10 minutes at 13000rpm and supernatant was collected and transferred to a QIAprep Spin column, which was centrifuged for one minute to bind DNA to the silica membrane. The QIAprep spin column was washed by adding 500µl buffer PB and centrifuging for one minute, discarding the flow-through, followed by a second wash with 750µl buffer PE to rid the column of endonucleases and salt, again centrifuging for one minute. Flow-through was discarded and the column was centrifuged for one minute to remove residual buffer. The column was placed in a clean 1.5ml Eppendorf and DNA was eluted in 30ul nuclease free water by centrifuging for one minute at 13000rpm. For purification of larger plasmid preps, the HiSpeed Plasmid Midi Kit (Qiagen, UK) was used according to manufacture's instructions.

2.9. Immunoblotting

2.9.1. Cell lysate preparation

For preparation of cell lysates, cells were washed twice with PBS at 4ºC, then harvested in RIPA (Radio-Immunoprecipitation Assay, Sigma, Poole, UK) Buffer: 150 mM NaCl, 1.0% w/v IGEPAL® CA-630, 0.5% w/v sodium deoxycholate, 0.1% w/v SDS, and 50 mM Tris, pH 8.0, supplemented with protease and phosphatase inhibitors (Roche, Burgess Hill, UK) at 4ºC. Cell lysates were transferred to a 1.5ml Eppendorf and incubated on ice for 30 minutes, then were spun at 13000*g* at 4ºC for 12 minutes. The supernatant was transferred to a fresh Eppendorf and an equal volume of 2x sample buffer containing SDS and 2-ME (Sigma, Poole, UK) was added. The samples were boiled at 100ºC for 10 minutes and centrifuged at 13000*g* for 1 minute before gel loading. For non-reducing sample conditions, no 2-ME was added to the 2x sample buffer and samples were not boiled prior to gel loading.

2.9.2. Bradford Protein Assay

The Bio-Rad Protein Assay (Bio-Rad) was used to determine protein concentrations. A differential colour change of the protein assay dye, Coomassie Brilliant blue G-250, occurs as the absorbance maximum shifts from 465 nm to 595 nm when protein binding occurs. Measurement at 595 nm with a spectrophotometer or microplate reader and comparison to a standard curve provides a relative measurement of protein concentration.

Serial dilutions of bovine serum albumin (BSA) ranging in concentration from 0 to 1mg/ml were used as protein standards. Test proteins were diluted 1 in 2 and the protein assay dye was diluted 1 in 5 with dH_20. 10µl of standard or test sample were added to a 96-well plate in duplicate, followed by 200µl protein assay dye, and mixed by gentle pipetting. The samples were left to incubate at room temperature for 5 minutes, then absorbance at 595 nm was read using a standard plate reader. A standard curve was produced by plotting OD595 against the concentration of the BSA standard, and the protein concentration of each sample was determined by extrapolating from the linear equation.

2.9.3. SDS-PAGE

The samples were run on precast 4-12% polyacrylamide NuPAGE Bis-Tris gels (Life Technologies, Paisley, UK). The gels were run in 1x 3-(Nmorpholino) propanesulfonic acid (MOPS) running buffer (Life Technologies, Paisley, UK), consisting of 50mM MOPS, 50mM Tris, 0.1% w/v SDS, 1mM EDTA, pH 7.7. High Molecular Weight Marker protein ladder or Novex Sharp Pre-stained Protein Standard (Life Technologies, Paisley, UK) were run alongside all samples. 20-25µl of sample per well was loaded and the samples were run at 100-150V for 1.5-3 hours.

2.9.4. Immunoblotting

After separation by electrophoresis, the samples were transferred to a nitrocellulose membrane (Whatman) by either semi-dry transfer using a Trans-Blot SD semi-dry transfer cell (Bio-Rad, Hemel Hempstead, UK) or wet transfer using a mini Trans-Blot cell (Bio- Rad, Hemel Hempstead, UK), depending on the size of the protein.

Semi-dry transfer was carried out at 15V for 40 minutes using a transfer buffer containing 20mM Tris base, 120mM glycine and 20% (v/v) methanol. Wet transfer was carried out at 45V overnight (16 hours) at 4ºC using a transfer buffer containing 20mM Tris base, 120mM glycine, 0.1% (w/v) sodium dodecyl sulfate (SDS) and 10% (v/v) methanol.

After transfer the membrane was blocked with 5% milk powder in PBS with 0.1% Tween20 (PBST) for 1 hour to prevent non-specific binding of the antibody, then incubated in 5ml 5% (w/v) milk in PBST containing appropriate primary antibodies (Table 2.10) for 3 hours or overnight. After washing in PBST three times for 10 minutes the membranes were incubated with appropriate species-specific infrared secondary antibodies (Licor, Cambridge, UK, Table 2.11) at a dilution of 1:5000 for 1 hour. After three washes in PBST, the membranes were scanned using the Licor Odyssey infrared scanner. This system involves direct scanning of the membrane by two independent lasers, allowing detection of the infrared fluorescence emitted by two different secondary antibodies. The two colour detection system uses a 700 nm red channel, and 800 nm green channel. Images of the blots were quantified using the Licor Odyssey imaging systems software.

2.9.5. Coomassie Blue staining

Coomassie brilliant blue is a triphenylmethane dye that stains proteins in polyacrylamide gels. Protein lysates were run on precast 4-12% polyacrylamide NuPAGE Bis-Tris gels. Gels were then washed briefly in sterile deionised ultrapure water prior to soaking in Coomassie Brilliant Blue staining solution (0.05% (w/v) Coomassie Brilliant Blue R-250, 50% (v/v) methanol and 10% (v/v) glacial acetic acid) at room temperature for 1 hour with gentle shaking. The gels were then destained in Coomassie destaining buffer (20% (v/v) methanol and 10% (v/v) glacial acetic acid) at room temperature with gentle shaking until the desired contrast was achieved (approximately 5 minutes). Gels were dried overnight between two moistened sheets of clear cellulose film using a gel drying kit (Promega).

2.10. Immunoprecipitation

2.10.1. Crosslinking

SH-SY5Y cells were subjected to chemical cross-linking at 24 hours post-transfection. The cleavable, homo-bifunctional cross-linker dithiobis[succinimidylpropionate] (DSP; Pierce, Rockford, IL, USA) was diluted to a final concentration of 1mM in PBS and added to the cultured cells. After incubation for 1 hour at room temperature, cross-linking was stopped by addition of Tris (pH 7.5) to a final concentration of 20mM. Cells were then lysed in preparation for immunoprecipitation and immunoblotting.

2.10.2. Cell lysis

SH-SY5Y cells in T25 culture flask were transfected with Dynactin-6-FLAG and/or DRP1-GFP, or empty vectors. After 24 hours the cells were washed twice in ice-cold PBS, before the cells were harvested in 750µl Lysis buffer (50mM Tris-HCl pH7.4, 150mM NaCl, 1mM EDTA and 0.5% (v/v) Triton X-100) supplemented with protease inhibitors (Roche, Burgess Hill, UK) and incubated on ice for 15 minutes. The cells were homogenised by passing ten times through a 23G needle. The lysate was centrifuged at 17500*g* on a table top microcentrifuge to separate the nuclei, and the supernatant was used for immunoprecipitation. A small aliquot (120µl) of supernatant was removed for analysis by immunoblotting (input fraction).

2.10.3. Tag-coupled bead immunoprecipitation

40µl of anti-FLAG-M2 Magnetic beads (Sigma, Poole, UK) were washed twice in 200ml lysis buffer, before being recovered in a magnetic separator. The remaining cell lysate was added to the washed beads and incubated overnight at 4ºC on a rotor. After approximately 16 hours the beads were placed in the magnetic separator and the supernatant was removed. The beads were then washed three times with 400µl lysis buffer. After washing the beads were eluted in 50µl 2x sample buffer (Sigma, Poole, UK) and heated at 100ºC for 3 minutes before being placed in the magnetic separator to collect the supernatant, which was subsequently used for immunoblotting.

2.11. Subcellular fractionation

2.11.1. Mitochondrial Isolation

Cells were seeded in 10cm cell culture dishes and allowed to reach 90-100% confluence. The cells were washed twice in ice cold PBS, before being harvested in 1ml of ice cold trypsin and transferred to a 15ml Falcon. The cells were spun at 200*g* for 5 minutes to pellet the cells, and the pellet was washed in 10ml of PBS. The cells were re-pelleted at 200*g* for 5 minutes, before resuspending in 100µl of homogenisation buffer (10mM Tris-HCL (pH 7.4), 1mM EDTA, 250mM sucrose) with protease inhibitors (Roche, Burgess Hill, UK). The cells were frozen overnight at -80ºC. The homogenisation buffer containing the cell pellet was thawed on ice and transferred to an ice cold 1.5ml Eppendorf. The Falcon was washed with 300µl of homogenisation buffer and added to the Eppendorf. The cell pellet was resuspended by pipetting (around 20x titrations) before being frozen again at -80ºC for 1 hour. After thawing on ice, the lysate was spun at 1500*g* for 10 minutes at 4ºC to generate a supernatant (S1; homogenate fraction) and pellet (P1; nuclei and cell debris). The S1 fraction was transferred to a new Eppendorf and a 30µl aliquot taken before centrifugation at 11500*g* for 12 minutes to generate a supernatant (S2; cytoplasm) and pellet (P2; mitochondria). The S2 fraction was transferred to a new Eppendorf and a 30µl aliquot taken. 4x sample buffer (Life Technologies, Paisley, UK) was added to the S2 fraction and samples heated at 70ºC for 10 minutes. The P2 fraction was washed by resuspension in 1ml of homogenisation buffer before being re-pelleted at 11500*g* for 12 minutes. The supernatant was discarded and the mitochondrial pellet resuspended in 50µl of homogenisation buffer. An equal volume of 2x sample buffer (Sigma, Poole, UK) was added to each sample and heated at 70ºC for 10 minutes. Additionally, the mitochondrial fraction was sonicated at 10,000 kHz for 10 seconds to break up the DNA. All fractions were subsequently analysed by SDS-PAGE and immunoblotting.

2.11.2. Cytoskeletal Fraction

Cells were seeded in a 10cm cell culture dish and allowed to reach 90-100% confluence. The cells were washed three times with ice-cold PBS and incubated for 10 minutes with 1ml of lysis buffer (50 mM HEPES, pH 7.4, 20 mM EGTA, 0.5% (v/v) Triton-X100), supplemented with protease and phosphatase inhibitors (Roche, Burgess Hill, UK), at

room temperature. Cell lysates were centrifuged at 15000*g* for 15 minutes at 4ºC to obtain a detergent-insoluble pellet. The supernatant (soluble fraction) was transferred to a 1.5 ml Eppendorf and the insoluble pellet was washed with lysis buffer and re-pelleted at 15000*g* for 10 minutes at 4ºC. Insoluble pellets were resuspended in 60µl of urea (6 M). Fractions were mixed with equal volume of 2x concentrated Laemmli's sample buffer, heated at 100ºC for 10 minutes, and subsequently analysed by SDS-PAGE.

2.11.3. Intermediate-filament-rich-fractions

Intermediate filaments (IFs) are extremely stable. Even after extraction in solutions containing detergents and high salt concentrations, most IFs in a cell remain intact, whereas microfilaments and microtubules depolymerise into their soluble subunits. Hence, IF purification methods use detergents and high salt concentrations to seperate IFs from other proteins. The IFs are then treated with urea, a denaturing solvent.

Cells were seeded in 10cm cell culture dishes and allowed to reach 90-100% confluence. The cells were washed three times with ice-cold PBS, before being harvested in 1ml of homogenisation buffer containing 1% (v/v) Nonidet P-40, 10% (v/v) glycerol , 20 mM HEPES, pH 7.6, and 150 mM NaCl, supplemented with protease and phosphatase inhibitors (Roche, Burgess Hill, UK). Lysates were transferred to 1.5ml Eppendorfs, homogenised by passing through a 23-gauge needle ten times, and incubated at 37°C for 30 minutes. The soluble (supernatant) and insoluble (pellet) fractions were collected after centrifugation at 5200 rpm for 30 minutes at 4ºC. The soluble supernatant was transferred to a 1.5 ml Eppendorf and the insoluble pellet washed once with homogensiation buffer and re-pelleted at 5200 rpm for 20 minutes at 4ºC. Insoluble pellets were resuspended in 60µl of urea (6 M) and sonicated at 10,000 kHz for 10 seconds. Fractions were mixed with equal volume of 2x concentrated Laemmli's sample buffer, heated at 100ºC for 10 minutes, and subsequently analysed by SDS-PAGE.

2.12. Immunocytochemistry

SH-SY5Y and human dermal fibroblast cells were grown on glass 8-well Lab-Tek II chamber slides (Nalge Nunc International Corp.) or 12-well plates until 80% confluent or 24-48 hours post-transfection. After washing three times in PBS, cells were treated with 3.7% (v/v) paraformaldehyde for 20 minutes to fix the cells, followed by PBS with

0.2% (v/v) Triton X-100 for 5 minutes to permeabilise the cell membranes. The cells were washed in PBS, and then blocked in 0.02% (v/v) Triton X-100 containing 10% (v/v) normal goat serum (NGS) and 1% (w/v) bovine serum albumin (BSA), hereafter called Buffer A, for 45 minutes. After blocking the cells were incubated with primary antibodies (Table 2.10) at the appropriate concentration in Buffer A for 2 hours. After incubation with primary antibodies the cells were washed three times in PBS and then incubated with species-specific secondary antibodies (Table 2.11) in Buffer A for 45 minutes. After two washes in PBS, the cells were briefly (1 minute) incubated with 2mg/ml 4',6-diamidino-2-phenylindole dihydrochloride (DAPI, Sigma, Poole, UK) to counterstain nuclei and then washed twice in PBS. Fluorescent mounting medium (Dako, Ely, UK) was used to apply coverslips to slides, or in the case of chamber slides, the chamber was removed from the slide and fluorescent mounting medium (Dako, Ely, UK) was used to apply cover glass.

2.12.1. MitoTracker

MitoTracker (Life Technologies, Paisley, UK) is a cell permeant mitochondrial probe that stains the mitochondria within cells. A stock solution was initially prepared by dissolving 50µg of lyophilised marker in DMSO to a concentration of 1mM. This was then stored at -20°C. The excitation and emission maxima are given as 579 nm and 599 nm, respectively, by Life Technologies. The stock MitoTracker solution was diluted to a working concentration of 100nM in complete medium (DMEM, 10% (v/v) FBS, 1% (v/v) Pen/Strep). MitoTracker was added to the cells and incubated for 30 minutes at 37ºC in 5% CO_2 atmosphere. After washing twice in PBS, cells were treated with 3.7% (v/v) paraformaldehyde for 20 minutes to fix the cells. Immunocytochemistry was then performed as above.

Table 2.10. Primary antibodies used in immunoblotting and immunocytochemistry

Antibody	Species	Dilution	Company
Acetylated-α-tubulin (monoclonal, 6-11B-1)	Mouse	1:2000 (IC) 1:2000 (IB)	Sigma, Poole, UK
Arl13b (polyclonal)	Rabbit	1:500 (IC)	Proteintech, Manchester, UK
β-actin (monoclonal, AC-15)	Mouse	1:10000 (IB)	Sigma, Poole, UK
β-tubulin (monoclonal, TUB 2.1)	Mouse	1:200 (IC) 1:500 (IB)	Sigma, Poole, UK
BiP (monoclonal, C50B12)	Rabbit	1:300 (IB)	Cell Signaling Technology, Danvers, MA, USA
Calnexin (monoclonal, 37)	Mouse	1:1000 (IB)	BD Biosciences, Oxford, UK
DRP1 (monoclonal, 8/DLP1)	Mouse	1:500 (IB) 1:100 (IC)	BD Biosciences, Oxford, UK
DCTN6 (polyclonal)	Rabbit	1:500 (IB)	Atlas Antibodies, Stockholm, Sweden
FLAG (monoclonal, M2)	Mouse	1:1000 (IB) 1:250 (IC)	Sigma, Poole, UK
EEA1 (monoclonal, 14)	Mouse	1:100 (IC)	BD Biosciences, Oxford, UK
GAPDH (polyclonal)	Rabbit	1:5000 (IB)	Abcam, Cambridge, UK
GFP (monoclonal, GFP-20)	Mouse	1:2000 (IB)	Roche, Burgess Hill, UK
GS28 (monoclonal, HFD9)	Mouse	1:500 (IC)	Enzo Life Sciences, Exeter, UK
HSP60 (monoclonal, LK1)	Mouse	1:500 (IB)	Sigma, Poole, UK
HSP70 (monoclonal, BRM-22)	Mouse	1:5000 (IB) 1:100 (IC)	Sigma, Poole, UK
HSP90 (polyclonal)	Rabbit	1:100 (IC)	Abcam, Cambridge, UK
KDEL (monoclonal, 10C3)	Mouse	1:1000 (IB)	Stressgen, Ann Arbor, MI, USA
LAMP-2 (monoclonal, H4B4)	Mouse	1:5000 (IB) 1:100 (IC)	Santa Cruz, Santa Cruz, CA, USA
p62/SQSTM1 (polyclonal)	Mouse	1:1000 (IB) 1:100 (IC)	Abcam, Cambridge, UK
Sacsin (monoclonal, EPR11864)	Rabbit	1:1600 (IB) 1:100 (IC)	Abcam, Cambridge, UK
TOM20 (polyclonal)	Rabbit	1:1000 (IB)	Santa Cruz, Santa Cruz, CA,

		1:500 (IC)	USA
Ubiquitin (polyclonal)	Rabbit	1:500 (IB) 1:100 (IC)	Abcam, Cambridge, UK
V5 (monoclonal, V5-10)	Mouse	1:1000 (IB)	Sigma, Poole, UK
Vimentin (monoclonal, Vim 3B4)	Mouse	1:2000 (IB) 1:100 (IC)	Abcam, Cambridge, UK
Vimentin (monoclonal, SP20)	Rabbit	1:2000 (IB) 1:100 (IC)	Abcam, Cambridge, UK

IB = Immunoblotting, IC = Immunocytochemistry

Table 2.11. Secondary fluorescent antibodies used in immunoblotting and immunocytochemistry

Antibody	Emission	Species	Dilution	Company
Alexa Fluor 488	Green	Mouse/rabbit	1:1000	Life Technologies, Paisley, UK
Alexa Fluor 568	Red	Mouse/rabbit	1:1000	Life Technologies, Paisley, UK
Alexa Fluor 647	Far-red	Mouse/rabbit	1:1000	Life Technologies, Paisley, UK
DAPI[1]	Blue	n/a	1:5000	Sigma, Poole, UK
MitoTracker Red CMXRos	Red	n/a	100nM	Life Technologies, Paisley, UK
ActinGreen 488 ReadyProbes	Green	n/a	2 drops/ml	Life Technologies, Paisley, UK
TMRM[2]	Red	n/a	10nM	Life Technologies, Paisley, UK
IRDye®680LT	Far-red	Mouse	1:5000	Life Technologies, Paisley, UK
IRDye®800CW	Far-red	Rabbit	1:5000	Life Technologies, Paisley, UK

[1] DAPI = 4','6-diamido-2-phenylindole stain
[2] TMRM = Tetramethylrhodamine, Methyl Ester, Perchlorate

2.13. Confocal Microscopy

Cells stained for various intracellular markers were visualised and imaged using the Zeiss LSM510 inverted laser scanning confocal microscope (Carl Zeiss Ltd, UK). Super resolution microscopy of sacsin localisation was performed using a Zeiss LSM710 ELYRA PS.1 (Carl Zeiss Ltd, UK). Images were taken using a 63x oil immersion objective. The pinhole was set to 1 Airy unit, with Cy2 green fluorophore detected by the 458 nm Argon laser, Cy3 red fluorophore detected by the 543 nm HeNe laser, Cy5 far-red fluorophore detected by the 633 nm HeNe laser, and blue wavelengths, such as that emitted by DAPI, detected by the 405 nm Diode laser. Images were acquired at 1024 x 1024 pixels; 8-line averaging, and 12-bit depth. Image processing was performed using Zen 2009 software (Carl Zeiss Ltd, UK), and Imaris (Biplane, Switzerland). Maximum intensity projection images of Z-stacks were also produced using the Zen software.

Fluorescence recovery after photobleaching (FRAP) was performed using the 63x oil immersion objective, a scan area of 512 x 512 pixels, 12-bit depth, 1-line averaging and the 458 nm argon laser power was 100%. Photobleaching of a 15 x 15 μm area was started after 2 or 3 scans.

Tetramethylrhodamine methyl ester (TMRM) fluorescence analysis was performed using the 63x oil immersion objective, a scan area of 512 x 512 pixels, 12-bit depth, 2-line averaging and the gain in the red channel was 405 and the digital offset -1.36.

2.14. Statistics

Where mean values are presented, error bars represent ± SEM. An unpaired two-tailed Student's *t-test* was performed in excel to compare means between two conditions, for example *SCRM* vs. *DCTN6* siRNA. P-values <0.05 were considered to be statistically significant.

CHAPTER 3: DISRUPTED MITOCHONDRIAL FISSION IN ARSACS

3.1. Introduction and Aims

Disruption to mitochondrial morphology has recently been implicated in ARSACS disease pathogenesis. Specifically, an elongated and interconnected mitochondrial network is observed in ARSACS patient fibroblasts (Criscuolo et al., 2015, Blumkin et al., 2015, Pilliod et al., 2015, Girard et al., 2012), *SACS* knockout mouse neurons (Lariviere et al., 2015), and *SACS* knockdown cells (Girard et al., 2012). This mitochondrial phenotype is suggestive of perturbed mitochondrial dynamics, more specifically reduced fission or enhanced fusion. Reduced fission seems a more likely mechanistic explanation of the ARSACS mitochondrial phenotype, since a co-IP experiment performed in our lab identified that a heterologously expressed N-terminal portion of sacsin (amino acids 1-1368) interacted with DRP1, the main mediator of mitochondrial fission in mammalian cells (Girard et al., 2012). Furthermore, immunocytochemistry analysis revealed that sacsin localisation partially overlaps with DRP1 foci at mitochondria (Girard et al., 2012). This data suggests a potential role for sacsin in mitochondrial fission.

For mitochondrial fission to occur, DRP1, which mainly exists as small oligomers in the cytosol, is recruited to the outer mitochondrial membrane (OMM). The mechanisms and regulation of DRP1 recruitment to mitochondria are not yet fully understood in mammalian cells (Otera and Mihara, 2011). FIS1 and MFF are thought to be important in facilitating DRP1 recruitment onto mitochondria (Loson et al., 2013; Otera et al., 2010; Yoon et al., 2001b). Other factors, such as, mitochondrial dynamics protein of 49kDa and 51kDa (MiD49 and MiD51, respectively), and the mitochondrial E3 ubiquitin ligase MARCH5 (Karbowski et al., 2007) are also known to regulate DRP1 recruitment/activation (Palmer et al., 2011).

Once recruited to the OMM, DRP1 self-assembles into larger multimeric structures at discrete foci and forms spirals around the outside of mitochondria (Chang and Blackstone, 2010; Yoon et al., 2001b; Smirnova et al., 2001). This is mediated by the coiled-coil domain (Okamoto et al., 1999) and is driven by GTP hydrolysis-dependent conformational change. Mitochondrial fission is then thought to occur through spiral constriction of the DRP1 ring (Hoppins et al., 2007; Mears et al., 2011; Smirnova et al., 2001; Strack and Cribbs, 2012). This resembles the action of dynamin at sites of endocytosis. Dynamin, along with its accessory proteins, assembles into a fission complex, which begins constriction of the clathrin-coated pit neck. The assembled

dynamin polymer then undergoes GTP-dependent conformational changes that constrict the neck further and lead to plasma membrane fission (Hinshaw, 2000; Ingerman et al., 2005; Sundborger and Hinshaw, 2014).

To gain further mechanistic insights into how loss of sacsin function modulates mitochondrial dynamics, our lab has previously performed a yeast two-hybrid (Y2H) screen using residues 1-649 of sacsin as bait. This identified dynactin-6 (DCTN6) to be a putative sacsin interactor. DCTN6, also known as p27, is a component of the dynein-dynactin motor complex, which drives retrograde transport of various cargoes, including mitochondria, on microtubules (section 1.8.1.1). Interestingly, this motor complex has previously been shown to be required for the recruitment of DRP1 to mitochondria (Varadi et al., 2004). Varadi *et al* (2004) found that overexpressing dynamitin (p50), another subunit of the dynein-dynactin complex, lead to a collapsed mitochondrial phenotype, with long, interconnected mitochondria, which is accompanied by a large reduction in the association of DRP1 with mitochondria. Additionally, mutations in another dynactin subunit, $p150^{Glued}$, were shown to lead to a similar mitochondrial phenotype (Levy et al., 2006). These studies indicate that the dynein-dynactin complex is involved in DRP1 recruitment to mitochondria and thus, mitochondrial fission.

Since putative interactions have been identified between both sacsin and DRP1, and sacsin with DCTN6; this indicates the potential for a joint function between sacsin and the dynein-dynactin complex in the recruitment of DRP1 to mitochondria. To test this hypothesis, several approaches were taken. Initially, interactions between sacsin, DRP1 and DCTN6 were further investigated by co-immunoprecipitation (co-IP) experiments. Secondly, a role for sacsin in the mitochondrial translocation of DRP1 and its assembly into scission complexes was investigated through *SACS* siRNA knockdown experiments. Thirdly, it is hypothesised that changes in DCTN6 expression may also lead to alterations in mitochondrial morphology and dynamics like that shown for sacsin and other subunits of the dynein-dynactin complex. So, the effects of DCTN6 overexpression and siRNA knockdown on mitochondrial morphology and DRP1 localisation were investigated using confocal microscopy. The objective was to further establish the cellular mechanisms contributing to the highly elongated and interconnected mitochondrial network seen in ARSACS.

3.2. Results

3.2.1. Identification of an interaction between DRP1 and DCTN6

As it is hypothesised that sacsin and DCTN6 could form a complex, possibly with DRP1, interactions between these three proteins were further investigated. A direct interaction between sacsin and DCTN6 could not be verified by co-IP due to technical issues related to the available reagents. Specifically, a FLAG-tagged construct encoding residues 1–1368 of sacsin, which was used to detect a putative interaction with DRP1 (Girard et al., 2012), was no longer available and attempts to reproduce this construct failed. Sacsin and DCTN6 antibodies were also not suitable for use in immunoprecipitation (IP) experiments.

Full-length DCTN6 vectors with a GFP- or 3xFLAG-tag were constructed to carry out heterologous expression experiments to investigate a predicted interaction between DCTN6 and DRP1. An endogenous IP would be preferable but was not possible due to difficulties in the detection of DCTN6 using the available antibodies to the endogenous protein.

3.2.1.1. *Verification of DCTN6-FLAG and DCTN6-GFP construct expression*

Prior to using the DCTN6-FLAG and DCTN6-GFP constructs (generation of constructs is detailed in section 2.8.1), confirmation that cells expressed a protein of the predicted size was performed. SH-SY5Y cells were transfected with either construct, and after 48 hours cell lysates were analysed by immunoblotting. Specific bands of approximately 24 kDa and 48 kDa for DCTN6-FLAG and DCTN6-GFP (Figure 3.1), which are the respective predicted molecular weights of these fusion proteins, were detected.

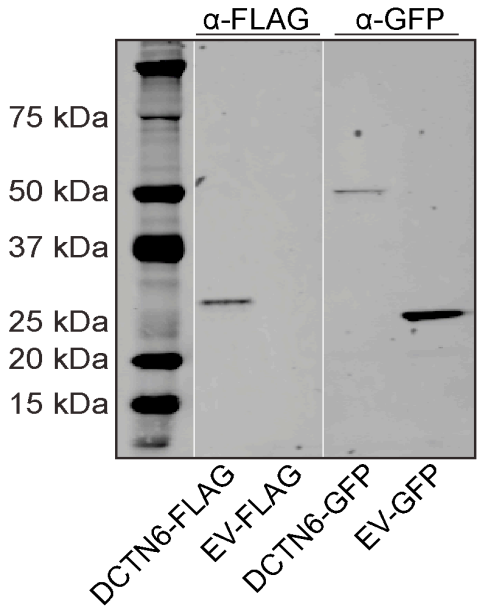

Figure 3.1. Verification of DCTN6-FLAG and DCTN6-GFP expression. Immunoblot analysis of SH-SY5Y cells transfected with DCTN6-FLAG (~24 kDa) or DCTN6-GFP (~48 kDa). The corresponding tagged empty vector (EV) constructs were transfected as controls.

3.2.1.2. *Co-immunoprecipitation between DRP1 and DCTN6*

SH-SY5Y cells were transiently transfected with a FLAG-tagged construct expressing DCTN6 and/or a GFP-tagged construct expressing DRP1, or were transfected with an empty FLAG or empty GPF vector (controls). 24 hours post transfection; cells were chemically crosslinked using dithiobis[succinimidylpropionate] (DSP; Pierce, Rockford, IL, USA) and lysed. Following this, cell lysates were incubated with anti-FLAG magnetic beads overnight.

Immunoblot analysis of inputs (Figure 3.2) shows specific bands corresponding to endogenous DRP1 (monomeric ~80 kDa, oligomeric ~240 kDa), along with successful transfection of DCTN6-FLAG (~24 kDa) and DRP1-GFP (monomeric ~107 kDa, oligomeric ~270 kDa). Immunoblot analysis of immunoprecipitated lysates (Figure 3.2) shows that the anti-FLAG magnetic beads successfully captured DCTN6-FLAG. Importantly, distinct bands were revealed, which correspond to monomeric DRP1-GFP (~107 kDa) and oligomeric DRP1-GFP (~270 kDa) in the immunoprecipitated sample that was dual transfected with DCTN6-FLAG and DRP1-GFP (indicated by arrows in figure 3.2). These bands are absent in the control samples. The DRP1 antibody

recognises some strong non-specific bands between 70-85 kDa (¶ in figure 3.2). This is unlikely to be the antibody heavy chain, which is approximately 50 kDa, but is possibly non-specific protein binding to the beads. This obscures endogenous monomeric DRP1 in immunoprecipitated samples; hence an interaction between endogenous DRP1 and DCTN6-FLAG cannot be reliably determined here. In summary, this data shows an interaction between DCTN6-FLAG and DRP1-GFP by co-IP. This interaction may be transient, since the experiment was carried out under cross-linking conditions, which stabilises labile interactions.

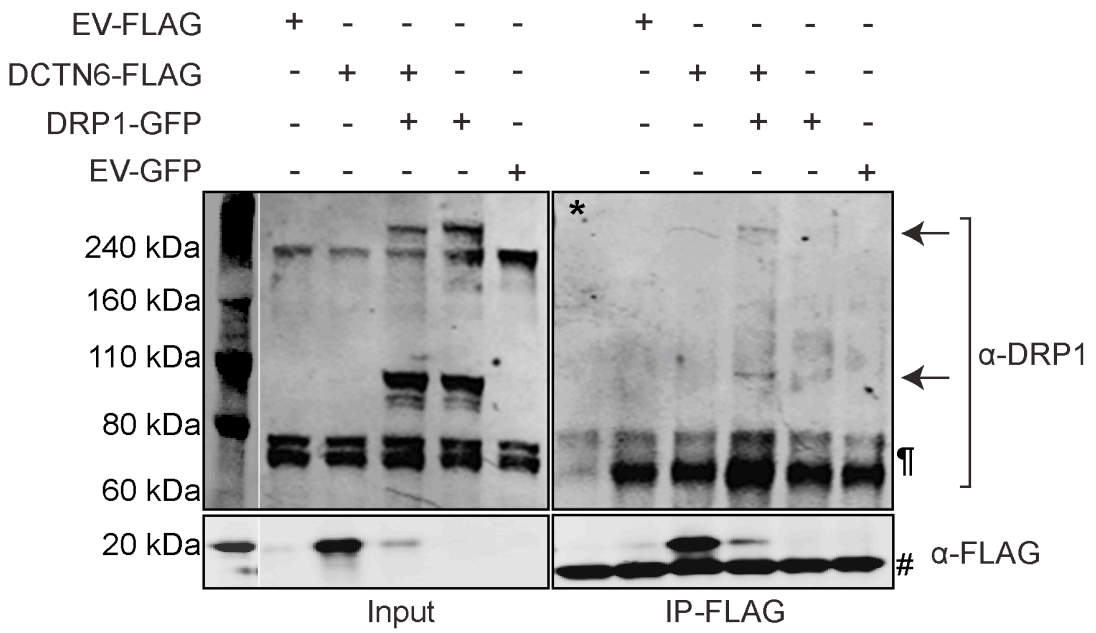

Figure 3.2. Co-IP of DCTN6-FLAG and DRP1-GFP. SH-SY5Y cells were transfected with a FLAG-tagged construct encoding DCTN6 and/or a GFP-tagged construct encoding DRP1. Transfections of empty vectors (EV) were also performed as controls. Immunoprecipitation (IP) was performed with FLAG-tagged magnetic beads, and immunoblots were performed with anti-FLAG or anti-DRP1 antibodies. The inputs of DCTN6-FLAG and DRP1 are indicated (endogenous monomeric and oligomeric DRP1 are ~80 kDa and ~240 kDa, respectively). Arrows indicate monomeric and oligomeric DRP1-GFP (~107 kDa and ~270 kDa, respectively). *Negative IP control, ♯ antibody light chain, ¶ non-specific bands.

3.2.2. A role for sacsin in the mitochondrial translocation of DRP1

Since a putative interaction between sacsin and DRP1 has previously been identified, siRNA-mediated knockdown was used to investigate the effect of loss of sacsin on the mitochondrial localisation of DRP1 and on the assembly of DRP1 multimeric complexes.

3.2.2.1. *Sacsin expression can be reduced in SH-SY5Y cells by siRNA*

SH-SY5Y neuroblastoma cells were transiently transfected with a combination of previously validated siRNA molecules to sacsin exons 7, 8 and 10 (*SACS*) or a scrambled non-targeting siRNA (*SCRM*) control. Mito-DsRed was used to identify transfected cells. It is assumed that the cells expressing Mito-DsRed will also be transfected with siRNA. Immunocytochemistry followed by confocal imaging, reverse transcription PCR (RT-PCR) and immunoblot analyses of cell lysates transfected with each siRNA were used to confirm effective knockdown of sacsin (Figure 3.3). A commercially available sacsin antibody was used (this reagent was not used in previous work from our lab as it was not available), which binds to a specific sequence within amino acids 4100-4200 (Abcam). This antibody also detects a fainter band on immunoblotting, which is around 450 kDa (Figure 3.3B). This may be an alternatively spliced isoform of sacsin, although no experimental evidence exists for this. Originally, sacsin was thought to be encoded by a single gigantic exon (now exon 10), which contains an ATG initiation codon; hence this may be responsible for the lower molecular weight protein product. The confocal images also confirm the previously identified localisation of a proportion of sacsin at or near the cytoplasmic face of mitochondria (Figure 3.3A).

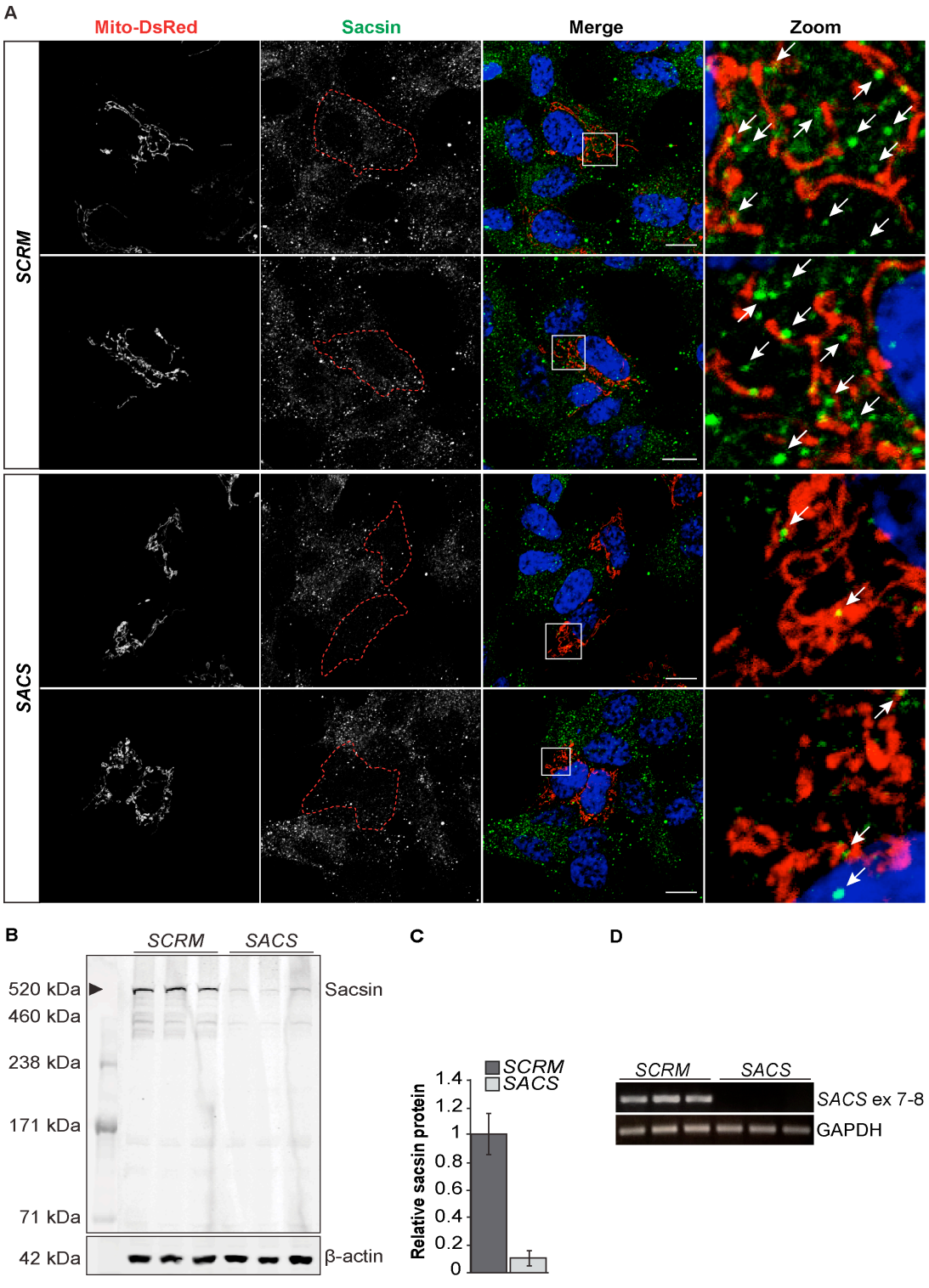
A
Mito-DsRed
Sacsin
Merge
Zoom
SCRM
SACS
B
SCRM
SACS
520 kDa
460 kDa
238 kDa
171 kDa
71 kDa
42 kDa
Sacsin
β-actin
C
SCRM
SACS
Relative sacsin protein
1.4
1.2
1
0.8
0.6
0.4
0.2
0
D
SCRM
SACS
SACS ex 7-8
GAPDH

Figure 3.3. Cellular levels of sacsin can be significantly reduced by targeting *SACS* with siRNAs. SH-SY5Y cells were transfected with siRNA to *SACS* exons 7, 8 and 10, or a *SCRM* siRNA control, and after 48 hours cells were analysed for *SACS* mRNA and protein expression. **(A)** Representative images of cells transfected with Mito-DsRed and either *SCRM* or *SACS* siRNA. Cells were fixed and stained with a rabbit anti-sacsin antibody. Maximum intensity projections of z-stacks were taken via confocal microscopy. The white box in the merged panel is shown zoomed in the panel on the far right, and white arrows indicate sacsin puncta. Red dashed lines in the sacsin panels outline transfected cells. **(B)** Immunoblot analysis was performed using the rabbit anti-sacsin antibody, along with β-actin as a loading control. Lane 1: HiMark pre-stained protein standard (Life Technologies). **(C)** Densitometric analysis of sacsin protein levels normalized to β-actin shows 0.9-fold reduction in *SACS* compared to *SCRM* siRNA treated cells. The full blot is shown to allow assessment of any non-specific binding by the antibody. **(D)** RT-PCR was performed using intron spanning primers for exons (ex) 7-8 of *SACS*, which reveals a reduction in *SACS* mRNA in *SACS* compared to *SCRM* siRNA treated cells. GAPDH was used as a control.

3.2.2.2. *Reduced levels of mitochondrial associated DRP1 in sacsin deficient cells*

DRP1 localisation in relation to the mitochondrial network was investigated in sacsin deficient cells compared to controls by immunocytochemistry. SH-SY5Y cells were transfected with Mito-DsRed and either *SCRM* or *SACS* siRNA. 48 hours after transfection, cells were treated with vehicle control or 20 μM of the mitochondrial uncoupler carbonyl cyanide m-chlorophenylhydrazone (CCCP) for 40 minutes. CCCP is one of the most widely used protonophore uncouplers, along with 2,4-Dinitrophenol (Kenwood et al., 2014). It causes dissipation of the proton gradient across the inner mitochondrial membrane, which is used to drive ATP synthesis in oxidative phosphorylation, leading to mitochondrial membrane depolarisation and mitochondrial fission. Possible off-target effects of these uncouplers are plasma membrane depolarisation, mitochondrial inhibition, and cytotoxicity (Kenwood et al., 2014; Park et al., 2002), which may interfere with the measurement of mitochondrial function. Other know inducers of mitochondrial fission include the mitochondrial complex I inhibitor, Rotenone (Barsoum et al., 2006; Hwang et al., 2014), and Oligomycin, an inhibitor of mitochondria ATP synthase (De Vos et al., 2005; Guillery et al., 2008).

Following treatment, cells were processed for immunocytochemistry, as detailed in the methods, using an anti-DRP1 antibody. Cells were imaged using confocal microscopy (Figure 3.4) and the number of DRP1 foci per micrometer (μm) of mitochondrial length was measured using the line trace function of the LSM510 confocal ZEN software (Zeiss). This gives the intensity of both the red and green channel along individual mitochondria, with green intensity peaks representing DRP1 foci. The number of DRP1 foci along the measured mitochondria length was then collated from the graphical and tabular output. Ten cells per siRNA condition and six mitochondria per cell (total of 60 mitochondria per condition) were measured. Two or three independent sets of cells, transfected on different days, were analysed. The number of DRP1 foci per μm of mitochondria significantly decreased in *SACS* cells compared to *SCRM*, decreasing from 0.91 ± 0.03 to 0.75 ± 0.02 (Figure 3.4). Inducing mitochondrial fission with CCCP significantly increased the number of DRP1 foci per μm of mitochondria in *SCRM* cells from 0.91 ± 0.03 to 1.41 ± 0.05, and hence mitochondrial fragmentation. Despite a significant increase in DRP1 foci per μm of mitochondria in *SACS* cells in response to CCCP mediated induction of mitochondrial fission, there was still a significant reduction in mitochondrial associated DRP1 foci incidence compared to *SCRM* siRNA

controls (0.86 ± 0.03 for *SACS*, compared to 1.41 ± 0.05 for *SCRM*, Figure 3.4).

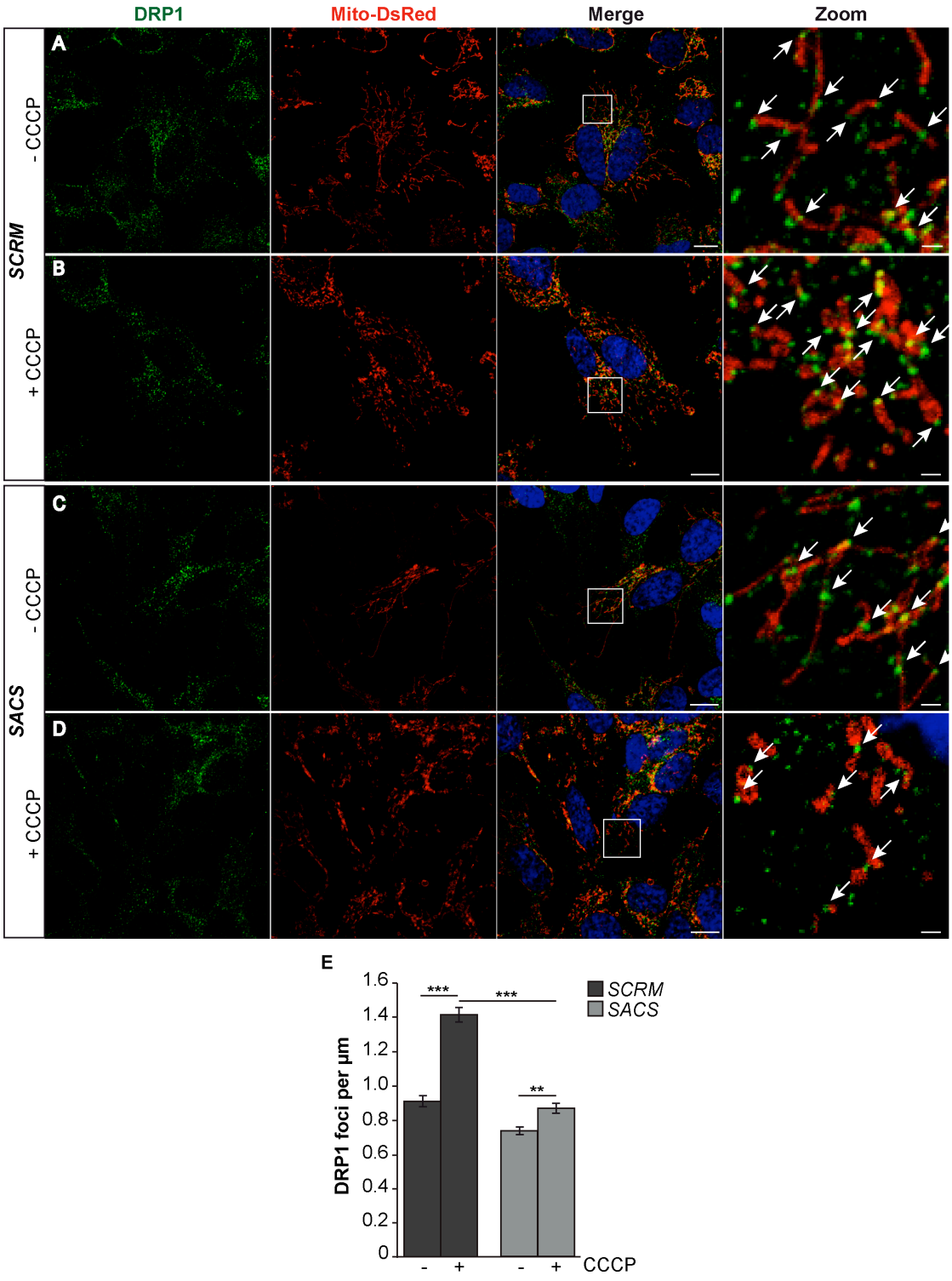

Figure 3.4. Reduced mitochondrial localisation of DRP1 in sacsin knockdown cells. Representative confocal images of SH-SY5Y cells transfected with Mito-DsRed and either **(A, B)** *SCRM*, or **(C, D)** *SACS* siRNA, all treated with either vehicle control or 20 μM CCCP for 40 minutes. 48 hours post transfection; cells were fixed and stained with an anti-DRP1 antibody (green). The white box in the merged panel is shown zoomed in the panel on the far right. White arrows indicate DRP1 foci in close proximity to mitochondria. The number of DRP1 foci on mitochondria was measured using ZEN software. **(E)** Quantification of the mean number of DRP1 foci per μm of mitochondria in *SCRM* and *SACS* cells. Ten cells per siRNA condition and six mitochondria per cell (total of 60 mitochondria per condition) were measured in at least two independent experiments. Error bars represent SEM, *** = $p<0.001$, ** = $p<0.01$. Scale bars = 10μm and 1μm in merged and zoom panels, respectively.

This observation of reduced DRP1 localisation to mitochondria in sacsin deficient cells was further investigated by subcellular fractionation of SH-SY5Y cells transfected with either *SACS* or *SCRM* siRNA. Briefly, 48 hours after transfection, cells were lysed and homogenized before centrifugation to separate nuclei and cell debris from the cytosol. The cytosolic fraction was then subjected to further centrifugation to create a mitochondrial pellet (detailed in section 2.11). After immunoblot analysis, total DRP1 levels were found to be similar in cells treated with *SCRM* control or *SACS* siRNA. However, DRP1 was present in the mitochondrial fraction at a reduced level in cells treated with *SACS* siRNA compared to *SCRM* siRNA (Figure 3.5), which supports the immunocytochemistry data in figure 3.4. This result was consistently observed, however was difficult to quantify due to variability between immunoblots from different experiments.

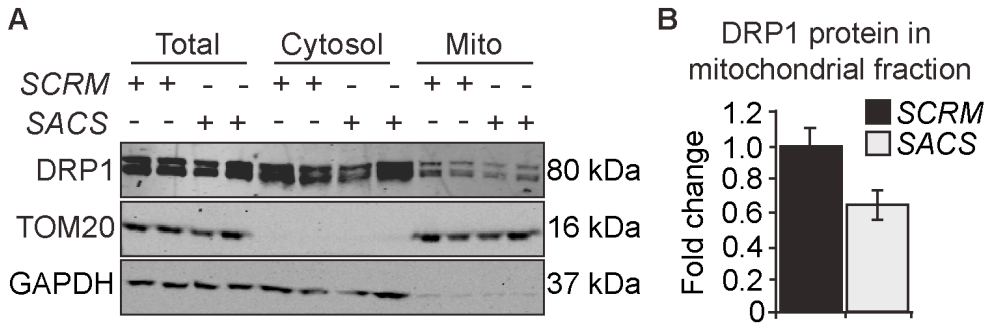

Figure 3.5. Reduced DRP1 in the mitochondrial fraction of sacsin knockdown cells. **(A)** Representative immunoblot of SH-SY5Y cells transiently transfected with *SACS* or *SCRM* siRNA and subjected to subcellular fractionation. Transfections were performed in duplicate. Analysis with antibodies to TOM20 (mitochondria) and GAPDH (cytosol) confirmed that the fractionation protocol had enriched mitochondrial (mito) proteins. **(B)** Densitometric analysis of DRP1 levels in the mitochondrial fraction relative to TOM20 shows a 0.35-fold reduction in *SACS* compared to *SCRM* siRNA treated cells (n = 2).

3.2.2.3. *Reduction in higher order DRP1 complexes in sacsin deficient cells*

Since a reduction in DRP1 mitochondrial localisation has been identified in sacsin deficient cells, it is hypothesised that there may be a reduction in DRP1 self-assembly into multimeric structures on the OMM. This was investigated in SH-SY5Y cells by siRNA knockdown. Following transfection of *SACS* or *SCRM* siRNA, cells were subjected to chemical cross-linking using DSP. Cells were lysed and a non-reducing sample buffer (without the reducing agent 2-Mercaptoethanol, 2-ME) was added to lysates. This approach was similar to that used by Cho *et al.* for detecting oligomeric DRP1 (Cho et al., 2014). Immunoblot analysis using an anti-DRP1 antibody revealed several high molecular weight DRP1 complexes (>230kDa, Figure 3.6). Cells transfected with *SACS* siRNA showed a reduction in the higher molecular weight DRP1 complexes when compared to *SCRM* controls (Figure 3.6). Expression of monomeric (~80 kDa) and lower order oligomeric (dimer and tetramer) DRP1 shows similar levels in *SCRM* and *SACS* siRNA treated cells. The reduction in the higher molecular weight DRP1 complexes may reflect an absence of DRP1:sacsin complexes, but could also indicate that DRP1 higher order oligomers, or complexes between DRP1 and other components of the fission machinery are reduced.

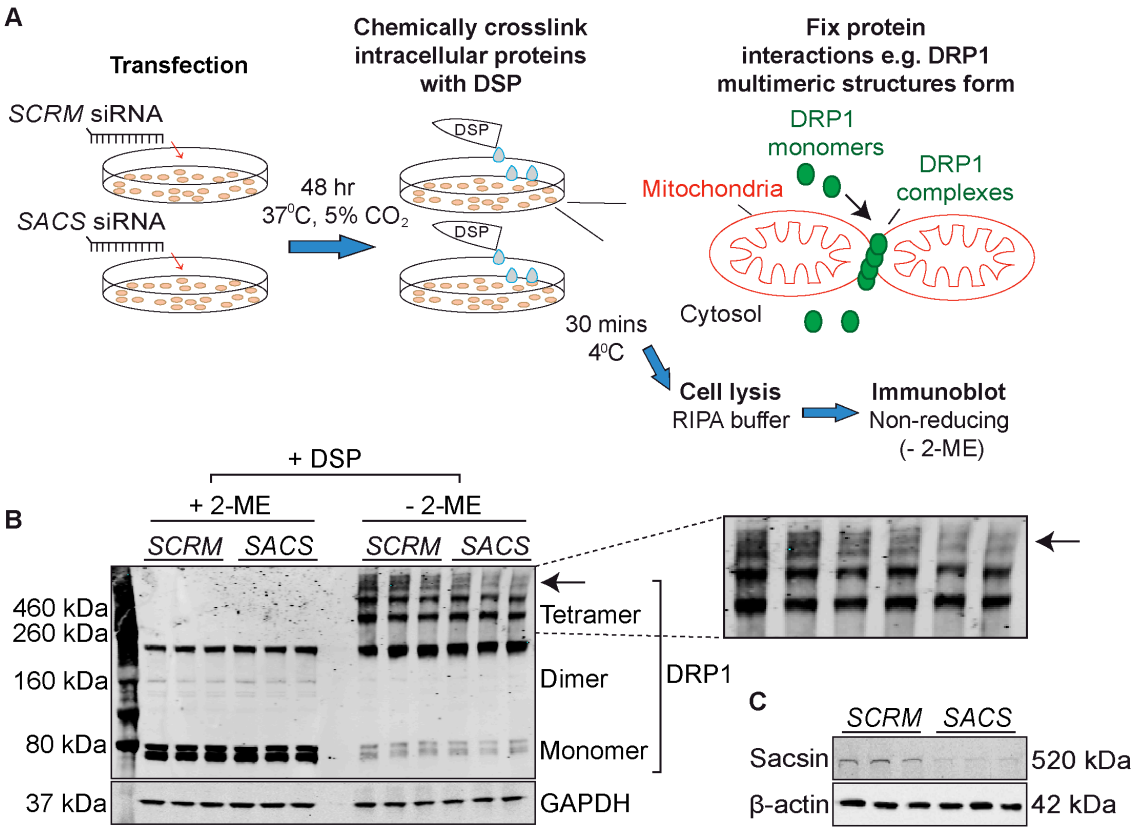

Figure 3.6. Reduced higher molecular weight DRP1 complexes in sacsin knockdown cells. (A) Schematic of the method to detect DRP1 complexes. **(B)** Representative immunoblot showing high molecular weight DRP1 complexes are reduced in sacsin knockdown cells. SH-SY5Y cells were transfected with *SACS* or *SCRM* siRNA. After 48 hours cells were treated with the crosslinker DSP and lysed. Total cell lysates were immunoblotted under reducing (+ 2-ME) and non-reducing conditions (- 2-ME) for DRP1. GAPDH was used as a loading control. Arrow indicates high molecular weight DRP1 species. DSP: dithiobis[succinimidylpropionate]. **(C)** Immunoblotting for sacsin confirms effective *SACS* siRNA knockdown. β-actin was used as a loading control.

3.2.3. A role for DCTN6 in the regulation of mitochondrial fission

The identified interaction between DCTN6 and DRP1, along with previous data showing that loss of function of components of the dynein-dynactin complex leads to altered mitochondrial morphology and dynamics (Varadi et al., 2004; Levy et al., 2006), suggests that the dynein-dynactin complex may have a role in mitochondrial fission. The effect of DCTN6 expression on mitochondrial morphology has not yet been explored and was thus investigated here. Human dermal fibroblasts (HDFs) were selected for this imaging based analysis due to the mitochondrial network being more evenly distributed throughout the cell than that seen in SH-SY5Y cells.

3.2.3.1. *DCTN6 overexpression leads to mitochondrial fragmentation*

HDFs were transiently transfected with Mito-DsRed and either the empty vector pEGFP-N3 (indicated as EV-GFP from here on) or DCTN6-GFP. After 48 hours, live cell imaging was performed using a confocal microscope. Maximum intensity projections of z-stack images suggested that the mitochondrial network in cells transfected with DCTN6-GFP was more fragmented than in EV-GFP control cells (Figure 3.7).

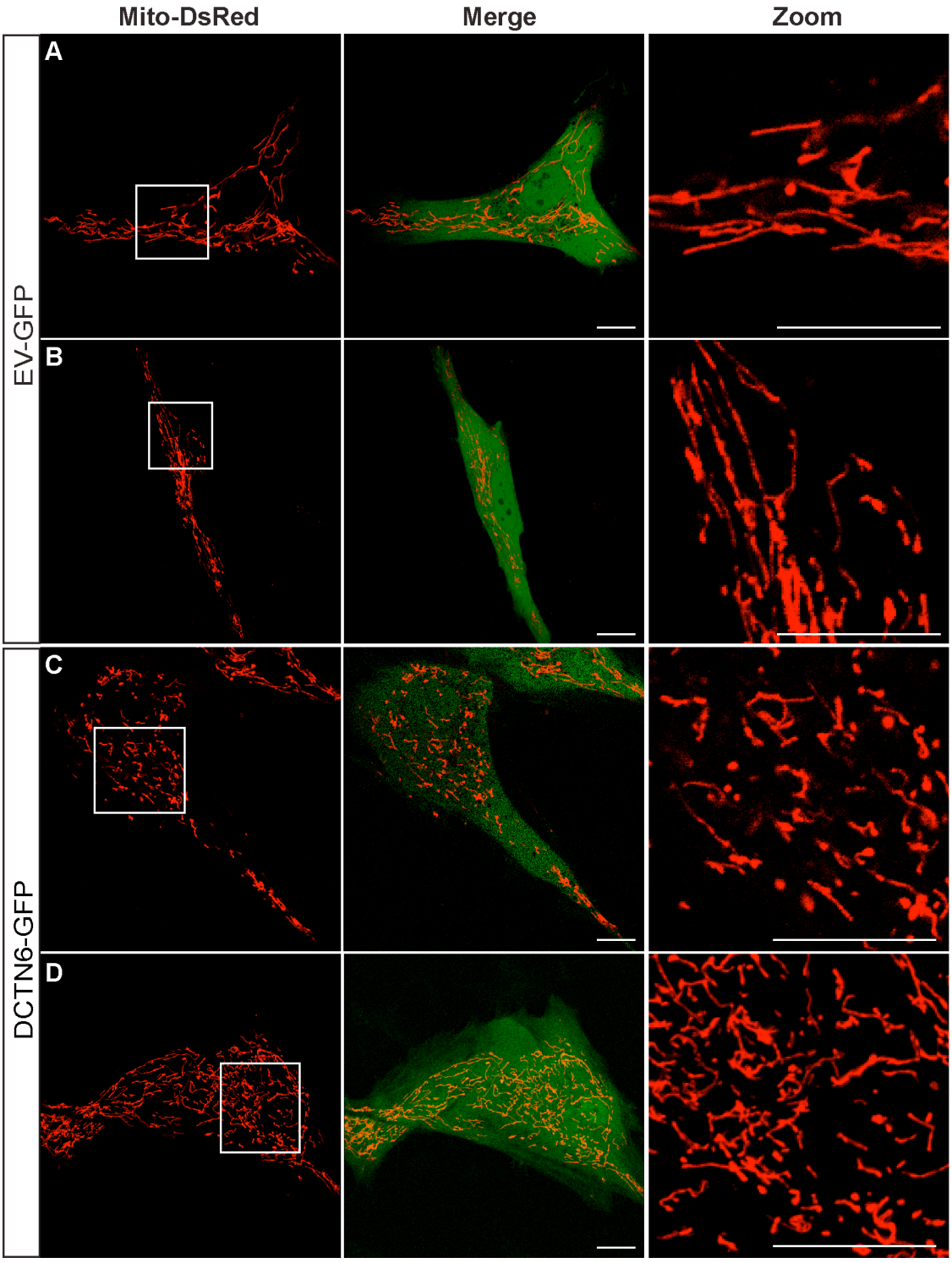

Figure 3.7. The mitochondrial network appears more fragmented in DCTN6-GFP overexpressing cells. Representative confocal images of normal HDFs transfected with mito-DsRed and either **(A, B)** EV-GFP, or **(C, D)** DCTN6-GFP. After 48 hours, maxiumum intensity projections of z-stacks were obtained by live cell confocal imaging. The white box in the mito-DsRed panel is shown zoomed in the panel on the far right. Scale bar = 10μm.

3.2.3.2. *DCTN6 siRNA knockdown leads to mitochondrial elongation*

HDFs were transfected with previously validated siRNAs targeting exons 3 and 6 of *DCTN6,* or a *SCRM* siRNA control, and incubated for 48 hours. Immunoblot analysis of cell lysates expressing each siRNA was used to confirm effective knockdown of DCTN6 protein compared to β-actin loading control. The predicted molecular weight of DCTN6 is 21 kDa (Figure 3.8). It is important to note that the anti-DCTN6 antibody used detects a non-specific band of approximately 75 kDa (Figure 3.8). The expression of this band does not reduce after DCTN6 siRNA knockdown, so is unlikely to be a DCTN6 oligomer. For this reason the antibody is not suitable for use in immunocytochemistry.

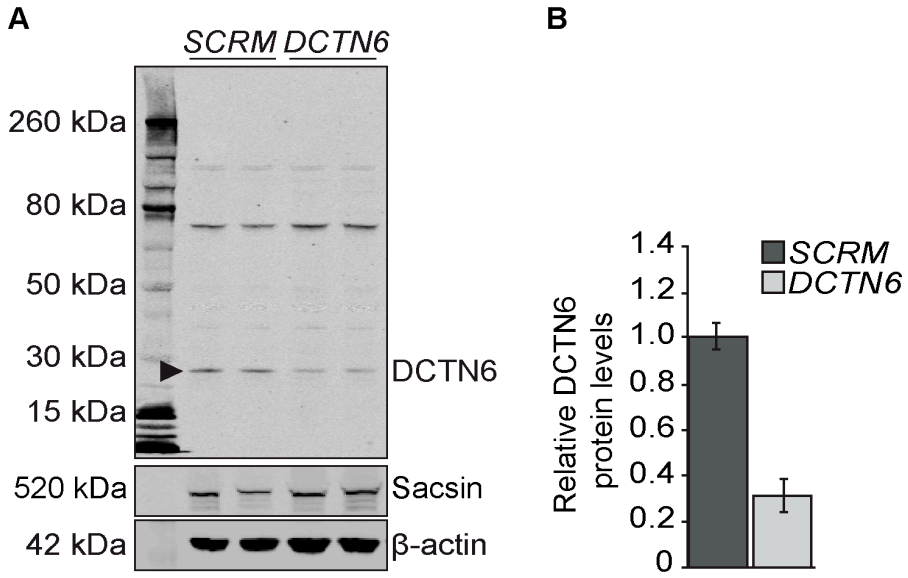

Figure 3.8. DCTN6 expression can be reduced by RNA interference using siRNA. **(A)** HDFs were transfected with siRNA to *DCTN6* exons 3 and 6, or *SCRM* siRNA control. After 48 hours cells were analysed for DCTN6 protein expression by immunoblotting using a rabbit anti-DCTN6 antibody (Proteintech). β-actin (Sigma) was used as a loading control. Arrowhead indicates the band corresponding to DCTN6 protein. Sacsin levels were not reduced by siRNA targeting DCTN6. **(B)** Densitometric analysis of DCTN6 protein levels normalised to β-actin shows 0.7-fold reduction in *DCTN6* compared to *SCRM* siRNA treated cells.

To study the effect of *DCTN6* knockdown on mitochondrial morphology, HDFs were transfected with Mito-DsRed and either *SCRM* or *DCTN6* siRNA, as detailed in the methods. After 48 hours, live cell imaging was performed using a confocal microscope. Maximum intensity projections of z-stack images showed the mitochondrial network in cells transfected with *DCTN6* siRNA appeared to be much more elongated and interconnected than in *SCRM* siRNA control cells (Figure 3.9).

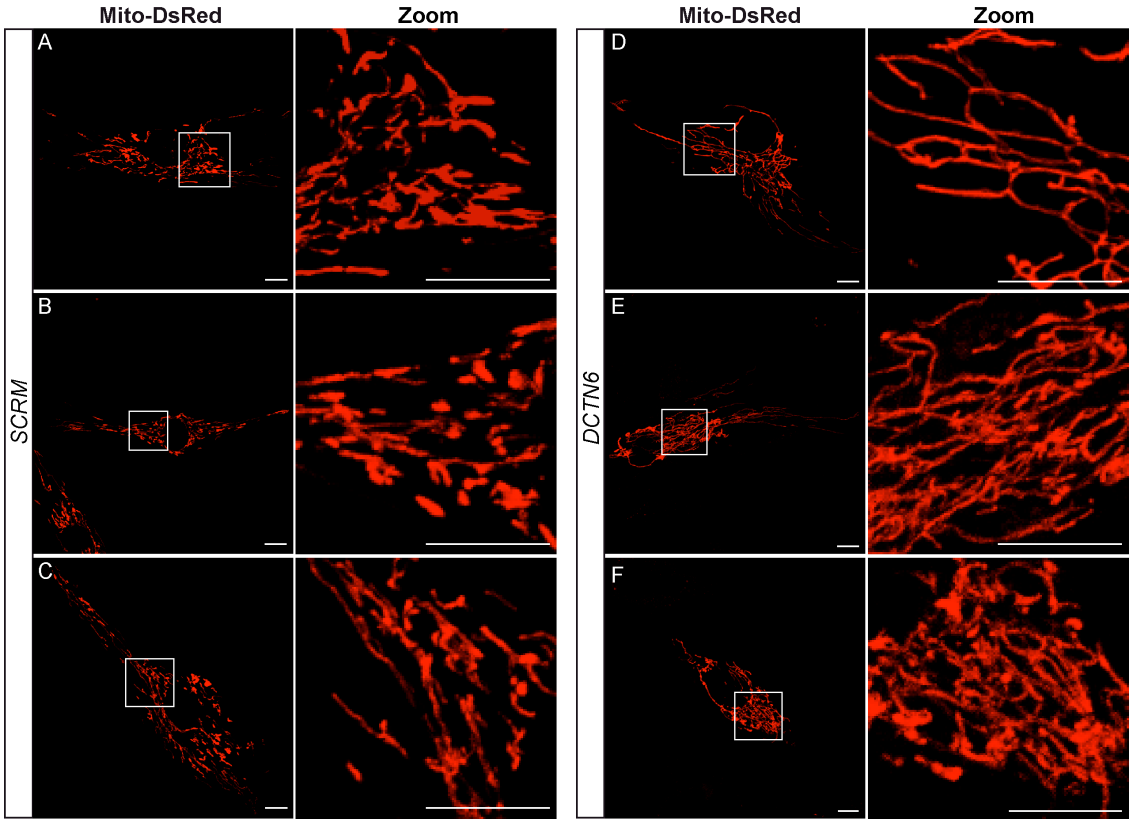

Figure 3.9. *DCTN6* knockdown leads to elongated and interconnected mitochondria. Representative confocal images of HDFs transfected with Mito-DsRed and either (**A-C**) *SCRM*, or (**D-F**) *DCTN6* siRNAs. After 48 hours, maximum intensity projections of z-stacks were taken via confocal microscopy. The white boxes in the mito-DsRed panels are shown zoomed in the panels on the right of each image. Scale bars = 10μm.

Fluorescence recovery after photobleaching (FRAP) studies have been widely used as a measure of mitochondrial dynamics (Mitra and Lippincott-Schwartz, 2010; Tanaka et al., 2010). SH-SY5Y cells were transfected with a mitochondrial-targeted GFP, in combination with either *SCRM* or *DCTN6* siRNA. After 48 hours FRAP analysis was performed on 15-20 cells for each treatment. Briefly, this involved photobleaching a small area of mitochondrial-targeted GFP (mitoGFP) within a cell and then monitoring the diffusion of the fluorescent signal within mitochondria back into the region of interest from the surrounding region. Confocal settings were kept constant for all imaging. There was a higher level of recovery from photobleaching in *DCTN6* cells compared to *SCRM* control (Figure 3.10). The mitoGFP fluorescence recovers to 71 ± 5.7 % of the initial intensity in *DCTN6* siRNA transfected cells, whereas in *SCRM* siRNA transfected cells, the fluorescence recovers to only 58 ± 6.5 % of the initial intensity after 20 seconds (Figure 3.10). This indicates a more interconnected mitochondrial network in *DCTN6* cells, as the mitoGFP can diffuse back into the bleached zone more rapidly than that seen in *SCRM* control cells.

Additional methods for quantifying this alteration in mitochondrial morphology are discussed in section 3.3.1.

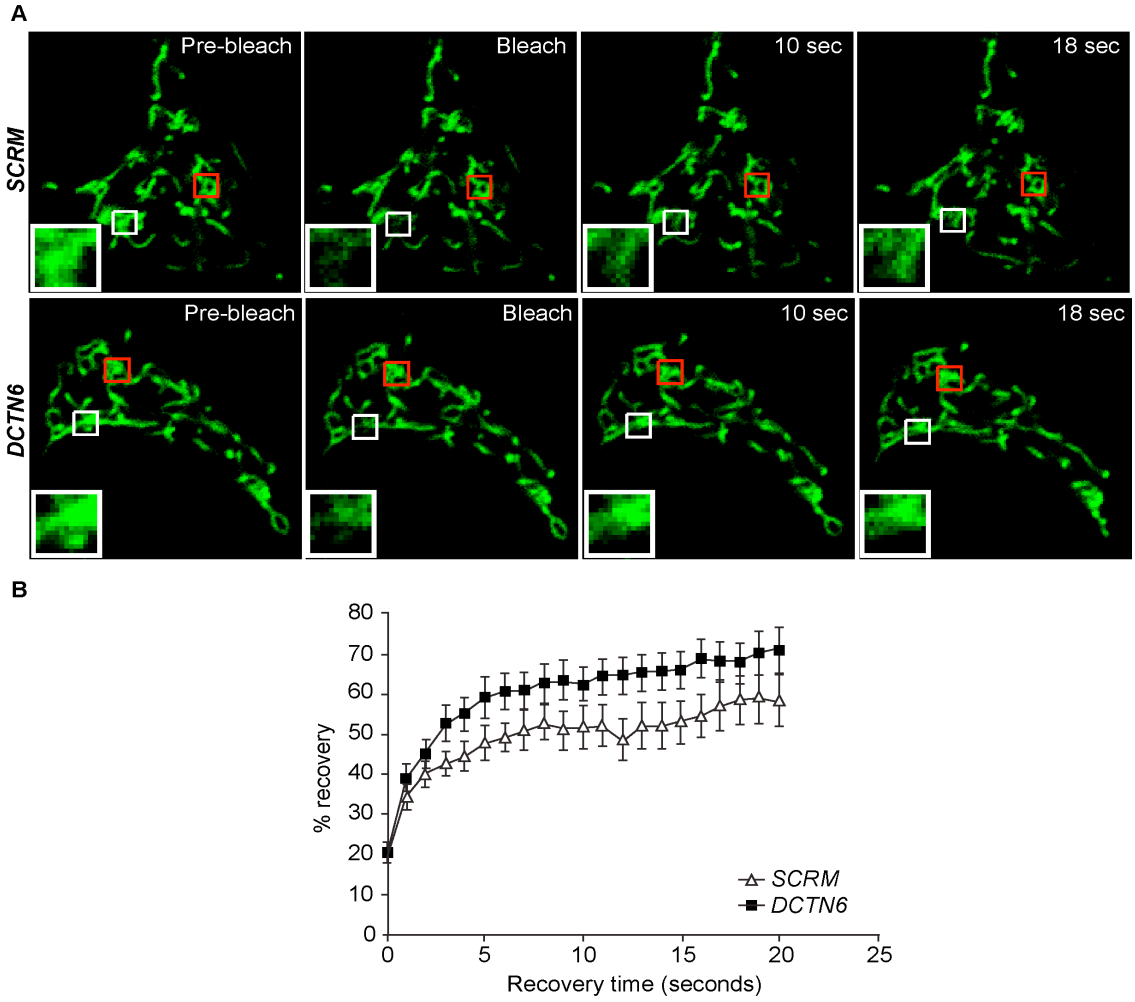

Figure 3.10. FRAP analysis of *DCTN6* knockdown cells indicates a more interconnected mitochondrial network. (A) Representative images of SH-SY5Y cells co-transfected with mitoGFP and either *SCRM* or *DCTN6* siRNA. A 15 x 15 µm area of the mitochondrial network corresponding to the white-boxed area was photobleached and the cells imaged every second for 20 seconds. Red boxes indicate a 15 x 15 µm area of the mitochondrial network not photobleached and fluorescence measurements of this area were used as a control for any loss of fluorescence over time that was not due to photobleaching. **(B)** Graphical representation of recovery after photobleaching from 15-20 cells/siRNA condition/experiment (n=3). Fluorescent intensities of the 15 x 15 µm area were normalised to pre-bleach levels at 100%. Error bars represent SEM.

3.2.4. DCTN6 knockdown leads to reduced mitochondrial localisation of DRP1

Earlier in this chapter, sacsin knockdown was demonstrated to reduce the mitochondrial localisation of DRP1 (3.2.2), which could explain the elongation of mitochondria due to reduced fission. Here, *DCTN6* knockdown also results in a more interconnected mitochondrial network, and evidence has been provided for an interaction between DCTN6 and DRP1 (Figure 3.2). Therefore, the effect of *DCTN6* siRNA knockdown on DRP1 localisation was investigated, as a reduced mitochondrial localisation of DRP1 could also explain the elongated mitochondria in this case.

SH-SY5Y cells were transfected with Mito-DsRed and either *SCRM* or *DCTN6* siRNA. 48 hours after transfection, cells were treated with vehicle control or 20 μM of the mitochondrial uncoupler CCCP for 40 minutes to induce mitochondrial fission. Cells were processed for immunocytochemistry, as detailed in the methods, using an anti-DRP1 antibody. Cells were visualized by confocal microscopy (Figure 3.11) and the number of DRP1 foci per μm of mitochondrial length was measured using the line trace function of the LSM510 confocal ZEN software, as in section 3.2.2. Ten cells per siRNA condition and six mitochondria per cell (total of 60 mitochondria per condition) were measured. At least two independent sets of cells, transfected on different days, were analysed. The number of DRP1 foci per μm of mitochondria significantly decreased in *DCTN6* cells compared to *SCRM*, decreasing from 0.91 ± 0.03 to 0.61 ± 0.02 (Figure 3.11). Inducing mitochondrial fission with CCCP significantly increased the number of DRP1 foci per μm of mitochondria in *SCRM* cells from 0.91 ± 0.03 to 1.41 ± 0.05, and hence mitochondrial fragmentation. Despite a significant increase in DRP1 foci per μm of mitochondria in *DCTN6* cells in response to CCCP mediated induction of mitochondrial fission, there was still a significant reduction in mitochondrial associated DRP1 foci incidence compared to *SCRM* siRNA controls (0.76 ± 0.03 for *DCTN6*, compared to 1.41 ± 0.05 for *SCRM*, Figure 3.11).

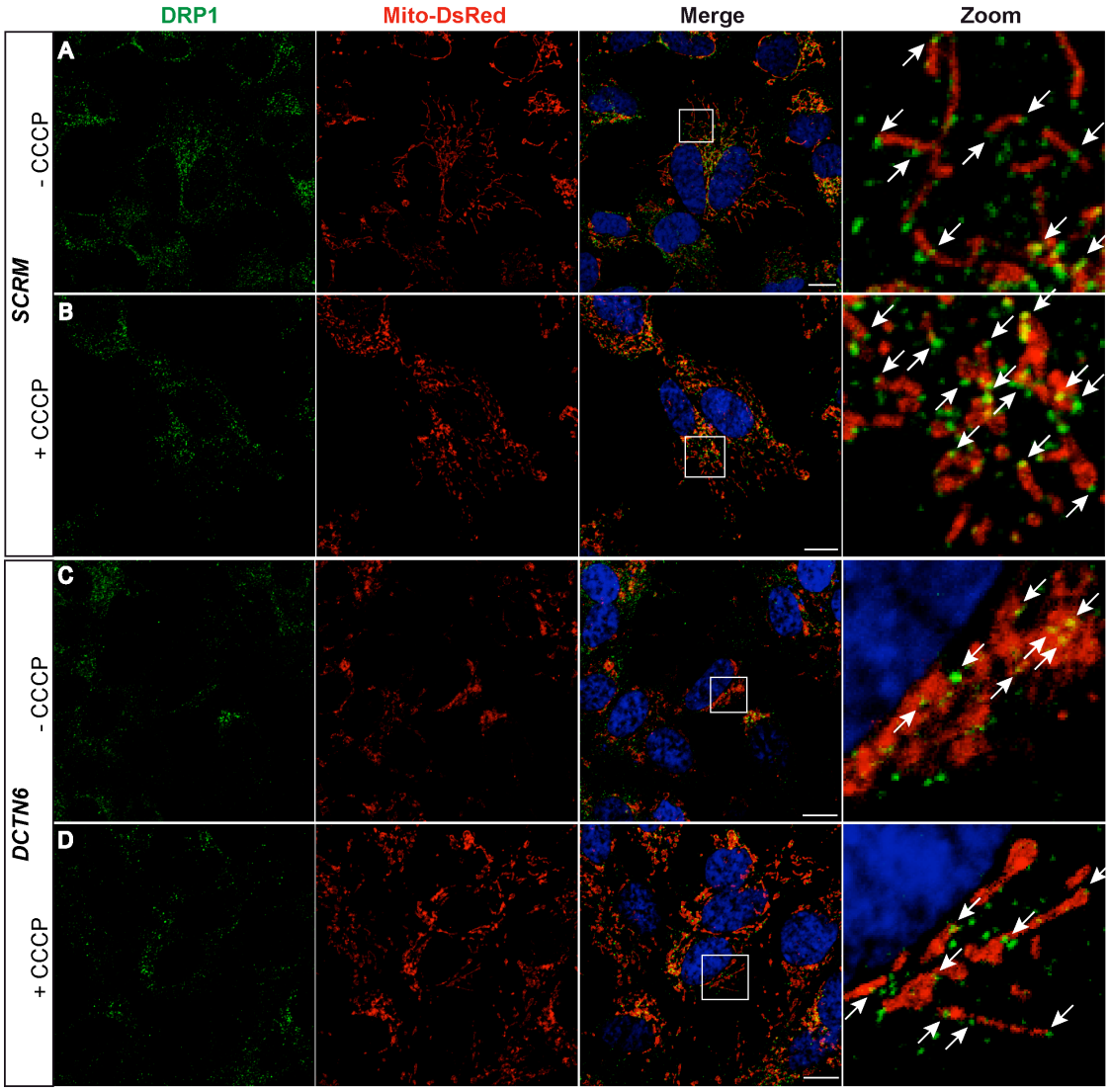
DRP1
Mito-DsRed
Merge
Zoom
SCRM
DCTN6
- CCCP
+ CCCP
A
B
C
D
E
DRP1 foci per µm
1.6
1.4
1.2
1.0
0.8
0.6
0.4
0.2
0
***
***
***
SCRM
DCTN6
- + - +
CCCP

Figure 3.11. Reduced mitochondrial localisation of DRP1 in *DCTN6* knockdown cells. Representative confocal images of SH-SY5Y cells transfected with mito-DsRed and either (**A, B**) *SCRM*, or (**C**, **D**) *DCTN6* siRNA, all treated with either vehicle control (0 μM) or 20 μM CCCP for 40 minutes. 48 hours post transfection; cells were fixed and stained with an anti-DRP1 antibody. The white box in the merged panel is shown zoomed in the panel on the far right. White arrows indicate DRP1 foci in close proximity to mitochondria. The number of DRP1 foci on mitochondria was measured using ZEN software (Zeiss). (**E)** Quantification of the mean number of DRP1 foci per μm of mitochondria in *SCRM* and *DCTN6* cells. Ten cells per siRNA condition and six mitochondria per cell (total of 60 mitochondria per condition) were measured in at least two independent experiments. Error bars represent SEM, *** = $p<0.001$. Scale bar = 10μm.

3.2.5. DCTN6 knockdown leads to reduced mitochondrial membrane potential

Mitochondrial membrane potential ($\Delta\psi_m$) is generated by oxidative phosphorylation and is thus an indicator of mitochondrial function. Loss of sacsin expression reduces $\Delta\psi_m$, suggesting impaired mitochondrial function (Girard et al., 2012). The effect of loss of *DCTN6* expression on $\Delta\psi_m$ was determined using the potential-sensitive dye, tetramethylrhodamine methyl ester (TMRM) in live cell imaging studies. SH-SY5Y cells were transfected with either *SCRM* or *DCTN6* siRNA, along with EV-GFP to allow identification of transfected cells. After 48 hours the cells were incubated with 10nM TMRM for 30 minutes before live cell imaging using the confocal microscope. TMRM fluorescence was quantified using LSM510 software, using GFP fluorescence to delineate the edge of the cell (Appendix 1). A total of 25 cells per treatment were analysed. Confocal settings were kept constant for all imaging. *DCTN6* knockdown cells have a significantly reduced TMRM fluorescence intensity by 29 ± 7% compared to *SCRM* control cells ($p<0.01$, Figure 3.12), indicating that loss of *DCTN6* expression leads to reduced $\Delta\psi_m$. This reduction may be due to a disruption to electron transport chain (ETC) complex assembly and function, which is discussed further in section 3.3.1.

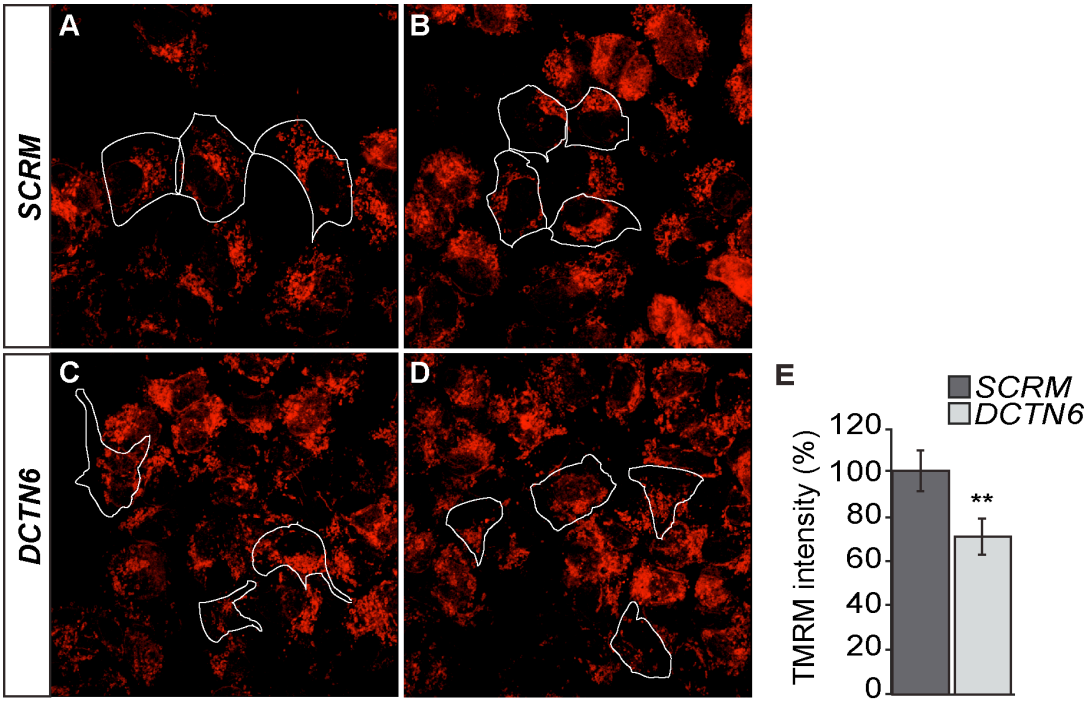

Figure 3.12. *DCTN6* knockdown leads to reduced mitochondrial membrane potential. Representative images of SH-SY5Y cells transfected with either **(A, B)** *SCRM* or **(C, D)** *DCTN6* siRNA, along with EV-GFP (images including GFP are shown in appendix 1). 48 hours post transfection; cells were incubated with 10nM TMRM for 30 minutes before live cell imaging. Maximum intensity projection images from z-stacks are shown. TMRM fluorescence was quantified using LSM510 software (Zeiss). White lines represent the edge of cells. **(E)** The mean TMRM intensity from at least two independent experiments was calculated. Error bars represent SEM, ** = $p<0.01$.

3.3. Conclusions

Previously, a putative interaction was identified between sacsin and DCTN6, a component of the dynein-dynactin motor complex. This complex has been shown to be an important modulator of DRP1 distribution, and therefore mitochondrial fission (Varadi et al., 2004). Thus, a role for sacsin in mitochondrial fission may involve DCTN6. In this chapter, evidence for a novel interaction was demonstrated between DCTN6 and DRP1 using heterologous expression vectors. Interactions have previously been identified between DRP1 and other dynactin subunits, namely p50 and p150^{Glued} (Varadi et al., 2004) thus, the data presented here is in support of an interaction between DRP1 and the dynactin complex. This putative interaction between DRP1 and DCTN6, together with the previous data indicating that sacsin interacts with both of these proteins, suggests that sacsin, DCTN6 and DRP1 may function together in mitochondrial fission (Figure 3.13). However, verification of an interaction between sacsin and DCTN6 by co-IP is required to support this hypothesis.

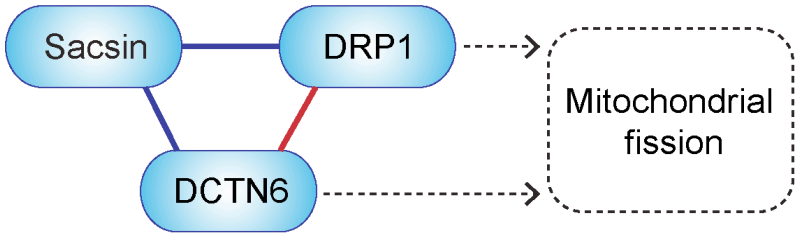

Figure 3.13. Putative interactions identified between sacsin, DCTN6 and DRP1 may provide a mechanistic link for sacsin in mitochondrial fission. Blue lines: previously identified interactions, red line: interaction identified in this thesis.

Moreover, data produced in this chapter provides evidence for a reduction in the localisation of DRP1 at the OMM in cells with reduced levels of sacsin. Importantly, this is also the case after mitochondrial fission is induced by the uncoupler CCCP; indicating that DRP1 recruitment to mitochondria is impaired. Similar results have been reported due to loss of function of mitochondrial fission accessory proteins. For example, reduced MFF expression leads to a reduction in mitochondrial recruitment of DRP1 and elongation of the mitochondrial network (Otera et al., 2010). Likewise, loss of MiD49 or MiD51 expression has been shown to reduce DRP1 association with

mitochondria, leading to unopposed fusion (Palmer et al., 2011). This suggests that, like MFF, Mid49 and Mid51, sacsin may play a role in the recruitment or stabilisation of DRP1 at mitochondrial fission sites, hence maintaining normal mitochondrial dynamics. Sacsin may affect the function of an already known, or unknown mitochondrial fission accessory protein, thus exerting an indirect influence on DRP1 localisation and mitochondrial fission. However, this is unlikely due to the identification of an interaction between sacsin and DRP1 (Girard et al., 2012), which may indicate a more direct affect on DRP1 traffic.

Additionally, diminished cellular levels of sacsin expression were shown to lead to a reduction in higher order DRP1 complexes. These high molecular weight complexes may be DRP1 in complex with another protein(s). Since an interaction has been shown between sacsin (520 kDa) and DRP1 (~80 kDa), this complex may include sacsin (~600 kDa). Hence, loss of sacsin expression leads to reduced complex formation with DRP1. The size of the higher molecular weight protein(s) that are reduced in figure 3.6 corresponds with this hypothesis. Alternatively, loss of sacsin may affect DRP1 interactions with other proteins, possibly other mitochondrial fission accessory proteins. This may explain how loss of sacsin can lead to perturbations in mitochondrial fission.

On the other hand, the high molecular weight complexes could be DRP1 oligomers, which suggests that the self-assembly of DRP1 into multimeric structures on the OMM may be impaired. The fission-promoting activity of DRP1 would thus be reduced, consequently leading to increased fusion of mitochondria. If the mitochondrial localisation of DRP1 is impaired, less DRP1 will be available to form a multimeric constriction complex. Alternatively, loss of sacsin may impair DRP1 self-assembly itself, perhaps through affecting GTP hydrolysis of DRP1, which is known to be important for DRP1 oligomerisation on the OMM (Chang et al., 2010). Defective self-assembly of DRP1 at the OMM is likely to destabilise the mitochondrial pool of DRP1, hence reducing its mitochondrial localisation.

Perturbed DRP1 self-assembly on the OMM was identified to be the cause of an elongated mitochondrial network in HDFs from a neonate with a lethal *de novo* mutation within the middle domain of DRP1 (A395D, (Chang et al., 2010; Pitts et al., 1999)). On the other hand, disassembly of DRP1 complexes is also important for mitochondrial fission to occur. A dominant-negative DRP1 mutation, K38A, impairs GTP hydrolysis, which in turn prevents the disassembly of DRP1 complexes (Chang et

al., 2010), inhibiting OMM constriction, leading to mitochondrial elongation (Smirnova et al., 1998). This highlights that mitochondrial fission is dependent on having correct DRP1 cycling dynamics.

It is also important to note that loss of sacsin does not eliminate mitochondrial fission. This is concordant with what is shown when the function of known mitochondrial fission accessory proteins are lost (Gandre-Babbe and van der Bliek, 2008; Palmer et al., 2011), and emphasises the complexity of the fission process and the multiple contributing factors.

Also in this chapter, changes in *DCTN6* expression levels were observed to alter mitochondrial morphology. Specifically, *DCTN6* overexpression lead to a more fragmented mitochondrial network, whereas siRNA-mediated knockdown of *DCTN6* lead to a more elongated and interconnected mitochondrial network. FRAP analysis also supports the confocal imaging showing a more interconnected mitochondrial network due to reduced *DCTN6* expression. Interestingly, this phenocopies the effect when sacsin function is perturbed (Blumkin et al., 2015; Criscuolo et al., 2015; Girard et al., 2012; Lariviere et al., 2015; Pilliod et al., 2015), which further supports a joint role for sacsin and DCTN6 in mitochondrial dynamics.

Like when reducing sacsin expression, impaired mitochondrial fission seems to be the cause of the elongated mitochondrial network in cells with reduced DCTN6 expression. siRNA-mediated knockdown of *DCTN6* lead to a significant reduction in DRP1 foci localised with mitochondria. This is concordant with that shown by Varadi *et al* (2004) when disrupting dynein-dynactin function. They suggest that the dynein-dynactin complex is required for the correct targeting of DRP1 to mitochondria (Varadi et al., 2004). This observation also further supports the interaction identified between DRP1 and DCTN6 by co-IP.

Finally, reducing *DCTN6* expression significantly decreases $\Delta\psi_m$. This again, is also a consequence of reducing cellular levels of sacsin (Girard et al., 2012), which further supports a joint role for sacsin and DCTN6, and indicates the potential involvement of these proteins in maintaining normal mitochondrial health. It is conceivable that the reduction in DRP1-mediated mitochondrial fission, which is required to maintain mitochondrial quality control, leads to an accumulation of dysfunctional mitochondria that cannot be degraded by mitophagy and thus, a reduction in $\Delta\psi_m$ is observed. This is

reflected in recent studies showing mitochondrial dysfunction in ARSACS (Girard et al., 2012, Criscuolo et al., 2015, Bradshaw et al., 2016).

In summary, several observations suggest that DCTN6 and sacsin may function in the same pathway. Firstly, there is evidence that they both interact with DRP1, secondly, loss of function of either protein leads to elongated and overly interconnected mitochondria, and thirdly, loss of function of either protein leads to a reduction in the mitochondrial localisation of DRP1. Collectively, this data suggests that sacsin and DCTN6 may function together in the recruitment or stabilisation of DRP1 on mitochondria.

Considering all of the data, it is plausible that the high molecular weight DRP1 complexes in figure 3.6 could be a complex including DRP1, sacsin and DCTN6, and loss of sacsin leads to reduced formation of this complex, which ultimately results in reduced mitochondrial fission. Taking into account that sacsin is a putative co-chaperone; sacsin may act as a co-chaperone, regulating complex assembly and/or disassembly, in order for DRP1 to be recruited to mitochondria *via* the dynein-dynactin motor. However, further research is required to investigate this.

The data also supports that the alterations in mitochondrial dynamics observed in ARSACS are a consequence of impaired fission, rather than an increase in fusion.

3.3.1. Further work

It is essential that the protein interactions identified in this chapter, and previously, are now verified. For example, an interaction between the N-terminus of sacsin and DCTN6, identified by a Y2H screen, needs to be verified by performing a co-IP. Sacsin 1-1368-FLAG, representing the N-terminus, would be heterologously expressed along with DCTN6-GFP, followed by incubation of cell lysates with anti-FLAG magnetic beads.

The development of super-resolution microscopy allows for more accurate determination of the co-localisation of proteins, such as sacsin, DRP1 and DCTN6. This anaylsis is less reliable using confocal microscopy due to the limits in resolution. This data would provide further evidence to support interactions between these proteins.
A proximity ligation assay using antibodies to sacsin, DRP1 and DCTN6 could also be performed to verify interactions between these proteins.

To further investigate whether the high molecular weight DRP1 complexes in figure 3.6 include sacsin and DCTN6, the same experiment could be performed (as in section 3.2.2), but for DCTN6 knockdown. If the high molecular weight DRP1 complexes are also reduced with loss of DCTN6 expression, this would add support to the hypothesis that DRP1, sacsin and DCTN6 work together in a complex.

Further quantification of the changes in mitochondrial network morphology due to altered DCTN6 levels (figures 3.7 and 3.9) could be performed to verify this data. Methods include quantifying the number and length of mitochondria per cell and comparing between conditions. Also, the degree of branching of the mitochondrial network (form factor) in DCTN6 siRNA treated cells compared to controls could be quantified using the length of the mitochondria outline and area of mitochondrion (Grunewald et al., 2010; Koopman et al., 2005; Mortiboys et al., 2008).

It has previously been found that mitochondrial dynamics, including DRP1-mediated fission, modulates oxidative phosphorylation complex assembly and function (Hroudova et al., 2014; Liu et al., 2011). The reduced mitochondrial membrane potential in cells with loss of DCTN6 (figure 3.12) is suggestive of disrupted oxidative phosphorylation, which may be mediated by reduced DRP1-mediated fission (figure 3.11) and thus, disrupted assembly and function of electron transport chain (ETC) complexes. This could be assessed through blue native polyacrylamide gel electrophoresis (BN PAGE) to quantify the protein content and activities of the ETC complexes in *DCTN6* siRNA treated cells compared to controls. Spectrophotometric enzyme assays can also be performed, for example, complex I (NADH dehydrogenase) activity can be measured by NADH oxidation, with or without the complex I inhibitor rotenone (Jung et al., 2000). Furthermore, a perturbation to oxidative phosphorylation could be confirmed using a seahorse extracellular flux (XF) analyser (Seahorse Biosciences) to measure bioenergetic function.

Post-translational modifications are important in regulating DRP1 function and recruitment to mitochondria. The reduced localisation of DRP1 at the OMM seen in both sacsin and DCTN6 deficient cells may be mediated through a change in DRP1 post-translational modifications. Therefore, it is important to investigate if there is a relationship between loss of these proteins and key regulatory modifications of DRP1, such as phosphorylation and SUMOylation. Phosphorylation of DRP1 at serine 637 is known to inhibit DRP1 activation leading to retention of the protein in the cytosol while

dephosphorylation of serine 637 promotes translocation of DRP1 to the mitochondria (Cereghetti et al., 2008; Knott and Bossy-Wetzel, 2008). Phosphorylation of DRP1 at serine 616 inhibits mitochondrial translocation and oligomerisation of DRP1 (Cho et al., 2014).

Preliminary experiments were performed to optimise detection of phosphorylated DRP1 at Ser616 and Ser637 by immunoblotting (not shown). Cell lysates were analysed under both crosslinked and un-crosslinked, and reduced (+2-ME) and non-reduced (-2-ME) conditions. Interestingly, DRP1 appears to be phosphorylated at Ser616 at the monomeric and higher oligomeric levels, whereas phosphorylation at Ser637 is at the monomeric and dimeric levels, but not the higher oligomeric level. Comparisons now need to be made in the levels of DRP1 phosphorylation at Ser616 and Ser637 in cells transfected with *SCRM*, *SACS* or *DCTN6* siRNAs.

SUMOylation stabilizes the mitochondrial pool of DRP1 and stimulates mitochondrial fission (Braschi et al., 2009; Harder et al., 2004). This occurs via SUMO proteins (Figueroa-Romero et al., 2009), and E3 ligases such as MAPL (mitochondrial-anchored protein ligase). Hence, the phosphorylation and SUMOylation state of DRP1 could be compared between sacsin or DCTN6 deficient cells and controls, which would give further mechanistic insight into the reduced mitochondrial localisation of DRP1.

CHAPTER 4: INTRACELLULAR DISORGANISATION IN ARSACS

4.1. Introduction and Aims

As described in the introduction to this thesis, the cytoskeleton is a heterogeneous network of filamentous structures, composed of microfilaments, intermediate filaments (IFs) and microtubules. This interconnected network of cytoskeletal elements allows eukaryotic cells to resist deformation, transport intracellular cargo, and change shape. Moreover, it is integral to the spatial organisation of organelles within the cell. Neurons are particularly dependent on the cytoskeleton to deliver the proteins and other components synthesised in the cell body to the axons and nerve terminals. Therefore, it is not suprising that dysfunction of cytoskeletal components is linked to neurodegenerative diseases including amyotrophic lateral sclerosis (ALS), Alzheimer's, Parkinson's, tauopathies, polyQ disorders and Charcot-Marie-Tooth disease (Al-Chalabi and Miller, 2003; Gunawardena and Goldstein, 2005; Lariviere and Julien, 2004; Liem and Messing, 2009; McMurray, 2000; Perrot and Eyer, 2009).

One example of a neurodegenerative disease with multiple cytoskeletal components affected is Spinocerebellar Ataxia Type 3 (SCA3), also known as Machado-Joseph Disease (MJD), which is caused by expansion of a polyglutamine tract in ataxin-3 (ATXN3). ATXN3 is a deubiquitinating enzyme, so binds to ubiquitinylated proteins, and is thought to modulate substrate degradation through the ubiquitin-proteasome pathway (Rodrigues et al., 2010). Depletion of *ATXN3* using siRNA in both human and mouse cell lines leads to severely compromised and disorganised microtubule, microfilament and IF networks (Rodrigues et al., 2010). This cytoskeletal phenotype was found to be reversible and dependent on ATXN3 levels.

A striking example of a neurodegenerative disease where IFs alone appear to be disrupted in isolation to other cytoskeletal elements is giant axonal neuropathy (GAN), which is caused by autosomal recessive mutations in *GAN*, resulting in loss of the gigaxonin protein. Peripheral nerves from patients show accumulations of neurofilaments within enlarged axons (Gordon, 2004), muscle fibres have accumulations of desmin, glial fibrillary acidic protein (GFAP) accumulates in astrocytes, and vimentin accumulates in multiple cell types, including dermal fibroblasts (Cleveland et al., 2009; Peiffer et al., 1977).

Recently, disrupted neurofilament organisation was identified as a pathophysiological feature of ARSACS (Lariviere et al., 2015). Specifically, loss of sacsin function results in abnormal accumulations of non-phosphorylated neurofilament heavy chain (npNFH)

bundles in the somatodendritic region of various neuronal populations in sacsin knockout mice and ARSACS brains (Lariviere et al., 2015).

This leads to the overarching aim of this chapter, which was to investigate the organisation of IFs in ARSACS patient dermal fibroblasts and *SACS* siRNA knockdown cells. IFs connect with many other cellular structures, including actin and microtubules (Chang and Goldman, 2004), the Golgi complex (Gao and Sztul, 2001; Gao et al., 2002), endosomes (Sarria et al., 1992), and mitochondria (Nekrasova et al., 2011; Winter et al., 2008). Disorganisation of the IF network may effect the spatial organisation of these cellular components; hence the distribution of these organelles in cells with depleted sacsin function were also characterised. Moreover, the subcellular localisation of sacsin was further investigated using a newly available antibody.

4.2. Results

4.2.1. Colocalisation of a proportion of sacsin with vimentin intermediate filaments

Sacsin is expressed at detectable levels in SH-SY5Y cells and has a predominantly cytoplasmic distribution, with a clear punctate component. Previously, a proportion of sacsin has been shown to localise at or near the cytoplasmic face of the OMM (Parfitt et al., 2009; Girard et al., 2012), with defects in mitochondrial dynamics and function identified as an important factor in ARSACS disease pathogenesis (Girard et al., 2012). Due to the recent discovery of alterations in neurofilaments as an additional underlying pathophysiological feature of ARSACS (Lariviere et al., 2015), the subcellular localisation of sacsin in relation to IFs was investigated using immunocytochemistry in SH-SY5Y cells. These neuroblastoma-derived cells have vimentin as their primary IF rather than neurofilaments.

Vimentin IFs were analysed for overlap with sacsin localisation using antibodies to vimentin and sacsin, followed by visualisation using confocal microscopy. As previously shown, sacsin displays a cytoplasmic localisation with a punctate component. Importantly, a proportion of sacsin punctate were identified to be on or near the vimentin cytoskeleton (Figure 4.1).

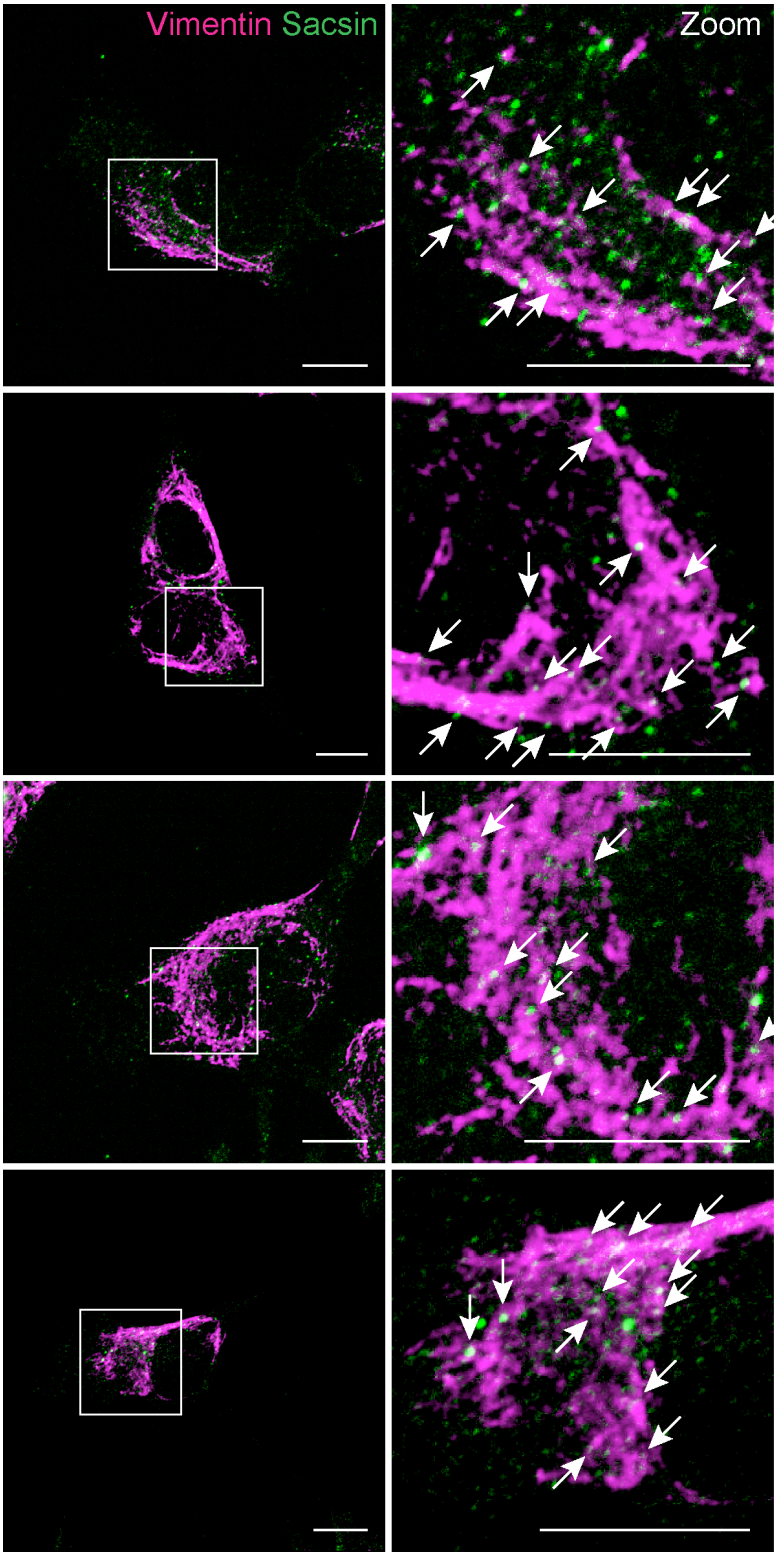

Figure 4.1. Sacsin localises in close proximity to vimentin intermediate filaments. Representative confocal images of SH-SY5Y cells fixed and permeabilised, followed by staining with antibodies to sacsin (green) and vimentin (magenta). White boxes in vimentin/sacsin panels are shown zoomed in the right panels. White arrows indicate sacsin punctate on or near vimentin filaments. Scale bars = 10μm.

The localisation of sacsin in relation to vimentin was further analysed using super-resolution structured illumination microscopy (SR-SIM, LSM 710 ELYRA PS.1). This allows higher-resolution imaging, generating images of approximately 100 nm in lateral resolution compared to the 200 nm obtained by standard confocal microscopy (Figure 4.2). Antibodies to vimentin and sacsin were used, along with MitoTracker Red to label mitochondria. Z-stacks were acquired and SIM processing performed. The previously identified localisation of a proportion of sacsin at or near the cytoplasmic face of mitochondria was also evident in these images (Figure 4.2D). In addition, the ability to visualise the cells in super-resolution identified areas where sacsin punctae are localised between mitochondria and vimentin filaments (indicated by white arrows in Figure 4.2D), suggesting that sacsin may contact both mitochondria and vimentin simultaneously.

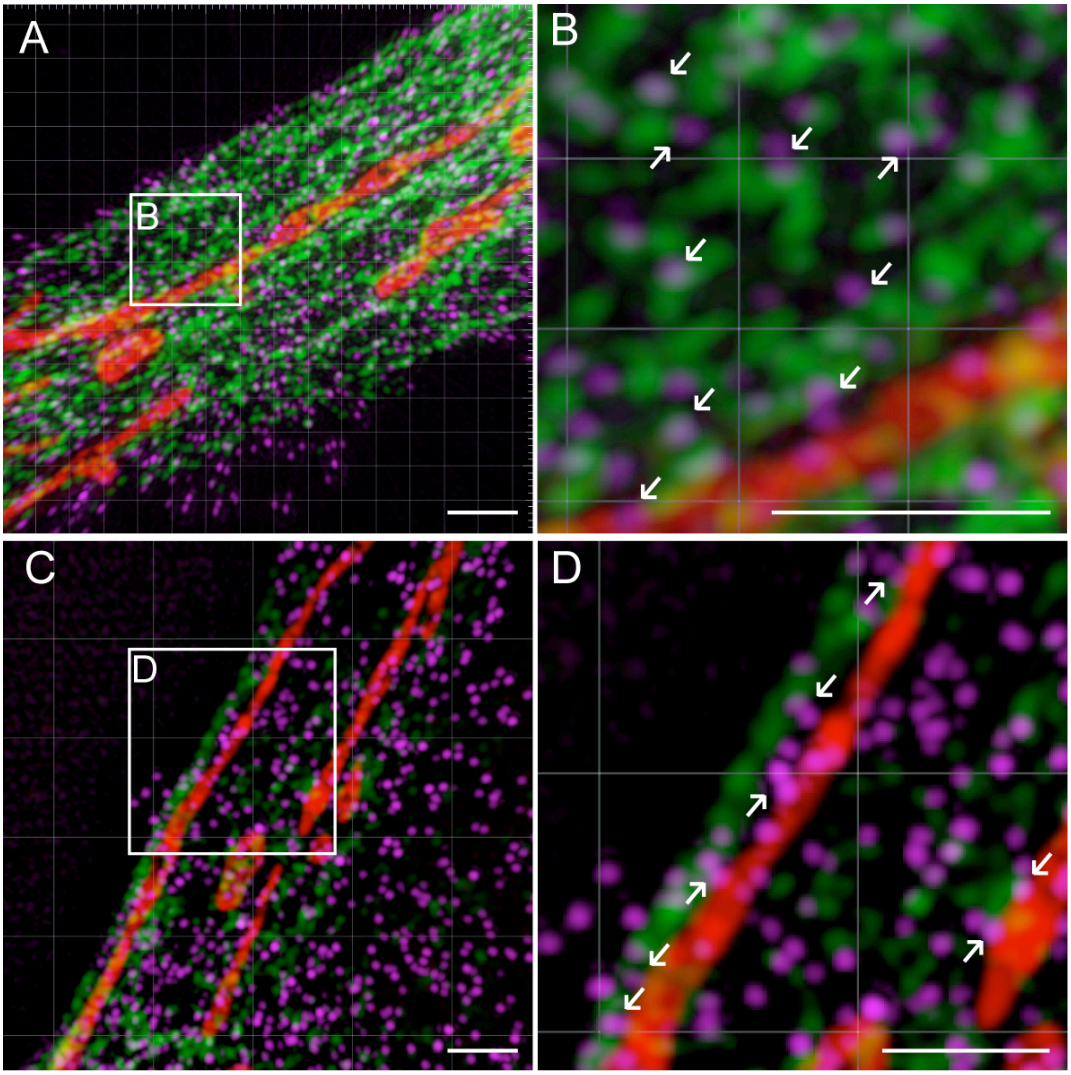

Figure 4.2. Sacsin localises in close proximity to both vimentin intermediate filaments and mitochondria. Representative super-resolution images of SH-SY5Y cells incubated with MitoTracker Red and stained with antibodies to sacsin (magenta) and vimentin (green). Panels B and D are zoomed in images of A and C. White arrows in panel B indicate sacsin puncta adjacent to vimentin. White arrows in panel D indicate sacsin puncta localised between mitochondria and vimentin IF. Scale bars = 20μm.

4.2.2. Cellular fractionation of SH-SY5Y cells and human dermal fibroblasts

Given the strong overlap between sacsin and vimentin IF localisation, subcellular fractionation of SH-SY5Y cells and control human dermal fibroblasts (HDFs) was performed (see section 2.11.2) to investigate if sacsin purifies in the cytoskeletal fraction, and more specifically in an IF-enriched fraction of cell lysate. Immunoblot analyses showed sacsin to be enriched in an insoluble cytoskeletal fraction, as was the case for the cytoskeletal proteins vimentin and β-actin (Figure 4.3).

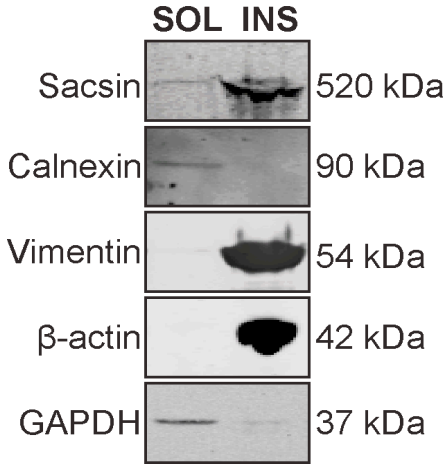

Figure 4.3. Sacsin is enriched in an insoluble cytoskeletal fraction. Subcellular fractionation of control HDFs to separate cytoskeletal proteins and subsequent immunoblot analysis reveals that although sacsin is present in the soluble (SOL) cytosolic fraction, it is significantly enriched in the insoluble (INS) cytoskeletal fraction. Analysis with antibodies to calnexin (ER), vimentin (IF), β-actin (actin filaments) and GAPDH (cytosol) confirmed that the fractionation protocol had enriched cytoskeletal proteins relative to other cellular components.

Using an alternative fractionation protocol designed to specifically enrich IFs, sacsin's cytoskeletal association was further investigated. Sacsin was present in an IF-enriched fraction generated from HDF and SH-SY5Y cell lysates (Figure 4.4). This is more evident in SH-SY5Y cells as sacsin has a higher abundance in these cells compared to HDFs. However, the fractionation of HDFs was cleaner with no detection of β-tubulin, GAPDH and HSP60 in the insoluble IF-enriched fraction (INS, Figure 4.4). This data is consistent with the immunocytochemistry data and further suggests that sacsin is associated with the cytoskeleton and specifically with IFs.

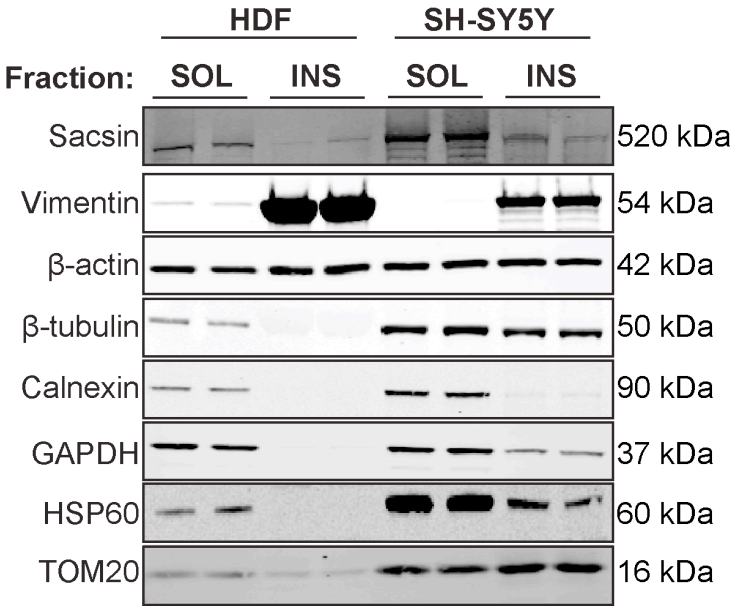

Figure 4.4. Sacsin is present in an insoluble IF-enriched fraction. IF fractionation of normal HDF and SH-SY5Y cells, followed by immunoblot analysis reveals that sacsin is present in the soluble cytosolic fraction and the insoluble intermediate filament fraction. The relative mobility of sacsin is the same across cell types and in soluble and insoluble fractions. Analysis with antibodies to vimentin (IF), β-actin (actin filaments), β-tubulin (microtubles), calnexin (ER), GAPDH (cytosol), HSP60 and TOM20 (mitochondria) are shown as controls for the fractionation. SOL = soluble, INS = Insoluble.

4.2.3. Disorganisation of the vimentin IF network in ARSACS patient HDFs

The discovery of alterations in the neurofilament cytoskeleton in neurons from *Sacs*$^{-/-}$ mice and in ARSACS brains (Lariviere et al., 2015), along with the identification that sacsin localises within close proximity of vimentin IFs, indicates a potential function of sacsin with IFs. Here, HDFs from ARSACS patients were analysed for evidence of alterations in IF networks. These patient HDFs contain pathological mutations in *SACS,* in the context of the genetic background of the affected individual, hence they are a useful cellular model to study ARSACS. It is also important to note that a mitochondrial phenotype has previously been observed in these patient HDFs. Details of the *SACS* mutations present in the five ARSACS HDF lines used, and the location of the mutations within sacsin are given in table 4.1 and figure 4.5.

ARSACS patient	Age at onset (yrs)	Disease duration (yrs)	Gender (M/F)	SACS mutations	Type of mutation	Sacsin protein detected?[#]
1	1	39	F	Q4054* and c.2094-2A>G	Nonsense/ Splice-site	No
2	3	33	F	R2002fs and Q4054*	Frameshift/ Nonsense	No
3	3	60	F	F2780C, S3892*, L4139S	Missense/ Nonsense/ Missense	No
4	1	25	F	p.2801delQ	In frame deletion	Yes
5	8	45	M	K1715* and R4331Q	Nonsense/ Missense	Yes

Table 4.1. ARSACS HDF lines used in this thesis. These were obtained from Dr. Sasha Vemeer, Radboud University, Nijmegen and Dr. Paola Giunti, UCL Institute of Neurology, London. Amino acid change to an * indicates a truncated protein, fs indicates a frameshift and del indicates a deletion. [#]Using an anti-sacsin antibody recognising a fragment within human sacsin amino acids 4100-4200 (abcam). ARSACS HDF lines were not age or gender matched with WT controls (appendix 2).

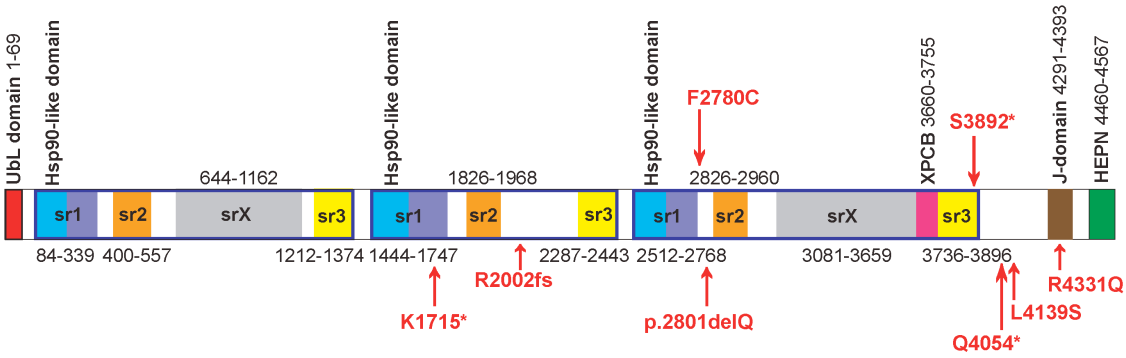

Figure 4.5. Schematic showing location of ARSACS patient mutations in sacsin. Schematic representation of the sacsin domains from N- to C-terminus. Amino acid residues are indicated in numbers. sr1: subrepeat 1, sr2: subrepeat 2, sr3: subrepeat 3, srX: subrepeat X.

Sacsin expression in the HDFs was also analysed by immunoblotting. Three of the five ARSACS HDFs have no detectable sacsin protein, whereas two have reduced cellular levels of sacsin compared to WT controls (Figure 4.6). This is consistent with what is expected from the types of *SACS* mutations present in the patients. For example, patient 5 in table 4.1 is a compound heterozygote, with one allele having a point mutation affecting residue 4331, which is beyond the region of antibody binding (4100-4200), hence this mutation does not affect binding and sacsin levels are detectable. The other allele has a mutation at residue 1715, which leads to a premature STOP codon and truncation of the protein, which is why they have reduced sacsin expression compared to wild-type (WT) controls. Patient 4 has a homozygous in-frame deletion of a single amino acid at residue 2801. This does not affect sacsin levels; hence this patient has comparable sacsin levels to WT controls.

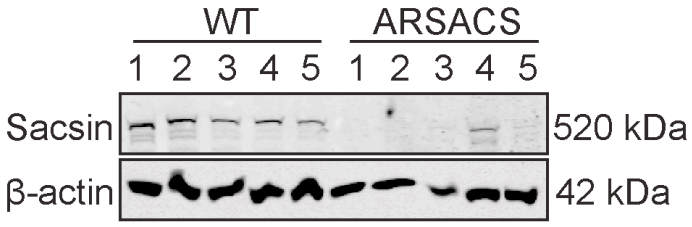

Figure 4.6. Sacsin protein levels in WT control and ARSACS HDFs. Immunoblotting of lysates from ARSACS HDF lines and WT controls was performed using a rabbit monoclonal anti-sacsin antibody against an undefined sequence between residues 4100 and 4200. This detected a sacsin band in cells homozygous for the single amino acid deletion mutation 2801delQ, which was of similar intensity to that seen in WT control HDFs (patient 4). In cells with the K1715*/R4331Q mutation a significantly fainter sacsin band was just visible (patient 5). This is consistent with the K1715*/R4331Q HDF line expressing detectable levels of protein from a single allele. No sacsin was detected in the other three ARSACS HDF lines, although we could not preclude expression of a truncated protein. The relative mobility of sacsin was the same across all patients and controls. Patient numbers correspond with table 4.1.

4.2.3.1 *Collapsed and bundled vimentin IFs in ARSACS*

The vimentin network of the five ARSACS patient and five WT control HDF lines was visualised by immunocytochemistry, using antibodies to sacsin and vimentin, along with MitoTracker Red to label the mitochondria. Confocal imaging identified a striking collapse and perinuclear bundling of the vimentin network in all ARSACS HDF lines compared to WT controls (Figure 4.7). Interestingly, a perinuclear 'hole' in the mitochondrial network occurs where the vimentin bundles, and in the two patient cells with some remaining sacsin protein detected (p.2801delQ, K1715* and R4331Q), there is a re-localisation of sacsin from being throughout the cytoplasm, to the perinuclear area where the vimentin is bundling and mitochondria are excluded (as indicated by white arrows in figure 4.7).

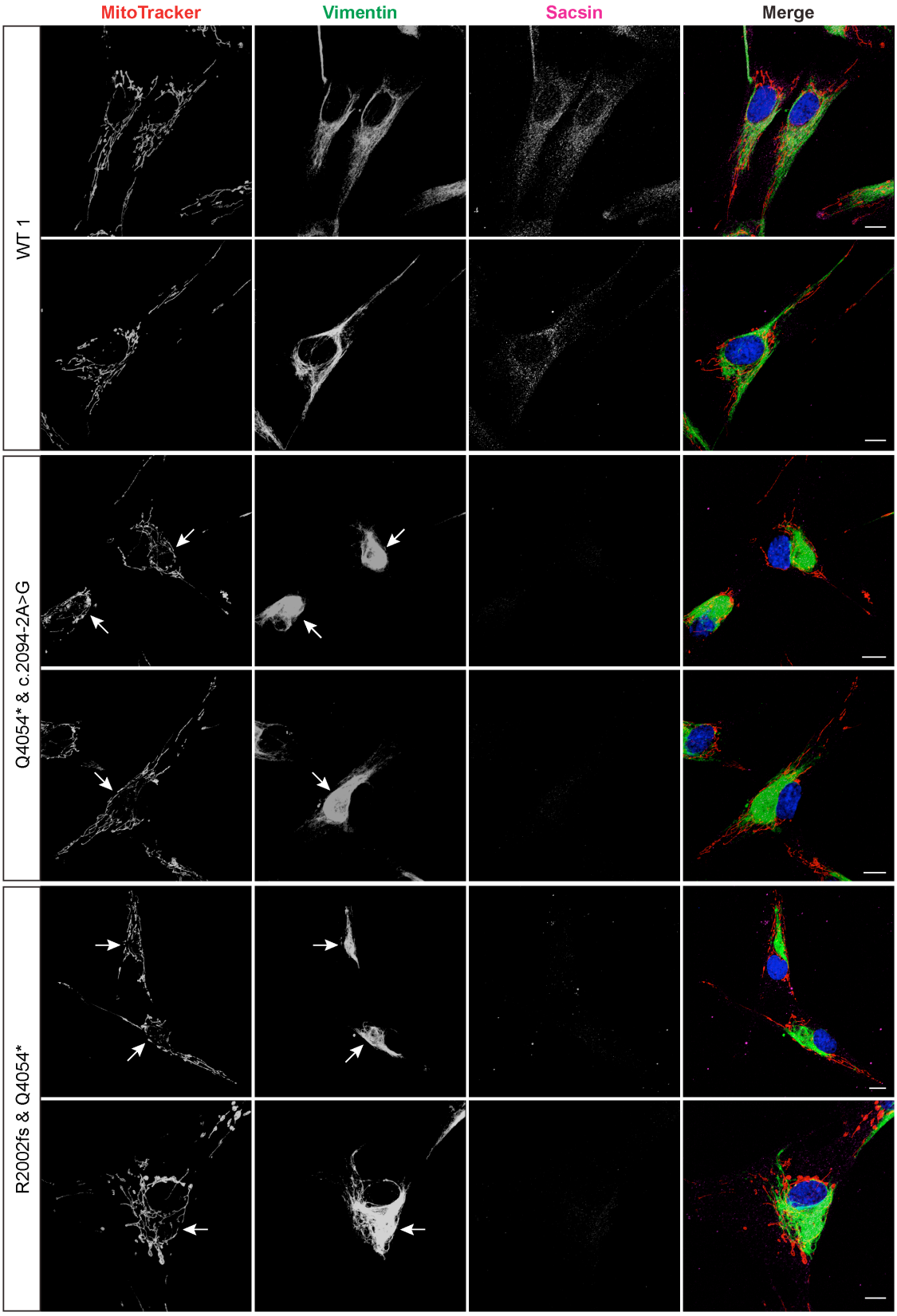
MitoTracker
Vimentin
Sacsin
Merge
WT 1
Q4054* & c.2094-2A>G
R2002fs & Q4054*

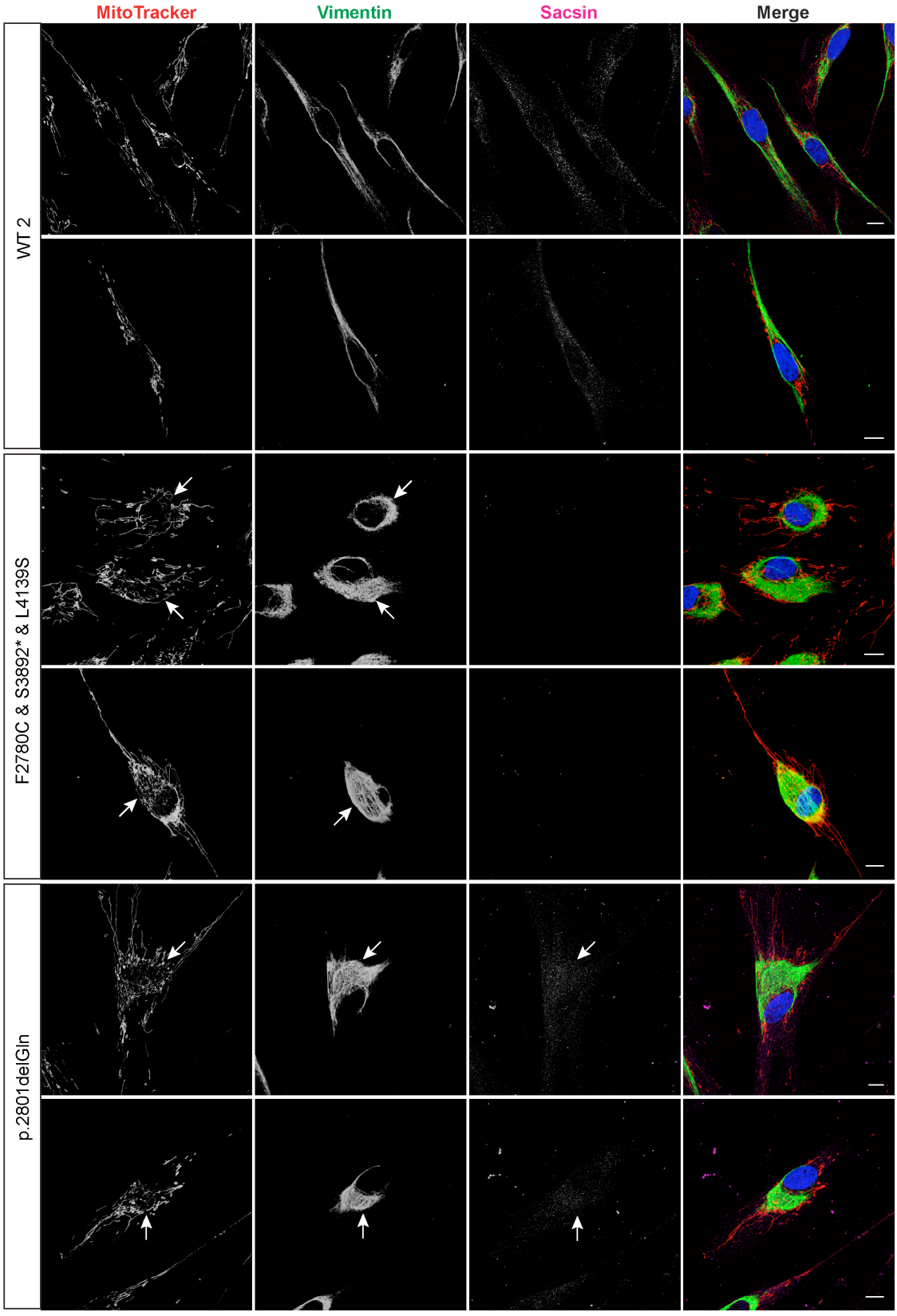
MitoTracker
Vimentin
Sacsin
Merge
WT 2
F2780C & S3892* & L4139S
p.2801delGln

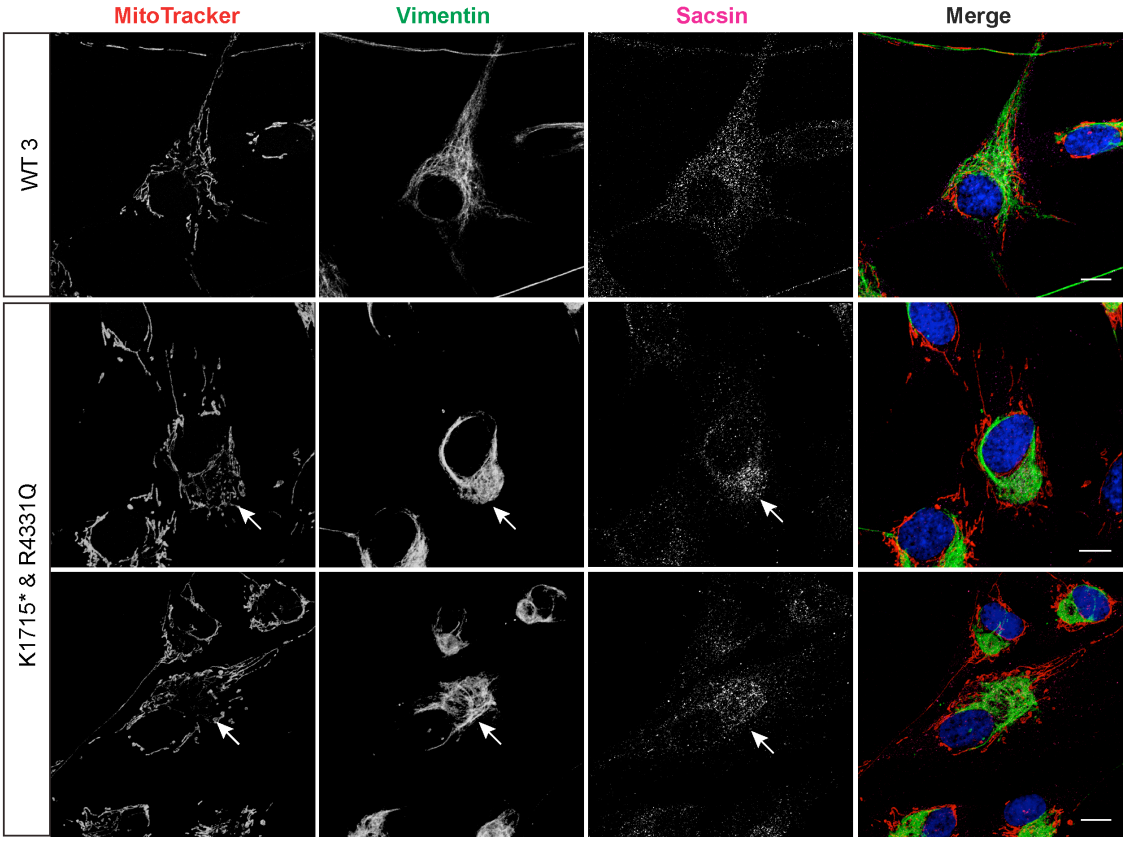

Figure 4.7. Collapsed and bundled vimentin IFs in ARSACS patient HDFs. Representative confocal images of five ARSACS patient HDF and WT control lines. Fibroblasts were incubated with MitoTracker Red and were stained with rabbit anti-sacsin and mouse anti-vimentin antibodies. Confocal analysis showed collapsed and bundled vimentin IFs in all five ARSACS patient HDFs. Arrows indicate areas of vimentin network distruption. The mitochondrial network is disrupted and sacsin accumulates in the same location. Scale bars = 10 μm. Further images for ARSACS HDF and WT control cells are shown in appendix 3.

The incidence of HDFs with vimentin bundling was compared by quantifying the phenotype in each ARSACS patient and each WT control line. This was done blind to experimental status. The total number of cells counted per cell line was >120 from at least two different cover slips. This revealed that, on average, 79.6 ± 1.9 % of cells from the five ARSACS patients have a collapsed vimentin network, which is a highly significant increase from control cells ($p<0.001$, Figure 4.8). These results indicate that loss of sacsin disrupts both the IF and mitochondrial network in ARSACS patient cells.

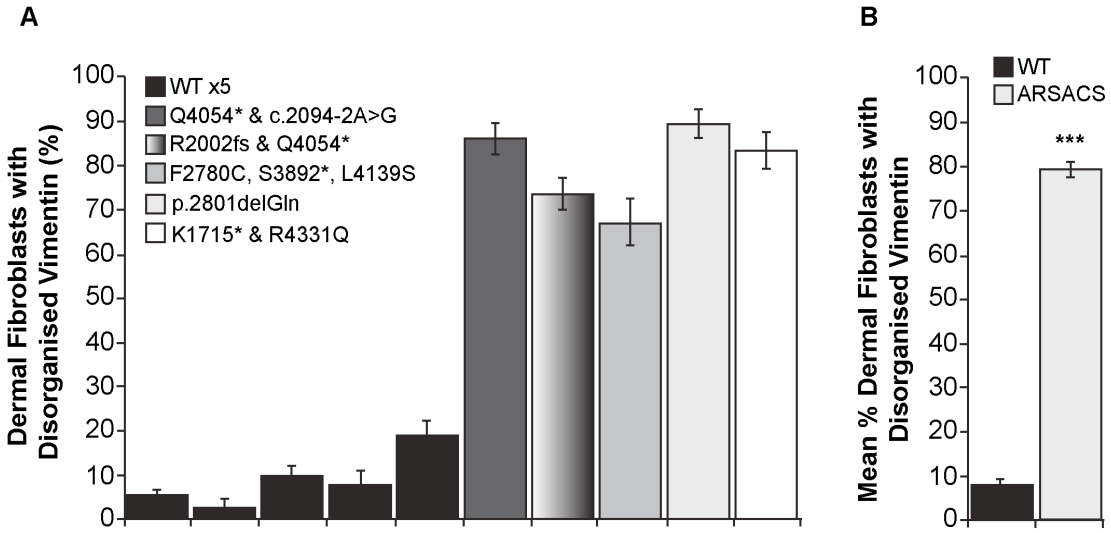

Figure 4.8. Quantification of the collapsed and bundled vimentin IF phenotype in ARSACS patient HDFs. (A) The vimentin phentoype was quantified by counting the number of cells with a collapsed vimentin network for each cell line, blind to experimental status. The total number of cells counted per cell line was >120 from two cover slips. Results are expressed as mean ± SEM for each control and patient cell line. **(B)** Results from all five WT and five patient cell lines were combined to give an overall mean ± SEM, *** $p<0.001$. Statistics were carried out using an unpaired two-tailed Students t-test.

The compound heterozygote ARSACS patient with *SACS* mutations K1715* and R4331Q has some remaining sacsin expression (patient 5 in table 4.1 and figure 4.6). Interestingly, sacsin localisation mirrors the collapsed vimentin network in HDFs from this patient (Figure 4.9). The same is observed in HDFs from another patient with some remaining sacsin expression (patient 4 in table 4.1 and figure 4.6), which can be seen in figure 4.7. This provides further data to suggest an association between sacsin and vimentin.

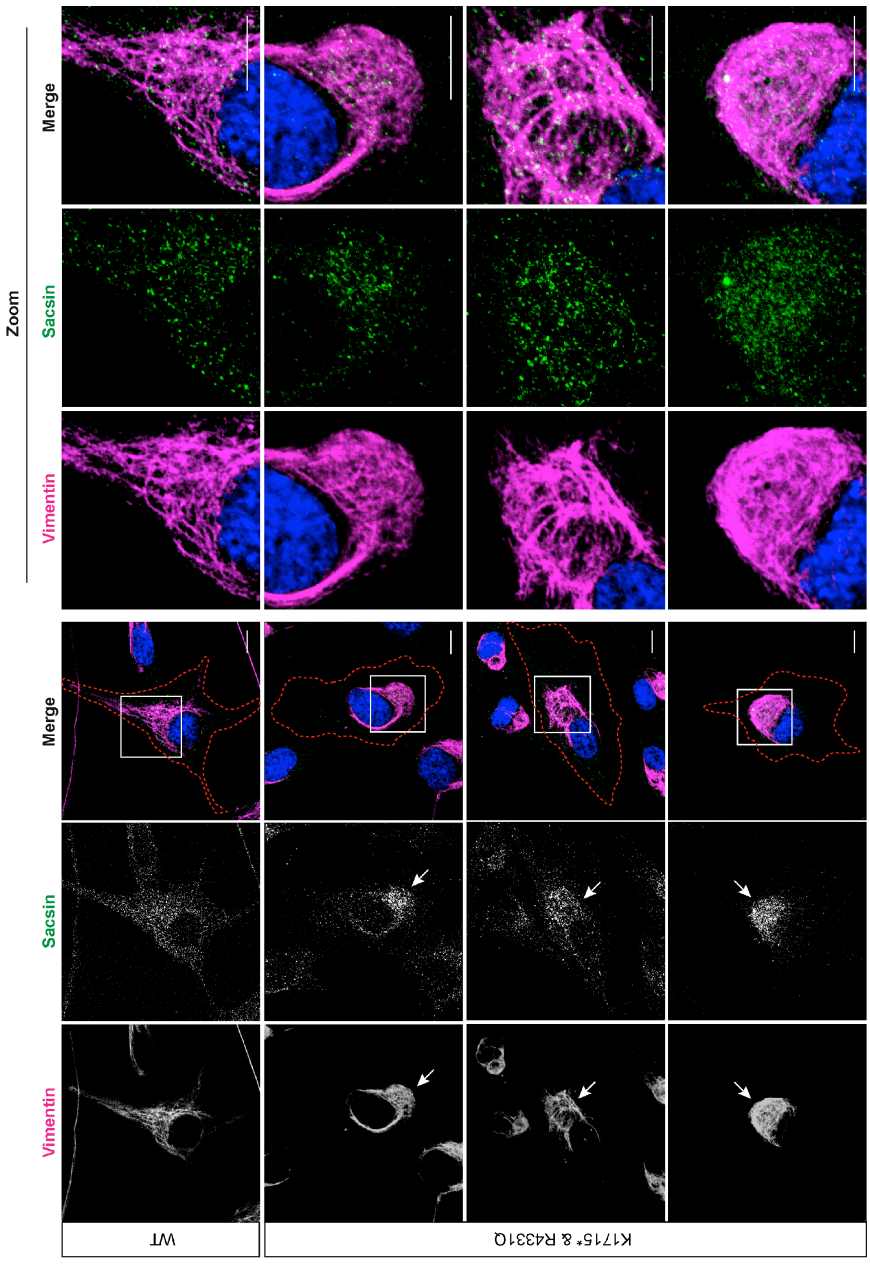

Figure 4.9. Sacsin localisation is consistent with vimentin localisation in ARSACS patient HDFs with *SACS* mutations K1715* and R4331Q. Representative confocal images of HDFs from a compound heterozygote ARSACS patient and a WT control line. Fibroblasts were incubated with rabbit anti-sacsin and mouse anti-vimentin antibodies. Confocal analysis showed sacsin relocalisation to the perinuclear vimentin bundles in the ARSACS patient HDFs, indicated by white arrows. Red dotted line indicates the edge of the cell. White boxes in the merged panel are shown zoomed in the right-hand side of the figure. Scale bars = 10 µm.

4.2.3.2 *Vimentin protein levels were unchanged in ARSACS patient HDFs*

Due to the re-localisation of vimentin in ARSACS patient HDFs, the total levels of vimentin protein were analysed for any change compared to controls by immunoblotting using an anti-vimentin antibody. There were no significant differences in total vimentin protein levels, normalised to β-actin, in ARSACS patient HDFs compared to WT controls (Figure 4.10).

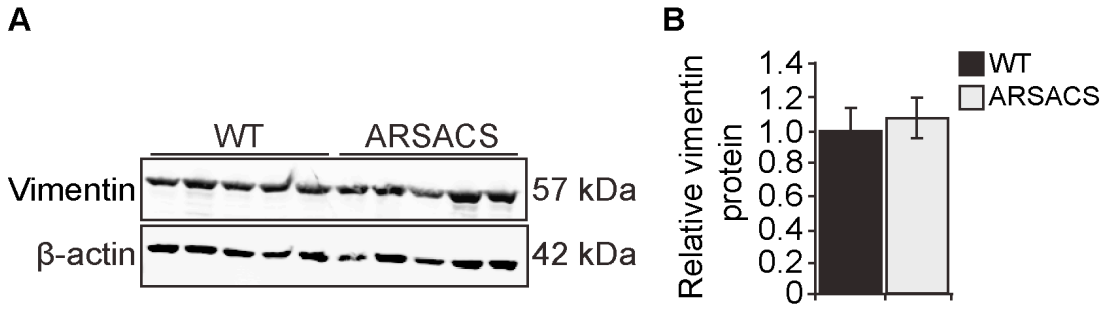

Figure 4.10. Total cellular levels of vimentin were unchanged in ARSACS patient HDFs. (A) Immunoblot analysis of protein lysates from five ARSACS patient and five WT control HDFs probed with an anti-vimentin antibody. β-actin was used as a loading control. (**B**) Densitometric analyses were performed and mean relative vimentin protein levels calculated for the ARSACS patient and WT control HDF lines. Data were normalised to β-actin. Total cellular protein levels of vimentin did not significantly differ.

Together this data suggests that loss of sacsin function leads to a significant remodeling of the vimentin network, but overall cellular levels of the protein are unchanged.

4.2.4. Organisation of the microtubule and microfilament network in ARSACS patient HDFs

Due to the striking changes in both the mitochondria and IF network organisation in ARSACS HDFs, the distribution of microtubules and microfilaments were also analysed. This was by immunocytochemistry, using either a fluorescent marker of actin (ActinGreen 488 ready probes, Life Technologies), or an antibody to β-tubulin, along with MitoTracker Red to label the mitochondria. Confocal imaging revealed that the distribution of the microfilament network did not appear to be significantly altered in ARSACS HDFs compared to controls (Figure 4.11).

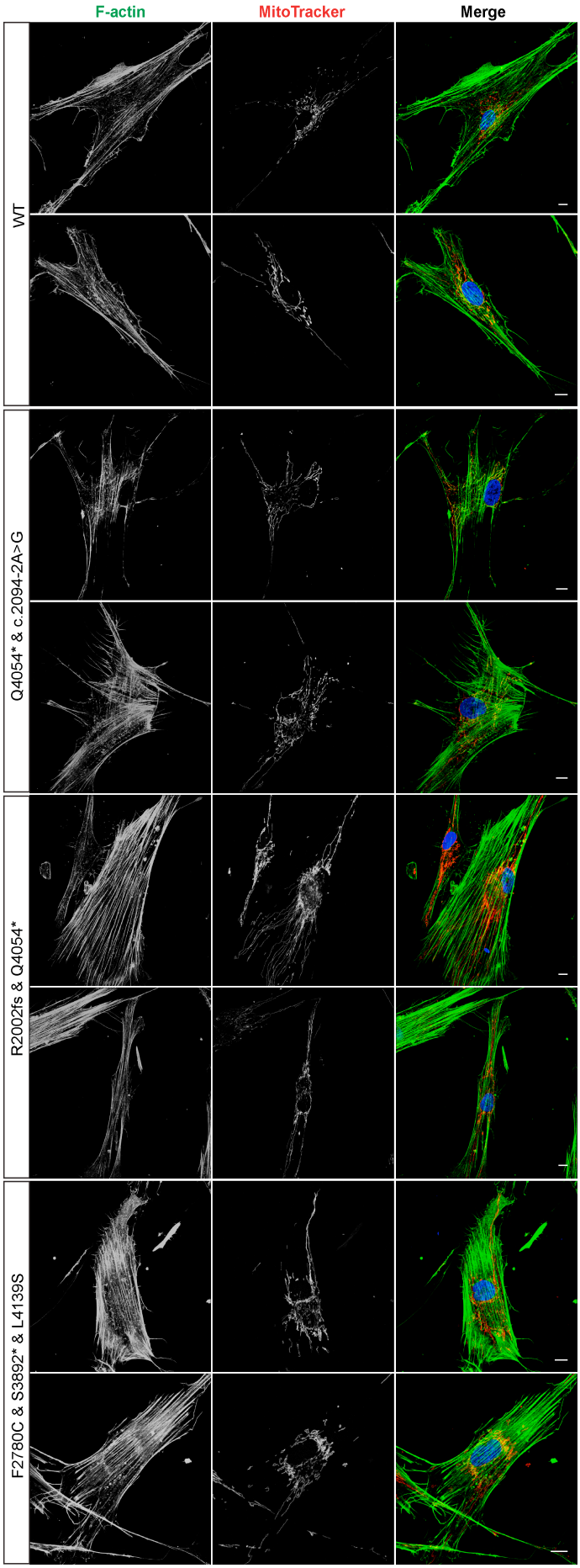
F-actin
MitoTracker
Merge
WT
Q4054* & c.2094-2A>G
R2002fs & Q4054*
F2780C & S3892* & L4139S

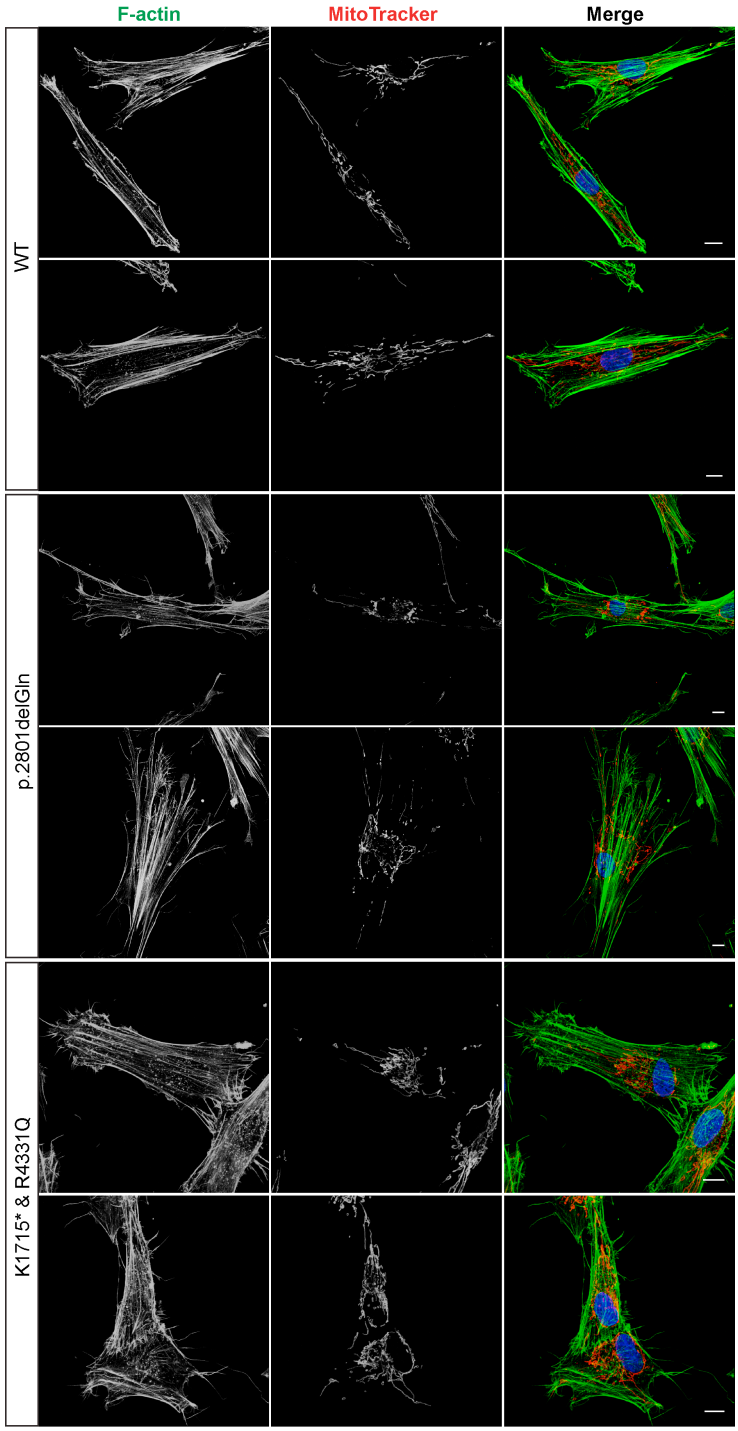

Figure 4.11. Organisation of the F-actin network in ARSACS patient HDFs. Representative confocal images of five ARSACS patient and WT control HDFs. Fibroblasts were incubated with both MitoTracker Red and an ActinGreen fluorescent marker. Confocal imaging showed the F-actin network in all ARSACS patient HDFs appeared unaltered from WT controls. Scale bars = 10 μm.

Likewise, ARSACS patient HDFs appear to have a normal microtubule distribution when compared to WT control cells (Figure 4.12). Microtubule nucleation from the microtubule organising centre (MTOC) did not appear compromised, but interestingly, the perinuclear accumulation of vimentin in ARSACS patient HDFs is spatially related to the MTOC. This is highlighted in the zoomed panels in figure 4.12.

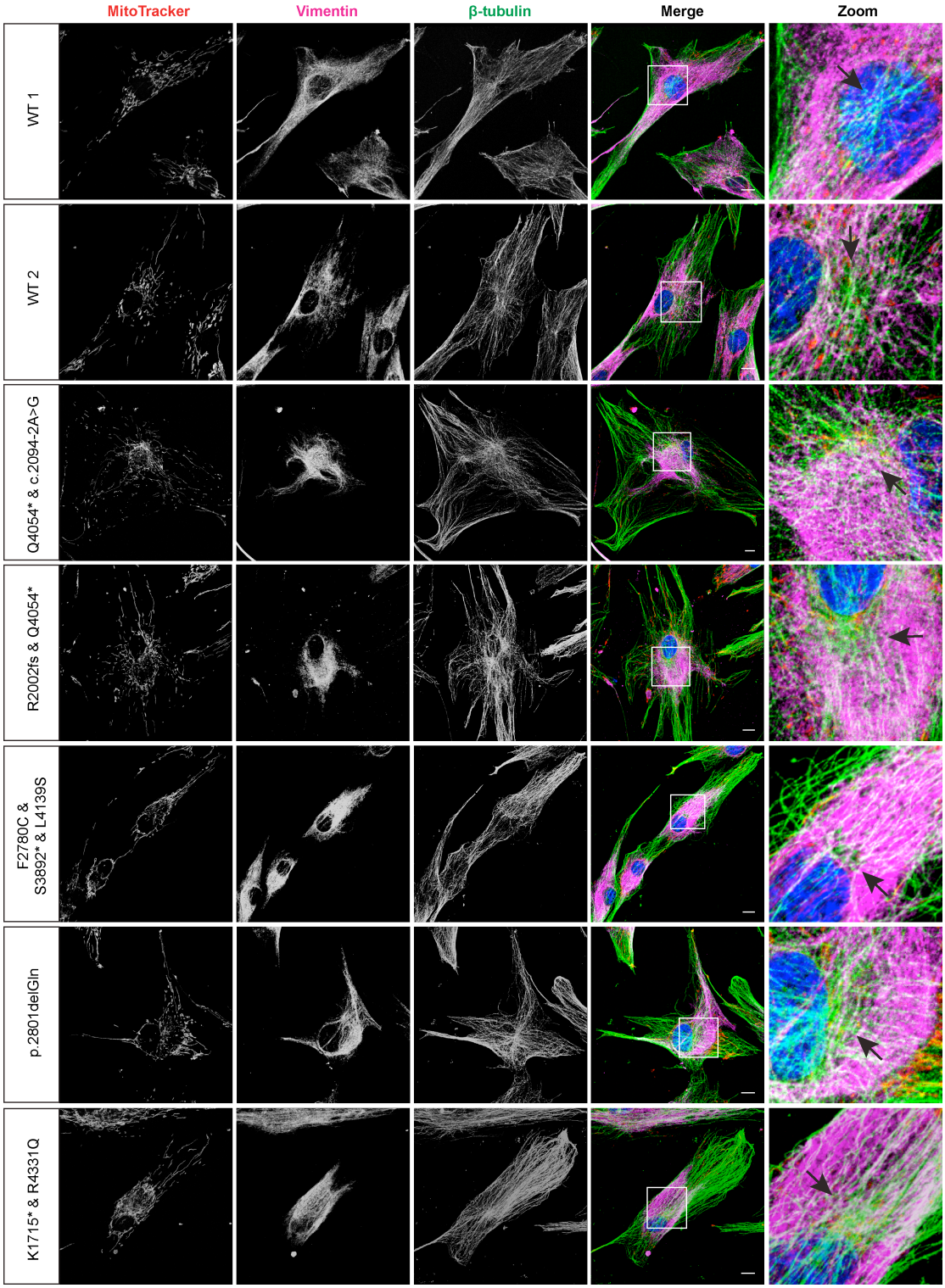

Figure 4.12. Organisation of the microtubule network in ARSACS patient HDFs. Representative confocal images of five ARSACS patient and WT control HDFs. Fibroblasts were incubated with MitoTracker Red and were stained with rabbit anti-vimentin and mouse anti-β-tubulin antibodies. The microtubule network in all ARSACS patient HDFs appeared unaltered from WT controls. White boxes in the merged panels are shown zoomed in the far right panels and highlight the MTOC, which is indicated by the black arrows. Scale bars = 10 μm.

4.2.4.1. *Altered acetylated α-tubulin in ARSACS patient HDFs*

Acetylation is a post-translational modification that occurs to many proteins, including tubulins. α–tubulin acetylation enhances microtubule stability (Piperno et al., 1987). Cellular structures that contain acetylated α–tubulin include primary cilia, centrioles, mitotic spindles, midbodies and a subset of cytoplasmic microtubules. Visualisation of acetylated α–tubulin by confocal microscopy, keeping confocal settings constant for all imaging, revealed an increase in fluorescence intensity in all five ARSACS HDFs compared to WT controls (Figure 4.13).

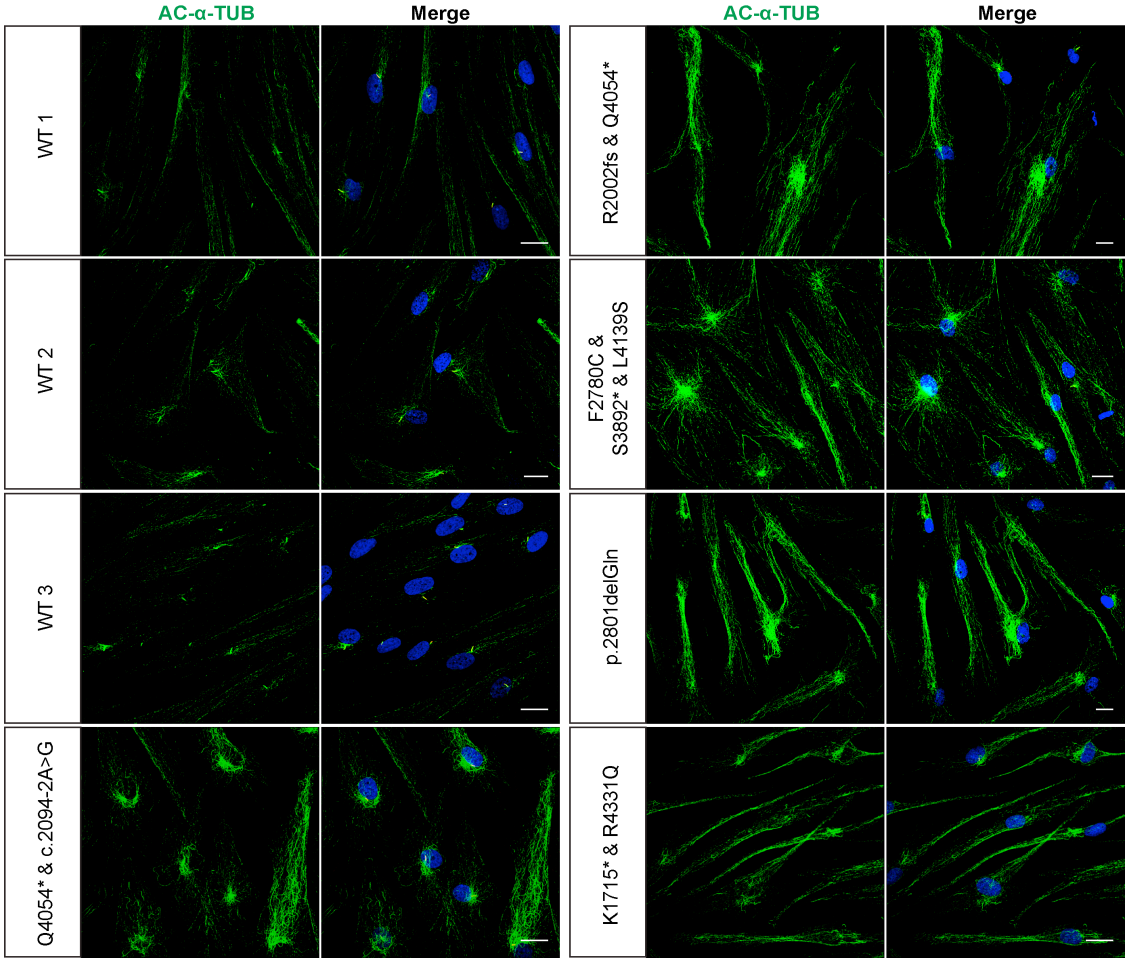

Figure 4.13. Altered acetylated α-tubulin in ARSACS patient HDFs. Representative confocal images of five ARSACS patient and WT control HDFs. All cells were serum starved for 72 hours prior to immunocytochemistry. Fibroblasts were stained with an acetylated α-tubulin antibody, while nuclei were counterstained with DAPI (blue). Scale bars = 20 μm.

In summary, the microtubule network, the MTOC, and the actin network have a normal distribution in ARSACS patient HDFs when compared with WT controls, indicating a specific disruption to IF distribution with loss of sacsin function. An exception to this is in the acetylation of α-tubulin, which appears to be increased and shows disorganisation in the ARSACS patient HDFs.

4.2.5. Disrupted localisation of other cellular organelles in ARSACS patient HDFs

IFs help to orchestrate the positioning and function of cellular organelles, including mitochondria, Golgi, endosomes, and lysosomes (Toivola et al., 2005). Therefore, it is not suprising that pertubations of the IF network can lead to alterations in the subcellular distribution of other organelles (Gao and Sztul, 2001; Gao et al., 2002; Styers et al., 2004). Due to the collapse of the IF network in ARSACS patient HDFs, the distribution of other organelles was investigated.

4.2.5.1. *Golgi apparatus*

Disruption of the IF network has previously been shown to affect Golgi localisation. For example, expression of CMT-like neurofilament mutant proteins in cultured neurons leads to Golgi fragmentation, along with alterations in other organelles (Perez-Olle et al., 2005). Also, expression of a keratin 18 (K18) mutation, which disrupts keratin IFs in cultured cells, alters Golgi distribution (Kumemura et al., 2004).

The organisation and location of the Golgi apparatus was analysed in the control and ARSACS HDFs by immunocytochemistry, using an antibody to GS28, a marker for a 28 kDa membrane protein of the cis-Golgi, along with MitoTracker Red to label the mitochondria. The Golgi apparatus becomes dispersed and fragmented around the perinuclear area of mitochondrial exclusion in all five ARSACS HDF lines compared to controls (Figure 4.14).

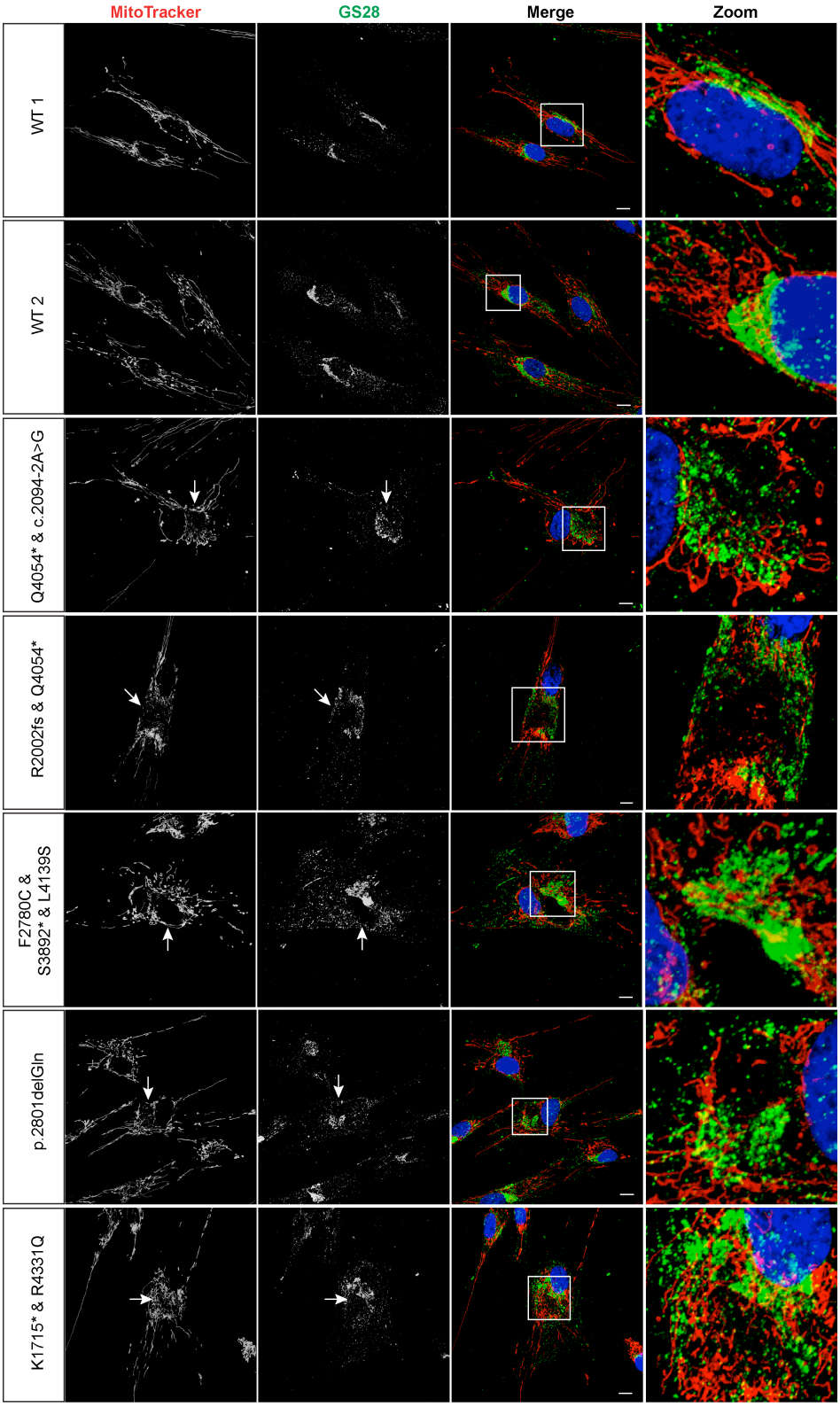

Figure 4.14. Fragmentation of the Golgi apparatus in ARSACS patient HDFs. Representative confocal images of five ARSACS patient and WT control HDFs. Fibroblasts were incubated with MitoTracker Red and were stained with a mouse anti-GS28 antibody, a marker for a 28 kDa membrane protein of the cis-Golgi. Confocal analysis showed fragmentation of the Golgi apparatus in all five ARSACS HDF lines. White boxes are shown as zoomed images in the far right panels. White arrows indicate areas of mitochondrial network disruption and Golgi exclusion. Scale bars = 10 μm.

4.2.5.2. *Primary cilia*

Virtually all cells have a single primary cilium during interphase of the cell cycle. Structurally the cilium comprises a centriole-derived basal body from which projects an axoneme composed of acetylated microtubules. It has a fundamental role in numerous cellular signalling pathways, such as the hedgehog (Corbit et al., 2005; Rohatgi et al., 2007), Wnt (Corbit et al., 2008), and insulin growth factor (IGF) pathways (Zhu et al., 2009). Cilia have functional roles in differentiation (Clement et al., 2009; Hoey et al., 2012), mechanobiology (Malone et al., 2007; Wann et al., 2012), as a cell cyle checkpoint (Kim and Tsiokas, 2011), and it is critical to the development and health of many tissues.

The base of the primary cilium lies in close proximity to the Golgi apparatus, therefore disruption in Golgi localisation and organisation may indicate disruption of the primary cilium. Also, the ARSACS HDFs display a disorganisation of acetylated α-tubulin (Figure 4.13), which is a marker for primary cilia, again indicating that primary cilia may be disrupted. Hence, primary cilia incidence and length were assessed in ARSACS patient HDFs compared to WT controls.

Cells were serum starved for 72 hours (media without FBS) before being processed for immnuocytochemistry using antibodies to ADP-ribosylation factor-like protein 13B (ARL13B), and acetylated α-tubulin, which are both markers of the ciliary axoneme. Primary cilia were visualised by confocal microscopy. Over 250 cells were scored for the presence/absence of a primary cilium per cell line (20 image fields from 2 cover slips per cell line). This quantification identified a significant reduction of 26.9 ± 2 % ($p<0.001$) in the mean number of ciliated cells in ARSACS HDF lines compared to WT controls (Figure 4.15 A,B). The lengths of at least 100 cilia per cell line (2 cover slips per cell line) were measured using ImageJ software (rsb.info.nih.gov/ij). This shows a significant reduction in the average cilium length in ARSACS patient HDFs compared to WT controls ($p<0.001$), reducing from a mean length of 4.37 ± 0.04 μm in WT controls to 3.90 ± 0.04 μm in the ARSACS HDFs (Figure 4.15 A,C).

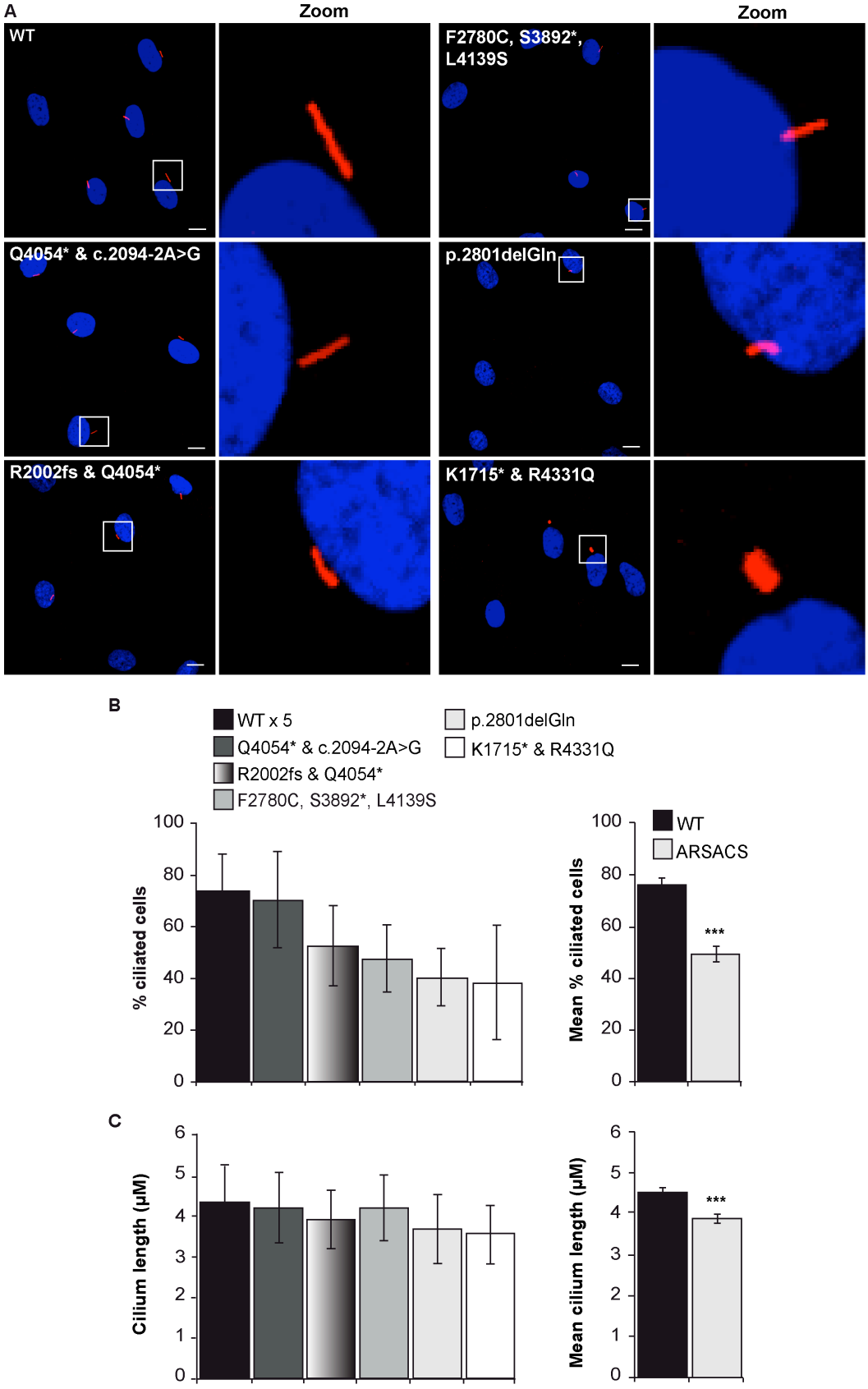
A
Zoom
Zoom
WT
F2780C, S3892*, L4139S
Q4054* & c.2094-2A>G
p.2801delGln
R2002fs & Q4054*
K1715* & R4331Q
B
WT x 5
Q4054* & c.2094-2A>G
R2002fs & Q4054*
F2780C, S3892*, L4139S
p.2801delGln
K1715* & R4331Q
% ciliated cells
Mean % ciliated cells
WT
ARSACS
***
C
Cilium length (µM)
Mean cilium length (µM)
***

Figure 4.15. Cilia incidence and length are reduced in ARSACS HDFs. (A) Representative confocal images of five ARSACS patient and a WT control HDF line. All cells were serum starved for 72 hours prior to processing for immunocytochemistry. Primary cilia were labelled with antibodies directed to ARL13B (red) while nuclei were counterstained with DAPI (blue). White boxes are shown as zooms to the right of each image. Scale bar represents 10 μm. **(B)** Primary cilia incidence and **(C)** primary cilia length for WT and five ARSACS patient HDFs. Results are expressed as mean ± SD for WT control and each patient cell line. WT is pooled data from five different control HDF lines (the five WT control HDF lines are shown seperately in appendix 4). Bar graphs on the far right represent the combined results from all five WT control and five patient HDF lines to give an overall mean ± SEM, $^{***}p<0.001$. Statistics were carried out using an unpaired two-tailed Students t-test.

4.2.5.3. *Early endosomes*

There is evidence for IF involvement in the endosomal-lysosomal pathway. For example, IFs bind to the adapter protein AP-3, which carries vesicles between endosomal-lysosomal compartments (Styers et al., 2005; Styers et al., 2004) IF disruption may affect the positioning of endosomes and lysosomes.

The localisation of early endosomes was analysed in the control and ARSACS HDFs by immunocytochemistry. Fibroblasts were incubated with MitoTracker Red before being processed via immunocytochemistry using an antibody to early endosome antigen 1 (EEA1). Confocal microscopy reveals a disruption in the normal localisation of early endosomes in all five ARSACS HDFs compared to five WT controls (Figure 4.16). Early endosomes are relatively dispersed around the perinuclear regions in WT control cells; however, they appear to become trapped around the edge of the mitochondrial 'hole' in ARSACS HDFs (indicated by white arrows in figure 4.16).

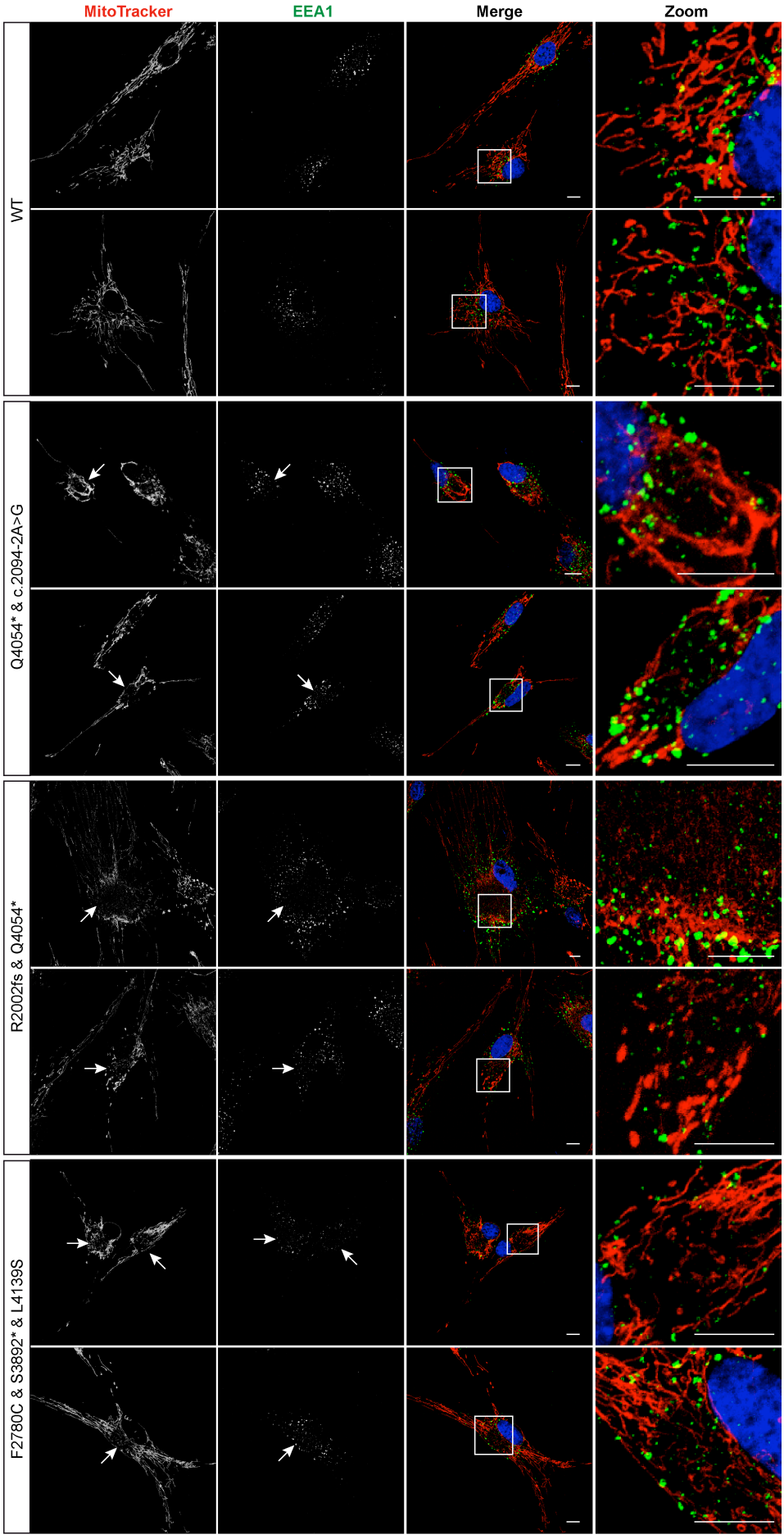
MitoTracker
EEA1
Merge
Zoom
WT
Q4054* & c.2094-2A>G
R2002fs & Q4054*
F2780C & S3892* & L4139S

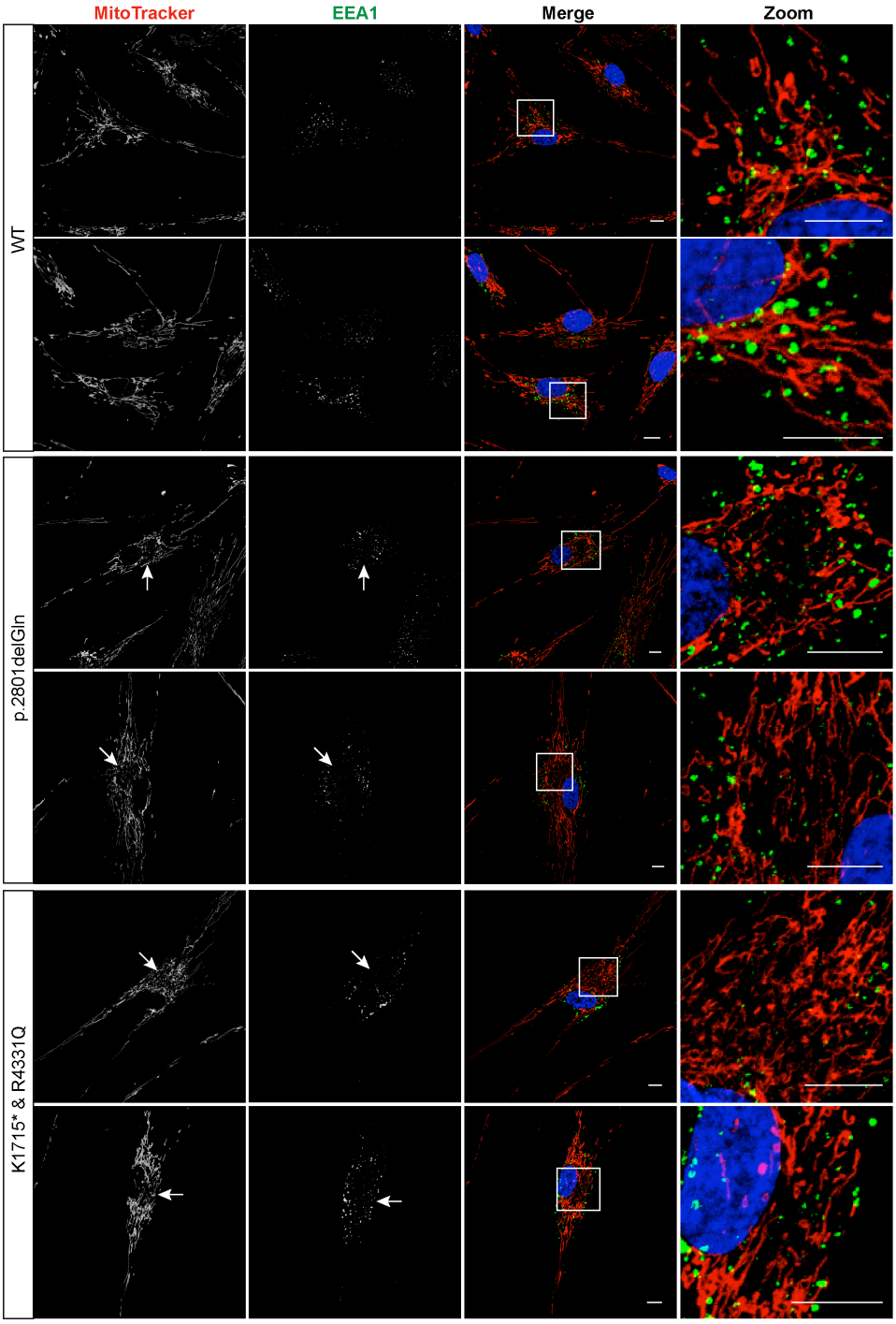

Figure 4.16. Early endosome relocalisation around the area of perinuclear mitochondrial disruption in ARSACS patient HDFs. Representative confocal images of five ARSACS patient and WT control HDFs. Fibroblasts were incubated with MitoTracker Red and were stained with a mouse anti-EEA1 antibody (green), a marker for a 180 kDa membrane-associated protein to early endosomes. Confocal analysis shows disruption in the localisation of early endosomes in all five ARSACS patient HDFs. White boxes in the merged panels are shown as zoomed images in the far right panels. White arrows indicate areas of mitochondrial network and early endosome disruption. Scale bars = 10 μm.

4.2.6. Disorganisation of the vimentin network in sacsin knockdown cells

The vimentin network was also analysed in WT HDFs that were transiently transfected with *SACS* siRNA or *SCRM* siRNA. This cellular knockdown model allows the comparison of cells with loss of sacsin to an isogenic control.

4.2.6.1. *Collapsed and bundled vimentin IF network*

The effect of *SACS* siRNA knockdown on the vimentin network was investigated in normal HDFs. Cells were transfected with mito-DsRed and either *SCRM* or *SACS* siRNA, as detailed in the methods. After 48 hours, cells were processed for immunocytochemistry using an antibody to vimentin. Confocal microscopy shows that the vimentin network appears to be collapsed, with some perinuclear bundling, in cells transfected with *SACS* siRNA compared to *SCRM* controls (Figure 4.17).

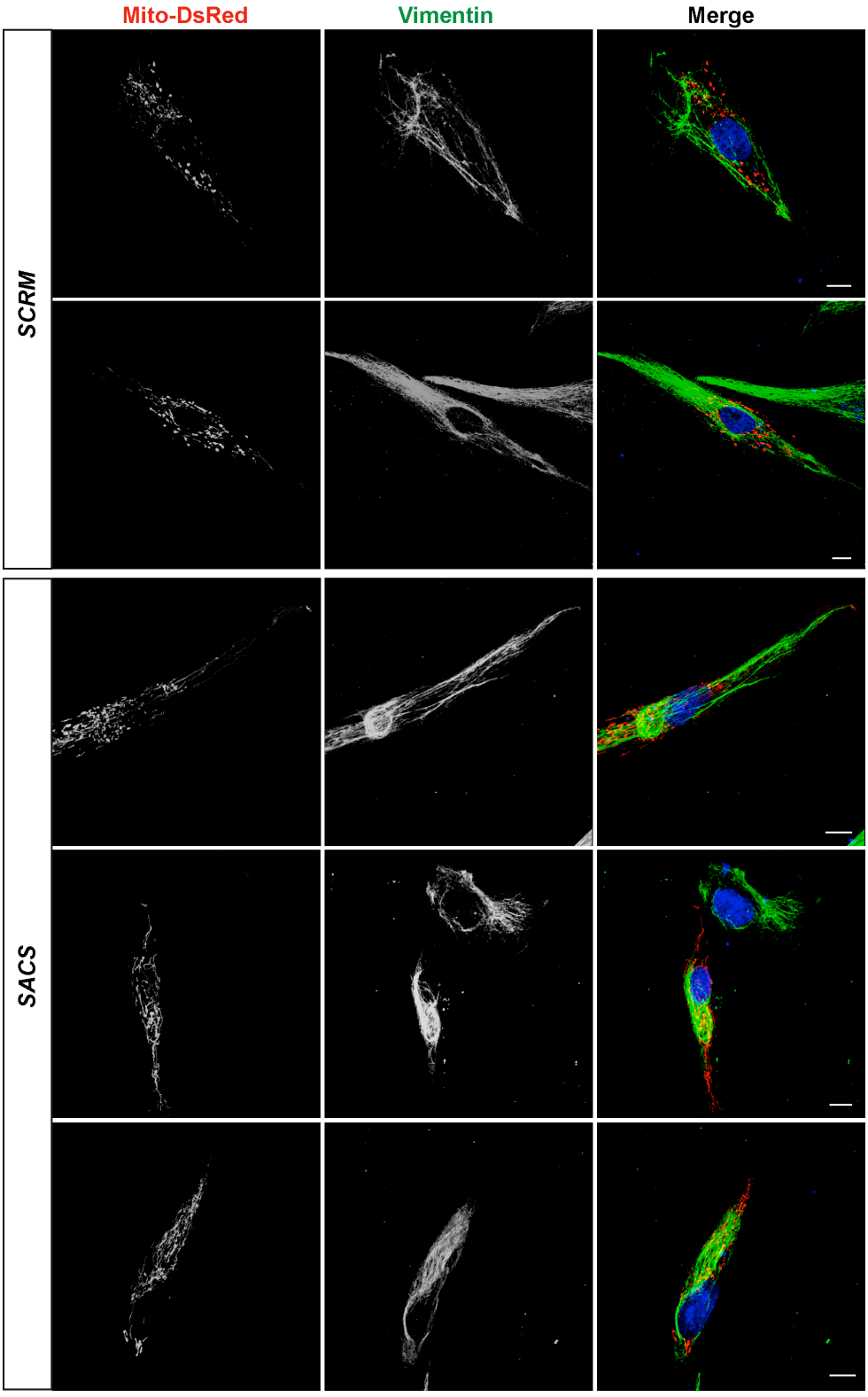

Figure 4.17. Sacsin knockdown leads to collapsed and bundled vimentin IFs. Representative images of normal HDFs transfected with mito-DsRed and either *SCRM* or *SACS* siRNA. After 48 hours, cells were fixed and permeabilised, and incubated with an anti-vimentin antibody. Maximum intensity projections of z-stacks were taken via confocal microscopy. The vimentin network appears collapsed and bundled in *SACS* siRNA transfected cells compared to *SCRM* control. Scale bars = 10µm.

4.2.6.2. *Reduced fluorescence recovery of vimentin-GFP in sacsin knockdown cells*

IF assembly requires the polymerisation of individual IF monomers. A dimer forms through the coiled-coil interactions of two parallel IF protein chains. Two dimers associate in a staggered and antiparallel fashion to form tetramers. On average, eight tetramers combine to form structures known as unit length filaments (ULFs). These ULFs link up end-to-end and assemble into mature IFs (Colakoglu and Brown, 2009; Vikstrom et al., 1992).

As sacsin deficiency leads to alterations in the arrangement of the vimentin network, there may be an impact on the dynamic assembly of the vimentin network. To assess this we analysed protein dynamics by fluorescence recovery after photobleaching (FRAP). FRAP studies have been widely used as a measure of IF dynamics (Perez-Sala et al., 2015; Vikstrom et al., 1992; Winter et al., 2014; Yoon et al., 2001a; Yoon et al., 1998). SH-SY5Y cells were transfected with a vimentin-targeted GFP, in combination with either *SCRM* or *SACS* siRNA. After 48 hours FRAP analysis was performed on 20-25 cells for each treatment. Briefly, this involved photobleaching a small area of vimentin-targeted GFP within a cell and then monitoring the diffusion of the fluorescent signal within vimentin back into the region of interest from the surrounding region.

Confocal settings were kept constant for all imaging, and areas of vimentin bundling in the *SACS* siRNA treated cells were avoided. There was a reduced level of fluorescence recovery from photobleaching in *SACS* cells compared to *SCRM* control. The vimentin-GFP fluorescence recovers to 56 ± 4.2 % of the initial intensity in *SCRM* siRNA transfected cells, whereas in *SACS* siRNA transfected cells, the fluorescence recovers to only 35 ± 2.5 % of the initial intensity after 85 seconds (Figure 4.18). So the vimentin-targeted GFP diffuses back into the bleached zone at a slower rate in *SACS vs*. *SCRM* siRNA transfected cells. This indicates that the mobility of vimentin molecules is reduced in cells with loss of *SACS* expression, suggesting that the vimentin network is less dynamic.

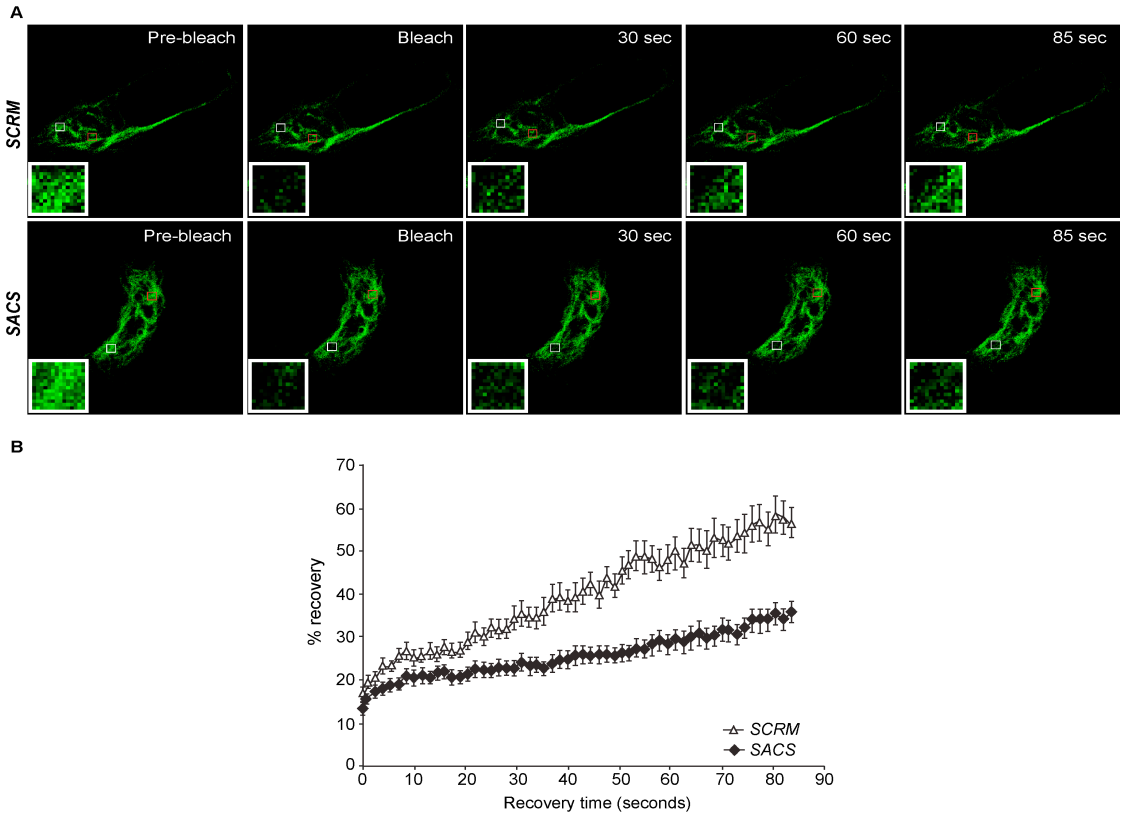

Figure 4.18. FRAP analysis showed reduced vimentin-GFP fluorescence recovery in sacsin knockdown cells. (A) Representative images of SH-SY5Y cells co-transfected with vimentin-GFP and either *SCRM* or *SACS* siRNA. A 15 x 15 µm area of the cell containing vimentin IFs, indicated by the white box, was photobleached and the cells imaged every 1.5 seconds for 85 seconds. A 15 x 15 µm area of the cell containing vimentin IFs that was not photobleached is indicated by the red box. Fluorescence measurements of this area were used as a control for any loss of fluorescence over time that was not due to photobleaching. **(B)** Graphical representation of recovery after photobleaching. Fluorescent intensities of the 15 x 15 µm area were normalised to pre-bleach levels at 100%. Error bars represent SEM.

4.3. Conclusions

The subcellular localisation of sacsin has previously been shown to be predominantly cytoplasmic with a significant mitochondrial component (Parfitt et al., 2009). In this chapter, the localisation of sacsin was further investigated in SH-SY5Y cells using a monoclonal antibody that recognises a fragment within human sacsin amino acids 4100-4200. With the recent advancement of super-resolution microscopy, cells, organelles and proteins can be visualised to a much higher resolution. Using the SIM approach to super-resolution imaging, a proportion of sacsin was found to be in close proximity to vimentin IFs. The previously identified localisation of sacsin with mitochondria was also confirmed. Importantly, areas where sacsin localised between the mitochondrial and vimentin network were observed. This is a feature of scaffold or cytolinker proteins, such as plectin, so intriguingly; this may suggest sacsin has a cytoskeletal linker function. This is discussed further in Chapter 6.

In addition, cellular fractionation studies showed that sacsin was detected in an IF-enriched fraction, further indicating an association between sacsin and vimentin. The mechanism of how sacsin may be associating with vimentin is unknown. However, sacsin contains three repeating regions, each with homology to the N-terminal ATPase domain of HSP90, the first of which has been shown to have ATPase activity (Anderson et al., 2010). The ATPase domain of HSP90 is important for an interaction with vimentin, and this interaction protects vimentin from apoptotic cleavage (Zhang et al., 2006). Hence, the three regions within sacsin, which have homology to the ATPase domain of HSP90, may interact with vimentin.

Sacsin appears to relocalise from being throughout the cell to concentrating in the perinuclear area of vimentin bundling in two ARSACS patient HDFs with some remaining sacsin expression (Figures 4.7 and 4.9). This further supports an association between sacsin and vimentin because the relocalisation of vimentin is consistent with the relocalisation of sacsin. The sacsin mutations present in these two patients (p.2801delQ, K1715* and R4331Q, Figure 4.5) do not affect the three HSP90-like domains. Therefore, the presence of these HSP90-like domains could explain an association between vimentin and sacsin.

Recently, disrupted neurofilament organisation was identified in somatodendritic regions of various neuronal populations from sacsin knockout mice and ARSACS brains (Lariviere et al., 2015). In this chapter, a dramatic collapse of vimentin IFs into a

perinuclear bundle was observed in almost 80% of dermal fibroblasts from five ARSACS patients, all with different *SACS* mutations. This vimentin phenotype was also identified in WT HDFs transfected with *SACS* siRNA, but was not present in *SCRM* siRNA control cells. This data demonstrates that the neurofilament defect identified in neurons of sacsin knockout mice and ARSACS brains extends to other IFs and other cell types. Neurons are perhaps more vulnerable to a perturbation of the IF network; hence there is more of a detrimental effect in neurons.

Disruption to the microtubule network, for example with drugs such as colchicine, nocodazole or vinblastine, can induce IF disorganisation (Lazarides, 1980). There were no apparent changes in morphology of the microtubule and microfilament network in the ARSACS patient HDFs, suggesting that the vimentin collapse is not a consequence of a disorganised microtubule network. However, there may be an increase in stability of the microtubule network, as indicated by increased acetylation of α-tubulin in the ARSACS patient HDFs, although this needs to be verified by immunoblotting. It would be interesting to investigate whether ARSACS patient HDFs are resistant to destabilisation of their microtubule network, for example using nocodazole, as this would indicate reduced microtubule dynamics. Also, it is known that inhibiting the tubulin deacetylase, HDAC6, enhances microtubule acetylation (Asthana et al., 2013; Haggarty et al., 2003; Zhang et al., 2008) thus, HDAC6 levels and activity could be analysed in ARSACS patient cells as this may account for the enhanced acetylation of α-tubulin.

Intriguingly, a disruption in the mitochondrial network is seen in the same perinuclear location of vimentin bundling. It seems likely that the abnormal vimentin bundle is either forcing mitochondria out of this area and/or preventing mitochondria from being transported to this region, so mitochondria are seen to accumulate at the periphery of the vimentin bundle.

The organisation of other organelles was also shown to be disrupted in all five ARSACS patient HDFs compared to WT controls, and importantly, the disruption is also spatially related to the perinuclear vimentin bundling. For example, the Golgi becomes dispersed and fragmented around the edge of the vimentin bundle, early endosomes become relocalised around the edge of the vimentin bundle, and primary cilia, which usually form at the centrosome, are reduced in incidence and length. This

suggests that the perinuclear collapse and bundling of vimentin may be disrupting the normal localisation of other cellular organelles in ARSACS patient HDFs.

In fact, the cellular phenotype observed in cells with loss of sacsin function is characteristic of what has been shown to occur in cells due to the formation of aggresomes (Garcia-Mata et al., 1999; Johnston et al., 1998; Kopito, 2000). Aggresomes form due to a disruption in normal cellular protein homeostasis meaning that misfolded proteins accumulate and aggregate. Specific characteristic features indicative of aggresome formation include a collapse of the IF network into perinuclear cage-like structures, and various organelles including mitochondria, Golgi and early endosomes are re-localised around the edge of the IF cage (Garcia-Mata et al., 1999; Johnston et al., 1998; Kopito, 2000). Aggresomes form at the microtubule organising centre (MTOC, (Garcia-Mata et al., 1999; Johnston et al., 1998) and interestingly the vimentin bundling in the ARSACS HDFs is spatially related to the MTOC, although this needs to be verified using the centrosomal protein, gamma-tubulin, as a marker of the MTOC.

The data also shows that vimentin network dynamics are reduced in cells with loss of sacsin function. FRAP analysis was performed in cells transfected with vimentin-GFP along with *SCRM* or *SACS* siRNA. This shows a reduced level of fluorescence recovery in cells with loss of sacsin as the vimentin-targeted GFP moved back into the bleached zone at a slower rate, indicating that subunit exchange is slower and less dynamic in cells with loss of sacsin. Increased stability and reduced turnover of IFs have previously been shown to be consequences of IF bundling (Flitney et al., 2009; Kim et al., 2010b; Lee and Coulombe, 2009; Windoffer et al., 2011), hence the reduction in vimentin dynamics due to loss of sacsin may be a consequence of alterations in vimentin architecture. Vimentin is likely to become more stable in order to form a perinuclear cage around protein aggregates. Alternatively, vimentin dynamics may be reduced due to misfolding of vimentin itself as a result of loss of sacsin. Interestingly, the molecular chaperone HSP27 binds to vimentin and ameliorates vimentin insolubilisation and vimentin filament collapse induced by the cytotoxic effects of cadmium, a toxic heavy metal (Lee et al., 2005). This suggests that HSP27 may maintain the structure and integrity of vimentin filaments under stress conditions. It is possible that sacsin may have a similar role as a molecular chaperone for IFs.

Collectively, the data here shows that loss of sacsin function leads to a cellular phenotype that indicates the formation of an aggresome-like structure. Such structures are known to form due to the accumulation of misfolded proteins. This will be investigated further in Chapter 5.

4.3.1. Further work

This chapter has identified that a proportion of sacsin protein localises in close proximity to vimentin IFs and is present in an IF-enriched fraction of cells. To investigate whether an association between sacsin and vimentin is mediated through sacsins HSP90-like domains, these domains could be disrupted by site-directed mutagenesis experiments to see if sacsin localisation is altered. This would also provide more evidence of an interaction between sacsin and vimentin.

Also, inhibiting the ATPase activity of HSP90 with geldanamycin has been shown to prevent an interaction between HSP90 and vimentin and leads to dramatically reduced vimentin levels (Zhang et al., 2006). Perhaps geldanamycin also inhibits the ATPase activity of the HSP90-like domains within sacsin. Thus, it would be interesting to investigate whether treating cells with geldanamycin affects the association of sacsin with vimentin and/or affects the cellular levels of sacsin. This would provide evidence that the sacsin-vimentin association is mediated through sacsins HSP90-like domains.

CHAPTER 5:
DISRUPTED PROTEOSTASIS IN ARSACS

5.1. Introduction and Aims

Cellular stresses, such as thermal or oxidative stress, and alterations in protein structure caused by mutations, RNA modifications, translational errors or post-translational modifications, can lead to unfolded or partially folded proteins (Hurle et al., 1994; Princiotta et al., 2003; Wetzel, 1994). This may subsequently lead to protein aggregation due to undesirable interactions with other molecules. Protein misfolding is not rare, with approximately 30% of newly synthesised proteins estimated to be misfolded (Schubert et al., 2000). The existence of a cellular 'quality control' machinery means that misfolded proteins do not normally accumulate in unstressed cells. As detailed in the introduction to this thesis, the initial cellular defense against misfolded proteins is mediated by molecular chaperone networks, which assist in the refolding or degradation of misfolded proteins. If a protein that is normally structured cannot be refolded, it is targeted for degradation by the ubiquitin/proteasome system (UPS, (Ciechanover, 2006; Muchowski and Wacker, 2005)) or the autophagy-lysosome pathway (ALP). However, when these lines of defense fail or are overwhelmed, an accumulation of misfolded proteins can ultimately lead to the formation of proteinacious aggregates. This is a feature of many neurodegenerative diseases, for example, Alzheimer's disease (AD), Parkinson's disease (PD), Huntington's disease (HD), spinocerebellar ataxias (SCA), and amyotrophic lateral sclerosis (ALS, (Ross and Poirier, 2004; Soto and Estrada, 2008; Tran and Miller, 1999)).

Misfolded protein aggregates are transported along microtubules, in a retrograde direction, by the cytoplasmic dynein-dynactin motor complex. This facilitates their delivery to the MTOC where they subsequently accumulate (Garcia-Mata et al., 1999; Johnston et al., 1998, Figure 5.1). The perinuclear location into which aggregated proteins are sequestered has been termed the aggresome (Johnston et al., 1998). Hence, an intact microtubule cytoskeleton is necessary for aggresome formation (Johnston et al., 1998). In addition, the correct function of the dynein-dynactin complex is required for aggresome formation. Overexpression of the dynamitin (p50) subunit of the dynactin complex leads to dissociation of the dynactin complex and inhibits dynein-mediated transport on microtubules (Burkhardt et al., 1997; Presley et al., 1997), resulting in the accumulation of peripherally distributed small protein aggregates rather than perinuclear aggresomes (Garcia-Mata et al., 1999; Johnston et al., 1998).

Depolymerisation of microtubules does not lead to the rapid dispersal of aggresomes, suggesting that they are not dynamic structures (Johnston et al., 1998).

5.1.1. Characteristics of aggresome formation

One of the most consistent and robust markers of aggresome formation is the relocalisation of the IF cytoskeleton from its normal extended cytoplasmic distribution to a collapsed perinuclear cage-like structure that surrounds the aggresome (Figure 5.1, (Iwata et al., 2005a; Johnston et al., 1998; Kopito, 2000; Wang et al., 2005a)). The type of IF that surrounds the aggresome depends on the cell type. For example, in mesenchymal cells this will be vimentin and in cardiomyocytes it will be desmin, whereas in neurons, aggresomes are surrounded by neurofilaments (Taylor et al., 2003). The molecular events that lead to this IF rearrangement are not yet understood. The pericentriolar accumulation of protein aggregates also frequently results in expansion of the centrosome, as assessed by γ tubulin and pericentrin (Wigley et al., 1999).

Aggresomes form in the region of the cell usually occupied by the Golgi. The Golgi becomes displaced and fragmented around the aggresome, and this becomes more apparent as the aggresome grows in size (Garcia-Mata et al., 1999). This has been observed in cultured cells overexpressing aggregation-prone proteins (Garcia-Mata et al., 1999), in neurons from AD brains, in spinal cords from ALS patients, and in a transgenic mouse model of ALS (Gonatas et al., 1998). Surprisingly, in cells that contain aggresomes, Golgi function does not seem to be compromised and cargo moves from the ER through the Golgi to the plasma membrane as normal (Garcia-Mata et al., 2002).

Aggresomes are enriched with the protein that is misfolding, as well as proteins involved in maintaining proteostasis, including HSP70, the HSP40 proteins Hdj1 and Hdj2, and the chaperonin TriC/TCP (Garcia-Mata et al., 1999; Wigley et al., 1999). In addition to chaperones, the presence of both 19S and 26S proteasome subunits in aggresomes has been reported (Anton et al., 1999; Fabunmi et al., 2000; Wigley et al., 1999), whereas the presence of ubiquitin localisation is inconsistent (Johnston et al., 2002; Garcia-Mata et al., 1999; Wigley et al., 1999; Johnston et al., 1998).

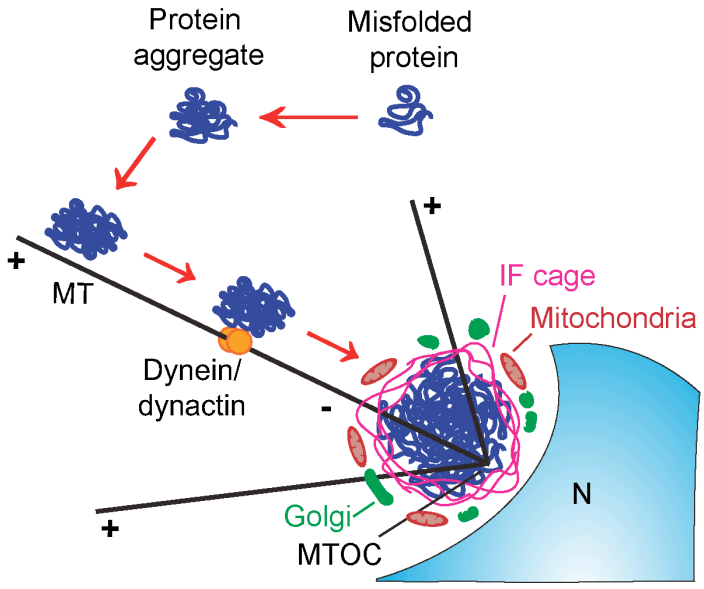

Figure 5.1. Schematic model of aggresome formation. Aggresome formation is a cellular response to misfolded proteins that aggregate and resist degradation by the proteasome. Aggregated proteins are transported along microtubules (MT), in a retrograde manner, by the dynein-dynactin motor to the microtubule-organising centre (MTOC). At the MTOC they are surrounded by a cage of IFs, and the localisation of other cellular organelles is disrupted. Aggresomes accumulate components of the ubiquitin-proteasome pathway of protein degradation, including molecular chaperones, ubiquitin, and proteasomes (Garcia-Mata et al., 2002; Kopito, 2000). N: nucleus.

The overall structure of aggresomes varies depending on the aggregating substrate and the 'host' cells. For example, mutant ATP7B protein, which is responsible for Wilson disease, forms spherical aggresomes, with a diameter of 1-3μm, in HEK293 cells, but forms extended ribbon aggresomes in HuH-7 cells (Harada et al., 2001). The molecular mechanisms that define the shape of an aggresome are unknown.

The function of aggresome formation is not fully understood, but it is thought it acts to sequester cytotoxic proteins, preventing abnormal interactions with other proteins and cell organelles (Chen et al., 2011; Garcia-Mata et al., 2002; Kopito, 2000). Studies have found that aggresome formation reduces the amount of mutant huntingtin protein present in the rest of the cell and is associated with increased cell survival (Arrasate and Finkbeiner, 2005; Arrasate et al., 2004).

Accumulating evidence suggests that aggresomes are substrates for autophagy, and in support of this, autophagic machinery has been found to localise to aggresomes (Fortun et al., 2003; Iwata et al., 2005a; Iwata et al., 2005b; Ravikumar et al., 2002; Taylor et al., 2003; Yamamoto et al., 2006; Zaarur et al., 2014).

5.1.2. Autophagy

As detailed in the introduction to this thesis (section 1.4.4), macroautophagy involves the formation of autophagosomes, which engulf cytoplasmic proteins and organelles and deliver them to lysosomes for degradation. Various autophagy (ATG) proteins are essential for the formation of autophagosomes (Reggiori and Klionsky, 2002; Rubinsztein et al., 2007). A complex of ATG5-ATG12-ATG16 is required for fusion of vesicles, and this complex requires the catalytic activities of ATG7 and ATG10. The processing of microtubule-associated protein 1 light chain 3 (LC3, also known as ATG8) is also important for autophagosome biogenesis. LC3 is cleaved by ATG4B to form LC3-I, which is then conjugated to phosphatidylethanolamine by ATG7 and ATG3 to form LC3-II (Kabeya et al., 2000).

As autophagosome formation completes, the ATG5-ATG12-ATG16 complex dissociates, whereas LC3-II remains associated with the completed autophagosome. Autophagosomes are then trafficked by dynein-dynactin motors along microtubules (Ravikumar et al., 2005) to the perinuclear region where they fuse with lysosomes and their contents are degraded. Efficient degradation of autophagy substrates can only occur if the acidic lysosomal pH is correctly maintained and the lysosomal hydrolases are functioning correctly.

Autophagy is particularly important in neurons because the total content of dysfunctional proteins and damaged organelles cannot be reduced through cell division (Tooze and Schiavo, 2008; Winslow and Rubinsztein, 2008). Abnormal numbers of autophagosomes are indicative of autophagic dysfunction (Nixon et al., 2005; Yang et al., 2007), which may be due to an upregulation of autophagy or impaired clearance of autophagosomes (Boland et al., 2008; Rubinsztein et al., 2009). Autophagic dysfunction has been implicated in the pathogenesis of many neurodegenerative diseases (Boland et al., 2008; Kegel et al., 2000; Nixon et al., 2005; Ravikumar et al., 2002).

As described in Chapter 1, sacsin contains multiple domains linking to molecular chaperone and protein degradation pathways. In addition, previous research has shown that sacsin is recruited to inclusions of mutant ataxin-1 (Parfitt et al., 2009). When sacsin levels were reduced by siRNA, expression of mutant ataxin-1 led to increased cell death compared to SCRM siRNA control, which suggests enhanced toxicity of mutant ataxin-1 with loss of sacsin (Parfitt et al., 2009). Collectively, this data suggests that sacsin has a role in protein quality control pathways. Therefore, loss of sacsin could

lead to a disruption in protein quality control and potentially an accumulation of misfolded proteins.

In Chapter 4, data was provided showing that cells with loss of sacsin function have several characteristics of aggresome formation. The vimentin network collapses into perinuclear cage-like structures, the Golgi complex becomes displaced and fragmented, and other organelles, such as mitochondria and early endosomes become relocalised around the periphery of the vimentin bundle. Therefore, the aim of this chapter was to further investigate whether loss of normal sacsin function leads to an accumulation of misfolded proteins and subsequent perinuclear aggregate formation. Molecular chaperones, ubiquitin, proteosomal subunits, and markers of autophagy have all previously been shown to be recruited to protein aggregates (Garcia-Mata et al., 1999; Iwata et al., 2005b; Wigley et al., 1999; Zaarur et al., 2014); hence immunocytochemistry for these proteostasis components was performed, followed by confocal microscopy. Evidence for an accumulation of misfolded proteins in cells with loss of sacsin function would support a role for sacsin in the cellular protein quality control system and would indicate a novel factor contributing to disease pathogenesis in ARSACS.

5.2. Results

5.2.1. Perinuclear accumulation of HSP70 in ARSACS patient HDFs

Molecular chaperones, such as HSP70, are known to be abundantly present in, and are actively recruited to aggresomes (Garcia-Mata et al., 1999; Johnston et al., 1998; Saliba et al., 2002). Therefore, HSP70 localisation was investigated in ARSACS patient HDFs compared to WT controls. Cells were incubated with MitoTracker Red, followed by immunocytochemistry using antibodies to HSP70 and vimentin. Confocal microscopy revealed that HSP70 strongly accumulates in a single perinuclear region in the ARSACS patient HDFs, which is where the vimentin network also concentrates. In contrast, HSP70 is dispersed throughout the cytoplasm in WT controls (Figure 5.2).

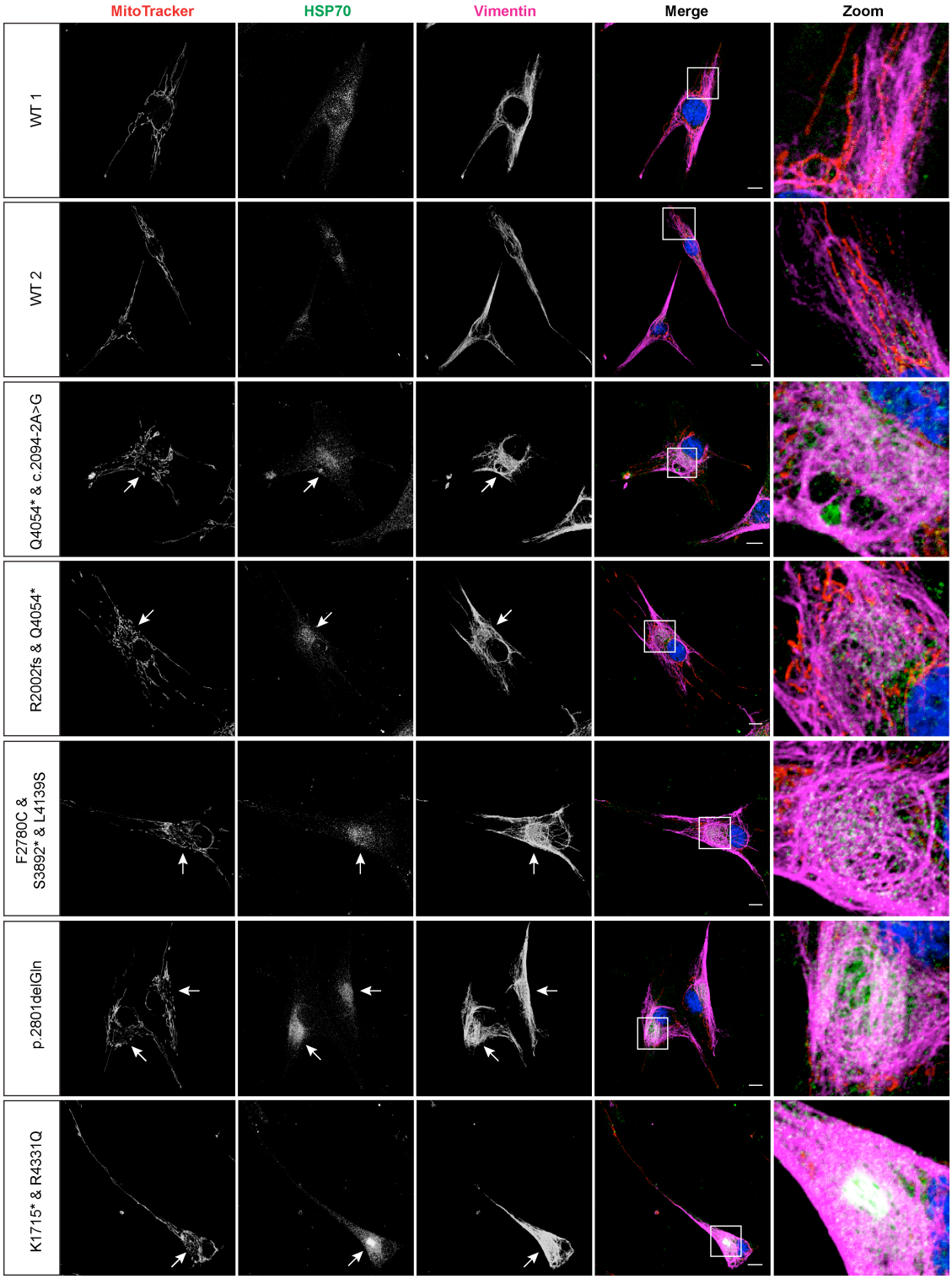

Figure 5.2. Perinuclear accumulation of HSP70 in ARSACS patient HDFs. Representative confocal images of ARSACS patients and WT control HDFs. Cells were incubated with MitoTracker Red, followed by staining with antibodies to HSP70 and vimentin. Confocal analysis showed accumulation of HSP70 in perinuclear regions in all five ARSACS patient HDFs. White boxes in merged panels are shown zoomed in the far right panels. Scale bars = 10 μm.

5.2.2. HSP70 protein levels were unchanged in ARSACS patient HDFs

Cellular stresses leading to an accumulation of misfolded proteins can result in altered expression of molecular chaperones, such as HSP70 (Hartl et al., 2011; Mosser et al., 1988). Due to the re-localisation of HSP70 in ARSACS patient HDFs, an immunoblot was performed to analyse total HSP70 protein levels in ARSACS patient HDFs compared to WT controls. There was no significant difference in total cellular levels of HSP70 in ARSACS patient cells compared to WT controls (Figure 5.3).

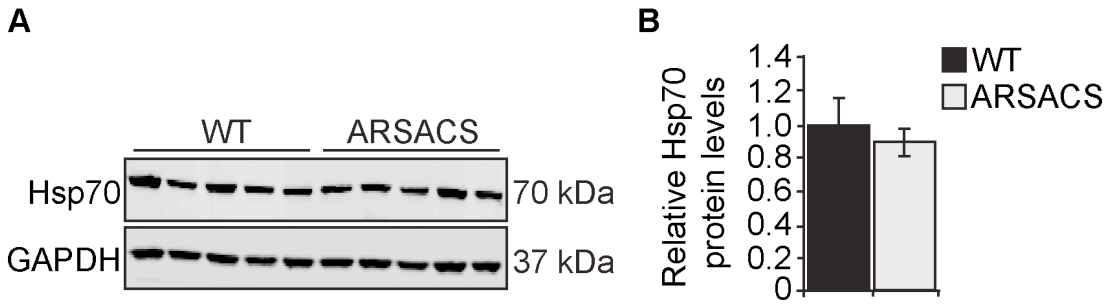

Figure 5.3. Total cellular levels of HSP70 were unchanged in ARSACS patient HDFs. (A) Immunoblot analysis of protein lysates from five ARSACS patient and five WT control HDFs probed with an anti-HSP70 antibody. GAPDH was used as a loading control. **(B)** Densitometric analyses were performed and mean relative protein levels calculated for the five WT and five patient cell lines. Data were normalised to GAPDH. Total cellular protein levels of HSP70 did not significantly differ between ARSACS patients and WT controls.

5.2.3. HSP90 colocalisation with vimentin in WT control and ARSACS patient HDFs

HSP90 has been shown to be recruited to protein aggregates (Leu et al., 2011). For example, HSP90 is found in Lewy bodies in PD (Auluck et al., 2002; Kalia et al., 2010; McLean et al., 2002), and HSP90 levels are increased in the brain of PD patients (Uryu et al., 2006). In addition, an interaction between HSP90 and vimentin has previously been demonstrated (Zhang et al., 2006). With this in mind, the localisation of HSP90 was investigated in the ARSACS patient HDFs compared to WT controls. Cells were incubated with MitoTracker Red, followed by immunocytochemistry using antibodies to HSP90 and vimentin. As previously shown by Zhang *et al.* (2006), confocal microscopy revealed a co-localisation between vimentin and HSP90. This was apparent in both WT control and ARSACS patient HDFs (Figure 5.4). HSP90 appeared to be associated with perinuclear vimentin bundling in the ARSACS patient cells; however it was not exclusively localised in this region and was found in other areas within the cytoplasm. Thus, HSP90 does not appear to significantly re-localise in the perinuclear region, as was seen for HSP70, in the ARSACS patient HDFs.

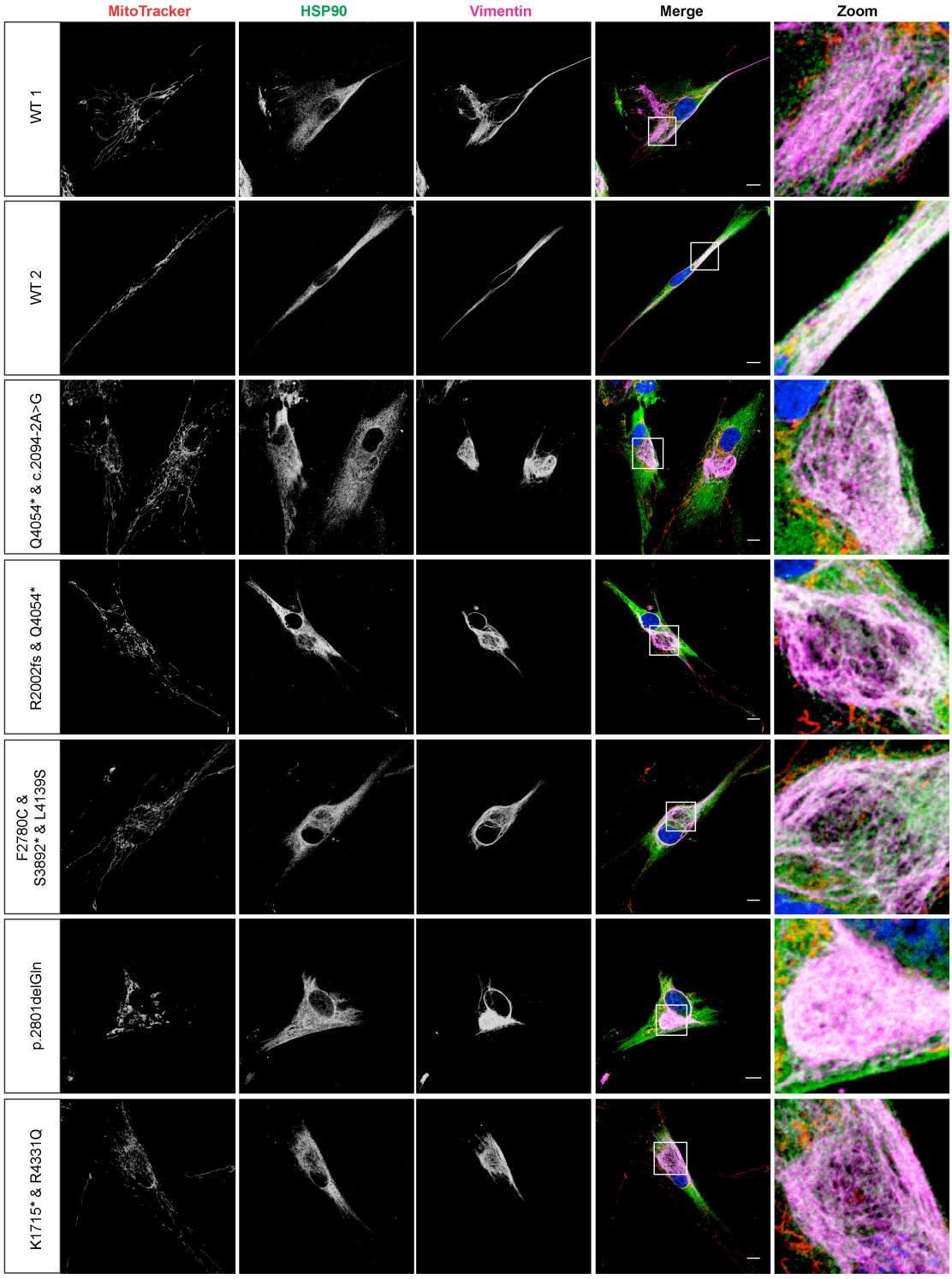

Figure 5.4. HSP90 co-localises with vimentin in WT and ARSACS patient HDFs. Representative confocal images of ARSACS patient and WT control HDFs. Cells were incubated with MitoTracker Red and were stained with rabbit anti-HSP90 and mouse anti-vimentin antibodies. Confocal analysis showed co-localisation of HSP90 with vimentin in both WT and ARSACS patient HDFs. White boxes in the merged panels are shown zoomed in the far right panels. Scale bars = 10 μm.

5.2.4. HSP90 protein levels were unchanged in ARSACS patient HDFs

Cellular stresses such as heat shock, nutrient deprivation and oxidative stress are reported to induce HSP90 expression levels by as much as two-fold (Bagatell et al., 2000). Total HSP90 protein levels were analysed in the ARSACS patient HDFs compared to WT controls by immunoblot analysis using an anti-HSP90 antibody. There was no significant difference in total HSP90 protein expression levels relative to β-actin in ARSACS patient HDFs compared to WT controls (Figure 5.5).

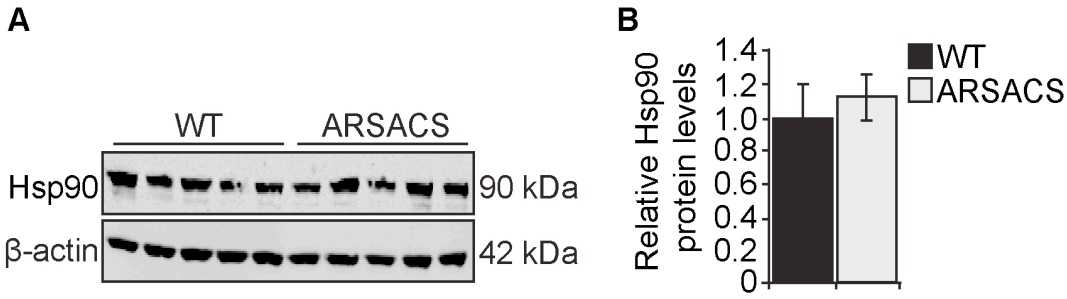

Figure 5.5. Total cellular levels of HSP90 were unchanged in ARSACS patient HDFs. (A) Immunoblot analysis of protein lysates from five ARSACS patient and five WT control HDF lines probed with an anti-HSP90 antibody. β-actin was used as a loading control. **(B)** Densitometric analyses were performed and mean relative protein levels calculated for the five WT control and five patient cell lines. Data were normalised to β-actin. Total cellular protein levels of HSP90 did not significantly differ.

5.2.5. Perinuclear accumulation of ubiquitin in ARSACS patient HDFs

The key signal for targeting proteins, including misfolded proteins, for degradation *via* the UPS or ALP is polyubiquitination. Intracellular inclusion bodies containing ubiquitinated proteins are detected in a variety of neurodegenerative diseases (Lowe et al., 1988). So far, the ARSACS patient cells appear to show cellular characteristics resembling the formation of an aggresome-like structure, therefore the presence of ubiquitinated proteins within this structure was investigated.

ARSACS patient and WT control HDFs were incubated with MitoTracker Red, followed by immunocytochemistry using antibodies to ubiquitin and vimentin. Confocal microscopy revealed an accumulation of ubiquitin in all of the ARSACS patient HDFs. This was in the same perinuclear region as vimentin bundling and HSP70 accumulation. In contrast, ubiquitin was dispersed throughout the cytoplasm in WT control cells (Figure 5.6).

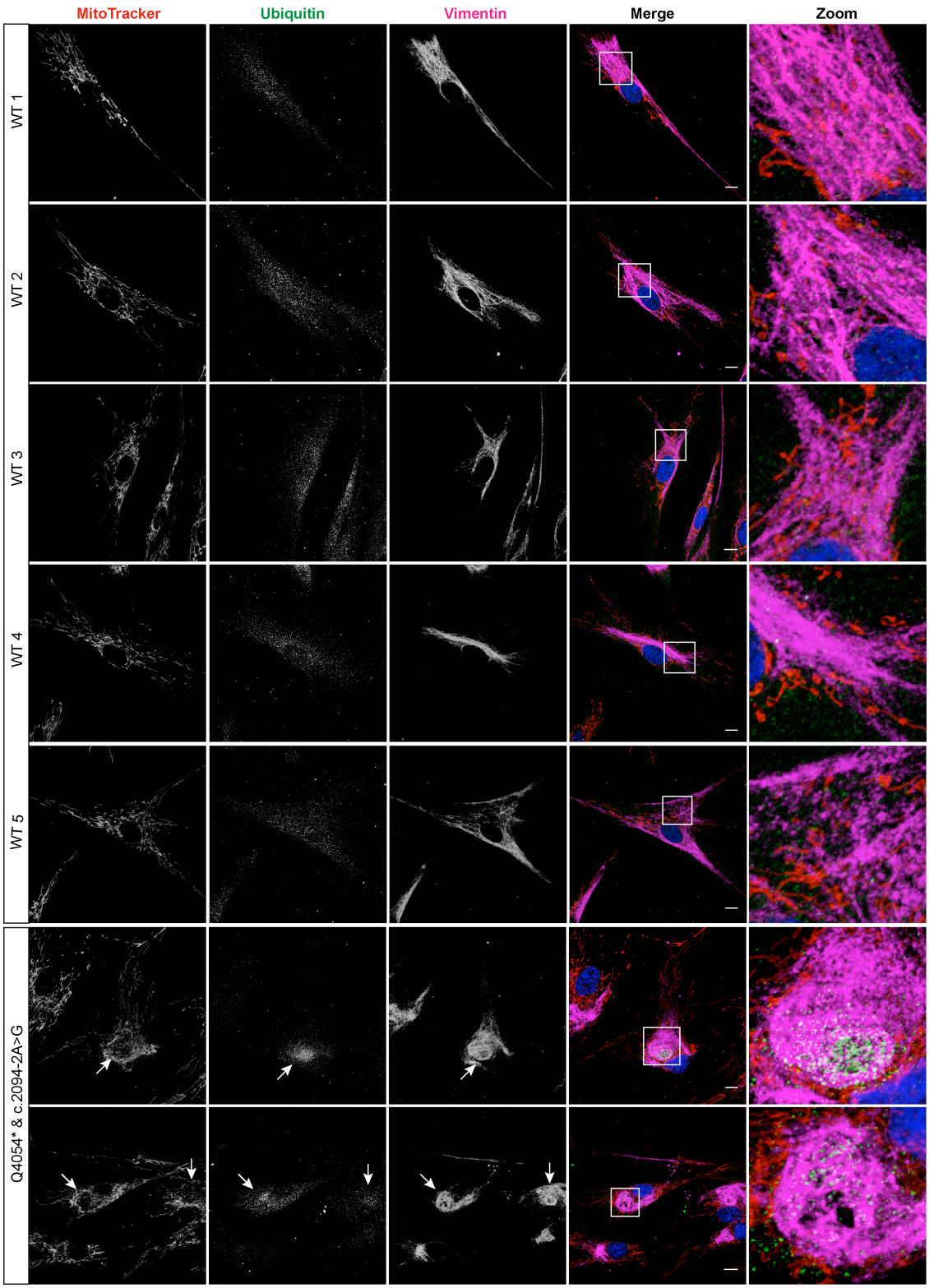
MitoTracker
Ubiquitin
Vimentin
Merge
Zoom
WT 1
WT 2
WT 3
WT 4
WT 5
Q4054* & c.2094-2A>G

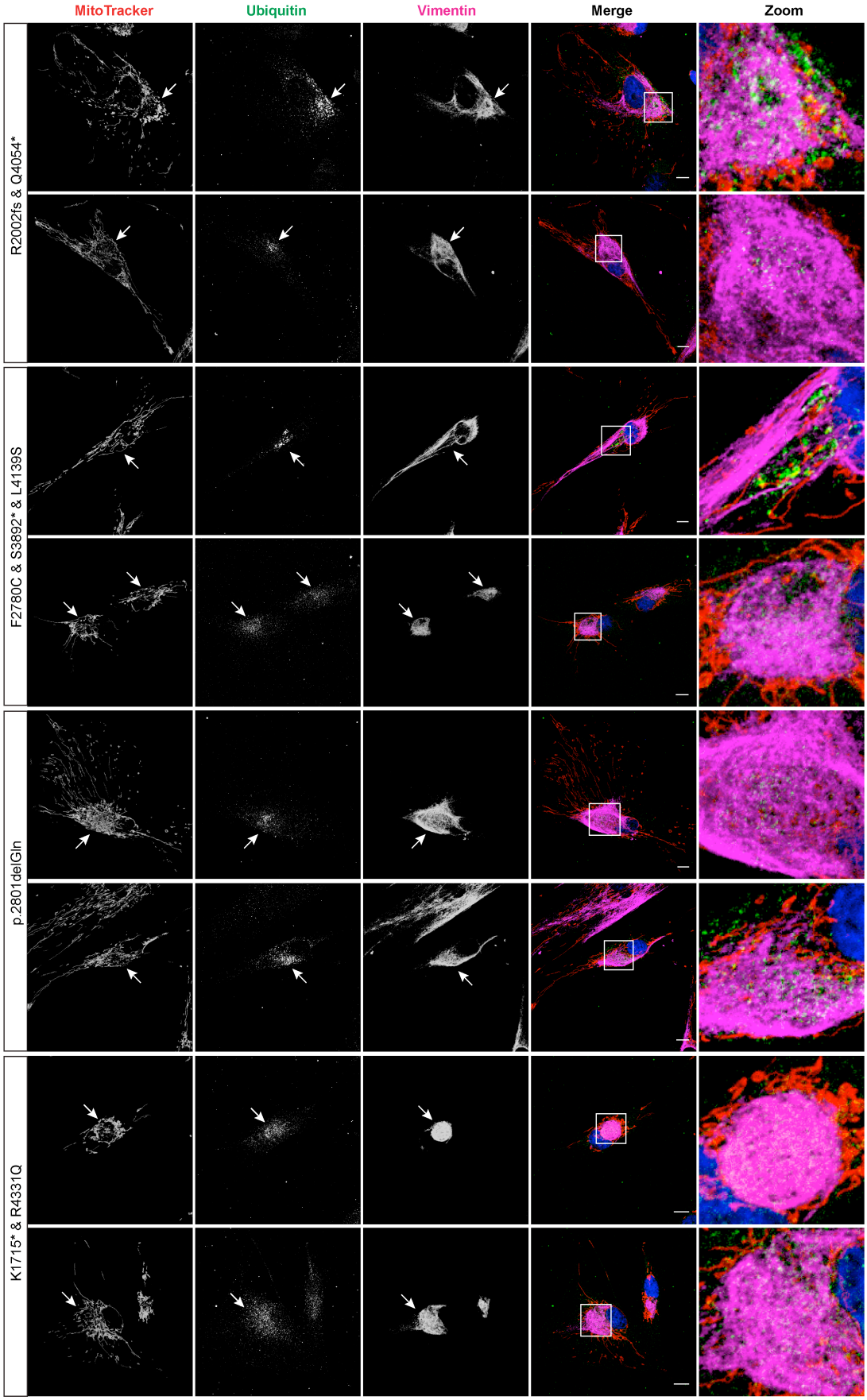
MitoTracker
Ubiquitin
Vimentin
Merge
Zoom
R2002fs & Q4054*
F2780C & S3892* & L4139S
p.2801delGln
K1715* & R4331Q

Figure 5.6. Perinuclear accumulation of ubiquitin in ARSACS patient HDFs. Representative confocal images of ARSACS patient and WT control HDFs. Cells were incubated with MitoTracker Red, followed by staining with antibodies to ubiquitin and vimentin. Confocal analysis showed accumulation of ubiquitin in perinuclear regions in all five ARSACS patient HDFs. White boxes in the merged panels are shown zoomed in the far right panels. White arrows indicate perinuclear accumulation of ubiquitin, vimentin bundling and mitochondrial disruption. Scale bars = 10 μm.

5.2.6. Perinuclear accumulation of p62/SQSTM1 in ARSACS patient HDFs

p62/SQSTM1 binds ubiquinated proteins, targeting them for autophagy, and has been shown to accumulate with ubiquitin-containing aggregates when autophagy is disrupted (Nagaoka et al., 2004; Zatloukal et al., 2002). As the ARSACS patient HDFs show an accumulation of ubiquitinated protein, p62 localisation was also explored.

ARSACS patient and WT control HDFs were incubated with MitoTracker Red, followed by immunocytochemistry using an antibody to p62/SQSTM1. Confocal microscopy revealed an accumulation of p62 in the same perinuclear region as seen for HSP70 and ubiquitin, in all of the ARSACS patient HDF lines (Figure 5.7). There seemed to be some variation in the amount of p62 accumulation between the five ARSACS patient HDFs. The heterozygous patient with the *SACS* mutations R2002fs and Q4054* appeared to show the highest intensity of p62 accumulation.

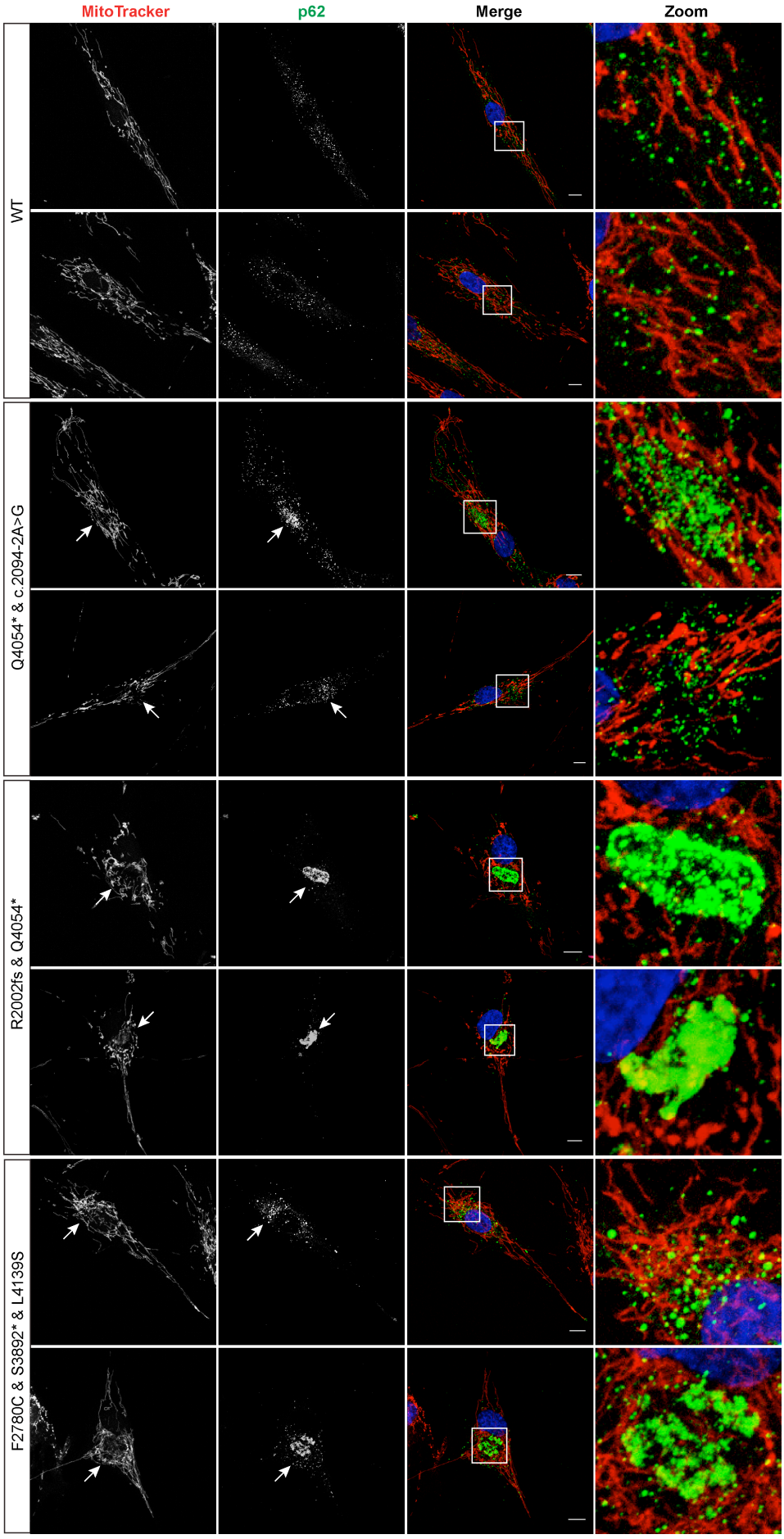
MitoTracker
p62
Merge
Zoom
WT
Q4054* & c.2094-2A>G
R2002fs & Q4054*
F2780C & S3892* & L4139S

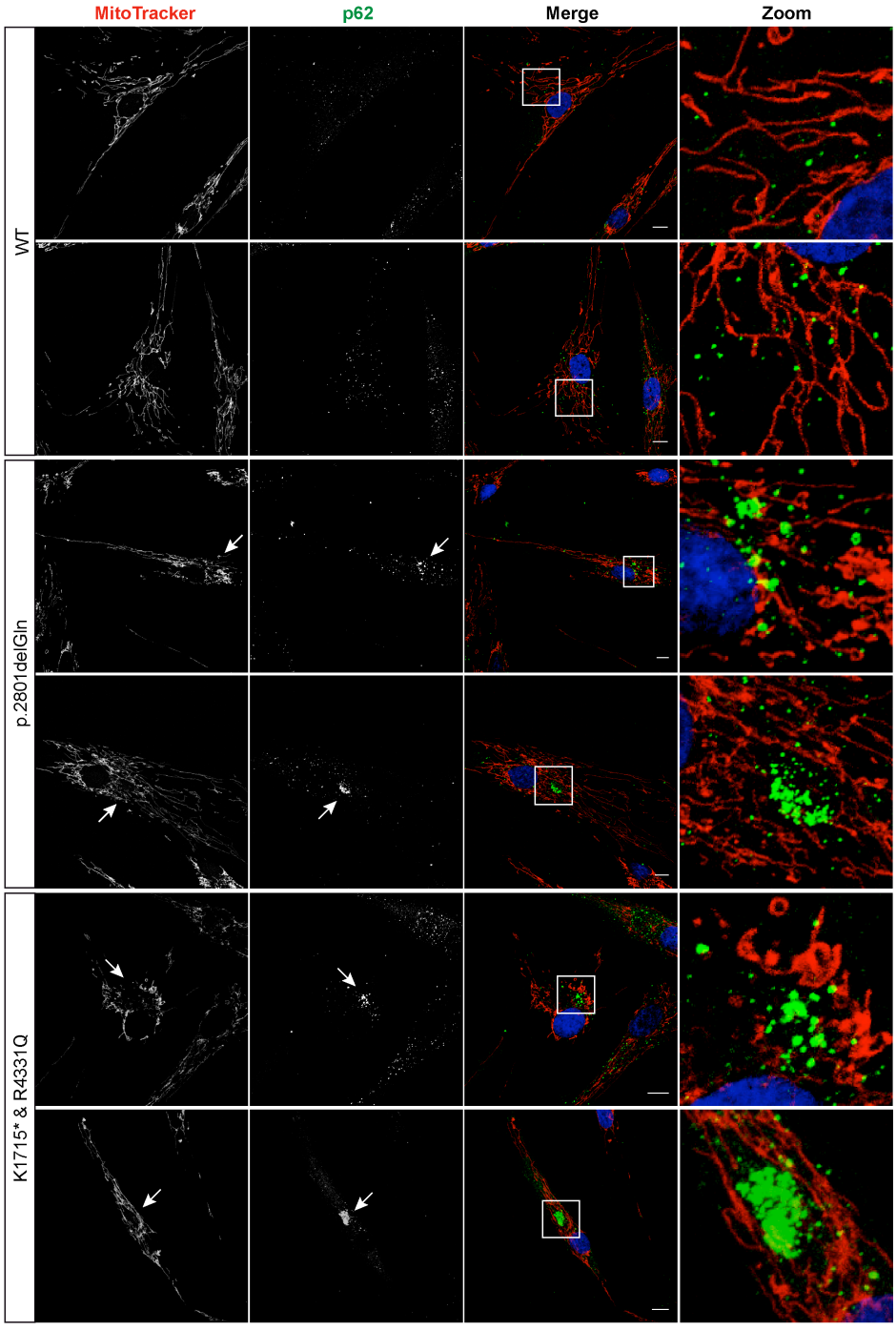

Figure 5.7. Perinuclear accumulation of p62 in ARSACS patient HDFs. Representative confocal images of ARSACS patient and WT control HDFs. Cells were incubated with MitoTracker Red, followed by staining with an antibody to p62/SQSTM1. Confocal analysis showed accumulation of p62 in perinuclear regions in all five ARSACS patient HDFs, indicated by white arrows. White boxes in the merged panels are shown zoomed in the far right panels. Scale bars = 10 μm.

5.2.7. Re-localisation of lysosomes in ARSACS patient HDFs

Lysosomes are membrane-bound organelles that contain many hydrolytic enzymes capable of degrading proteins, nucleic acids, carbohydrates and lipids. The lysosomal enzymes are active only at an acidic pH (4.5-5). To maintain their acidic pH, lysosomes actively transport protons into the lysosome via a proton pumping vacuolar-type ATPase (V-ATPase) in the membrane, a process that requires energy through ATP hydrolysis. Pertubation of the activity of V-ATPases leads to compromised lysosome acidification, so hydrolytic enzymes can no longer degrade the contents, which in turn leads to accumulation of lysosomes and their undegraded protein contents.

As lysosomes are involved in the final step of autophagic degradation, their localisation and expression levels were investigated in ARSACS patient HDFs compared to WT controls. Cells were incubated with MitoTracker Red, followed by immunocytochemistry using antibodies to vimentin and lysosome-associated membrane protein 2 (LAMP-2), which as the name suggests, is found in the membrane of lysosomes. Confocal microscopy revealed that lysosomes become re-localised from being dispersed throughout the perinuclear region in WT control HDFs, to having a strong perinuclear accumulation of lysosomes in a single region in ARSACS patient HDFs (Figure 5.8). This accumulation is in the same cellular region of vimentin bundling and mitochondrial disruption, indicated by the white arrows in figure 5.8. The same accumulation pattern was observed for HSP70, ubiquitin and p62. Confocal settings remained constant throughout imaging.

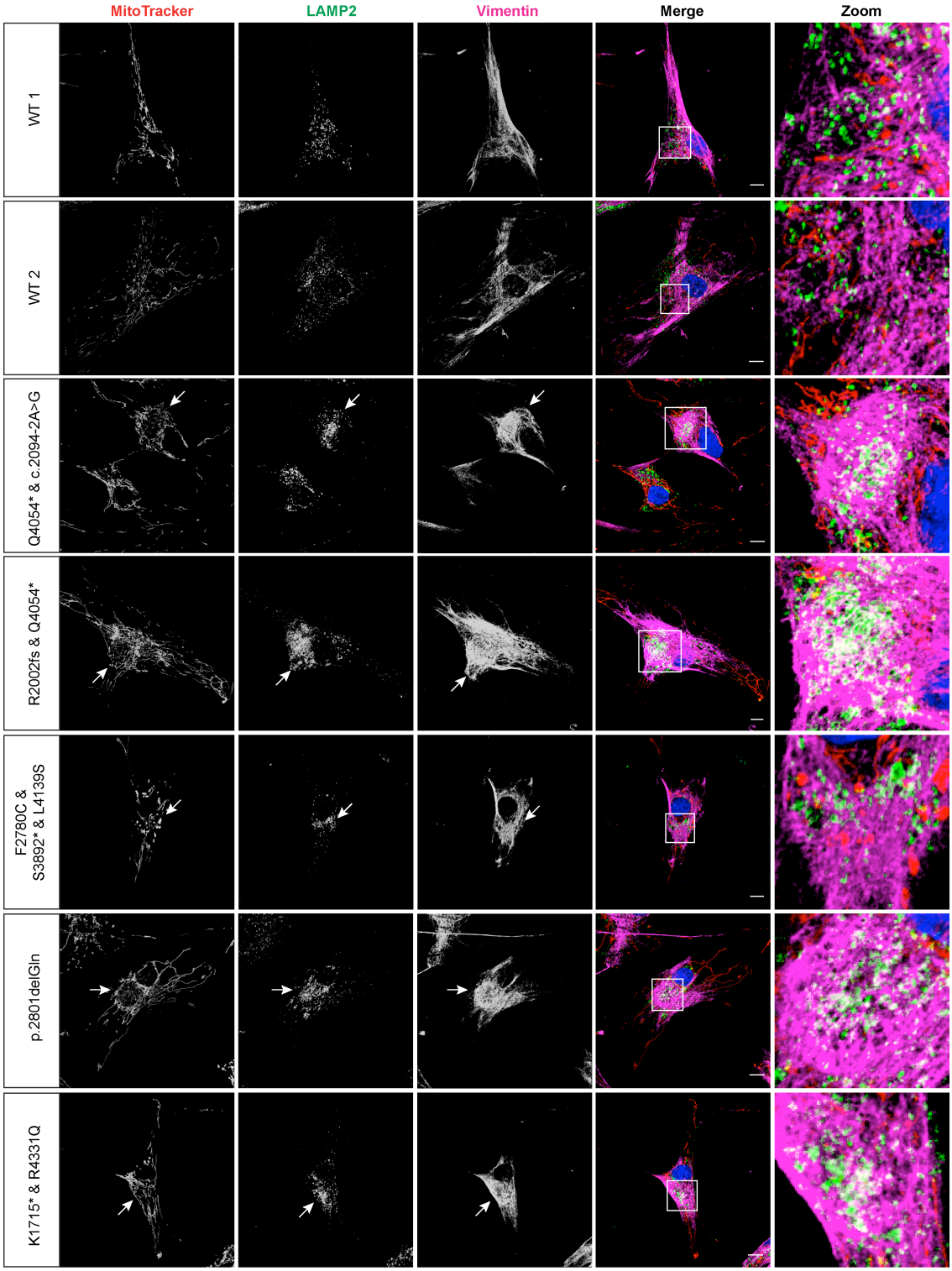

Figure 5.8. Perinuclear accumulation of LAMP-2 in ARSACS patient HDFs. Representative confocal images of ARSACS patient and WT control HDFs. Cells were incubated with MitoTracker Red, followed by staining with antibodies to LAMP-2 and vimentin. Confocal analysis showed perinuclear accumulation of LAMP-2 in all five ARSACS patient HDFs. White boxes in the merged panels are shown zoomed in the far right panels. White arrows indicate perinuclear accumulation of LAMP-2, vimentin bundling and mitochondrial disruption. Scale bars = 10 μm.

5.2.8. LAMP2 upregulation in sacsin knockdown cells

Our research group perfomed a microarray experiment using a human Illumina Whole Genome Gene Expression BeadChip (HT-12 v.4.0). Transcript levels were compared in SH-SY5Y cells transfected with *SCRM* or *SACS* siRNA (transfections, RNA extraction and purification were performed by Teisha Bradshaw and Suran Nethisinghe). Data analyses (carried out by Lisa Romano) identified a 0.5-fold increase in *LAMP2* gene expression in *SACS* siRNA treated cells compared to *SCRM* siRNA (Figure 5.9A). This upregulation was verified in an independent experiement by RT-qPCR (Figure 5.9B, 0.47-fold increase, work performed by Lisa Romano). To further confirm the *LAMP2* gene expression result, LAMP-2 protein levels were measured by immunoblot analysis using an anti-LAMP2 antibody. LAMP-2 protein levels were also significantly increased by 0.6-fold in cell lysates from *SACS* siRNA transfected cells compared to those transfected with *SCRM* siRNA control (Figure 5.9C,D **$p<0.01$). This was consistent with the gene expression result from the microarray analyses and RT-qPCR.

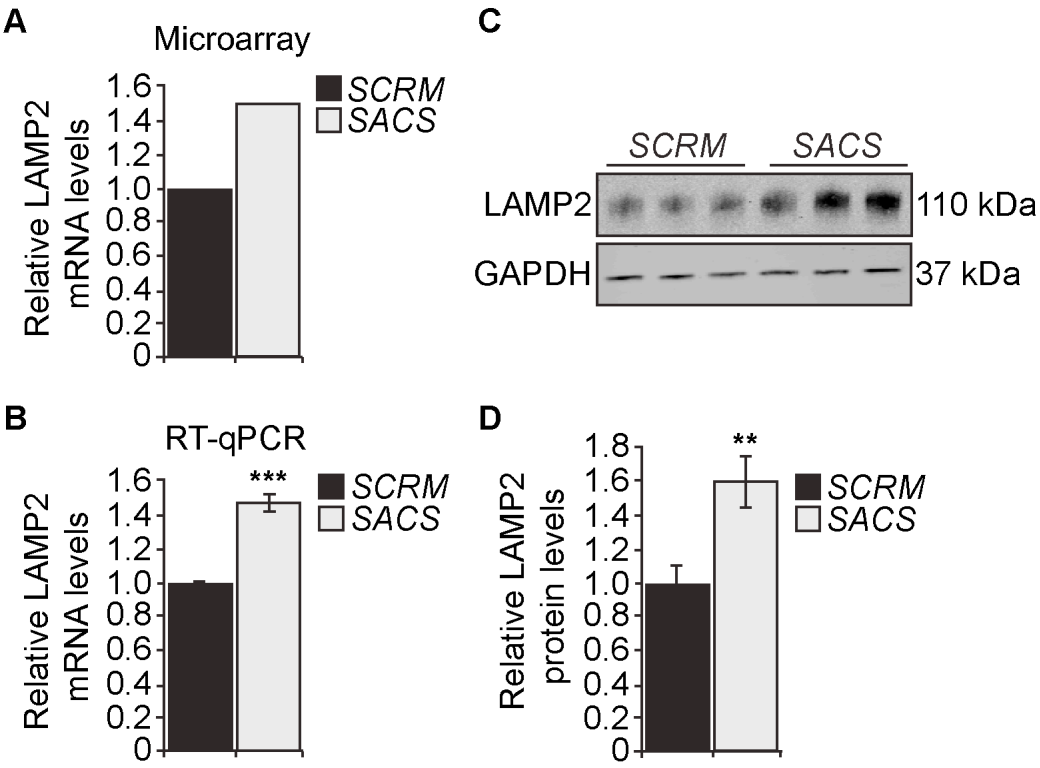

Figure 5.9. Upregulation of LAMP2 mRNA and protein expression in sacsin knockdown cells. RNA and protein were extracted from SH-SY5Y cells transfected with *SCRM* or *SACS* siRNA. Endogenous LAMP2 mRNA and protein were assayed by microarray, RT-qPCR and immunoblotting. Differential *LAMP2* mRNA levels determined by microarray **(A)** and RT-qPCR **(B)**. Results are expressed as mean ± SEM. Microarray n=2. RT-qPCR reactions were performed in triplicate. SYBR-green was used for RT-qPCR (ThermoFisher Scientific). **(C)** Representative immunoblot of total LAMP-2 protein expression levels in *SCRM* or *SACS* siRNA treated cells. Blots were probed with an anti-LAMP-2 antibody, along with GAPDH as a loading control. **(D)** Densitometric analyses were performed and mean relative protein levels calculated (n=8). Data were normalised to GAPDH and are expressed as mean ± SEM. Statistics were carried out using an unpaired, two-tailed Students t-test. $^{**}p<0.01$, $^{***}p<0.001$.

Together these data indicate a strong perinuclear accumulation of LAMP-2 in ARSACS patient HDFs, along with an upregulation of LAMP-2 mRNA and protein in *SACS* knockdown cells. This suggests lysosomal accumulation due to loss of sacsin function.

5.2.9. Investigating mitophagy in ARSACS patient HDFs

In the immunocytochemistry experiments described in this chapter and Chapter 4, mitochondria were stained with MitoTracker Red CMXRos (ThermoFisher Scientific). This is a lipophilic cationic fluorescent dye that accumulates inside mitochondria in response to highly negative mitochondrial membrane potential (Kholmukhamedov et al., 2013; Pendergrass et al., 2004). Therefore, loss of a membrane potential would mean MitoTracker is not taken up by mitochondria. This is a potential explanation for the perinuclear area of mitochondrial exclusion in ARSACS patient HDFs, as there may be mitochondria in this region that are not being detected because they have lost membrane potential. This occurs in damaged/unhealthy mitochondria.

To investigate this in the ARSACS patient and WT control HDFs, dual immunocytochemistry was performed using MitoTracker Red along with the mitochondrial marker, TOM20 (Translocase of Outer Mitochondrial Membrane 20 homolog), which is not dependent on membrane potential so will stain healthy and unhealthy mitochondria. Cells were incubated with MitoTracker Red, followed by immunocytochemistry using an antibody to TOM20. Confocal microscopy revealed that MitoTracker and TOM20 staining overlap in both the ARSACS patient and WT control HDFs (Figure 5.10). Importantly, like MitoTracker Red fluorescence, staining the mitochondria using an antibody to TOM20 also shows a perinuclear area of mitochondrial exclusion in the ARSACS patient HDFs (highlighted in zoomed panels of figure 5.10), which suggests that unheathly mitochondria without a membrane potential are not accumulating in this region.

This data indicates that an increased degradation of dysfunctional mitochondria through mitophagy is not the explanation for the perinuclear accumulation of proteostasis components and area of mitochondrial network disruption seen in the ARSACS patient cells.

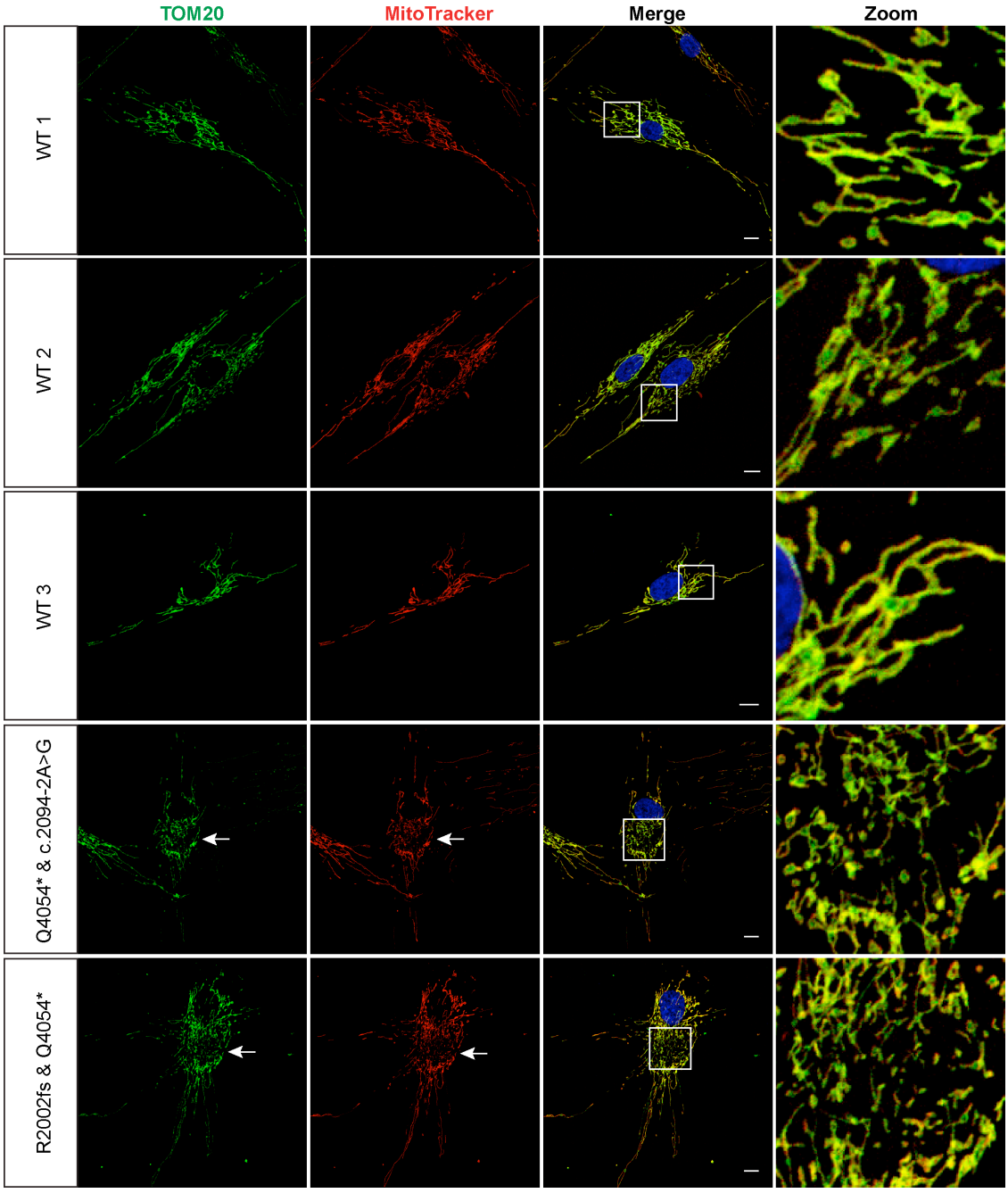
TOM20
MitoTracker
Merge
Zoom
WT 1
WT 2
WT 3
Q4054* & c.2094-2A>G
R2002fs & Q4054*

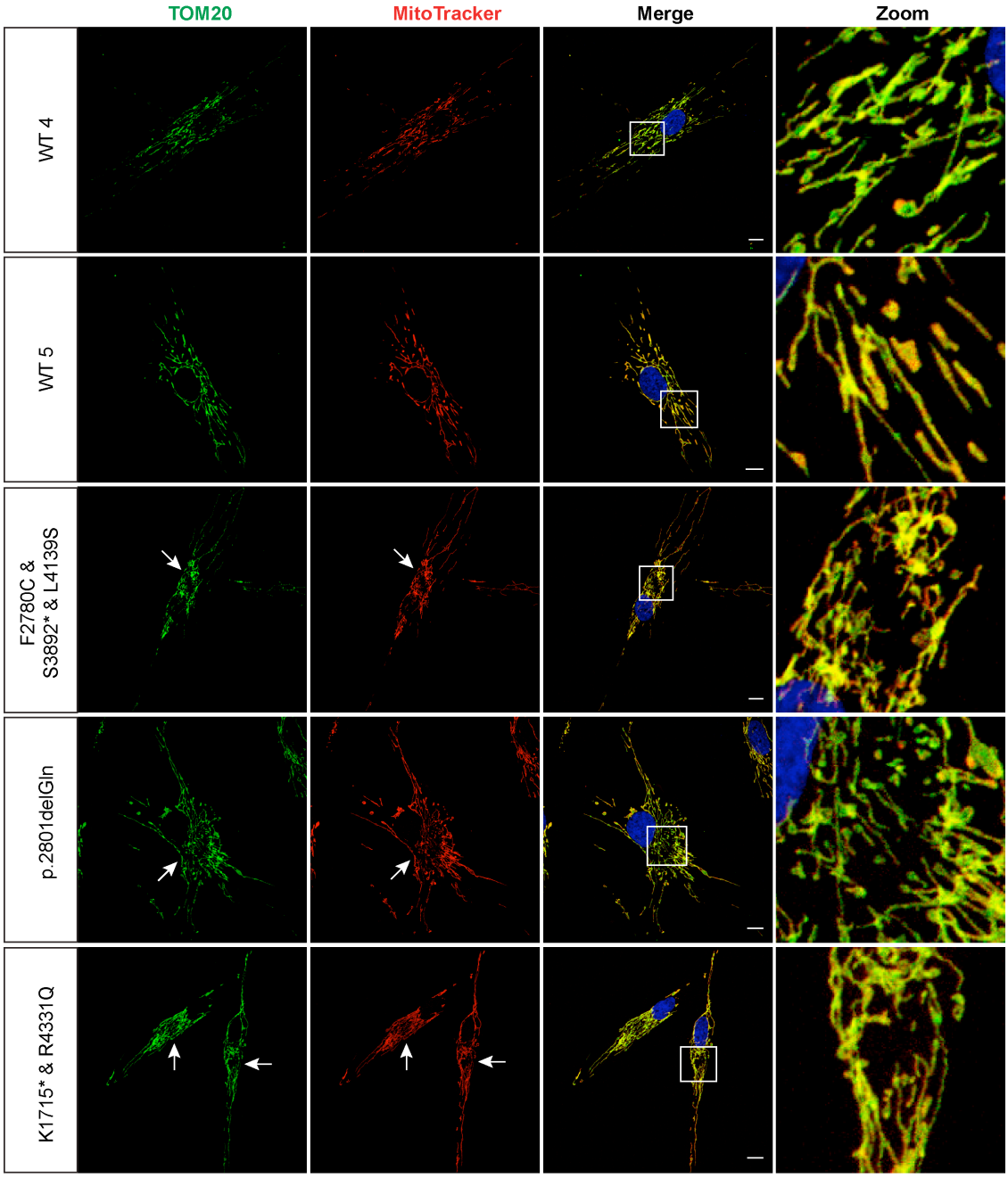

Figure 5.10. TOM20 and MitoTracker co-localise on mitochondria. Representative confocal images of ARSACS patient and WT control HDFs. Cells were incubated with MitoTracker Red and were stained with rabbit anti-TOM20 antibody. Confocal z-stacks show co-localisation of TOM20 and MitoTracker Red throughout the cell in both WT and ARSACS patient HDFs. White boxes in the merged panels are shown zoomed in the far right panels. Scale bars = 10 μm.

5.3. Conclusions

This chapter has demonstrated a perinuclear accumulation of some markers of proteostasis, which resembles an aggresome-like structure. This has been observed in the five ARSACS patient HDF lines studied, all of which have different *SACS* mutations. Firstly, the molecular chaperone HSP70 accumulates in a single area adjacent to the nucleus in the ARSACS patient HDFs, and this is in the same subcellular region where the vimentin network is bundling and the mitochondrial network is disrupted (described in Chapter 4). Molecular chaperones are known to accumulate with aggregates of misfolded protein as they have a key role in refolding proteins or targeting misfolded proteins for degradation (Hartl and Martin, 1995). For example, the molecular chaperones HSP70 and HSP40 associate with insoluble, cytoplasmic polyglutamine-containing protein aggregates in a cellular model of HD (Waelter et al., 2001). Furthermore, these molecular chaperones have been shown to be associated with Parkin-containing protein aggregates (Junn et al., 2002), and in Lewy bodies of PD brains (Auluck et al., 2002).

Additionally, a perinuclear accumulation of ubiquitinated proteins and p62/SQSTM1 occurs in the same region as HSP70 in the ARSACS patient HDFs. Ubiquitin tags misfolded proteins and targets them for degradation *via* the UPS or ALP, so this suggests the presence of accumulated misfolded proteins that have been targeted for degradation. Intracellular protein aggregates containing ubiquitinated proteins are detected in many neurodegenerative diseases (Bence et al., 2001; Juenemann et al., 2015; Ross and Pickart, 2004). This is likely due to UPS impairment and/or its functional overload. The ubiquitin-containing protein aggregates identified in multiple neurodegenerative disorders also contain p62 (Kuusisto et al., 2001; Nakano et al., 2004; Zatloukal et al., 2002). p62 binds to ubiquitinated proteins via its ubiquitin-associated (UBA) domain, targeting them to the autophagy pathway for degradation. Inhibition of autophagy has been shown to lead to an increase in the size and number of p62-containing protein aggregates and p62 protein levels (Bjorkoy et al., 2005). So the observation that ARSACS patient HDFs show perinuclear accumulation of p62, suggests autophagy may be impaired.

Collectively, the demonstration of HSP70, ubiquitin and p62 perinuclear accumulation in a single location in the ARSACS patient HDFs is reminiscent to that observed when intracellular protein aggregates form in many other neurodegenerative diseases. This

data adds support for the presence of perinuclear aggregates of misfolded protein in ARSACS.

Furthermore, LAMP-2, a lysosome membrane marker required for lysosomal fusion with autophagosomes, also shows a perinuclear accumulation in the same region of the cell as HSP70, ubiquitin and p62, in the ARSACS patient HDFs. This indicates that lysosomes have been recruited to the area of the cell where other modulators of proteostasis are relocalising. This is potentially to promote removal of misfolded proteins that the data suggests has accumulated. Moreover, a microarray experiment performed on SH-SY5Y cells transfected with *SCRM* or *SACS* siRNA highlighted that *LAMP2* is upregulated in *SACS* siRNA transfected cells compared to *SCRM* controls, a result which was verified by both RT-qPCR and immunoblotting.

LAMP2 is upregulated in lysosomal storage diseases (LSDs), a family of disorders that result from inherited gene mutations that perturb lysosomal degradation. This ultimately leads to neurodegeneration in infancy/childhood (Wraith, 2002), and less commonly in adulthood (Nixon et al., 2008; Shapiro et al., 2008; Spada et al., 2006). An example is Gaucher disease, where a mouse model shows increased protein levels of LAMP-2 (Sun and Grabowski, 2010). Similar to other more common neurodegenerative diseases, LSDs also have cellular accumulations of dysfunctional mitochondria that cannot be degraded through mitophagy (Ezaki et al., 1996; Jennings et al., 2006; Takamura et al., 2008), along with an accumulation of ubiquitinated and aggregate-prone proteins, including p62, α-synuclein and Huntingtin protein (Settembre et al., 2008; Suzuki et al., 2007; Tessitore et al., 2009). Additionally, an increase in *LAMP2* gene expression and protein levels has recently been identified in the peripheral leukocytes of coronary artery disease (CAD) patients due to an accumulation of lysosomes (Wu et al., 2011). Thus, like LSDs and CAD, an increase in LAMP-2 expression in cells with loss of sacsin function may indicate that autophagy-lysosome degradation is impaired, although this requires further investigation.

Due to the research implicating mitochondrial dysfunction in ARSACS (Blumkin et al., 2015; Criscuolo et al., 2015; Girard et al., 2012; Pilliod et al., 2015), a perturbation to autophagic degradation, and thus mitophagy, may lead to an accumulation of dysfunctional mitochondria in ARSACS patient cells. Dysfunctional mitochondria usually have a loss of membrane potential; hence MitoTracker Red, which is membrane potential dependent, would not accumulate in these mitochondria. So a perinuclear

accumulation of dysfunctional mitochondria would appear as negative MitoTracker Red staining, which could explain the presence of the perinuclear region of mitochondrial exclusion in the ARSACS patient HDFs. However, upon investigation using a TOM20 antibody, which detects mitochondria regardless of membrane potential, the perinuclear area of mitochondrial disruption/exclusion was still present. Perhaps the elongated and hyperfused mitochondria in ARSACS patient cells are too large to be engulfed by autophagosomes, and are thus not being degraded through mitophagy and are accumulating within the cell.

In conclusion, the data provided in both chapters 4 and 5 points towards the formation of an aggresome-like structure in cells due to loss of sacsin function. This may be forming due to an accumulation of misfolded protein, which is consistent with sacsin having a chaperone-linked role, with ablation of its function leading to problems with protein folding and/or degradation. Further work is required to verify this, as a disruption to normal proteostasis may contribute to disease pathogenesis in ARSACS.

5.3.1. Further Work

Further evidence is required to determine if misfolded proteins are accumulating in ARSACS. Most importantly, the next step is to determine the identity of any aberrantly folded protein species in the ARSACS patient cells. Since aggregated proteins tend to have reduced solubility, insoluble protein fractions from ARSACS patient and WT control HDF cell lysates could be generated. These protein fractions may then be analysed by SDS-PAGE, followed by Coomassie Blue staining, in order to observe protein bands that may be present in the ARSACS patients, but are absent in control protein. If a protein band(s) was observed to be present only in protein from ARSACS patient cells, this would be excised from the gel and submitted for mass spectrometry (MS) to determine the identity of the protein(s). Identified proteins would be prioritised for further analyses based on whether they have previously been linked to neurodegenerative or misfolding diseases. Following this, immunocytochemistry and confocal microscopy would be performed to investigate whether these candidate proteins are indeed localised to the aggresome-like structure in ARSACS patient HDFs.

Additionally, in order to further characterise the perinuclear aggresome or aggresome-like structures, transmission electron microscopy could be carried out on ARSACS patient HDFs. Aggresomes appear as large accumulations of closely packed electron-

dense particles in the region of the centrosome, which are wrapped by bundles of filamentous material (Johnston et al., 1998).

Furthermore, the subcellular localisation of other known markers of aggresomes, such as proteosomal subunits and other molecular chaperones, could be analysed in cells with loss of sacsin function, to further characterise the formation of aggresome-like structures in these cells. Additionally, mutant proteins that are known to form aggresomes, such as mutant rhodopsin (Saliba et al., 2002) and the ΔF508 mutation within CFTR (Burnett and Pittman, 2005), could be heterologously expressed in sacsin null cells to determine if these mutant proteins form aggresomes in the same perinuclear region of disruption identified in sacsin null cells. Immunoblotting of p62/SQSTM1 and ubiquitin to determine if their levels are increased in sacsin null cells would also increase the evidence for proteostasis disruption.

Our research group is currently generating neurons derived from the ARSACS patient HDFs used in this thesis *via* induced pluripotent stem cell (iPSC) technologies. It will be necessary to confirm that the ARSACS cellular phenotypes identified in this thesis hold true in neurons, where the disease manifests. It is expected that the evidence produced for an accumulation of misfolded protein and formation of perinuclear aggresome-like structures in the ARSACS patient HDFs would also be identified in neuronal cells.

Mitophagy could be further investigated in cells lacking normal sacsin, using PINK1 and Parkin as markers of mitophagy. PINK1 accumulates at the OMM of defective mitochondria, which in-turn elicits the translocation of Parkin from the cytosol to mitochondria to mediate the clearance of damaged mitochondria (Geisler et al., 2010; Narendra et al., 2008; Narendra et al., 2009). Thus, immunoblotting for PINK1 and parkin in a mitochondrial fraction could be used to investigate mitophagy, along with immunocytochemistry to investigate the localisation of PINK1 and parkin in relation to mitochondria. Since a reduction in mitochondrial membrane potential is known to accompany mitophagy, the uncoupling agent CCCP, which induces mitochondrial membrane depolarisation, has been frequently used when investigating mitophagy (Khalil et al., 2015; Tanaka, 2010; Vives-Bauza et al., 2010). Additionally, the co-localisation of LC3-II, a marker of autophagosomes, with mitochondria has been widely used to study mitophagy (Gomez-Sanchez et al., 2014; Kim et al., 2007; Narendra et al., 2008). Mitophagy is also known to induce ubiquitination of the OMM fusion proteins

MFN-1 and MFN-2; hence this could be investigated by immunoblotting of mitochondrial fractions (Gegg et al., 2010; Gegg and Schapira, 2011).

A microarray experiment on SH-SY5Y cells transfected with *SCRM* or *SACS* siRNA, and also on ARSACS patient and WT control HDF cell lines has been carried out in our group. In addition to *LAMP2* (section 5.2.8), preliminary analysis of the results from this highlight other lysosome related genes that are dysregulated in cells with loss of sacsin, for example, the minor lysosome membrane protein sortilin 1 (SORT1), CD68, which is a member of the LAMP protein family, and several lysosomal acid hydrolases (cathepsins) are upregulated, while the V-ATPase subunits $ATP6V_{0C}$ and $ATP6V_{0B}$ are downregulated. These need to be verified by RT-qPCR and immunoblotting as this data would provide evidence suggesting lysosome dysfunction in cells due to loss of sacsin, which in-turn would lead to impaired autophagic protein degradation.

In a sacsin knockout mouse model, an accumulation of non-phosphorylated NFH was identified (Lariviere et al., 2015). Similarly, alterations in neurofilament organisation have been identified in other neurodegenerative diseases (Al-Chalabi and Miller, 2003; Forno et al., 1986; Perrot and Eyer, 2009). Vimentin assembly and function is known to be regulated by phosphorylation state (Ivaska et al., 2007; Sihag et al., 2007). Site-specific phosphorylation induces disassembly of vimentin filaments, and an increase in phosphorylation accompanies vimentin filament reorganisation *in vivo* (Inagaki et al., 1987). Vimentin phosphorylation occurs at several sites by different kinases, for example, Rab-7a interacts with and modulates vimentin phosphorylation at positions Ser-38 and Ser-55, which affects assembly (Cogli et al., 2013). The site-specific phosphorylation state of vimentin could be investigated in the ARSACS patient cells as alterations to the phosphorylation state may accompany the vimentin filament reorganisation observed.

CHAPTER 6: DISCUSSION

The ultimate aim of this thesis was to decipher the cellular role of sacsin by determining how loss of its function leads to the mitochondrial and intermediate filament defects identified in ARSACS. Data produced in this thesis provides evidence that the mitochondrial and intermediate filament defects may be the result of disrupted proteostasis. This is indicated by the formation of aggresome-like structures in sacsin deficient cells. Moreover, loss of sacsin leads to reduced DRP1-mediated mitochondrial fission, which is necessary for mitochondrial quality control. This likely explains the elongated and interconnected mitochondrial network in ARSACS, along with the mitochondrial dysfunction. Thus, the data suggests that sacsin has a key role in proteostasis, and defects in proteostasis likely have indirect consequences that disrupt mitochondrial quality control.

6.1. Disrupted Mitochondrial Fission in ARSACS

The data produced in Chapter 3 provides evidence that the elongated mitochondrial network observed in ARSACS is a consequence of impaired DRP1-mediated fission, and implicates sacsin as a regulator of DRP1 mitochondrial association. This is important as mechanisms that modulate recruitment of DRP1 to the OMM are not fully defined.

DRP1-mediated mitochondrial fission is crucial for survival. A complete loss of DRP1-mediated mitochondrial fission is embryonic lethal in mice (Ishihara et al., 2009; Wakabayashi et al., 2009) and humans (Chang et al., 2010). DRP1 association with mitochondria is reduced rather than abolished in sacsin null cells, thus loss of sacsin is not embryonic lethal in mice or humans. This less severe ARSACS phenotype signifies that sacsin is not essential for DRP1-mediated fission, but may be required for normal regulation of mitochondrial division in some cell types.

An important regulator of DRP1-mediated fission is the dynein-dynactin motor complex (Varadi et al., 2004). In Chapter 3, a novel role for the DCTN6 subunit in DRP1-mediated fission was identified. Specifically, a putative interaction between DCTN6 and DRP1 was observed by co-IP using heterologously expressed proteins. DRP1 (Girard et al., 2012) and DCTN6 (Parfitt, 2011) have both previously been shown to have putative interactions with sacsin, and interestingly, the mitochondrial phenotype observed due to loss of DCTN6 is analogous to that observed due to loss of sacsin. This consists of an elongated and overly interconnected mitochondrial network, reduced mitochondrial localisation of DRP1, and significantly reduced mitochondrial membrane potential, which is indicative of an increase in dysfunctional mitochondria. These findings have lead to the hypothesis that sacsin and DCTN6 may function together in the recruitment or stabilisation of DRP1 on mitochondria. It is conceivable that sacsin may function as a chaperone in the complex assembly of DRP1 with the dynein-dynactin subunit DCTN6, or perhaps sacsin stabilises DRP1 at the dynein-dynactin complex. DRP1 can then be transferred to mitochondria, which are also transported by the dynein-dynactin motor complex (Hollenbeck and Saxton, 2005). Once at mitochondria, it is known that DRP1 is recruited to the OMM by receptors, such as MFF and FIS1, in order to initiate fission (Figure 6.1).

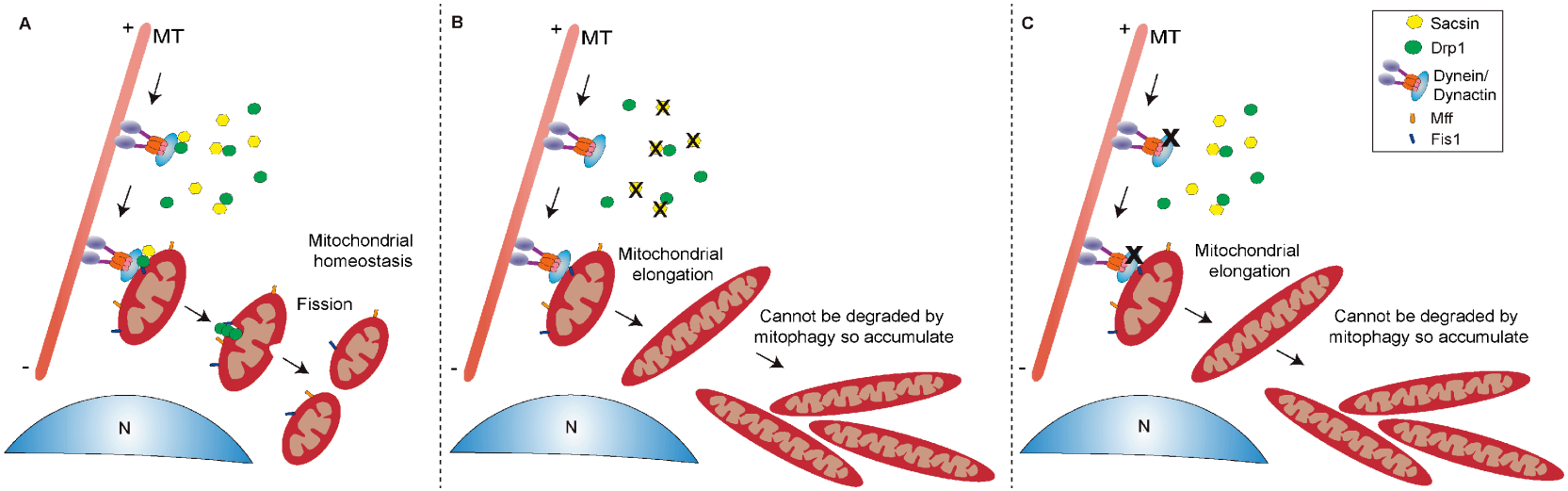

Figure 6.1. Schematic representation of the hypothesis that sacsin and DCTN6 function together in the mitochondrial translocation of DRP1. (A) Sacsin (yellow) may function as a chaperone in the complex assembly of DRP1 (green) with the dynein-dynactin subunit DCTN6. This complex may then be transferred to mitochondria, which are transported along microtubules (MT), in a retrograde manner, by the dynein-dynactin motor. Once at mitochondria, receptors, such as MFF and FIS1, recruit DRP1 for fission. **(B)** Loss of sacsin may lead to reduced complex assembly of DRP1 and DCTN6. Therefore, less DRP1 would be available at mitochondria for fission, resulting in elongation of the mitochondrial network. **(C)** Similarly, loss of DCTN6 may lead to reduced complex assembly with DRP1 and sacsin. Therefore, less DRP1 is able to be recruited to mitochondria for fission to occur. Reduced DRP1-mediated fission resulting from loss of sacsin or DCTN6 may lead to reduced degradation of damaged mitochondria through mitophagy. Hence, an accumulation of damaged mitochondria could occur. N: nucleus.

DRP1-mediated fission is essential for mitochondrial quality control as it allows damaged parts of the mitochondrial network to be isolated from healthy mitochondria. Damaged mitochondrial fragments can then be engulfed by autophagosomes for their degradation by mitophagy (Arnoult et al., 2005; Gomes and Scorrano, 2008; Kageyama et al., 2014; Lu, 2009; Tanaka et al., 2010). Thus, the impairment in DRP1-mediated fission observed in sacsin or DCTN6 deficient cells likely leads to perturbations in mitophagy. Failure to remove dysfunctional mitochondria may explain the reduction in mitochondrial membrane potential observed in sacsin (Girard et al., 2012) and DCTN6 deficient cells. This is discussed further in section 6.4.2.4.

Impaired mitochondrial quality control is likely to be particularly detrimental in neurons. This is supported by the evidence that defects in mitochondrial dynamics, and thus quality control, contribute to numerous neurodegenerative diseases, including Alzheimer's and Parkinson's (Bereiter-Hahn, 2014; Chen and Chan, 2009; Itoh et al., 2013). An accumulation of dysfunctional mitochondria in ARSACS patient neurons due to impaired mitophagy could mean that the relatively high energetic demands of the neurons cannot be met. This likely leads to neurotoxicity and contributes to the Purkinje cell death in ARSACS (Winslow and Rubinsztein 2008; Nixon et al., 2008).

Mitochondrial transport to the cell periphery is also impaired in ARSACS. Specifically, an accumulation of mitochondria occurs in the soma and proximal dendrites of cultured hippocampal neurons after sacsin knockdown (Girard et al., 2012). Mitochondrial motility is also significantly reduced in axons of *Sacs*$^{-/-}$ mice motor neurons (Lariviere et al., 2015). This may be due to a direct effect of loss of sacsin on mitochondrial transport, or an indirect effect, through reduced mitochondrial fission. In support of the latter, it has previously been suggested that elongated mitochondria are poorer substrates for anterograde motors, such as kinesin. Hence, mitochondrial transport to the cell periphery becomes impaired, resulting in a perinuclear accumulation of elongated mitochondria (Varadi et al., 2004). Disruption of mitochondrial transport into dendrites has been shown to lead to abnormal dendritic morphology, and striking alterations are observed in the organisation of dendritic fields in the cerebellum of *Sacs*$^{-/-}$ mice, which precedes Purkinje cell death (Lariviere et al., 2015). Thus, the reduction in DRP1-mediated mitochondrial fission in sacsin deficient cells may ultimately contribute to the Purkinje cell death and neurodegeneration in ARSACS.

6.2. Cellular Localisation of Sacsin

In Chapter 4, evidence was provided to suggest a novel association of sacsin with vimentin, and the possibility that this association may be mediated through sacsin's HSP90-like domains was discussed (section 4.3). Due to its massive size, heterologous expression of full-length sacsin (open reading frame of >12000bp) is difficult. Hence, previous studies investigating sacsin interactors have used specific regions of sacsin, for example the N-terminal (Girard et al., 2012; Parfitt, 2011) or C-terminal (Lim et al., 2006) regions. Since two of sacsin's HSP90-like domains are located outside of these regions, this may explain why an interaction between sacsin and vimentin has not yet been identified.

Sacsin is a co-chaperone/putative chaperone and several molecular chaperones are known to associate with IFs. Thus, sacsin may have a role related to, or as part of, a functional chaperone network with these other molecular chaperones. The small heat shock proteins (sHSP), HSP27 and αB-crystallin, associate with several types of IFs, such as vimentin, GFAP, keratin and desmin (Perng et al., 1999; Vicart et al., 1998; Wisniewski and Goldman, 1998). It has been proposed that one of the major functions of this association of sHSPs with IFs is to manage inter-filament interactions (Perng et al., 1999). The association of these sHSP is not restricted to a particular IF type, hence it would be interesting to investigate whether sacsin associates with other IFs besides vimentin.

HSP27 and αB-crystallin also associate with IF aggregates in certain human pathologies (Iwaki et al., 1993; Iwaki et al., 1989), and mutations in αB-crystallin lead to desmin aggregation in desmin-related myopathies (Vicart et al., 1998). Both desmin and αB-crystallin are found in the aggregates. The co-collapse of IFs with mutated sHSPs is comparable to what is observed for mutated sacsin and vimentin filaments in some ARSACS patient HDF lines (Figure 4.9). HSP27 and αB-crystallin may also associate with the vimentin bundles in the ARSACS patient HDFs, although this requires investigation.

So perhaps, similar to these sHSPs, sacsin has a chaperone-like function with IFs, and is important for inter-filament interactions or IF interactions with other proteins.

6.2.1. Sacsin as a cytoskeletal linker

In Chapter 4, with the aid of super resolution microscopy, areas where sacsin punctae localised between mitochondria and vimentin filaments were identified, indicating that sacsin may contact both mitochondria and vimentin simultaneously. This is a feature of cytolinker proteins, and suggests that sacsin may bridge together mitochondria and IFs.

Plectin, a cytoskeletal linker protein of a similarly large size to sacsin (500 kDa), mediates interactions between IFs and mitochondria (Winter et al., 2008), as well as acting as a mechanical linker between IFs and other cytoskeletal structures and organelles, including actin and microtubules (Wiche et al., 2015). Mutations in plectin cause epidermolysis bullosa simplex with muscular dystrophy (EBS-MD), which is characterised by a severe disorganisation and aggregation of desmin IFs, along with mitochondrial dysfunction (Schroder et al., 2002). Interestingly, IF aggregation and mitochondrial dysfunction are the two most prominent cellular phenotypes identified in sacsin deficient cells; therefore sacsin may have a similar cellular role to plectin.

Intriguingly, MitoTracker staining of mitochondria in muscle fibres of plectin 1b or plectin 1d knockout mice revealed mitochondria-free areas, which the authors denoted as ‘black holes’ (Winter et al., 2015). This may be similar to the perinuclear ‘holes’ in the mitochondrial network seen in the ARSACS patient HDFs. Aggregation of the desmin IF network is also observed in these knockout mice (Winter et al., 2015).

Since a proportion of sacsin is seen to be localised between mitochondria and IFs, and loss of sacsin leads to similar cellular phenotypes to those seen with loss of plectin function, this may indicate that sacsin has a similar cytoskeletal linker function as plectin.

Supporting a role for sacsin with the cytoskeleton, putative interactions have been observed between the C-terminus of sacsin and several cytoskeletal-linked proteins, namely the microtubule-associated protein 1A (MAP1A, (Anderson, 2011)) and α-actinin-4 (ACTN4, (Lim et al., 2006)).

MAP1A is expressed almost exclusively in the brain (Huber and Matus, 1984) and binds to microtubules, forming cross-bridges between microtubules and/or microtubules with other cellular structures, including actin and IFs (Pedrotti et al., 1994; Shiomura and Hirokawa, 1987). Thus, if this putative interaction was real, MAP1A may represent an important link between sacsin and IFs.

ACTN4 belongs to a family of actin-binding proteins that cross-link and bundle actin filaments (Otey and Carpen, 2004). They are also involved in the organisation of the submembranous cortical cytoskeleton (Pelletier et al., 2003; Wachsstock et al., 1993). Microtubules, actin and IFs networks are interlinked through multiple cytoskeletal associated proteins (CAPs (Fuchs and Cleveland, 1998; Leung et al., 1999)); hence sacsin may be an important organiser of the cytoskeletal network, perhaps indirectly through its interactions with other CAPs, like MAP1A and ACTN4.

Moreover, preliminary analysis of sacsins protein sequence using the bioinformatics tool, Homology detection & structure prediction (HHpred), predicts that sacsin may contain a CAP-Gly (glycine-rich cytoskeleton-associated protein)-like domain within the C-terminal 4175-4304 amino acids (Figure 6.2). CAP-Gly domains are conserved motifs (GKNDG) identified in numerous CAPs, including restin, dynactins and CLIP-170 (Figure 6.2 (Riehemann and Sorg, 1993)).

```
Sacsin      4175 FYPGEYVGYLVDAEGGDIYGSYQPTYTYAIIVQEVEREDADNSS
Dynactin-1  52   FATGKWVGVILDEAKGKNDGTVQG--------------------
Restin      82   FAPGQWAGIVLDEPIGKNDGSVAG--------------------
CLIP-170    318  FASGQWVGVELDEPEGKNDGSV----------GGV---------

Sacsin      4219 FLGKIYQIDIGYSEYKIVSSLDLYKFSRPEESSQSRDSAPSTPT
Dynactin-1  96   --RKYFTCDEGHGI-----------FVRQSQIQVFEDGADTTSP
Restin      126  --VRYFQCEPLKGI-----------FTRPSKLTRKVQAEDEANG
CLIP-170    362  ---RYFICPPKQGL-----------FASVSKISKAVDAPPSSVT

Sacsin      4259 SPTE--FLTPGLRSIPPLFSGRESHKTSSKHQSPKKLKVNSLP
Dynactin-1  140  ETPDSSASKVLKREGTDTTAKTSKLRGLKPKKAP
Restin      170  LQTT--PASRATSPLCTSTASMVSSSPSTPSNIPQKPSQPAA
CLIP-170    406  S------TPRTPRMDFSRVTGKGRREHKGKKKTPSSPSLGSL
```

Figure 6.2. Structure-aided alignment of the C-termius of sacsin with cytoskeletal associated proteins containing a CAP-Gly domain. Accession numbers of the proteins that sacsin aligns with are as follows: Dynactin-1: NP_004073.2, Restin: NP_002947.1, CLIP-170: NP_056341.1. The position of each sequence is indicated at the start of each sequence. Identical amino acids between the sequences are indicated in bold red. The conserved CAP-Gly motif (GKNDG) is indicated by the blue box.

The predicted CAP-Gly domain is in the same C-terminal region of sacsin that was used to identify a putative interaction with ACTN4 (Lim et al., 2006), and part of the same region used to identify a putative interaction with MAP1A (Anderson, 2011). Thus,

perhaps a CAP-Gly domain within sacsin is mediating interactions with these proteins, and possibly other cytoskeletal proteins. This adds further support indicating that sacsin may have a role in mediating cytoskeletal interactions or functions.

Sacsins predicted CAP-Gly domain could be investigated in future work. Cellular localisation and fractionation studies could be performed using C-terminal constructs of sacsin to investigate an interaction with the cytoskeleton. Also, site-directed mutagenesis within this C-terminal region could be performed to investigate whether mutations in this region affect an association with the cytoskeleton.

6.3. Intermediate Filament Disruption in ARSACS

It is intriguing that not only an association between sacsin and vimentin was identified in this thesis, but that a collapse and perinuclear bundling of the vimentin network was identified in ARSACS patient HDFs and SH-SY5Y cells transfected with siRNA targeting sacsin. This data suggests that sacsin may have a role in maintaining the vimentin IF network.

In addition to the vimentin network disruption in ARSACS patient HDFs, neurons from *Sacs*$^{-/-}$ knockout mice and ARSACS brains display specific accumulations of non-phoshorylated NFH (npNFH, Lariviere et al., 2015). Aberrantly phosphorylated IF accumulations may be the result of disrupted turnover or abnormal post-translational modifications. Many properties of IFs are tightly associated with phosphorylation state, thus disrupting this may affect IF assembly and organisation. For example, mutating a phosphorylation site in NF-L leads to the formation of NF-L inclusions in the cell bodies of neurons from transgenic mice, along with the development of swollen Purkinje cell axons (Gibb et al., 1998). The phosphorylation state of the vimentin accumulations in ARSACS patient HDFs is yet to be determined.

So like the previously identified mitochondrial phenotype, multiple cell types display IF disruptions in ARSACS, which suggests that a neurofilament-specific function for sacsin is unlikely, and rather, sacsin has a more general role with IFs.

Giant axonal neuropathy (GAN) is also characterised by abnormal accumulations of IF proteins in multiple cell types (Bomont and Koenig, 2003; Cleveland et al., 2009; Gordon, 2004). The defective protein, gigaxonin, is proposed to function as a substrate adaptor for an E3 ubiquitin ligase, which affects proteasome-dependent degradation of

microtubule-related proteins, including MAP1B, MAP8 and the tubulin folding chaperone TBCB (Allen et al., 2005; Cleveland et al., 2009; Ding et al., 2006; Wang et al., 2005b). Ablation of gigaxonin causes a substantial accumulation of MAP1B in neurons (Allen et al., 2005).

IFs are known to redistribute into perinuclear cage-like structures that surround inclusion bodies and aggresomes that have formed due to proteostasis disruption in many neurodegenerative diseases (Mayer et al., 1989). Hence, the IF rearrangements observed in GAN may reflect the formation of IF-cage like structures around protein aggregates that have accumulated due to disrupted proteasome-dependent degradation. In support of this, the abnormal IF accumulations are in close proximity to the MTOC (Bomont and Koenig, 2003), which is where inclusion bodies/aggresomes are known to form.

Lewy bodies in PD and hyaline inclusions in ALS are surrounded by NFs, and the inclusion bodies in Pick's disease are surrounded by the IF protein GFAP (Mayer et al., 1989). The purpose of this cage-like IF structure is unclear, although it may promote the stability of the inclusion/aggresome or prevent non-specific interactions with other proteins within the cytoplasm (Mayer et al., 1989).

This IF rearrangement into a perinuclear cage-like structure coincides with what was observed in the ARSACS patient HDFs in Chapter 4. So rather than a direct effect of loss of sacsin function on the IF network, perhaps loss of sacsin leads to disrupted proteostasis, which in-turn leads to the collapse of the IF network around aggresomes. Further supporting this, other organelles, such as mitochondria, the Golgi, and early endosomes, become relocalised around the periphery of the IF cage-like structure. These are key characteristics seen in other cells when aggresomes form (Garcia-Mata et al., 1999; Lee et al., 2011; Saliba et al., 2002; Waelter et al., 2001).

This could also explain the accumulations of NFs in neurons from *Sacs*$^{-/-}$ mice and ARSACS brains. Interestingly, axonal torpedoes (rounded swellings of Purkinje cell axons) were identified in the *Sacs*$^{-/-}$ mice (Lariviere et al., 2015). Similar axonal torpedoes identified in essential tremor (ET), a common neurological disease, have accumulations of disorganised NFs within the torpedoes (Louis et al., 2009). Mitochondria and smooth ER were also abundant, particularly at the periphery of the torpedoes (Louis et al., 2009). Thus, the axonal torpedoes in the *Sacs*$^{-/-}$ mice may represent the formation of inclusions containing NF accumulations, possibly with

mitochondria and other organelles at the periphery of the torpedoes. These cellular characteristics are akin to those identified in the ARSACS patient HDFs.

The potential formation of aggresomes in ARSACS patient cells suggests that proteostasis may be disrupted due to loss of sacsin function.

6.4. Disrupted Proteostasis in ARSACS

Many neurodegenerative diseases are now recognised as 'conformational diseases', because they are characterised by an accumulation of misfolded protein and the formation of intracellular or extracellular protein aggregates. Together with the misfolded protein, aggregates tend to include the presence of proteostasis components, such as ubiquitin and HSP70 (Table 6.1). Similar to these conformational diseases, ARSACS patient HDFs display the characteristic features of aggresomes, which includes the accumulation of proteostasis components, such as HSP70, ubiquitin and p62 (Table 6.1). This suggests the possibility of protein aggregate formation due to disrupted proteostasis. Thus, further research may lead to ARSACS also being categorised as a conformational disease.

Table 6.1. Characteristics of protein aggregates in conformational diseases

Disease	Proteins involved	Protein deposit	Additional protein components
Alexander's disease	GFAP	Cytoplasmic	αB-crystallin, HSP27, ubiquitin, p62
Alzheimer's disease	Presenilin, Tau , β-amyloid	Extracellular, cytoplasmic	Ubiquitin, p62
Amyotrophic lateral sclerosis	Superoxide dismutase	Cytoplasmic	Neurofilaments, ubiquitin, vimentin
Cystic Fibrosis	CFTR	Cytoplasmic	Ubiquitin, vimentin, HSP70, proteasome, ataxin-3
Huntington's disease	Huntingtin	Nuclear, cytoplasmic	HSP70, HSP40, BiP, ubiquitin, vimentin, proteasome, α-synuclein
Parkinson's disease	α-synuclein, UCH-LI	Cytoplasmic, extracellular	p62, ubiquitin, proteasome, neurofilaments, β-amyloid
Prion diseases	Prion protein	Extracellular, cytoplasmic	HSP70, ubiquitin, p62
Spinocerebellar ataxias	Ataxins, atrophin-1	Nuclear	HSP40, HSP70, proteasome, ubiquitin

GFAP: glial fibrillary protein, CFTR: cystic fibrosis transmembrane regulator, UCH-L1: ubiquitin carboxy-terminal hydrolase L1, SCAs: Spinocerebellar ataxia. Adapted from (Garcia-Mata et al., 2002).

Some conformational diseases are caused by mutations in proteins that are key regulators of proteostasis (Cataldo et al., 1996; Kegel et al., 2000; Keller et al., 2000; McNaught et al., 2001; Mittal and Ganesh, 2010). These proteins typically contain domains that mediate interactions with polyubiquitinated proteins or the proteasome, such as an UbL or UbA domain, or UIMs (Grabbe and Dikic, 2009; Su and Lau, 2009). An example is the E3 ubiquitin ligase Parkin, which localises to Lewy bodies in sporadic PD patients (Murakami et al., 2004; Schlossmacher et al., 2002; Shimura et al., 2001), and to aggresomes formed in cultured cells induced by proteasomal impairment

(Junn et al., 2002; Muqit et al., 2004; Zhao et al., 2003). Similarly, ataxin-3 interacts with subunits of the proteasome and has a putative role in protein degradation (Berke et al., 2005; Doss-Pepe et al., 2003; Tsai et al., 2003). WT ataxin-3 is found in intranuclear inclusions in spinocerebellar ataxia (Uchihara et al., 2001) and in aggresomes formed by expression of the ΔF508 mutation within the cystic fibrosis transmembrane conductance regulator (CFTR, (Burnett and Pittman, 2005)). Ablation of ataxin-3 function leads to cytoskeletal disorganisation, ubiquitin-positive aggregate formation and specific neuronal death.

As described in the introduction to this thesis (section 1.4.3.2), mutations have also been identified in DNAJ co-chaperones, which cause disrupted proteostasis, aggregate formation and neurodegeneration (Blumen et al., 2012; Chapple and Cheetham, 2003; Gess et al., 2014; Koutras and Braun, 2014; Mitsuhashi and Kang, 2012).

Sacsin is a member of the DNAJ family of proteins (DNAJC29) due to the presence of a J-domain. Additionally, sacsin also contains an UbL domain and UIMs, and several HSP90-like domains, which all suggest that sacsin may be a key regulator of proteostasis. Furthermore, this thesis has demonstrated that loss of sacsin function leads to cellular characteristics that resemble what is observed when proteostasis is disrupted. Specifically, the intracellular organisation of ARSACS patient HDFs dramatically alters and is indicative of the formation of aggresomes. This is comparable to cells from patients with autosomal dominant, demyelinating CMT type 1C (CMT1C), where aggresomes are encaged by vimentin and enriched with ubiquitin and HSP70 (Lee et al., 2011). Moreover, the intracellular organisation of ARSACS patient HDFs is analogous to cells that have formed aggresomes due to mutant rhodopsin (Kaushal and Khorana, 1994; Olsson et al., 1992; Roof et al., 1994; Saliba et al., 2002). This includes the relocalisation of vimentin into cage-like structures close to the MTOC, disruption to Golgi localisation, recruitment of HSC70 and ubiquitin to the aggresome, and the structures were surrounded by mitochondria (Saliba et al., 2002).

These are all cellular phenotypes that were identified in the ARSACS patient HDFs, thus indicating that aggresomes may be forming as a result of disrupted proteostasis. In line with this hypothesis, the microtubule network appears to be intact in ARSACS patient HDFs, so protein aggregates can be transported along microtubules to the MTOC where aggresomes form. Additionally, like WT ataxin-3, WT sacsin is recruited to expanded ataxin-1 nuclear inclusions (82Q), implying that sacsin may have a

protective role against expanded ataxin-1 induced toxicity (Parfitt et al., 2009). It would be interesting to investigate if sacsin is recruited to inclusions formed in other neurodegenerative diseases, such as intranuclear inclusions of aggregated huntingtin containing polyQ expansions in HD. Considering the data, the pathogenesis of ARSACS may be caused by similar pathological mechanisms to that of other conformational diseases.

Originally, it was assumed that the formation of aggresomes or inclusion bodies containing aggregated proteins were the cause of cellular toxicity in neurodegenerative diseases. However, it is now thought that they may serve a neuroprotective role (Caughey and Lansbury, 2003; Tanaka et al., 2004; Taylor et al., 2003), and provide a way for cells to remove aggregated proteins from the cytosol, where they may interfere with cellular functions. Blocking aggresome formation has been shown to enhance the cytotoxicity of mutant proteins in various neurodegenerative diseases (Taylor et al., 2003; Tanaka et al., 2004), suggesting a protective role for aggresome formation.

Increasing evidence suggests that aggresome formation serves as a mechanism for concentrating misfolded and aggregated proteins for subsequent clearance by autophagy (Chin et al., 2010; Fortun et al., 2003; Iwata et al., 2005a; Taylor et al., 2003). Supporting this, autophagic machinery has been found to localise to inclusions, including those formed in mouse models of polyglutamine disease (Iwata et al., 2005a), and Lewy bodies in PD (Iwata et al., 2005a). Importantly, in Chapter 5, autophagic markers were shown to accumulate with the aggresome-like structures in the ARSACS patient HDFs (discussed further in section 6.4.1).

Studies have also shown that the clearance of aggresomes can be facilitated by the induction of autophagy and blocked by autophagic dysfunction (Fortun et al., 2003; Ravikumar et al., 2002; Yamamoto et al., 2006; Ravikumar et al., 2004). Interestingly, there is evidence for autophagic dysfunction in ARSACS.

6.4.1. Autophagy dysfunction in ARSACS

In neurons, protein quality control mechanisms are crucial to identify abnormal proteins and/or damaged organelles and assure their autophagic degradation before their accumulation leads to neurotoxicity (Winslow and Rubinsztein 2008; Nixon et al., 2008). Autophagic dysfunction has been directly linked to a growing number of

neurodegenerative diseases, including AD, PD, HD and ALS (Lee, 2012; Ravikumar et al., 2002; Stefanis et al., 2001; Webb et al., 2003).

Defective autophagy is indicated by an abnormal accumulation of autophagosomes, particularly in the affected neurons in neurodegenerative diseases (Nixon et al., 2005; Yang et al., 2007). This may be due to increased autophagic activity, meaning that more autophagosomes form, or because clearance of autophagosomes is impaired (Figure 6.3).

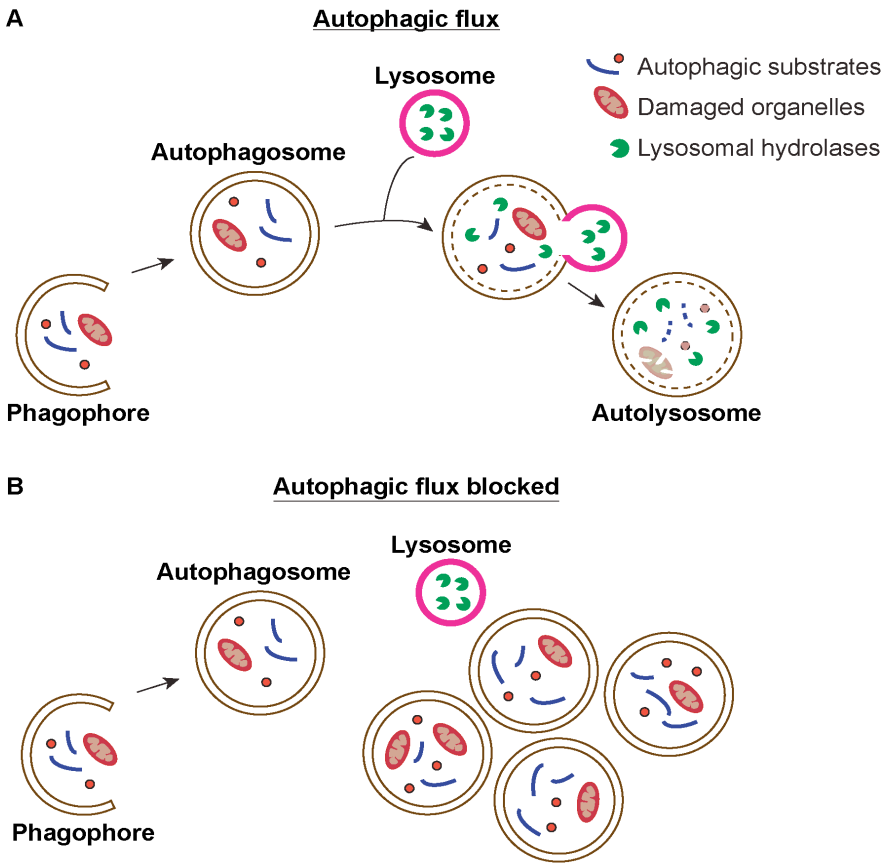

Figure 6.3. Schematic representation of autophagy when turnover is blocked *vs.* normal autophagic flux. (A) Following the induction of autophagy, autophagic substrates and/or damaged organelles are engulfed by an isolation membrane known as a phagophore. This expands into an autophagosome, which fuses with lysosomes (autolysosome) to degrade their contents by the action of lysosomal hydrolases, allowing complete flux through the pathway. **(B)** Autophagy is initiated, but a defect in autophagosome turnover due, for example, to a block in fusion with lysosomes or disruption of lysosomal functions, results in an increased number of autophagosomes. So, autophagy has been induced, but there is no or limited autophagic flux.

In AD, autophagy is induced and the clearance of autophagosomes is impaired, leading to autophagosome accumulation in dystrophic neurites (Boland et al., 2008). In PD, mutations in α-synuclein result in upregulated autophagy (Lynch-Day et al., 2012), and likewise, in HD, increased autophagy results in excess autophagosomes in brains from HD patients (Lynch-Day et al., 2012; Lee, 2012). Increased numbers of autophagosomes promotes neuronal cell death due to an accumulation of toxic proteins (Lee, 2012).

Several autophagosome and lysosome markers are typically used when investigating autophagy dysfunction. Inhibition of autophagy results in an increase in size and number of p62/SQSTM1-containing inclusion bodies, along with an increase in p62/SQSTM1 protein levels (Bjorkoy et al., 2005; Nagaoka et al., 2004; Rusten and Stenmark, 2010; Zatloukal et al., 2002). This is coupled with an accumulation of ubiquitin-containing aggregates (Nagaoka et al., 2004; Zatloukal et al., 2002). Intriguingly, perinuclear p62/SQSTM1 and ubiquitin accumulations were identified in the ARSACS patient HDFs, which is comparable to that observed in many other neurodegenerative diseases. For example, p62/SQSTM1 is present in neuronal and glial inclusions in AD and frontotemporal lobar degeneration (Pikkarainen et al., 2008), inclusions in Pick's disease and PD (Kuusisto et al., 2002), and polyQ-containing inclusions in SCAs (Pikkarainen et al., 2011).

Furthermore, during autophagy, a cytosolic form of microtubule-associated 1A/1B-light chain 3 (LC3-I) is conjugated to phosphatidylethanolamine to form LC3-phosphatidylethanolamine conjugate (LC3-II), which is recruited to autophagosomal membranes. So the number of autophagosomes is correlated with the amount of LC3-II protein. LC3-II is found in Lewy bodies in patients with sporadic PD (Alvarez-Erviti et al., 2010; Dehay et al., 2010). LC3-II protein levels and localisation are yet to be determined in sacsin deficient cells.

Additionally, an accumulation of lysosomes can be identified by observing the expression levels of the late endosome and lysosome membrane proteins LAMP-1 and LAMP-2 (Sun and Grabowski, 2010; Wu et al., 2011; Zaglia et al., 2014). LAMP-1 is found in Lewy bodies in patients with sporadic PD (Chu et al., 2009). Interestingly, LAMP-2 accumulations were observed within the aggresome-like structures in the ARSACS patient HDFs. Along with this, a significant increase in LAMP-2 was

identified at the transcript and protein level in sacsin deficient cells, which may suggest lysosome accumulation (Wu et al., 2011).

Together, increased levels of LC3-II, p62/SQSTM1, LAMP-1 and LAMP-2 indicate autophagy disruption (Fetalvero et al., 2013; Kinouchi et al., 2010). Thus, the data presented in the ARSACS patient HDFs points towards autophagic disruption.

Interestingly, acetylation of microtubules has been suggested to be required for the fusion of autophagosomes with lysosomes (Xie et al., 2010). This is because microtubule acetylation allows the recruitment of the molecular motors dynein and kinesin-1 to microtubules, enabling increased transport of vesicles along microtubules (Bulinski, 2007; Dompierre et al., 2007). This may explain the observed increase in acetylation of α-tubulin in the ARSACS patient HDFs (section 4.2.4.1). A disruption to autophagy may lead to an accumulation of autophagosomes, which in-turn may lead to a compensatory increase in the transport of autophagosomes to lysosomes in order for them to be degraded.

This thesis has presented evidence of disruption to autophagy-mediated protein degradation in ARSACS patient HDF. This is analogous to other neurodegenerative diseases and may be due to an upregulation of the pathway and/or impaired lysosomal degradation and reduced clearance of autophagosomes. If aggregates of misfolded proteins cannot be removed by autophagy, this could explain the aggresome-like structures observed in the ARSACS patient HDFs.

6.4.2. Potential mechanisms of autophagy dysfunction in ARSACS

Interestingly, Y2H screening previously carried out in our group identified putative interactions between the N-terminal region of sacsin encompassing the UbL domain (amino acids 1-650) and ATP6AP2 (ATPase 6 accessory protein 2), snapin, DCTN6, and CSN5, a component of the COP9 signalsome (Parfitt, 2011). This is also the same region of sacsin that has been shown to interact with DRP1 by co-IP (Girard et al., 2012). These proteins all link to roles in protein degradation *via* the UPS or autophagy pathways (Figure 6.4), so it is plausible that loss of sacsin function may affect the localisation or function of these interacting proteins, which may lead to impaired UPS and autophagy-mediated degradation, most likely of a specific client.

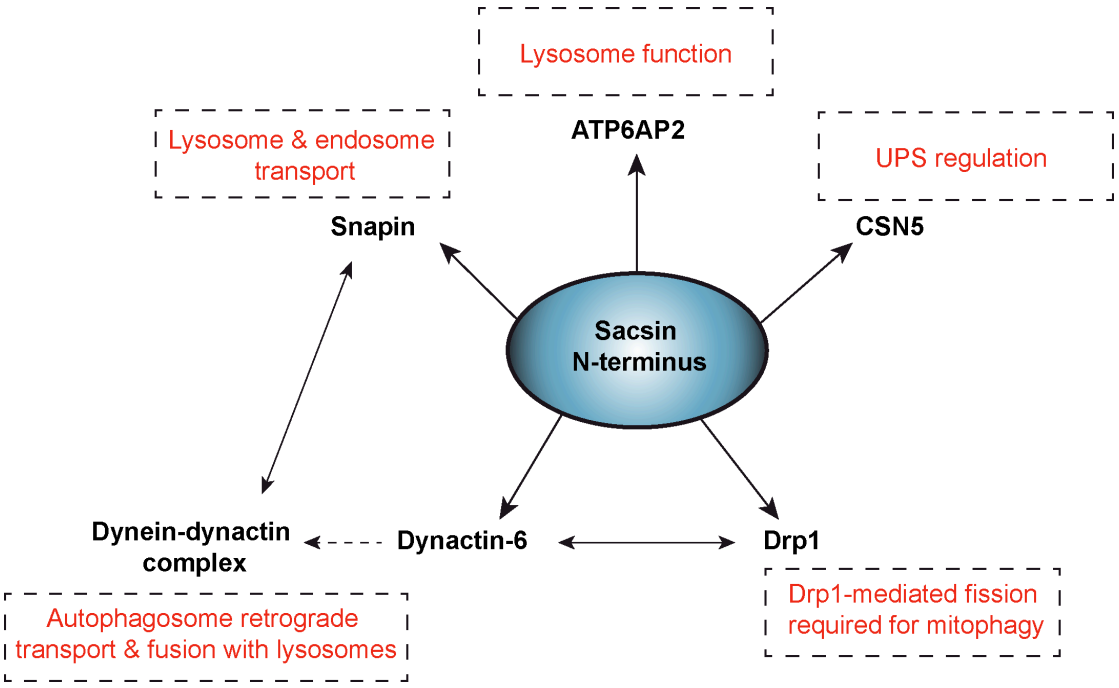

Figure 6.4. Putative interactions between the N-terminal region of sacsin encompassing the UbL domain and proteins implicated in protein degradation pathways.

6.4.2.1. *ATP6AP2*

ATP6AP2 is an essential accessory component of V-ATPase, a large multisubunit complex that has an important function in maintaining the acidic pH in lysosomes and endosomes, and in ensuring the fusion of autophagosomes with endosomes and lysosomes (Toei et al., 2010). Thus, the V-ATPase is required for lysosomal degradation.

V-ATPase is composed of an 8-subunit V_1 sector that is responsible for ATP hydrolysis and a 6-subunit V_0 sector that serves as a transmembrane proton channel (Peters et al., 2001; Yokoyama and Imamura, 2005). ATP6AP2 is specifically associated with the V_0 sector, and loss of ATP6AP2 protein destabilses V_0, preventing its assembly, which results in deacidification of lysosomes (Kinouchi et al., 2010). So, loss of sacsin may be detrimental to ATP6AP2 function, which in-turn may compromise V_0 assembly and disrupt lysosome function. This could explain the phenotypic characteristics indicating autophagy dysfunction in the ARSACS patient HDFs.

Intriguingly, preliminary observations from a microarray experiment performed by our group on four ARSACS patient and two WT control HDF lines indicate a

downregulation of the V_0 subunits $ATP6V_{0B}$ and $ATP6V_{0C}$ (0.77 and 0.75 fold change, respectively) in the ARSACS patient HDF lines. If this data is confirmed by RT-qPCR and immunoblotting, it provides evidence for destabilisation of the V_0 sector in ARSACS patient HDFs, which may be mediated by ATP6AP2 dysfunction. In-line with this, others have shown that loss of ATP6AP2 function leads to significantly decreased protein levels of V_0 subunits, including $ATP6V_{0C}$ (Kinouchi et al., 2010; Kinouchi et al., 2013).

Furthermore, ATP6AP2 loss of function studies describe cellular and molecular phenotypes that resemble what has been observed in the ARSACS patient HDFs (Hedera et al., 2002; Korvatska et al., 2013; Ramser et al., 2005). For example, cardiac-specific ATP6AP2 conditional-knockout mice show perinuclear accumulation of autophagosomes, along with an accumulation of LAMP-2, LC3-II and p62 (Kinouchi et al., 2010).

Perhaps sacsin has a role in targeting ATP6AP2 to the V_0 sector of the V-ATPase, or in targeting V-ATPase to lysosomes, which would be a similar role to the AD-related protein PS1 (Lee et al., 2010).

6.4.2.2. *Snapin*

Snapin has a critical role in the autophagy-lysosome pathway in neurons (Cai et al., 2010; Cai and Sheng, 2011). Snapin assists the dynein-driven retrograde transport of late endosomes to lysosomes for degradation of their contents. This is *via* a direct interaction between snapin and the dynein intermediate chain (DIC, (Cai et al., 2010)).

Snapin$^{-/-}$ neurons show an increase in expression of LAMP-1 and LAMP-2, along with increased LC3-II positive autophagosomes, polyubiquitinated proteins and p62/SQSTM1 (Cai et al., 2010; Lu et al., 2009). This suggests aberrant accumulation of autophagosomes and reduced lysosomal degradation, which results in reduced neuron viability and neurodegeneration (Cai et al., 2010; Lu et al., 2009; Zhou et al., 2011).

If an interaction between snapin and sacsin is verified by co-IP, then loss of sacsin may be detrimental to snapin function, which in-turn may compromise late endosome transport and lysosomal degradation in sacsin deficient cells.

6.4.2.3. *COP9 signalsome*

The COP9 signalosome (CSN) comprises of eight essential subunits (CSN1-CSN8) and is responsible for the regulation of the UPS (Su et al., 2011; Wei et al., 2008). A putative interaction was shown between sacsin and the CSN5 subunit, also known as COPS5. Interestingly, ablation of one of the subunits, CSN8, compromises UPS function and results in excessive accumulation of autophagosomes (Su et al., 2011). Loss of CSN5 function may have a similar effect, so if loss of sacsin function is detrimental to CSN5 function, a disruption to the UPS may occur and an accumulation of autophagosomes may be observed.

6.4.2.4. *DRP1*

A putative interaction has been identified between sacsin and DRP1 by co-IP (Girard et al., 2012), and importantly, a significant reduction in mitochondrial localised DRP1 in sacsin knockdown cells was demonstrated in Chapter 3 of this thesis. This is also observed in ARSACS patient HDFs (Bradshaw et al., 2016). Since DRP1-mediated mitochondrial fission is required for the removal of damaged/dysfunctional mitochondria by mitophagy, sacsin deficient cells potentially accumulate dysfunctional mitochondria. This is evident in various models of ARSACS, including sacsin knockdown cells (Girard et al., 2012), Purkinje neurons from *Sacs*$^{-/-}$ mice (Girard et al., 2012) and ARSACS patient HDFs (Criscuolo et al., 2015; Bradshaw et al., 2016). Thus, reduced Drp1-mediated fission represents a mechanism contributing to the decline of mitochondrial health in ARSACS.

Data from Chapter 5 (Figure 5.10) suggests that dysfunctional mitochondria are not accumulating within the perinuclear region where ubiquitin, HSP70, p62 and LAMP-2 accumulate in the ARSACS patient HDFs. This is consistent with the theory of impaired mitophagy in ARSACS. The hypothesis is that reduced DRP1-mediated mitochondrial fission in ARSACS means that dysfunctional mitochondrial fragments cannot be sequestered for autophagic degradation, thus are not transported to the MTOC. Additionally, as suggested by Gomes and Scorrano (2013), the resulting elongated and hyperfused mitochondria may be too large to be engulfed by autophagosomes (Gomes and Scorrano, 2013). This results in an accumulation of dysfunctional mitochondria, thus contributing to the molecular pathology of ARSACS. This hypothesis is in-line with previous data showing that reduced mitochondrial fission

impairs mitophagy (Arnoult et al., 2005; Gomes and Scorrano, 2013; Parone et al., 2008; Twig et al., 2008).

6.4.2.5. *DCTN6*

DCTN6 may be linked to the autophagy pathway of protein degradation *via* several avenues. Firstly, in Chapter 3, an interaction was identified between heterologously expressed DCTN6 and DRP1. *DCTN6* siRNA-mediated knockdown also resulted in a significant reduction in mitochondrial localised DRP1, along with an elongated mitochondrial network. Thus, DCTN6 function may also be important for mitochondrial quality control through maintaining DRP1-mediated mitochondrial fission. *DCTN6* knockdown also lead to a reduction in mitochondrial membrane potential, suggesting an accumulation of dysfunctional mitochondria may be occurring, which may be attributed to impaired mitophagy. Varadi *et al* (2004) have previously shown that the dynein-dynactin complex is required for DRP1 recruitment to mitochondria (Varadi et al., 2004), which supports that this motor complex may be, indirectly, necessary for mitophagy.

The dynein-dynactin motor is also required for the retrograde transport of autophagosomes along microtubules to lysosomes (Ravikumar et al., 2005; Rubinsztein et al., 2005). Reduced dynein-dynactin function impairs autophagic clearance of aggregate-prone proteins, leading to the accumulation of protein aggregates and inclusion formation. This is observed when the dynactin subunit, $p150^{Glued}$, is mutated, which causes a motor neuron disease (Levy et al., 2006; Puls et al., 2003).

So if loss of sacsin function interferes with DCTN6 function, this may impair autophagic degradation, which may contribute to the accumulation of dysfunctional mitochondria observed in ARSACS, and possibly protein aggregation and aggresome formation.

In summary, it is compelling that putative interactions have been identified between the N-terminus of sacsin and five proteins involved in protein degradation pathways. This, together with the evidence produced in this thesis for disrupted proteostasis in ARSACS, strongly suggests a role for sacsin in proteostasis. This could be a direct role, or an indirect role, through interactions with other key regulators of proteostasis, such as ATP6AP2, snapin, DCTN6, COPS5 and DRP1. Given the large size of sacsin and the

multiple functional domains, it is feasible that sacsin may act as a scaffold protein, interacting with multiple members of the proteostasis pathway.

6.4.3. Further work to investigate autophagy dysfunction in ARSACS

Further research is required to investigate a role for sacsin in proteostasis. The number of autophagosomes is correlated with the amount of LC3-II protein. Increased LC3-II along with reduced LC3-I levels would indicate an accumulation of autophagosomes in sacsin deficient cells, hence would help to determine if autophagy is impaired. This could be investigated using immunoblotting and immunocytochemistry in sacsin deficient cells compared to controls.

Also, dual immunocytochemistry for LC3-II and LAMP-2 followed by high-resolution confocal microscopy could be performed in sacsin deficient and control cells. If these two proteins do not co-localise, then it suggests that autophagosome-lysosome fusion may be perturbed, which blocks autophagic flux and autophagosome clearance (Zaglia et al., 2014).

Our research group carried out a microarray experiment on SH-SY5Y cells transfected with *SCRM* or *SACS* siRNA, and on ARSACS patient and WT control HDF cell lines. Preliminary analyses of the results from this highlight various autophagy-related genes that are dysregulated in cells with loss of sacsin. For example, *ATG5* is upregulated by 1.25-fold, and *CTSH* and *CTSB*, which encode lysosomal cathepsins, are upregulated by 1.22-fold and 1.24-fold, respectively. These need to be verified by RT-qPCR and immunoblotting as this data would provide evidence suggesting autophagic dysfunction in cells due to loss of sacsin.

The putative interactions between sacsin and ATP6AP2, snapin, COPS5, and DCTN6 also need to be verified. A number of methods could be used, for example, Co-IP studies, subcellular immunofluorescent co-localisation studies or tissue immunohistochemical studies. The protein and mRNA expression levels and the subcellular localisation of these proteins could also be investigated for any change in cells with loss of sacsin compared to controls. If these interactions are verified, then it may highlight a potential mechanism for disrupted proteostasis in sacsin deficient cells.

Moreover, lysosomal pH could be investigated in cells with loss of sacsin, for example by using LysoSensor (ThermoFisher Scientific). A deacidification of lysosomes would be indicated by an increase in pH.

6.5. Potential Therapeutic Strategies for ARSACS

There is currently no available therapy for ARSACS. Defining the molecular pathogenesis of ARSACS represents the first step in identifying a therapeutic strategy. The data produced in this thesis suggests that loss of sacsin function disrupts cellular proteostasis. Further investigation of the mechanisms leading to this disrupted proteostasis may provide a target for therapeutics. Also, the cellular phenotypes identified, such as the collapse of the vimentin network into perinuclear bundles, could be used in high-throughput screening to identify therapeutic targets for ARSACS.

If autophagic degradation is impaired, then manipulating this pathway may be a viable strategy for treating ARSACS. Mammalian target of rapamycin (mTOR) is an intracellular serine/threonine protein kinase that has a central role in several cellular processes, including autophagy (Hay and Sonenberg, 2004; Wullschleger et al., 2006; Zoncu et al., 2011). Inhibiting mTOR using rapamycin leads to the induction of autophagy. Data from studies of cell, animal, and fly models show that this may reduce toxicity in many neurodegenerative diseases where mutant proteins lead to aggresome/inclusion formation (Berger et al., 2006). For example, rapamycin treatment reduces protein aggregation and toxicity in HD (Ravikumar et al., 2002; Ravikumar et al., 2004), SCA3 (Menzies et al., 2010), and PD (Bove et al., 2011; Dehay et al., 2010; Malagelada et al., 2010; Xiong et al., 2011).

Another possible therapeutic strategy, that has been shown to reduce inclusion formation and prevent cell toxicity in several models of neurodegeneration, is to enhance chaperone levels. This may restore proteostasis by increasing protein folding, reducing aggregation, and promoting proteasomal degradation. For example, HSP70 overexpression reduced α-synuclein accumulation and toxicity in mouse and *Drosophila* models of PD (Auluck et al., 2002; Klucken et al., 2004). Furthermore, overexpression of the HSP40 protein HDJ-2 (DNAJA1) caused a significant reduction in the incidence of ataxin-1 inclusions (Cummings et al., 1998).

6.6. Final Conclusions

Sacsin is a large multi-domain protein, which contains regions of similarity to molecular chaperones and domains linking to protein degradation pathways, which suggests a potential role in maintaining proteostasis.

The main findings of this thesis include the observation that cells with loss of sacsin function display the characteristics of aggresome formation. Aggresomes form due to the accumulation and aggregation of misfolded proteins, which occurs when proteostasis is impaired. Thus, the potential presence of aggresome-like structures suggests proteostasis may be disrupted due to loss of sacsin function.

Furthermore, a reduction in DRP1-mediated mitochondrial fission has been identified in sacsin deficient cells. This may be due to loss of an interaction between sacsin, DRP1 and DCNT6, which may result in reduced transport of DRP1 to mitochondria *via* the dynein-dynactin complex. Since, DRP1-mediated mitochondrial fission is necessary for mitochondrial quality control, a disruption to mitochondrial quality control is likely to occur in sacsin deficient cells. This may explain the mitochondrial dysfunction, observed by our group and others, in ARSACS. Moreover, a disruption to dynein-dynactin-based microtubule transport may also have implications for IF network assembly and organisation (Helfand et al., 2002).

Mitochondrial dysfunction, cytoskeletal disruption, and protein misfolding and aggregation are particular detrimental in neurons and are characteristic features of many neurodegenerative diseases. Sacsin is highly expressed in neurons, particularly in motor neurons and Purkinje neurons in the cerebellum (Parfitt, 2011), indicating a vital role in these neurons. This may reflect the importance of proteostasis in these neurons.

In summary, the findings of this thesis, together with the knowledge of sacsins domain structure, indicate a role for sacsin in maintaining proteostasis. Impaired proteostasis likely leads to mitochondrial dysfunction and neurotoxicity, and may contribute to the cerebellar ataxia and neurodegeneration in ARSACS. Further work will be required to fully elucidate the role of sacsin in protein and mitochondrial quality control.

REFERENCES

Ahn, S., J. Kim, C.L. Lucaveche, M.C. Reedy, L.M. Luttrell, R.J. Lefkowitz, and Y. Daaka. 2002. Src-dependent tyrosine phosphorylation regulates dynamin self-assembly and ligand-induced endocytosis of the epidermal growth factor receptor. *The Journal of biological chemistry*. 277:26642-26651.

Al-Chalabi, A., P.M. Andersen, P. Nilsson, B. Chioza, J.L. Andersson, C. Russ, C.E. Shaw, J.F. Powell, and P.N. Leigh. 1999. Deletions of the heavy neurofilament subunit tail in amyotrophic lateral sclerosis. *Human molecular genetics*. 8:157-164.

Al-Chalabi, A., and C.C. Miller. 2003. Neurofilaments and neurological disease. *BioEssays : news and reviews in molecular, cellular and developmental biology*. 25:346-355.

Alberti, S., J. Demand, C. Esser, N. Emmerich, H. Schild, and J. Hohfeld. 2002. Ubiquitylation of BAG-1 suggests a novel regulatory mechanism during the sorting of chaperone substrates to the proteasome. *The Journal of biological chemistry*. 277:45920-45927.

Alexander, C., M. Votruba, U.E. Pesch, D.L. Thiselton, S. Mayer, A. Moore, M. Rodriguez, U. Kellner, B. Leo-Kottler, G. Auburger, S.S. Bhattacharya, and B. Wissinger. 2000. OPA1, encoding a dynamin-related GTPase, is mutated in autosomal dominant optic atrophy linked to chromosome 3q28. *Nature genetics*. 26:211-215.

Ali, A., S. Bharadwaj, R. O'Carroll, and N. Ovsenek. 1998. HSP90 interacts with and regulates the activity of heat shock factor 1 in Xenopus oocytes. *Molecular and cellular biology*. 18:4949-4960.

Ali, M.M., S.M. Roe, C.K. Vaughan, P. Meyer, B. Panaretou, P.W. Piper, C. Prodromou, and L.H. Pearl. 2006. Crystal structure of an Hsp90-nucleotide-p23/Sba1 closed chaperone complex. *Nature*. 440:1013-1017.

Allen, E., J. Ding, W. Wang, S. Pramanik, J. Chou, V. Yau, and Y. Yang. 2005. Gigaxonin-controlled degradation of MAP1B light chain is critical to neuronal survival. *Nature*. 438:224-228.

Alper, G., and V. Narayanan. 2003. Friedreich's ataxia. *Pediatr Neurol*. 28:335-341.

Alvarez-Erviti, L., M.C. Rodriguez-Oroz, J.M. Cooper, C. Caballero, I. Ferrer, J.A. Obeso, and A.H. Schapira. 2010. Chaperone-mediated autophagy markers in Parkinson disease brains. *Archives of neurology*. 67:1464-1472.

Anderson, J.F. 2011. The Role of Sacsin as a Molecular Chaperone.

Anderson, J.F., E. Siller, and J.M. Barral. 2010. The sacsin repeating region (SRR): a novel Hsp90-related supra-domain associated with neurodegeneration. *J Mol Biol*. 400:665-674.

Anesi, L., P. de Gemmis, M. Pandolfo, and U. Hladnik. 2011. Two novel homozygous SACS mutations in unrelated patients including the first reported case of paternal UPD as an etiologic cause of ARSACS. *J Mol Neurosci*. 43:346-349.

Anesti, V., and L. Scorrano. 2006. The relationship between mitochondrial shape and function and the cytoskeleton. *Biochimica et biophysica acta*. 1757:692-699.

Anheim, M., M. Fleury, B. Monga, V. Laugel, D. Chaigne, G. Rodier, E. Ginglinger, C. Boulay, S. Courtois, N. Drouot, M. Fritsch, J.P. Delaunoy, D. Stoppa-Lyonnet, C. Tranchant, and M. Koenig. 2010. Epidemiological, clinical, paraclinical and molecular study of a cohort of 102 patients affected with autosomal recessive progressive cerebellar ataxia from Alsace, Eastern France: implications for clinical management. *Neurogenetics*. 11:1-12.

Anheim, M., L.L. Mariani, P. Calvas, E. Cheuret, F. Zagnoli, S. Odent, C. Seguela, C. Marelli, M. Fritsch, J.P. Delaunoy, A. Brice, A. Durr, and M. Koenig. 2012a. Exonic deletions of FXN and early-onset Friedreich ataxia. *Archives of neurology*. 69:912-916.

Anheim, M., C. Tranchant, and M. Koenig. 2012b. The autosomal recessive cerebellar ataxias. *The New England journal of medicine*. 366:636-646.

Anton, L.C., U. Schubert, I. Bacik, M.F. Princiotta, P.A. Wearsch, J. Gibbs, P.M. Day, C. Realini, M.C. Rechsteiner, J.R. Bennink, and J.W. Yewdell. 1999. Intracellular localization of proteasomal degradation of a viral antigen. *The Journal of cell biology*. 146:113-124.

Anttonen, A.K., I. Mahjneh, R.H. Hamalainen, C. Lagier-Tourenne, O. Kopra, L. Waris, M. Anttonen, T. Joensuu, H. Kalimo, A. Paetau, L. Tranebjaerg, D. Chaigne, M. Koenig, O. Eeg-Olofsson, B. Udd, M. Somer, H. Somer, and A.E. Lehesjoki. 2005. The gene disrupted in Marinesco-Sjogren syndrome encodes SIL1, an HSPA5 cochaperone. *Nature genetics*. 37:1309-1311.

Ao, X., L. Zou, and Y. Wu. 2014. Regulation of autophagy by the Rab GTPase network. *Cell death and differentiation*. 21:348-358.

Arnoult, D., N. Rismanchi, A. Grodet, R.G. Roberts, D.P. Seeburg, J. Estaquier, M. Sheng, and C. Blackstone. 2005. Bax/Bak-dependent release of DDP/TIMM8a promotes Drp1-mediated mitochondrial fission and mitoptosis during programmed cell death. *Current biology : CB*. 15:2112-2118.

Arrasate, M., and S. Finkbeiner. 2005. Automated microscope system for determining factors that predict neuronal fate. *Proceedings of the National Academy of Sciences of the United States of America*. 102:3840-3845.

Arrasate, M., S. Mitra, E.S. Schweitzer, M.R. Segal, and S. Finkbeiner. 2004. Inclusion body formation reduces levels of mutant huntingtin and the risk of neuronal death. *Nature*. 431:805-810.

Asthana, J., S. Kapoor, R. Mohan, and D. Panda. 2013. Inhibition of HDAC6 deacetylase activity increases its binding with microtubules and suppresses microtubule dynamic instability in MCF-7 cells. *The Journal of biological chemistry*. 288:22516-22526.

Auluck, P.K., H.Y. Chan, J.Q. Trojanowski, V.M. Lee, and N.M. Bonini. 2002. Chaperone suppression of alpha-synuclein toxicity in a Drosophila model for Parkinson's disease. *Science*. 295:865-868.

Baets, J., T. Deconinck, K. Smets, D. Goossens, P. Van den Bergh, K. Dahan, E. Schmedding, P. Santens, V.M. Rasic, P. Van Damme, W. Robberecht, L. De Meirleir, B. Michielsens, J. Del-Favero, A. Jordanova, and P. De Jonghe. 2010. Mutations in SACS cause atypical and late-onset forms of ARSACS. *Neurology*. 75:1181-1188.

Bagatell, R., G.D. Paine-Murrieta, C.W. Taylor, E.J. Pulcini, S. Akinaga, I.J. Benjamin, and L. Whitesell. 2000. Induction of a heat shock factor 1-dependent stress response alters the cytotoxic activity of hsp90-binding agents. *Clinical cancer research : an official journal of the American Association for Cancer Research*. 6:3312-3318.

Baloh, R.H., R.E. Schmidt, A. Pestronk, and J. Milbrandt. 2007. Altered axonal mitochondrial transport in the pathogenesis of Charcot-Marie-Tooth disease from mitofusin 2 mutations. *The Journal of neuroscience : the official journal of the Society for Neuroscience*. 27:422-430.

Bardwell, J.C., and E.A. Craig. 1984. Major heat shock gene of Drosophila and the Escherichia coli heat-inducible dnaK gene are homologous. *Proceedings of the National Academy of Sciences of the United States of America*. 81:848-852.

Barouch, W., K. Prasad, L.E. Greene, and E. Eisenberg. 1994. ATPase activity associated with the uncoating of clathrin baskets by Hsp70. *The Journal of biological chemistry*. 269:28563-28568.

Barral, J.M., S.A. Broadley, G. Schaffar, and F.U. Hartl. 2004. Roles of molecular chaperones in protein misfolding diseases. *Seminars in cell & developmental biology*. 15:17-29.

Barsoum, M.J., H. Yuan, A.A. Gerencser, G. Liot, Y. Kushnareva, S. Graber, I. Kovacs, W.D. Lee, J. Waggoner, J. Cui, A.D. White, B. Bossy, J.C. Martinou, R.J. Youle, S.A. Lipton, M.H. Ellisman, G.A. Perkins, and E. Bossy-Wetzel. 2006. Nitric oxide-induced mitochondrial fission is regulated by dynamin-related GTPases in neurons. *The EMBO journal*. 25:3900-3911.

Bates, G. 1996. Expanded glutamines and neurodegeneration--a gain of insight. *BioEssays : news and reviews in molecular, cellular and developmental biology*. 18:175-178.

Becker, D., J. Richter, M.A. Tocilescu, S. Przedborski, and W. Voos. 2012. Pink1 kinase and its membrane potential (Deltapsi)-dependent cleavage product both localize to outer mitochondrial membrane by unique targeting mode. *The Journal of biological chemistry*. 287:22969-22987.

Benard, G., and M. Karbowski. 2009. Mitochondrial fusion and division: Regulation and role in cell viability. *Seminars in cell & developmental biology*. 20:365-374.

Bence, N.F., R.M. Sampat, and R.R. Kopito. 2001. Impairment of the ubiquitin-proteasome system by protein aggregation. *Science*. 292:1552-1555.

Benitez, B.A., D. Alvarado, Y. Cai, K. Mayo, S. Chakraverty, J. Norton, J.C. Morris, M.S. Sands, A. Goate, and C. Cruchaga. 2011. Exome-sequencing confirms DNAJC5 mutations as cause of adult neuronal ceroid-lipofuscinosis. *PloS one*. 6:e26741.

Berciano, J., J. Infante, A. Garcia, J.M. Polo, V. Volpini, and O. Combarros. 2005. Very late-onset Friedreich's ataxia with minimal GAA1 expansion mimicking multiple system atrophy of cerebellar type. *Movement disorders : official journal of the Movement Disorder Society*. 20:1643-1645.

Bereiter-Hahn, J. 1990. Behavior of mitochondria in the living cell. *Int Rev Cytol*. 122:1-63.

Bereiter-Hahn, J. 2014. Mitochondrial dynamics in aging and disease. *Progress in molecular biology and translational science*. 127:93-131.

Bereiter-Hahn, J., and M. Voth. 1994. Dynamics of mitochondria in living cells: shape changes, dislocations, fusion, and fission of mitochondria. *Microsc Res Tech*. 27:198-219.

Berger, Z., B. Ravikumar, F.M. Menzies, L.G. Oroz, B.R. Underwood, M.N. Pangalos, I. Schmitt, U. Wullner, B.O. Evert, C.J. O'Kane, and D.C. Rubinsztein. 2006. Rapamycin alleviates toxicity of different aggregate-prone proteins. *Human molecular genetics*. 15:433-442.

Berke, S.J., Y. Chai, G.L. Marrs, H. Wen, and H.L. Paulson. 2005. Defining the role of ubiquitin-interacting motifs in the polyglutamine disease protein, ataxin-3. *The Journal of biological chemistry*. 280:32026-32034.

Bhattacharyya, S., H. Yu, C. Mim, and A. Matouschek. 2014. Regulated protein turnover: snapshots of the proteasome in action. *Nature reviews. Molecular cell biology*. 15:122-133.

Biedler, J.L., S. Roffler-Tarlov, M. Schachner, and L.S. Freedman. 1978. Multiple neurotransmitter synthesis by human neuroblastoma cell lines and clones. *Cancer research*. 38:3751-3757.

Bignami, A., T. Raju, and D. Dahl. 1982. Localization of vimentin, the nonspecific intermediate filament protein, in embryonal glia and in early differentiating neurons. In vivo and in vitro immunofluorescence study of the rat embryo with vimentin and neurofilament antisera. *Developmental biology*. 91:286-295.

Bjorkoy, G., T. Lamark, A. Brech, H. Outzen, M. Perander, A. Overvatn, H. Stenmark, and T. Johansen. 2005. p62/SQSTM1 forms protein aggregates degraded by autophagy and has a protective effect on huntingtin-induced cell death. *The Journal of cell biology*. 171:603-614.

Bleazard, W., J.M. McCaffery, E.J. King, S. Bale, A. Mozdy, Q. Tieu, J. Nunnari, and J.M. Shaw. 1999. The dynamin-related GTPase Dnm1 regulates mitochondrial fission in yeast. *Nature cell biology*. 1:298-304.

Blumen, S.C., S. Astord, V. Robin, L. Vignaud, N. Toumi, A. Cieslik, A. Achiron, R.L. Carasso, M. Gurevich, I. Braverman, N. Blumen, A. Munich, M. Barkats, and L. Viollet. 2012. A rare recessive distal hereditary motor neuropathy with HSJ1 chaperone mutation. *Annals of neurology*. 71:509-519.

Blumkin, L., T. Bradshaw, M. Michelson, T. Kopler, D. Dahari, T. Lerman-Sagie, D. Lev, J.P. Chapple, and E. Leshinsky-Silver. 2015. Molecular and functional studies of retinal degeneration as a clinical presentation of SACS-related disorder. *European journal of paediatric neurology : EJPN : official journal of the European Paediatric Neurology Society*. 19:472-476.

Boland, B., A. Kumar, S. Lee, F.M. Platt, J. Wegiel, W.H. Yu, and R.A. Nixon. 2008. Autophagy induction and autophagosome clearance in neurons: relationship to autophagic pathology in Alzheimer's disease. *The Journal of neuroscience : the official journal of the Society for Neuroscience*. 28:6926-6937.

Boldogh, I.R., and L.A. Pon. 2006. Interactions of mitochondria with the actin cytoskeleton. *Biochimica et biophysica acta*. 1763:450-462.

Bomont, P., and M. Koenig. 2003. Intermediate filament aggregation in fibroblasts of giant axonal neuropathy patients is aggravated in non dividing cells and by microtubule destabilization. *Human molecular genetics*. 12:813-822.

Borkovich, K.A., F.W. Farrelly, D.B. Finkelstein, J. Taulien, and S. Lindquist. 1989. hsp82 is an essential protein that is required in higher concentrations for growth of cells at higher temperatures. *Molecular and cellular biology*. 9:3919-3930.

Bossy-Wetzel, E., A. Petrilli, and A.B. Knott. 2008. Mutant huntingtin and mitochondrial dysfunction. *Trends in neurosciences*. 31:609-616.

Bouchard, J.P. 1991. Ressesive spastic ataxia of Charlevoix-Saguenay. *In* Handbook of Clinical Neurology. J.M.B.V.d. Jong, editor. Elsevier, Amsterdam. 451-459.

Bouchard, J.P., A. Barbeau, R. Bouchard, and R.W. Bouchard. 1978. Autosomal recessive spastic ataxia of Charlevoix-Saguenay. *Can J Neurol Sci*. 5:61-69.

Bouchard, J.P., A. Richter, J. Mathieu, D. Brunet, T.J. Hudson, K. Morgan, and S.B. Melancon. 1998. Autosomal recessive spastic ataxia of Charlevoix-Saguenay. *Neuromuscular disorders : NMD*. 8:474-479.

Bouchard, J.P., Richter, A, Melancon, S.B, Mathieu, J, Michaud, J. 2000. Autosomal recessive spastic ataxia (Charlevoix-Saguenay). *In* Handbook of Ataxia Disorders. K. T, editor. Marcel Dekker, New York. 312-324.

Bouhlal, Y., R. Amouri, G. El Euch-Fayeche, and F. Hentati. 2011. Autosomal recessive spastic ataxia of Charlevoix-Saguenay: an overview. *Parkinsonism Relat Disord*. 17:418-422.

Bouhlal, Y., G. El Euch-Fayeche, F. Hentati, and R. Amouri. 2009. A novel SACS gene mutation in a Tunisian family. *J Mol Neurosci*. 39:333-336.

Bove, J., M. Martinez-Vicente, and M. Vila. 2011. Fighting neurodegeneration with rapamycin: mechanistic insights. *Nature reviews. Neuroscience*. 12:437-452.

Boya, P., R.A. Gonzalez-Polo, N. Casares, J.L. Perfettini, P. Dessen, N. Larochette, D. Metivier, D. Meley, S. Souquere, T. Yoshimori, G. Pierron, P. Codogno, and G. Kroemer. 2005. Inhibition of macroautophagy triggers apoptosis. *Molecular and cellular biology*. 25:1025-1040.

Bradley, J.L., J.C. Blake, S. Chamberlain, P.K. Thomas, J.M. Cooper, and A.H. Schapira. 2000. Clinical, biochemical and molecular genetic correlations in Friedreich's ataxia. *Human molecular genetics*. 9:275-282.

Bradshaw, T.Y., L.E. Romano, E.J. Duncan, S. Nethisinghe, R. Abeti, G.J. Michael, P. Giunti, S. Vermeer, and J.P. Chapple. 2016. A reduction in Drp1 mediated fission compromises mitochondrial health in autosomal recessive spastic ataxia of Charlevoix Saguenay. *Human molecular genetics*.

Brandt, R., M. Hundelt, and N. Shahani. 2005. Tau alteration and neuronal degeneration in tauopathies: mechanisms and models. *Biochimica et biophysica acta*. 1739:331-354.

Braschi, E., R. Zunino, and H.M. McBride. 2009. MAPL is a new mitochondrial SUMO E3 ligase that regulates mitochondrial fission. *EMBO reports*. 10:748-754.

Breckpot, J., Y. Takiyama, B. Thienpont, S. Van Vooren, J.R. Vermeesch, E. Ortibus, and K. Devriendt. 2008. A novel genomic disorder: a deletion of the SACS gene leading to spastic ataxia of Charlevoix-Saguenay. *Eur J Hum Genet*. 16:1050-1054.

Brickley, K., and F.A. Stephenson. 2011. Trafficking kinesin protein (TRAK)-mediated transport of mitochondria in axons of hippocampal neurons. *The Journal of biological chemistry*. 286:18079-18092.

Brownlees, J., S. Ackerley, A.J. Grierson, N.J. Jacobsen, K. Shea, B.H. Anderton, P.N. Leigh, C.E. Shaw, and C.C. Miller. 2002. Charcot-Marie-Tooth disease neurofilament mutations disrupt neurofilament assembly and axonal transport. *Human molecular genetics*. 11:2837-2844.

Bukau, B., and A.L. Horwich. 1998. The Hsp70 and Hsp60 chaperone machines. *Cell*. 92:351-366.

Bukau, B., J. Weissman, and A. Horwich. 2006. Molecular chaperones and protein quality control. *Cell*. 125:443-451.

Bulinski, J.C. 2007. Microtubule modification: acetylation speeds anterograde traffic flow. *Current biology : CB*. 17:R18-20.

Burkhardt, J.K., C.J. Echeverri, T. Nilsson, and R.B. Vallee. 1997. Overexpression of the dynamitin (p50) subunit of the dynactin complex disrupts dynein-dependent maintenance of membrane organelle distribution. *The Journal of cell biology*. 139:469-484.

Burnett, B., F. Li, and R.N. Pittman. 2003. The polyglutamine neurodegenerative protein ataxin-3 binds polyubiquitylated proteins and has ubiquitin protease activity. *Human molecular genetics*. 12:3195-3205.

Burnett, B.G., and R.N. Pittman. 2005. The polyglutamine neurodegenerative protein ataxin 3 regulates aggresome formation. *Proceedings of the National Academy of Sciences of the United States of America*. 102:4330-4335.

Cai, Q., L. Lu, J.H. Tian, Y.B. Zhu, H. Qiao, and Z.H. Sheng. 2010. Snapin-regulated late endosomal transport is critical for efficient autophagy-lysosomal function in neurons. *Neuron*. 68:73-86.

Cai, Q., and Z.H. Sheng. 2011. Uncovering the role of Snapin in regulating autophagy-lysosomal function. *Autophagy*. 7:445-447.

Calkins, M.J., and P.H. Reddy. 2011. Amyloid beta impairs mitochondrial anterograde transport and degenerates synapses in Alzheimer's disease neurons. *Biochimica et biophysica acta*. 1812:507-513.

Campuzano, V., L. Montermini, Y. Lutz, L. Cova, C. Hindelang, S. Jiralerspong, Y. Trottier, S.J. Kish, B. Faucheux, P. Trouillas, F.J. Authier, A. Durr, J.L. Mandel, A. Vescovi, M. Pandolfo, and M. Koenig. 1997. Frataxin is reduced in Friedreich ataxia patients and is associated with mitochondrial membranes. *Human molecular genetics*. 6:1771-1780.

Campuzano, V., L. Montermini, M.D. Molto, L. Pianese, M. Cossee, F. Cavalcanti, E. Monros, F. Rodius, F. Duclos, A. Monticelli, F. Zara, J. Canizares, H. Koutnikova, S.I. Bidichandani, C. Gellera, A. Brice, P. Trouillas, G. De Michele, A. Filla, R. De Frutos, F. Palau, P.I. Patel, S. Di Donato, J.L. Mandel, S. Cocozza, M. Koenig, and M. Pandolfo. 1996. Friedreich's ataxia: autosomal recessive disease caused by an intronic GAA triplet repeat expansion. *Science*. 271:1423-1427.

Capetanaki, Y. 2002. Desmin cytoskeleton: a potential regulator of muscle mitochondrial behavior and function. *Trends in cardiovascular medicine*. 12:339-348.

Cara, L., M. Baitemirova, J. Follis, M. Larios-Sanz, and A. Ribes-Zamora. 2016. The ATM- and ATR-related SCD domain is over-represented in proteins involved in nervous system development. *Scientific reports*. 6:19050.

Carden, M.J., M.E. Goldstein, J. Bruce, H.S. Cooper, and W.W. Schlaepfer. 1987. Studies of neurofilaments that accumulate in proximal axons of rats intoxicated with beta,beta'-iminodipropionitrile (IDPN). *Neurochemical pathology*. 7:189-205.

Cartelli, D., C. Ronchi, M.G. Maggioni, S. Rodighiero, E. Giavini, and G. Cappelletti. 2010. Microtubule dysfunction precedes transport impairment and mitochondria damage in MPP+ -induced neurodegeneration. *Journal of neurochemistry*. 115:247-258.

Cataldo, A.M., D.J. Hamilton, J.L. Barnett, P.A. Paskevich, and R.A. Nixon. 1996. Properties of the endosomal-lysosomal system in the human central nervous system: disturbances mark most neurons in populations at risk to degenerate in Alzheimer's disease. *The Journal of neuroscience : the official journal of the Society for Neuroscience*. 16:186-199.

Caughey, B., and P.T. Lansbury. 2003. Protofibrils, pores, fibrils, and neurodegeneration: separating the responsible protein aggregates from the innocent bystanders. *Annual review of neuroscience*. 26:267-298.

Cavadini, P., H.A. O'Neill, O. Benada, and G. Isaya. 2002. Assembly and iron-binding properties of human frataxin, the protein deficient in Friedreich ataxia. *Human molecular genetics*. 11:217-227.

Cereghetti, G.M., A. Stangherlin, O. Martins de Brito, C.R. Chang, C. Blackstone, P. Bernardi, and L. Scorrano. 2008. Dephosphorylation by calcineurin regulates translocation of Drp1 to mitochondria. *Proceedings of the National Academy of Sciences of the United States of America*. 105:15803-15808.

Cerveny, K.L., and R.E. Jensen. 2003. The WD-repeats of Net2p interact with Dnm1p and Fis1p to regulate division of mitochondria. *Molecular biology of the cell*. 14:4126-4139.

Chai, Y., S.L. Koppenhafer, N.M. Bonini, and H.L. Paulson. 1999. Analysis of the role of heat shock protein (Hsp) molecular chaperones in polyglutamine disease. *The Journal of neuroscience : the official journal of the Society for Neuroscience*. 19:10338-10347.

Chan, D.C. 2006. Mitochondria: dynamic organelles in disease, aging, and development. *Cell*. 125:1241-1252.

Chan, D.C. 2012. Fusion and fission: interlinked processes critical for mitochondrial health. *Annu Rev Genet*. 46:265-287.

Chang, C.R., and C. Blackstone. 2007. Cyclic AMP-dependent protein kinase phosphorylation of Drp1 regulates its GTPase activity and mitochondrial morphology. *The Journal of biological chemistry*. 282:21583-21587.

Chang, C.R., and C. Blackstone. 2010. Dynamic regulation of mitochondrial fission through modification of the dynamin-related protein Drp1. *Ann N Y Acad Sci*. 1201:34-39.

Chang, C.R., C.M. Manlandro, D. Arnoult, J. Stadler, A.E. Posey, R.B. Hill, and C. Blackstone. 2010. A lethal de novo mutation in the middle domain of the dynamin-related GTPase Drp1 impairs higher order assembly and mitochondrial division. *The Journal of biological chemistry*. 285:32494-32503.

Chang, D.T., G.L. Rintoul, S. Pandipati, and I.J. Reynolds. 2006. Mutant huntingtin aggregates impair mitochondrial movement and trafficking in cortical neurons. *Neurobiology of disease*. 22:388-400.

Chang, L., and R.D. Goldman. 2004. Intermediate filaments mediate cytoskeletal crosstalk. *Nature reviews. Molecular cell biology*. 5:601-613.

Chapman, A.L., E.J. Bennett, T.M. Ramesh, K.J. De Vos, and A.J. Grierson. 2013. Axonal Transport Defects in a Mitofusin 2 Loss of Function Model of Charcot-Marie-Tooth Disease in Zebrafish. *PloS one*. 8:e67276.

Chapple, J.P., and M.E. Cheetham. 2003. The chaperone environment at the cytoplasmic face of the endoplasmic reticulum can modulate rhodopsin processing and inclusion formation. *The Journal of biological chemistry*. 278:19087-19094.

Chapple, J.P., J. van der Spuy, S. Poopalasundaram, and M.E. Cheetham. 2004. Neuronal DnaJ proteins HSJ1a and HSJ1b: a role in linking the Hsp70 chaperone machine to the ubiquitin-proteasome system? *Biochemical Society transactions*. 32:640-642.

Chaturvedi, R.K., and M.F. Beal. 2013. Mitochondria targeted therapeutic approaches in Parkinson's and Huntington's diseases. *Mol Cell Neurosci*. 55:101-114.

Cheetham, M.E., and A.J. Caplan. 1998. Structure, function and evolution of DnaJ: conservation and adaptation of chaperone function. *Cell Stress Chaperones*. 3:28-36.

Chen, C.H., S.L. Hwang, S.L. Howng, C.K. Chou, and Y.R. Hong. 2000. Three rat brain alternative splicing dynamin-like protein variants: interaction with the glycogen synthase kinase 3beta and action as a substrate. *Biochemical and biophysical research communications*. 268:893-898.

Chen, H., and D.C. Chan. 2009. Mitochondrial dynamics--fusion, fission, movement, and mitophagy--in neurodegenerative diseases. *Human molecular genetics*. 18:R169-176.

Chen, H., and D.C. Chan. 2010. Physiological functions of mitochondrial fusion. *Ann N Y Acad Sci*. 1201:21-25.

Chen, H., S.A. Detmer, A.J. Ewald, E.E. Griffin, S.E. Fraser, and D.C. Chan. 2003a. Mitofusins Mfn1 and Mfn2 coordinately regulate mitochondrial fusion and are essential for embryonic development. *The Journal of cell biology*. 160:189-200.

Chen, H., J.M. McCaffery, and D.C. Chan. 2007. Mitochondrial fusion protects against neurodegeneration in the cerebellum. *Cell*. 130:548-562.

Chen, P., C. Peng, J. Luff, K. Spring, D. Watters, S. Bottle, S. Furuya, and M.F. Lavin. 2003b. Oxidative stress is responsible for deficient survival and dendritogenesis in purkinje neurons from ataxia-telangiectasia mutated mutant mice. *The Journal of neuroscience : the official journal of the Society for Neuroscience*. 23:11453-11460.

Chen, Y.F., I.J. Wang, L.L. Lin, and M.S. Chen. 2011. Examining rhodopsin retention in endoplasmic reticulum and intracellular localization in vitro and in vivo by using truncated rhodopsin fragments. *Journal of cellular biochemistry*. 112:520-530.

Chernoivanenko, I.S., E.A. Matveeva, V.I. Gelfand, R.D. Goldman, and A.A. Minin. 2015. Mitochondrial membrane potential is regulated by vimentin intermediate filaments. *FASEB journal : official publication of the Federation of American Societies for Experimental Biology*. 29:820-827.

Cheung, E.C., H.M. McBride, and R.S. Slack. 2007. Mitochondrial dynamics in the regulation of neuronal cell death. *Apoptosis*. 12:979-992.

Chin, L.S., J.A. Olzmann, and L. Li. 2010. Parkin-mediated ubiquitin signalling in aggresome formation and autophagy. *Biochemical Society transactions*. 38:144-149.

Cho, B., H.M. Cho, H.J. Kim, J. Jeong, S.K. Park, E.M. Hwang, J.Y. Park, W.R. Kim, H. Kim, and W. Sun. 2014. CDK5-dependent inhibitory phosphorylation of Drp1 during neuronal maturation. *Experimental & molecular medicine*. 46:e105.

Cho, D.H., T. Nakamura, J. Fang, P. Cieplak, A. Godzik, Z. Gu, and S.A. Lipton. 2009. S-nitrosylation of Drp1 mediates beta-amyloid-related mitochondrial fission and neuronal injury. *Science*. 324:102-105.

Chu, Y., H. Dodiya, P. Aebischer, C.W. Olanow, and J.H. Kordower. 2009. Alterations in lysosomal and proteasomal markers in Parkinson's disease: relationship to alpha-synuclein inclusions. *Neurobiology of disease*. 35:385-398.

Chuang, J.Z., H. Zhou, M. Zhu, S.H. Li, X.J. Li, and C.H. Sung. 2002. Characterization of a brain-enriched chaperone, MRJ, that inhibits Huntingtin aggregation and toxicity independently. *The Journal of biological chemistry*. 277:19831-19838.

Chun, H.H., and R.A. Gatti. 2004. Ataxia-telangiectasia, an evolving phenotype. *DNA Repair (Amst)*. 3:1187-1196.

Chung, K.T., Y. Shen, and L.M. Hendershot. 2002. BAP, a mammalian BiP-associated protein, is a nucleotide exchange factor that regulates the ATPase activity of BiP. *The Journal of biological chemistry*. 277:47557-47563.

Ciechanover, A. 2006. Intracellular protein degradation: from a vague idea thru the lysosome and the ubiquitin-proteasome system and onto human diseases and drug targeting. *Hematology / the Education Program of the American Society of Hematology. American Society of Hematology. Education Program*:1-12, 505-506.

Cipolat, S., O. Martins de Brito, B. Dal Zilio, and L. Scorrano. 2004. OPA1 requires mitofusin 1 to promote mitochondrial fusion. *Proceedings of the National Academy of Sciences of the United States of America*. 101:15927-15932.

Clement, C.A., S.G. Kristensen, K. Mollgard, G.J. Pazour, B.K. Yoder, L.A. Larsen, and S.T. Christensen. 2009. The primary cilium coordinates early cardiogenesis

and hedgehog signaling in cardiomyocyte differentiation. *Journal of cell science*. 122:3070-3082.

Cleveland, D.W., K. Yamanaka, and P. Bomont. 2009. Gigaxonin controls vimentin organization through a tubulin chaperone-independent pathway. *Human molecular genetics*. 18:1384-1394.

Cochard, P., and D. Paulin. 1984. Initial expression of neurofilaments and vimentin in the central and peripheral nervous system of the mouse embryo in vivo. *The Journal of neuroscience : the official journal of the Society for Neuroscience*. 4:2080-2094.

Cogli, L., C. Progida, R. Bramato, and C. Bucci. 2013. Vimentin phosphorylation and assembly are regulated by the small GTPase Rab7a. *Biochimica et biophysica acta*. 1833:1283-1293.

Colakoglu, G., and A. Brown. 2009. Intermediate filaments exchange subunits along their length and elongate by end-to-end annealing. *The Journal of cell biology*. 185:769-777.

Collins, T.J., M.J. Berridge, P. Lipp, and M.D. Bootman. 2002. Mitochondria are morphologically and functionally heterogeneous within cells. *The EMBO journal*. 21:1616-1627.

Connell, P., C.A. Ballinger, J. Jiang, Y. Wu, L.J. Thompson, J. Hohfeld, and C. Patterson. 2001. The co-chaperone CHIP regulates protein triage decisions mediated by heat-shock proteins. *Nature cell biology*. 3:93-96.

Corbit, K.C., P. Aanstad, V. Singla, A.R. Norman, D.Y. Stainier, and J.F. Reiter. 2005. Vertebrate Smoothened functions at the primary cilium. *Nature*. 437:1018-1021.

Corbit, K.C., A.E. Shyer, W.E. Dowdle, J. Gaulden, V. Singla, M.H. Chen, P.T. Chuang, and J.F. Reiter. 2008. Kif3a constrains beta-catenin-dependent Wnt signalling through dual ciliary and non-ciliary mechanisms. *Nature cell biology*. 10:70-76.

Cossee, M., M. Schmitt, V. Campuzano, L. Reutenauer, C. Moutou, J.L. Mandel, and M. Koenig. 1997. Evolution of the Friedreich's ataxia trinucleotide repeat expansion: founder effect and premutations. *Proceedings of the National Academy of Sciences of the United States of America*. 94:7452-7457.

Costa, V., M. Giacomello, R. Hudec, R. Lopreiato, G. Ermak, D. Lim, W. Malorni, K.J. Davies, E. Carafoli, and L. Scorrano. 2010. Mitochondrial fission and cristae disruption increase the response of cell models of Huntington's disease to apoptotic stimuli. *EMBO Mol Med*. 2:490-503.

Craig, E.A., P. Huang, R. Aron, and A. Andrew. 2006. The diverse roles of J-proteins, the obligate Hsp70 co-chaperone. *Rev Physiol Biochem Pharmacol*. 156:1-21.

Craig, E.A., B.J. McCarthy, and S.C. Wadsworth. 1979. Sequence organization of two recombinant plasmids containing genes for the major heat shock-induced protein of D. melanogaster. *Cell*. 16:575-588.

Cribbs, J.T., and S. Strack. 2007. Reversible phosphorylation of Drp1 by cyclic AMP-dependent protein kinase and calcineurin regulates mitochondrial fission and cell death. *EMBO reports*. 8:939-944.

Criscuolo, C., S. Banfi, M. Orio, P. Gasparini, A. Monticelli, Scarano, F.M. Santorelli, A. Perretti, L. Santoro, and G. Michele. 2004. A novel mutation in SACS gene in a family from southern Italy. *Neurology*. 62:100-102.

Criscuolo, C., C. Procaccini, M.C. Meschini, A. Cianflone, R. Carbone, S. Doccini, D. Devos, C. Nesti, I. Vuillaume, M. Pellegrino, A. Filla, G. De Michele, G. Matarese, and F.M. Santorelli. 2015. Powerhouse failure and oxidative damage

in autosomal recessive spastic ataxia of Charlevoix-Saguenay. *Journal of neurology*. 262:2755-2763.

Criscuolo, C., F. Saccà, G. De Michele, P. Mancini, O. Combarros, J. Infante, A. Garcia, S. Banfi, A. Filla, and J. Berciano. 2005. Novel mutation of SACS gene in a Spanish family with autosomal recessive spastic ataxia. *Mov Disord*. 20:1358-1361.

Cuervo, A.M. 2004. Autophagy: many paths to the same end. *Molecular and cellular biochemistry*. 263:55-72.

Cuervo, A.M., L. Stefanis, R. Fredenburg, P.T. Lansbury, and D. Sulzer. 2004. Impaired degradation of mutant alpha-synuclein by chaperone-mediated autophagy. *Science*. 305:1292-1295.

Cuervo, A.M., E.S. Wong, and M. Martinez-Vicente. 2010. Protein degradation, aggregation, and misfolding. *Movement disorders : official journal of the Movement Disorder Society*. 25 Suppl 1:S49-54.

Cummings, C.J., M.A. Mancini, B. Antalffy, D.B. DeFranco, H.T. Orr, and H.Y. Zoghbi. 1998. Chaperone suppression of aggregation and altered subcellular proteasome localization imply protein misfolding in SCA1. *Nature genetics*. 19:148-154.

Cummings, C.J., Y. Sun, P. Opal, B. Antalffy, R. Mestril, H.T. Orr, W.H. Dillmann, and H.Y. Zoghbi. 2001. Over-expression of inducible HSP70 chaperone suppresses neuropathology and improves motor function in SCA1 mice. *Human molecular genetics*. 10:1511-1518.

Dagda, R.K., S.J. Cherra, 3rd, S.M. Kulich, A. Tandon, D. Park, and C.T. Chu. 2009. Loss of PINK1 function promotes mitophagy through effects on oxidative stress and mitochondrial fission. *The Journal of biological chemistry*. 284:13843-13855.

Davey, K.M., J.S. Parboosingh, D.R. McLeod, A. Chan, R. Casey, P. Ferreira, F.F. Snyder, P.J. Bridge, and F.P. Bernier. 2006. Mutation of DNAJC19, a human homologue of yeast inner mitochondrial membrane co-chaperones, causes DCMA syndrome, a novel autosomal recessive Barth syndrome-like condition. *Journal of medical genetics*. 43:385-393.

De Braekeleer, M., F. Giasson, J. Mathieu, M. Roy, J.P. Bouchard, and K. Morgan. 1993. Genetic epidemiology of autosomal recessive spastic ataxia of Charlevoix-Saguenay in northeastern Quebec. *Genet Epidemiol*. 10:17-25.

De Jonghe, P., I. Mersivanova, E. Nelis, J. Del Favero, J.J. Martin, C. Van Broeckhoven, O. Evgrafov, and V. Timmerman. 2001. Further evidence that neurofilament light chain gene mutations can cause Charcot-Marie-Tooth disease type 2E. *Annals of neurology*. 49:245-249.

De Vos, K.J., V.J. Allan, A.J. Grierson, and M.P. Sheetz. 2005. Mitochondrial function and actin regulate dynamin-related protein 1-dependent mitochondrial fission. *Current biology : CB*. 15:678-683.

Deacon, S.W., A.S. Serpinskaya, P.S. Vaughan, M. Lopez Fanarraga, I. Vernos, K.T. Vaughan, and V.I. Gelfand. 2003. Dynactin is required for bidirectional organelle transport. *The Journal of cell biology*. 160:297-301.

Deas, E., H. Plun-Favreau, S. Gandhi, H. Desmond, S. Kjaer, S.H. Loh, A.E. Renton, R.J. Harvey, A.J. Whitworth, L.M. Martins, A.Y. Abramov, and N.W. Wood. 2011. PINK1 cleavage at position A103 by the mitochondrial protease PARL. *Human molecular genetics*. 20:867-879.

Dehay, B., J. Bove, N. Rodriguez-Muela, C. Perier, A. Recasens, P. Boya, and M. Vila. 2010. Pathogenic lysosomal depletion in Parkinson's disease. *The Journal of*

neuroscience : the official journal of the Society for Neuroscience. 30:12535-12544.

Del Monte, F., and G. Agnetti. 2014. Protein post-translational modifications and misfolding: new concepts in heart failure. *Proteomics. Clinical applications*. 8:534-542.

Delatycki, M.B., R. Williamson, and S.M. Forrest. 2000. Friedreich ataxia: an overview. *Journal of medical genetics*. 37:1-8.

Delettre, C., G. Lenaers, J.M. Griffoin, N. Gigarel, C. Lorenzo, P. Belenguer, L. Pelloquin, J. Grosgeorge, C. Turc-Carel, E. Perret, C. Astarie-Dequeker, L. Lasquellec, B. Arnaud, B. Ducommun, J. Kaplan, and C.P. Hamel. 2000. Nuclear gene OPA1, encoding a mitochondrial dynamin-related protein, is mutated in dominant optic atrophy. *Nature genetics*. 26:207-210.

Di Donato, S., C. Gellera, and C. Mariotti. 2001. The complex clinical and genetic classification of inherited ataxias. II. Autosomal recessive ataxias. *Neurological sciences : official journal of the Italian Neurological Society and of the Italian Society of Clinical Neurophysiology*. 22:219-228.

Diamant, S., and P. Goloubinoff. 1998. Temperature-controlled activity of DnaK-DnaJ-GrpE chaperones: protein-folding arrest and recovery during and after heat shock depends on the substrate protein and the GrpE concentration. *Biochemistry*. 37:9688-9694.

Dibilio, V., F. Cavalcanti, A. Nicoletti, G. Mostile, E. Bruno, G. Annesi, P. Tarantino, M. Gagliardi, A. Gambardella, A. Quattrone, and M. Zappia. 2013. Sacsin-related spastic ataxia caused by a novel missense mutation p.Arg272His in a patient from Sicily, southern Italy. *Cerebellum*. 12:589-592.

Dice, J.F. 1990. Peptide sequences that target cytosolic proteins for lysosomal proteolysis. *Trends in biochemical sciences*. 15:305-309.

DiFiglia, M., E. Sapp, K.O. Chase, S.W. Davies, G.P. Bates, J.P. Vonsattel, and N. Aronin. 1997. Aggregation of huntingtin in neuronal intranuclear inclusions and dystrophic neurites in brain. *Science*. 277:1990-1993.

Ding, J., E. Allen, W. Wang, A. Valle, C. Wu, T. Nardine, B. Cui, J. Yi, A. Taylor, N.L. Jeon, S. Chu, Y. So, H. Vogel, R. Tolwani, W. Mobley, and Y. Yang. 2006. Gene targeting of GAN in mouse causes a toxic accumulation of microtubule-associated protein 8 and impaired retrograde axonal transport. *Human molecular genetics*. 15:1451-1463.

Dodson, M.W., and M. Guo. 2007. Pink1, Parkin, DJ-1 and mitochondrial dysfunction in Parkinson's disease. *Current opinion in neurobiology*. 17:331-337.

Dompierre, J.P., J.D. Godin, B.C. Charrin, F.P. Cordelieres, S.J. King, S. Humbert, and F. Saudou. 2007. Histone deacetylase 6 inhibition compensates for the transport deficit in Huntington's disease by increasing tubulin acetylation. *The Journal of neuroscience : the official journal of the Society for Neuroscience*. 27:3571-3583.

Doss-Pepe, E.W., E.S. Stenroos, W.G. Johnson, and K. Madura. 2003. Ataxin-3 interactions with rad23 and valosin-containing protein and its associations with ubiquitin chains and the proteasome are consistent with a role in ubiquitin-mediated proteolysis. *Molecular and cellular biology*. 23:6469-6483.

DuBoff, B., J. Gotz, and M.B. Feany. 2012. Tau promotes neurodegeneration via DRP1 mislocalization in vivo. *Neuron*. 75:618-632.

Dupre, N., J.P. Bouchard, B. Brais, and G.A. Rouleau. 2006. Hereditary ataxia, spastic paraparesis and neuropathy in the French-Canadian population. *Can J Neurol Sci*. 33:149-157.

Durrenberger, P.F., M.D. Filiou, L.B. Moran, G.J. Michael, S. Novoselov, M.E. Cheetham, P. Clark, R.K. Pearce, and M.B. Graeber. 2009. DnaJB6 is present in the core of Lewy bodies and is highly up-regulated in parkinsonian astrocytes. *Journal of neuroscience research*. 87:238-245.

Eaton, J.S., Z.P. Lin, A.C. Sartorelli, N.D. Bonawitz, and G.S. Shadel. 2007. Ataxia-telangiectasia mutated kinase regulates ribonucleotide reductase and mitochondrial homeostasis. *The Journal of clinical investigation*. 117:2723-2734.

Ebneth, A., R. Godemann, K. Stamer, S. Illenberger, B. Trinczek, and E. Mandelkow. 1998. Overexpression of tau protein inhibits kinesin-dependent trafficking of vesicles, mitochondria, and endoplasmic reticulum: implications for Alzheimer's disease. *The Journal of cell biology*. 143:777-794.

Echeverri, C.J., B.M. Paschal, K.T. Vaughan, and R.B. Vallee. 1996. Molecular characterization of the 50-kD subunit of dynactin reveals function for the complex in chromosome alignment and spindle organization during mitosis. *The Journal of cell biology*. 132:617-633.

Eckley, D.M., S.R. Gill, K.A. Melkonian, J.B. Bingham, H.V. Goodson, J.E. Heuser, and T.A. Schroer. 1999. Analysis of dynactin subcomplexes reveals a novel actin-related protein associated with the arp1 minifilament pointed end. *The Journal of cell biology*. 147:307-320.

Edvardson, S., Y. Cinnamon, A. Ta-Shma, A. Shaag, Y.I. Yim, S. Zenvirt, C. Jalas, S. Lesage, A. Brice, A. Taraboulos, K.H. Kaestner, L.E. Greene, and O. Elpeleg. 2012. A deleterious mutation in DNAJC6 encoding the neuronal-specific clathrin-uncoating co-chaperone auxilin, is associated with juvenile parkinsonism. *PloS one*. 7:e36458.

El Euch-Fayache, G., I. Lalani, R. Amouri, I. Turki, K. Ouahchi, W.Y. Hung, S. Belal, T. Siddique, and F. Hentati. 2003. Phenotypic features and genetic findings in sacsin-related autosomal recessive ataxia in Tunisia. *Arch Neurol*. 60:982-988.

Ellis, R.J. 2001. Macromolecular crowding: an important but neglected aspect of the intracellular environment. *Current opinion in structural biology*. 11:114-119.

Embirucu, E.K., M.L. Martyn, D. Schlesinger, and F. Kok. 2009. Autosomal recessive ataxias: 20 types, and counting. *Arquivos de neuro-psiquiatria*. 67:1143-1156.

Engert, J.C., P. Berube, J. Mercier, C. Dore, P. Lepage, B. Ge, J.P. Bouchard, J. Mathieu, S.B. Melancon, M. Schalling, E.S. Lander, K. Morgan, T.J. Hudson, and A. Richter. 2000. ARSACS, a spastic ataxia common in northeastern Quebec, is caused by mutations in a new gene encoding an 11.5-kb ORF. *Nature genetics*. 24:120-125.

Engert, J.C., C. Dore, J. Mercier, B. Ge, C. Betard, J.D. Rioux, C. Owen, P. Berube, K. Devon, B. Birren, S.B. Melancon, K. Morgan, T.J. Hudson, and A. Richter. 1999. Autosomal recessive spastic ataxia of Charlevoix-Saguenay (ARSACS): high-resolution physical and transcript map of the candidate region in chromosome region 13q11. *Genomics*. 62:156-164.

Estaquier, J., and D. Arnoult. 2007. Inhibiting Drp1-mediated mitochondrial fission selectively prevents the release of cytochrome c during apoptosis. *Cell death and differentiation*. 14:1086-1094.

Exner, N., B. Treske, D. Paquet, K. Holmstrom, C. Schiesling, S. Gispert, I. Carballo-Carbajal, D. Berg, H.H. Hoepken, T. Gasser, R. Kruger, K.F. Winklhofer, F. Vogel, A.S. Reichert, G. Auburger, P.J. Kahle, B. Schmid, and C. Haass. 2007. Loss-of-function of human PINK1 results in mitochondrial pathology and can be

rescued by parkin. *The Journal of neuroscience : the official journal of the Society for Neuroscience*. 27:12413-12418.

Ezaki, J., L.S. Wolfe, and E. Kominami. 1996. Specific delay in the degradation of mitochondrial ATP synthase subunit c in late infantile neuronal ceroid lipofuscinosis is derived from cellular proteolytic dysfunction rather than structural alteration of subunit c. *Journal of neurochemistry*. 67:1677-1687.

Fabunmi, R.P., W.C. Wigley, P.J. Thomas, and G.N. DeMartino. 2000. Activity and regulation of the centrosome-associated proteasome. *The Journal of biological chemistry*. 275:409-413.

Faruq, M., A. Narang, R. Kumari, R. Pandey, A. Garg, M. Behari, D. Dash, A.K. Srivastava, and M. Mukerji. 2014. Novel mutations in typical and atypical genetic loci through exome sequencing in autosomal recessive cerebellar ataxia families. *Clinical genetics*. 86:335-341.

Fearnley, J.M., and A.J. Lees. 1991. Ageing and Parkinson's disease: substantia nigra regional selectivity. *Brain : a journal of neurology*. 114 (Pt 5):2283-2301.

Fekkes, P., K.A. Shepard, and M.P. Yaffe. 2000. Gag3p, an outer membrane protein required for fission of mitochondrial tubules. *The Journal of cell biology*. 151:333-340.

Ferre, M., P. Amati-Bonneau, Y. Tourmen, Y. Malthiery, and P. Reynier. 2005. eOPA1: an online database for OPA1 mutations. *Hum Mutat*. 25:423-428.

Fetalvero, K.M., Y. Yu, M. Goetschkes, G. Liang, R.A. Valdez, T. Gould, E. Triantafellow, S. Bergling, J. Loureiro, J. Eash, V. Lin, J.A. Porter, P.M. Finan, K. Walsh, Y. Yang, X. Mao, and L.O. Murphy. 2013. Defective autophagy and mTORC1 signaling in myotubularin null mice. *Molecular and cellular biology*. 33:98-110.

Figlewicz, D.A., A. Krizus, M.G. Martinoli, V. Meininger, M. Dib, G.A. Rouleau, and J.P. Julien. 1994. Variants of the heavy neurofilament subunit are associated with the development of amyotrophic lateral sclerosis. *Human molecular genetics*. 3:1757-1761.

Figueroa-Romero, C., J.A. Iniguez-Lluhi, J. Stadler, C.R. Chang, D. Arnoult, P.J. Keller, Y. Hong, C. Blackstone, and E.L. Feldman. 2009. SUMOylation of the mitochondrial fission protein Drp1 occurs at multiple nonconsensus sites within the B domain and is linked to its activity cycle. *FASEB journal : official publication of the Federation of American Societies for Experimental Biology*. 23:3917-3927.

Filosto, M., M. Scarpelli, M.S. Cotelli, V. Vielmi, A. Todeschini, V. Gregorelli, P. Tonin, G. Tomelleri, and A. Padovani. 2011. The role of mitochondria in neurodegenerative diseases. *Journal of neurology*. 258:1763-1774.

Finley, D. 2009. Recognition and processing of ubiquitin-protein conjugates by the proteasome. *Annual review of biochemistry*. 78:477-513.

Flitney, E.W., E.R. Kuczmarski, S.A. Adam, and R.D. Goldman. 2009. Insights into the mechanical properties of epithelial cells: the effects of shear stress on the assembly and remodeling of keratin intermediate filaments. *FASEB journal : official publication of the Federation of American Societies for Experimental Biology*. 23:2110-2119.

Fogel, B.L., and S. Perlman. 2007. Clinical features and molecular genetics of autosomal recessive cerebellar ataxias. *The Lancet. Neurology*. 6:245-257.

Forno, L.S., L.A. Sternberger, N.H. Sternberger, A.M. Strefling, K. Swanson, and L.F. Eng. 1986. Reaction of Lewy bodies with antibodies to phosphorylated and non-phosphorylated neurofilaments. *Neuroscience letters*. 64:253-258.

Fortun, J., W.A. Dunn, Jr., S. Joy, J. Li, and L. Notterpek. 2003. Emerging role for autophagy in the removal of aggresomes in Schwann cells. *The Journal of neuroscience : the official journal of the Society for Neuroscience*. 23:10672-10680.

Frank, S., B. Gaume, E.S. Bergmann-Leitner, W.W. Leitner, E.G. Robert, F. Catez, C.L. Smith, and R.J. Youle. 2001. The role of dynamin-related protein 1, a mediator of mitochondrial fission, in apoptosis. *Dev Cell*. 1:515-525.

Fuchs, E., and D.W. Cleveland. 1998. A structural scaffolding of intermediate filaments in health and disease. *Science*. 279:514-519.

Gandre-Babbe, S., and A.M. van der Bliek. 2008. The novel tail-anchored membrane protein Mff controls mitochondrial and peroxisomal fission in mammalian cells. *Molecular biology of the cell*. 19:2402-2412.

Gao, X.C., C.J. Zhou, Z.R. Zhou, Y.H. Zhang, X.M. Zheng, A.X. Song, and H.Y. Hu. 2011. Co-chaperone HSJ1a dually regulates the proteasomal degradation of ataxin-3. *PloS one*. 6:e19763.

Gao, Y., and E. Sztul. 2001. A novel interaction of the Golgi complex with the vimentin intermediate filament cytoskeleton. *The Journal of cell biology*. 152:877-894.

Gao, Y.S., A. Vrielink, R. MacKenzie, and E. Sztul. 2002. A novel type of regulation of the vimentin intermediate filament cytoskeleton by a Golgi protein. *European journal of cell biology*. 81:391-401.

Garcia-Cardena, G., R. Fan, V. Shah, R. Sorrentino, G. Cirino, A. Papapetropoulos, and W.C. Sessa. 1998. Dynamic activation of endothelial nitric oxide synthase by Hsp90. *Nature*. 392:821-824.

Garcia-Mata, R., Z. Bebok, E.J. Sorscher, and E.S. Sztul. 1999. Characterization and dynamics of aggresome formation by a cytosolic GFP-chimera. *The Journal of cell biology*. 146:1239-1254.

Garcia-Mata, R., Y.S. Gao, and E. Sztul. 2002. Hassles with taking out the garbage: aggravating aggresomes. *Traffic*. 3:388-396.

Gegg, M.E., J.M. Cooper, K.Y. Chau, M. Rojo, A.H. Schapira, and J.W. Taanman. 2010. Mitofusin 1 and mitofusin 2 are ubiquitinated in a PINK1/parkin-dependent manner upon induction of mitophagy. *Human molecular genetics*. 19:4861-4870.

Gegg, M.E., and A.H. Schapira. 2011. PINK1-parkin-dependent mitophagy involves ubiquitination of mitofusins 1 and 2: Implications for Parkinson disease pathogenesis. *Autophagy*. 7:243-245.

Geisler, S., K.M. Holmstrom, A. Treis, D. Skujat, S.S. Weber, F.C. Fiesel, P.J. Kahle, and W. Springer. 2010. The PINK1/Parkin-mediated mitophagy is compromised by PD-associated mutations. *Autophagy*. 6:871-878.

Georgiou, D.M., J. Zidar, M. Korosec, L.T. Middleton, T. Kyriakides, and K. Christodoulou. 2002. A novel NF-L mutation Pro22Ser is associated with CMT2 in a large Slovenian family. *Neurogenetics*. 4:93-96.

Gess, B., M. Auer-Grumbach, A. Schirmacher, T. Strom, M. Zitzelsberger, S. Rudnik-Schoneborn, D. Rohr, H. Halfter, P. Young, and J. Senderek. 2014. HSJ1-related hereditary neuropathies: novel mutations and extended clinical spectrum. *Neurology*. 83:1726-1732.

Gibb, B.J., J.P. Brion, J. Brownlees, B.H. Anderton, and C.C. Miller. 1998. Neuropathological abnormalities in transgenic mice harbouring a phosphorylation mutant neurofilament transgene. *Journal of neurochemistry*. 70:492-500.

Gill, S.R., T.A. Schroer, I. Szilak, E.R. Steuer, M.P. Sheetz, and D.W. Cleveland. 1991. Dynactin, a conserved, ubiquitously expressed component of an activator of vesicle motility mediated by cytoplasmic dynein. *The Journal of cell biology*. 115:1639-1650.

Gillis, J., S. Schipper-Krom, K. Juenemann, A. Gruber, S. Coolen, R. van den Nieuwendijk, H. van Veen, H. Overkleeft, J. Goedhart, H.H. Kampinga, and E.A. Reits. 2013. The DNAJB6 and DNAJB8 protein chaperones prevent intracellular aggregation of polyglutamine peptides. *The Journal of biological chemistry*. 288:17225-17237.

Girard, M., R. Lariviere, D.A. Parfitt, E.C. Deane, R. Gaudet, N. Nossova, F. Blondeau, G. Prenosil, E.G. Vermeulen, M.R. Duchen, A. Richter, E.A. Shoubridge, K. Gehring, R.A. McKinney, B. Brais, J.P. Chapple, and P.S. McPherson. 2012. Mitochondrial dysfunction and Purkinje cell loss in autosomal recessive spastic ataxia of Charlevoix-Saguenay (ARSACS). *Proceedings of the National Academy of Sciences of the United States of America*. 109:1661-1666.

Glater, E.E., L.J. Megeath, R.S. Stowers, and T.L. Schwarz. 2006. Axonal transport of mitochondria requires milton to recruit kinesin heavy chain and is light chain independent. *The Journal of cell biology*. 173:545-557.

Glenner, G.G., and C.W. Wong. 1984. Alzheimer's disease: initial report of the purification and characterization of a novel cerebrovascular amyloid protein. *Biochemical and biophysical research communications*. 120:885-890.

Goldberg, A.L. 2003. Protein degradation and protection against misfolded or damaged proteins. *Nature*. 426:895-899.

Gomes, L.C., and L. Scorrano. 2008. High levels of Fis1, a pro-fission mitochondrial protein, trigger autophagy. *Biochimica et biophysica acta*. 1777:860-866.

Gomes, L.C., and L. Scorrano. 2013. Mitochondrial morphology in mitophagy and macroautophagy. *Biochimica et biophysica acta*. 1833:205-212.

Gomez-Sanchez, R., M.E. Gegg, J.M. Bravo-San Pedro, M. Niso-Santano, L. Alvarez-Erviti, E. Pizarro-Estrella, Y. Gutierrez-Martin, A. Alvarez-Barrientos, J.M. Fuentes, R.A. Gonzalez-Polo, and A.H. Schapira. 2014. Mitochondrial impairment increases FL-PINK1 levels by calcium-dependent gene expression. *Neurobiology of disease*. 62:426-440.

Gonatas, N.K., J.O. Gonatas, and A. Stieber. 1998. The involvement of the Golgi apparatus in the pathogenesis of amyotrophic lateral sclerosis, Alzheimer's disease, and ricin intoxication. *Histochemistry and cell biology*. 109:591-600.

Gordon, N. 2004. Giant axonal neuropathy. *Developmental medicine and child neurology*. 46:717-719.

Grabbe, C., and I. Dikic. 2009. Functional roles of ubiquitin-like domain (ULD) and ubiquitin-binding domain (UBD) containing proteins. *Chemical reviews*. 109:1481-1494.

Greene, A.W., K. Grenier, M.A. Aguileta, S. Muise, R. Farazifard, M.E. Haque, H.M. McBride, D.S. Park, and E.A. Fon. 2012. Mitochondrial processing peptidase regulates PINK1 processing, import and Parkin recruitment. *EMBO reports*. 13:378-385.

Greer, P.L., R. Hanayama, B.L. Bloodgood, A.R. Mardinly, D.M. Lipton, S.W. Flavell, T.K. Kim, E.C. Griffith, Z. Waldon, R. Maehr, H.L. Ploegh, S. Chowdhury, P.F. Worley, J. Steen, and M.E. Greenberg. 2010. The Angelman Syndrome protein Ube3A regulates synapse development by ubiquitinating arc. *Cell*. 140:704-716.

Gregianin, E., G. Vazza, E. Scaramel, F. Boaretto, A. Vettori, E. Leonardi, S.C. Tosatto, R. Manara, E. Pegoraro, and M.L. Mostacciuolo. 2013. A novel SACS mutation

results in non-ataxic spastic paraplegia and peripheral neuropathy. *European journal of neurology*. 20:1486-1491.

Grieco, G.S., A. Malandrini, G. Comanducci, Leuzzi, M. Valoppi, A. Tessa, S. Palmeri, L. Benedetti, A. Pierallini, and S. Gambelli. 2004. Novel SACS mutations in autosomal recessive spastic ataxia of Charlevoix-Saguenay type. *Neurology*. 62:103-106.

Griffin, E.E., J. Graumann, and D.C. Chan. 2005. The WD40 protein Caf4p is a component of the mitochondrial fission machinery and recruits Dnm1p to mitochondria. *The Journal of cell biology*. 170:237-248.

Grundke-Iqbal, I., K. Iqbal, M. Quinlan, Y.C. Tung, M.S. Zaidi, and H.M. Wisniewski. 1986. Microtubule-associated protein tau. A component of Alzheimer paired helical filaments. *The Journal of biological chemistry*. 261:6084-6089.

Grunewald, A., L. Voges, A. Rakovic, M. Kasten, H. Vandebona, C. Hemmelmann, K. Lohmann, S. Orolicki, A. Ramirez, A.H. Schapira, P.P. Pramstaller, C.M. Sue, and C. Klein. 2010. Mutant Parkin impairs mitochondrial function and morphology in human fibroblasts. *PloS one*. 5:e12962.

Grynberg, M., H. Erlandsen, and A. Godzik. 2003. HEPN: a common domain in bacterial drug resistance and human neurodegenerative proteins. *Trends in biochemical sciences*. 28:224-226.

Guernsey, D.L., M.P. Dubé, H. Jiang, G. Asselin, S. Blowers, S. Evans, M. Ferguson, C. Macgillivray, M. Matsuoka, M. Nightingale, A. Rideout, M. Delatycki, A. Orr, M. Ludman, J. Dooley, C. Riddell, and M.E. Samuels. 2010. Novel mutations in the sacsin gene in ataxia patients from Maritime Canada. *Journal of the Neurological Sciences*. 288:79-87.

Guillery, O., F. Malka, P. Frachon, D. Milea, M. Rojo, and A. Lombes. 2008. Modulation of mitochondrial morphology by bioenergetics defects in primary human fibroblasts. *Neuromuscular disorders : NMD*. 18:319-330.

Gunawardena, S., and L.S. Goldstein. 2005. Polyglutamine diseases and transport problems: deadly traffic jams on neuronal highways. *Archives of neurology*. 62:46-51.

Guo, C., K.L. Hildick, J. Luo, L. Dearden, K.A. Wilkinson, and J.M. Henley. 2013a. SENP3-mediated deSUMOylation of dynamin-related protein 1 promotes cell death following ischaemia. *The EMBO journal*. 32:1514-1528.

Guo, X., M.H. Disatnik, M. Monbureau, M. Shamloo, D. Mochly-Rosen, and X. Qi. 2013b. Inhibition of mitochondrial fragmentation diminishes Huntington's disease-associated neurodegeneration. *The Journal of clinical investigation*. 123:5371-5388.

Guo, X., G.T. Macleod, A. Wellington, F. Hu, S. Panchumarthi, M. Schoenfield, L. Marin, M.P. Charlton, H.L. Atwood, and K.E. Zinsmaier. 2005. The GTPase dMiro is required for axonal transport of mitochondria to Drosophila synapses. *Neuron*. 47:379-393.

H'mida-Ben Brahim, D., A. M'zahem, M. Assoum, Y. Bouhlal, F. Fattori, M. Anheim, L. Ali-Pacha, F. Ferrat, M. Chaouch, C. Lagier-Tourenne, N. Drouot, C. Thibaut, T. Benhassine, Y. Sifi, D. Stoppa-Lyonnet, K. N'Guyen, J. Poujet, A. Hamri, F. Hentati, R. Amouri, F.M. Santorelli, M. Tazir, and M. Koenig. 2011. Molecular diagnosis of known recessive ataxias by homozygosity mapping with SNP arrays. *J Neurol*. 258:56-67.

Haga, R., Y. Miki, Y. Funamizu, T. Kon, C. Suzuki, T. Ueno, H. Nishijima, A. Arai, M. Tomiyama, H. Shimazaki, Y. Takiyama, and M. Baba. 2012. Novel compound

heterozygous mutations of the SACS gene in autosomal recessive spastic ataxia of Charlevoix-Saguenay. *Clin Neurol Neurosurg*. 114:746-747.

Hageman, J. 2008. The human HSP70/HSP40 chaperone family : a study on its capacity to combat proteotoxic stres. *In* Faculty of Medical Sciences. Vol. PhD. University of Groningen, Groningen. 188.

Hageman, J., and H.H. Kampinga. 2009. Computational analysis of the human HSPH/HSPA/DNAJ family and cloning of a human HSPH/HSPA/DNAJ expression library. *Cell Stress Chaperones*. 14:1-21.

Hageman, J., M.A. van Waarde, A. Zylicz, D. Walerych, and H.H. Kampinga. 2011. The diverse members of the mammalian HSP70 machine show distinct chaperone-like activities. *The Biochemical journal*. 435:127-142.

Haggarty, S.J., K.M. Koeller, J.C. Wong, C.M. Grozinger, and S.L. Schreiber. 2003. Domain-selective small-molecule inhibitor of histone deacetylase 6 (HDAC6)-mediated tubulin deacetylation. *Proceedings of the National Academy of Sciences of the United States of America*. 100:4389-4394.

Hailey, D.W., A.S. Rambold, P. Satpute-Krishnan, K. Mitra, R. Sougrat, P.K. Kim, and J. Lippincott-Schwartz. 2010. Mitochondria supply membranes for autophagosome biogenesis during starvation. *Cell*. 141:656-667.

Hainzl, O., M.C. Lapina, J. Buchner, and K. Richter. 2009. The charged linker region is an important regulator of Hsp90 function. *The Journal of biological chemistry*. 284:22559-22567.

Hales, K.G., and M.T. Fuller. 1997. Developmentally regulated mitochondrial fusion mediated by a conserved, novel, predicted GTPase. *Cell*. 90:121-129.

Hall, J. 2005. The Ataxia-telangiectasia mutated gene and breast cancer: gene expression profiles and sequence variants. *Cancer Lett*. 227:105-114.

Hammer, M.B., G. Eleuch-Fayache, J.R. Gibbs, S.K. Arepalli, S.B. Chong, C. Sassi, Y. Bouhlal, F. Hentati, R. Amouri, and A.B. Singleton. 2013. Exome sequencing: an efficient diagnostic tool for complex neurodegenerative disorders. *European journal of neurology*. 20:486-492.

Han, X.J., Y.F. Lu, S.A. Li, T. Kaitsuka, Y. Sato, K. Tomizawa, A.C. Nairn, K. Takei, H. Matsui, and M. Matsushita. 2008. CaM kinase I alpha-induced phosphorylation of Drp1 regulates mitochondrial morphology. *The Journal of cell biology*. 182:573-585.

Hara, K., O. Onodera, M. Endo, H. Kondo, H. Shiota, K. Miki, N. Tanimoto, T. Kimura, and M. Nishizawa. 2005. Sacsin-related autosomal recessive ataxia without prominent retinal myelinated fibers in Japan. *Movement disorders : official journal of the Movement Disorder Society*. 20:380-382.

Hara, K., J. Shimbo, H. Nozaki, K. Kikugawa, O. Onodera, and M. Nishizawa. 2007. Sacsin-related ataxia with neither retinal hypermyelination nor spasticity. *Mov Disord*. 22:1362-1363.

Harada, M., S. Sakisaka, K. Terada, R. Kimura, T. Kawaguchi, H. Koga, M. Kim, E. Taniguchi, S. Hanada, T. Suganuma, K. Furuta, T. Sugiyama, and M. Sata. 2001. A mutation of the Wilson disease protein, ATP7B, is degraded in the proteasomes and forms protein aggregates. *Gastroenterology*. 120:967-974.

Harder, Z., R. Zunino, and H. McBride. 2004. Sumo1 conjugates mitochondrial substrates and participates in mitochondrial fission. *Current biology : CB*. 14:340-345.

Harding, A.E. 1981. Friedreich's ataxia: a clinical and genetic study of 90 families with an analysis of early diagnostic criteria and intrafamilial clustering of clinical features. *Brain : a journal of neurology*. 104:589-620.

Harms, M.B., R.B. Sommerville, P. Allred, S. Bell, D. Ma, P. Cooper, G. Lopate, A. Pestronk, C.C. Weihl, and R.H. Baloh. 2012. Exome sequencing reveals DNAJB6 mutations in dominantly-inherited myopathy. *Annals of neurology*. 71:407-416.

Hartl, F.U., A. Bracher, and M. Hayer-Hartl. 2011. Molecular chaperones in protein folding and proteostasis. *Nature*. 475:324-332.

Hartl, F.U., and M. Hayer-Hartl. 2002. Molecular chaperones in the cytosol: from nascent chain to folded protein. *Science*. 295:1852-1858.

Hartl, F.U., and J. Martin. 1995. Molecular chaperones in cellular protein folding. *Current opinion in structural biology*. 5:92-102.

Hatch, A.L., P.S. Gurel, and H.N. Higgs. 2014. Novel roles for actin in mitochondrial fission. *Journal of cell science*. 127:4549-4560.

Hay, N., and N. Sonenberg. 2004. Upstream and downstream of mTOR. *Genes & development*. 18:1926-1945.

Hayashi-Nishino, M., N. Fujita, T. Noda, A. Yamaguchi, T. Yoshimori, and A. Yamamoto. 2009. A subdomain of the endoplasmic reticulum forms a cradle for autophagosome formation. *Nature cell biology*. 11:1433-1437.

He, C.Z., and A.P. Hays. 2004. Expression of peripherin in ubiquinated inclusions of amyotrophic lateral sclerosis. *Journal of the neurological sciences*. 217:47-54.

Hedera, P., D. Alvarado, A. Beydoun, and J.K. Fink. 2002. Novel mental retardation-epilepsy syndrome linked to Xp21.1-p11.4. *Annals of neurology*. 51:45-50.

Hendershot, L.M. 2004. The ER function BiP is a master regulator of ER function. *Mt Sinai J Med*. 71:289-297.

Henell, F., A. Berkenstam, J. Ahlberg, and H. Glaumann. 1987. Degradation of short- and long-lived proteins in perfused liver and in isolated autophagic vacuoles--lysosomes. *Experimental and molecular pathology*. 46:1-14.

Hennessy, F., A. Boshoff, and G.L. Blatch. 2005. Rational mutagenesis of a 40 kDa heat shock protein from Agrobacterium tumefaciens identifies amino acid residues critical to its in vivo function. *The international journal of biochemistry & cell biology*. 37:177-191.

Hermann, G.J., J.W. Thatcher, J.P. Mills, K.G. Hales, M.T. Fuller, J. Nunnari, and J.M. Shaw. 1998. Mitochondrial fusion in yeast requires the transmembrane GTPase Fzo1p. *The Journal of cell biology*. 143:359-373.

Herrmann, H., S.V. Strelkov, P. Burkhard, and U. Aebi. 2009. Intermediate filaments: primary determinants of cell architecture and plasticity. *The Journal of clinical investigation*. 119:1772-1783.

Hershko, A., and A. Ciechanover. 1998. The ubiquitin system. *Annual review of biochemistry*. 67:425-479.

Hinshaw, J.E. 2000. Dynamin and its role in membrane fission. *Annual review of cell and developmental biology*. 16:483-519.

Hoche, F., K. Seidel, M. Theis, S. Vlaho, R. Schubert, S. Zielen, and M. Kieslich. 2012. Neurodegeneration in ataxia telangiectasia: what is new? What is evident? *Neuropediatrics*. 43:119-129.

Hoey, D.A., M.E. Downs, and C.R. Jacobs. 2012. The mechanics of the primary cilium: an intricate structure with complex function. *Journal of biomechanics*. 45:17-26.

Hollenbeck, P.J., and W.M. Saxton. 2005. The axonal transport of mitochondria. *Journal of cell science*. 118:5411-5419.

Holt, S.E., D.L. Aisner, J. Baur, V.M. Tesmer, M. Dy, M. Ouellette, J.B. Trager, G.B. Morin, D.O. Toft, J.W. Shay, W.E. Wright, and M.A. White. 1999. Functional

requirement of p23 and Hsp90 in telomerase complexes. *Genes & development*. 13:817-826.

Hoppins, S., L. Lackner, and J. Nunnari. 2007. The machines that divide and fuse mitochondria. *Annual review of biochemistry*. 76:751-780.

Howarth, J.L., S. Kelly, M.P. Keasey, C.P. Glover, Y.B. Lee, K. Mitrophanous, J.P. Chapple, J.M. Gallo, M.E. Cheetham, and J.B. Uney. 2007. Hsp40 molecules that target to the ubiquitin-proteasome system decrease inclusion formation in models of polyglutamine disease. *Molecular therapy : the journal of the American Society of Gene Therapy*. 15:1100-1105.

Hoyt, C.S. 1980. Autosomal dominant optic atrophy. A spectrum of disability. *Ophthalmology*. 87:245-251.

Hroudova, J., N. Singh, and Z. Fisar. 2014. Mitochondrial dysfunctions in neurodegenerative diseases: relevance to Alzheimer's disease. *BioMed research international*. 2014:175062.

Huber, G., and A. Matus. 1984. Immunocytochemical localization of microtubule-associated protein 1 in rat cerebellum using monoclonal antibodies. *The Journal of cell biology*. 98:777-781.

Hundley, H.A., W. Walter, S. Bairstow, and E.A. Craig. 2005. Human Mpp11 J protein: ribosome-tethered molecular chaperones are ubiquitous. *Science*. 308:1032-1034.

Hurle, M.R., L.R. Helms, L. Li, W. Chan, and R. Wetzel. 1994. A role for destabilizing amino acid replacements in light-chain amyloidosis. *Proceedings of the National Academy of Sciences of the United States of America*. 91:5446-5450.

Hwang, R.D., L. Wiemerslage, C.J. LaBreck, M. Khan, K. Kannan, X. Wang, X. Zhu, D. Lee, and Y.W. Fridell. 2014. The neuroprotective effect of human uncoupling protein 2 (hUCP2) requires cAMP-dependent protein kinase in a toxin model of Parkinson's disease. *Neurobiology of disease*. 69:180-191.

Inagaki, M., Y. Nishi, K. Nishizawa, M. Matsuyama, and C. Sato. 1987. Site-specific phosphorylation induces disassembly of vimentin filaments in vitro. *Nature*. 328:649-652.

Ingerman, E., E.M. Perkins, M. Marino, J.A. Mears, J.M. McCaffery, J.E. Hinshaw, and J. Nunnari. 2005. Dnm1 forms spirals that are structurally tailored to fit mitochondria. *The Journal of cell biology*. 170:1021-1027.

Ishihara, N., M. Nomura, A. Jofuku, H. Kato, S.O. Suzuki, K. Masuda, H. Otera, Y. Nakanishi, I. Nonaka, Y. Goto, N. Taguchi, H. Morinaga, M. Maeda, R. Takayanagi, S. Yokota, and K. Mihara. 2009. Mitochondrial fission factor Drp1 is essential for embryonic development and synapse formation in mice. *Nature cell biology*. 11:958-966.

Itoh, K., K. Nakamura, M. Iijima, and H. Sesaki. 2013. Mitochondrial dynamics in neurodegeneration. *Trends in cell biology*. 23:64-71.

Ivaska, J., H.M. Pallari, J. Nevo, and J.E. Eriksson. 2007. Novel functions of vimentin in cell adhesion, migration, and signaling. *Experimental cell research*. 313:2050-2062.

Iwaki, T., A. Iwaki, J. Tateishi, Y. Sakaki, and J.E. Goldman. 1993. Alpha B-crystallin and 27-kd heat shock protein are regulated by stress conditions in the central nervous system and accumulate in Rosenthal fibers. *The American journal of pathology*. 143:487-495.

Iwaki, T., A. Kume-Iwaki, R.K. Liem, and J.E. Goldman. 1989. Alpha B-crystallin is expressed in non-lenticular tissues and accumulates in Alexander's disease brain. *Cell*. 57:71-78.

Iwata, A., J.C. Christianson, M. Bucci, L.M. Ellerby, N. Nukina, L.S. Forno, and R.R. Kopito. 2005a. Increased susceptibility of cytoplasmic over nuclear polyglutamine aggregates to autophagic degradation. *Proceedings of the National Academy of Sciences of the United States of America*. 102:13135-13140.

Iwata, A., B.E. Riley, J.A. Johnston, and R.R. Kopito. 2005b. HDAC6 and microtubules are required for autophagic degradation of aggregated huntingtin. *The Journal of biological chemistry*. 280:40282-40292.

Jana, N.R. 2012. Understanding the pathogenesis of Angelman syndrome through animal models. *Neural Plast*. 2012:710943.

Jayadev, S., and T.D. Bird. 2013. Hereditary ataxias: overview. *Genetics in medicine : official journal of the American College of Medical Genetics*. 15:673-683.

Jennings, J.J., Jr., J.H. Zhu, Y. Rbaibi, X. Luo, C.T. Chu, and K. Kiselyov. 2006. Mitochondrial aberrations in mucolipidosis Type IV. *The Journal of biological chemistry*. 281:39041-39050.

Jin, S.M., M. Lazarou, C. Wang, L.A. Kane, D.P. Narendra, and R.J. Youle. 2010. Mitochondrial membrane potential regulates PINK1 import and proteolytic destabilization by PARL. *The Journal of cell biology*. 191:933-942.

Johnston, J.A., M.E. Illing, and R.R. Kopito. 2002. Cytoplasmic dynein/dynactin mediates the assembly of aggresomes. *Cell motility and the cytoskeleton*. 53:26-38.

Johnston, J.A., C.L. Ward, and R.R. Kopito. 1998. Aggresomes: a cellular response to misfolded proteins. *The Journal of cell biology*. 143:1883-1898.

Jordanova, A., P. De Jonghe, C.F. Boerkoel, H. Takashima, E. De Vriendt, C. Ceuterick, J.J. Martin, I.J. Butler, P. Mancias, S. Papasozomenos, D. Terespolsky, L. Potocki, C.W. Brown, M. Shy, D.A. Rita, I. Tournev, I. Kremensky, J.R. Lupski, and V. Timmerman. 2003. Mutations in the neurofilament light chain gene (NEFL) cause early onset severe Charcot-Marie-Tooth disease. *Brain : a journal of neurology*. 126:590-597.

Juenemann, K., A. Wiemhoefer, and E.A. Reits. 2015. Detection of ubiquitinated huntingtin species in intracellular aggregates. *Frontiers in molecular neuroscience*. 8:1.

Jung, C., C.M. Higgins, and Z. Xu. 2000. Measuring the quantity and activity of mitochondrial electron transport chain complexes in tissues of central nervous system using blue native polyacrylamide gel electrophoresis. *Analytical biochemistry*. 286:214-223.

Junn, E., S.S. Lee, U.T. Suhr, and M.M. Mouradian. 2002. Parkin accumulation in aggresomes due to proteasome impairment. *The Journal of biological chemistry*. 277:47870-47877.

Kabeya, Y., N. Mizushima, T. Ueno, A. Yamamoto, T. Kirisako, T. Noda, E. Kominami, Y. Ohsumi, and T. Yoshimori. 2000. LC3, a mammalian homologue of yeast Apg8p, is localized in autophagosome membranes after processing. *The EMBO journal*. 19:5720-5728.

Kageyama, Y., M. Hoshijima, K. Seo, D. Bedja, P. Sysa-Shah, S.A. Andrabi, W. Chen, A. Hoke, V.L. Dawson, T.M. Dawson, K. Gabrielson, D.A. Kass, M. Iijima, and H. Sesaki. 2014. Parkin-independent mitophagy requires Drp1 and maintains the integrity of mammalian heart and brain. *The EMBO journal*. 33:2798-2813.

Kalia, S.K., L.V. Kalia, and P.J. McLean. 2010. Molecular chaperones as rational drug targets for Parkinson's disease therapeutics. *CNS & neurological disorders drug targets*. 9:741-753.

Kamada, S., S. Okawa, T. Imota, M. Sugawara, and I. Toyoshima. 2008. Autosomal recessive spastic ataxia of Charlevoix-Saguenay (ARSACS): novel compound heterozygous mutations in the SACS gene. *Journal of neurology*. 255:803-806.

Kamionka, M., and J. Feigon. 2004. Structure of the XPC binding domain of hHR23A reveals hydrophobic patches for protein interaction. *Protein Sci*. 13:2370-2377.

Kampinga, H.H., and E.A. Craig. 2010. The HSP70 chaperone machinery: J proteins as drivers of functional specificity. *Nature reviews. Molecular cell biology*. 11:579-592.

Kampinga, H.H., J. Hageman, M.J. Vos, H. Kubota, R.M. Tanguay, E.A. Bruford, M.E. Cheetham, B. Chen, and L.E. Hightower. 2009. Guidelines for the nomenclature of the human heat shock proteins. *Cell Stress Chaperones*. 14:105-111.

Kanazawa, T., M.D. Zappaterra, A. Hasegawa, A.P. Wright, E.D. Newman-Smith, K.F. Buttle, K. McDonald, C.A. Mannella, and A.M. van der Bliek. 2008. The C. elegans Opa1 homologue EAT-3 is essential for resistance to free radicals. *PLoS genetics*. 4:e1000022.

Kang-Decker, N., S. Cao, S. Chatterjee, J. Yao, L.J. Egan, D. Semela, D. Mukhopadhyay, and V. Shah. 2007. Nitric oxide promotes endothelial cell survival signaling through S-nitrosylation and activation of dynamin-2. *Journal of cell science*. 120:492-501.

Kaplan, M.P., S.S. Chin, K.H. Fliegner, and R.K. Liem. 1990. Alpha-internexin, a novel neuronal intermediate filament protein, precedes the low molecular weight neurofilament protein (NF-L) in the developing rat brain. *The Journal of neuroscience : the official journal of the Society for Neuroscience*. 10:2735-2748.

Karbowski, M., A. Neutzner, and R.J. Youle. 2007. The mitochondrial E3 ubiquitin ligase MARCH5 is required for Drp1 dependent mitochondrial division. *The Journal of cell biology*. 178:71-84.

Karbowski, M., J.H. Spodnik, M. Teranishi, M. Wozniak, Y. Nishizawa, J. Usukura, and T. Wakabayashi. 2001. Opposite effects of microtubule-stabilizing and microtubule-destabilizing drugs on biogenesis of mitochondria in mammalian cells. *Journal of cell science*. 114:281-291.

Kaushal, S., and H.G. Khorana. 1994. Structure and function in rhodopsin. 7. Point mutations associated with autosomal dominant retinitis pigmentosa. *Biochemistry*. 33:6121-6128.

Kaushik, S., and A.M. Cuervo. 2012. Chaperone-mediated autophagy: a unique way to enter the lysosome world. *Trends in cell biology*. 22:407-417.

Kegel, K.B., M. Kim, E. Sapp, C. McIntyre, J.G. Castano, N. Aronin, and M. DiFiglia. 2000. Huntingtin expression stimulates endosomal-lysosomal activity, endosome tubulation, and autophagy. *The Journal of neuroscience : the official journal of the Society for Neuroscience*. 20:7268-7278.

Keller, J.N., K.B. Hanni, and W.R. Markesbery. 2000. Impaired proteasome function in Alzheimer's disease. *Journal of neurochemistry*. 75:436-439.

Kelley, W.L. 1998. The J-domain family and the recruitment of chaperone power. *Trends in biochemical sciences*. 23:222-227.

Kenwood, B.M., J.L. Weaver, A. Bajwa, I.K. Poon, F.L. Byrne, B.A. Murrow, J.A. Calderone, L. Huang, A.S. Divakaruni, J.L. Tomsig, K. Okabe, R.H. Lo, G. Cameron Coleman, L. Columbus, Z. Yan, J.J. Saucerman, J.S. Smith, J.W. Holmes, K.R. Lynch, K.S. Ravichandran, S. Uchiyama, W.L. Santos, G.W. Rogers, M.D. Okusa, D.A. Bayliss, and K.L. Hoehn. 2014. Identification of a

novel mitochondrial uncoupler that does not depolarize the plasma membrane. *Molecular metabolism*. 3:114-123.

Khalil, B., N. El Fissi, A. Aouane, M.J. Cabirol-Pol, T. Rival, and J.C. Lievens. 2015. PINK1-induced mitophagy promotes neuroprotection in Huntington's disease. *Cell death & disease*. 6:e1617.

Kholmukhamedov, A., J.M. Schwartz, and J.J. Lemasters. 2013. Isolated mitochondria infusion mitigates ischemia-reperfusion injury of the liver in rats: mitotracker probes and mitochondrial membrane potential. *Shock*. 39:543.

Kim, E.K., K.B. Kwon, M.J. Han, M.Y. Song, J.H. Lee, N. Lv, S.O. Ka, S.R. Yeom, Y.D. Kwon, D.G. Ryu, K.S. Kim, J.W. Park, R. Park, and B.H. Park. 2007. Coptidis rhizoma extract protects against cytokine-induced death of pancreatic beta-cells through suppression of NF-kappaB activation. *Experimental & molecular medicine*. 39:149-159.

Kim, J., J.P. Moody, C.K. Edgerly, O.L. Bordiuk, K. Cormier, K. Smith, M.F. Beal, and R.J. Ferrante. 2010a. Mitochondrial loss, dysfunction and altered dynamics in Huntington's disease. *Human molecular genetics*. 19:3919-3935.

Kim, J.S., C.H. Lee, and P.A. Coulombe. 2010b. Modeling the self-organization property of keratin intermediate filaments. *Biophysical journal*. 99:2748-2756.

Kim, S., and L. Tsiokas. 2011. Cilia and cell cycle re-entry: more than a coincidence. *Cell cycle*. 10:2683-2690.

Kimura, S., T. Noda, and T. Yoshimori. 2008. Dynein-dependent movement of autophagosomes mediates efficient encounters with lysosomes. *Cell Struct Funct*. 33:109-122.

Kimura, Y., I. Yahara, and S. Lindquist. 1995. Role of the protein chaperone YDJ1 in establishing Hsp90-mediated signal transduction pathways. *Science*. 268:1362-1365.

Kinouchi, K., A. Ichihara, M. Sano, G.H. Sun-Wada, Y. Wada, A. Kurauchi-Mito, K. Bokuda, T. Narita, Y. Oshima, M. Sakoda, Y. Tamai, H. Sato, K. Fukuda, and H. Itoh. 2010. The (pro)renin receptor/ATP6AP2 is essential for vacuolar H+-ATPase assembly in murine cardiomyocytes. *Circulation research*. 107:30-34.

Kinouchi, K., A. Ichihara, M. Sano, G.H. Sun-Wada, Y. Wada, H. Ochi, T. Fukuda, K. Bokuda, H. Kurosawa, N. Yoshida, S. Takeda, K. Fukuda, and H. Itoh. 2013. The role of individual domains and the significance of shedding of ATP6AP2/(pro)renin receptor in vacuolar H(+)-ATPase biogenesis. *PloS one*. 8:e78603.

Kitada, T., S. Asakawa, N. Hattori, H. Matsumine, Y. Yamamura, S. Minoshima, M. Yokochi, Y. Mizuno, and N. Shimizu. 1998. Mutations in the parkin gene cause autosomal recessive juvenile parkinsonism. *Nature*. 392:605-608.

Kline, L.B., and J.S. Glaser. 1979. Dominant optic atrophy. The clinical profile. *Arch Ophthalmol*. 97:1680-1686.

Klucken, J., Y. Shin, E. Masliah, B.T. Hyman, and P.J. McLean. 2004. Hsp70 Reduces alpha-Synuclein Aggregation and Toxicity. *The Journal of biological chemistry*. 279:25497-25502.

Knaevelsrud, H., and A. Simonsen. 2010. Fighting disease by selective autophagy of aggregate-prone proteins. *FEBS letters*. 584:2635-2645.

Knott, A.B., and E. Bossy-Wetzel. 2008. Impairing the mitochondrial fission and fusion balance: a new mechanism of neurodegeneration. *Ann N Y Acad Sci*. 1147:283-292.

Koch, A., Y. Yoon, N.A. Bonekamp, M.A. McNiven, and M. Schrader. 2005. A role for Fis1 in both mitochondrial and peroxisomal fission in mammalian cells. *Molecular biology of the cell*. 16:5077-5086.

Koopman, W.J., H.J. Visch, S. Verkaart, L.W. van den Heuvel, J.A. Smeitink, and P.H. Willems. 2005. Mitochondrial network complexity and pathological decrease in complex I activity are tightly correlated in isolated human complex I deficiency. *American journal of physiology. Cell physiology*. 289:C881-890.

Kopeikina, K.J., G.A. Carlson, R. Pitstick, A.E. Ludvigson, A. Peters, J.I. Luebke, R.M. Koffie, M.P. Frosch, B.T. Hyman, and T.L. Spires-Jones. 2011. Tau accumulation causes mitochondrial distribution deficits in neurons in a mouse model of tauopathy and in human Alzheimer's disease brain. *The American journal of pathology*. 179:2071-2082.

Kopito, R.R. 2000. Aggresomes, inclusion bodies and protein aggregation. *Trends in cell biology*. 10:524-530.

Korvatska, O., N.S. Strand, J.D. Berndt, T. Strovas, D.H. Chen, J.B. Leverenz, K. Kiianitsa, I.F. Mata, E. Karakoc, J.L. Greenup, E. Bonkowski, J. Chuang, R.T. Moon, E.E. Eichler, D.A. Nickerson, C.P. Zabetian, B.C. Kraemer, T.D. Bird, and W.H. Raskind. 2013. Altered splicing of ATP6AP2 causes X-linked parkinsonism with spasticity (XPDS). *Human molecular genetics*. 22:3259-3268.

Koshiba, T., S.A. Detmer, J.T. Kaiser, H. Chen, J.M. McCaffery, and D.C. Chan. 2004. Structural basis of mitochondrial tethering by mitofusin complexes. *Science*. 305:858-862.

Koutras, C., and J.E. Braun. 2014. J protein mutations and resulting proteostasis collapse. *Frontiers in cellular neuroscience*. 8:191.

Kozlov, G., A.Y. Denisov, M. Girard, M.J. Dicaire, J. Hamlin, P.S. McPherson, B. Brais, and K. Gehring. 2011. Structural basis of defects in the sacsin HEPN domain responsible for autosomal recessive spastic ataxia of Charlevoix-Saguenay (ARSACS). *The Journal of biological chemistry*. 286:20407-20412.

Kriz, J., Q. Zhu, J.P. Julien, and A.L. Padjen. 2000. Electrophysiological properties of axons in mice lacking neurofilament subunit genes: disparity between conduction velocity and axon diameter in absence of NF-H. *Brain research*. 885:32-44.

Kumemura, H., M. Harada, M.B. Omary, S. Sakisaka, T. Suganuma, M. Namba, and M. Sata. 2004. Aggregation and loss of cytokeratin filament networks inhibit golgi organization in liver-derived epithelial cell lines. *Cell motility and the cytoskeleton*. 57:37-52.

Kuusisto, E., A. Salminen, and I. Alafuzoff. 2001. Ubiquitin-binding protein p62 is present in neuronal and glial inclusions in human tauopathies and synucleinopathies. *Neuroreport*. 12:2085-2090.

Kuusisto, E., A. Salminen, and I. Alafuzoff. 2002. Early accumulation of p62 in neurofibrillary tangles in Alzheimer's disease: possible role in tangle formation. *Neuropathology and applied neurobiology*. 28:228-237.

Labrousse, A.M., M.D. Zappaterra, D.A. Rube, and A.M. van der Bliek. 1999. C. elegans dynamin-related protein DRP-1 controls severing of the mitochondrial outer membrane. *Mol Cell*. 4:815-826.

Laco, M.N., C.R. Oliveira, H.L. Paulson, and A.C. Rego. 2012. Compromised mitochondrial complex II in models of Machado-Joseph disease. *Biochimica et biophysica acta*. 1822:139-149.

Lagier-Tourenne, C., L. Tranebaerg, D. Chaigne, M. Gribaa, H. Dollfus, G. Silvestri, C. Betard, J.M. Warter, and M. Koenig. 2003. Homozygosity mapping of Marinesco-Sjogren syndrome to 5q31. *Eur J Hum Genet*. 11:770-778.

Lariviere, R., R. Gaudet, B.J. Gentil, M. Girard, T.C. Conte, S. Minotti, K. Leclerc-Desaulniers, K. Gehring, R.A. McKinney, E.A. Shoubridge, P.S. McPherson, H.D. Durham, and B. Brais. 2015. Sacs knockout mice present pathophysiological defects underlying autosomal recessive spastic ataxia of Charlevoix-Saguenay. *Human molecular genetics*. 24:727-739.

Lariviere, R.C., and J.P. Julien. 2004. Functions of intermediate filaments in neuronal development and disease. *Journal of neurobiology*. 58:131-148.

Lawson, V.H., B.V. Graham, and K.M. Flanigan. 2005. Clinical and electrophysiologic features of CMT2A with mutations in the mitofusin 2 gene. *Neurology*. 65:197-204.

Lazarides, E. 1980. Intermediate filaments as mechanical integrators of cellular space. *Nature*. 283:249-256.

Lee, C.H., and P.A. Coulombe. 2009. Self-organization of keratin intermediate filaments into cross-linked networks. *The Journal of cell biology*. 186:409-421.

Lee, H.J., and S.J. Lee. 2002. Characterization of cytoplasmic alpha-synuclein aggregates. Fibril formation is tightly linked to the inclusion-forming process in cells. *The Journal of biological chemistry*. 277:48976-48983.

Lee, J.A. 2012. Neuronal autophagy: a housekeeper or a fighter in neuronal cell survival? *Experimental neurobiology*. 21:1-8.

Lee, J.H., W.H. Yu, A. Kumar, S. Lee, P.S. Mohan, C.M. Peterhoff, D.M. Wolfe, M. Martinez-Vicente, A.C. Massey, G. Sovak, Y. Uchiyama, D. Westaway, A.M. Cuervo, and R.A. Nixon. 2010. Lysosomal proteolysis and autophagy require presenilin 1 and are disrupted by Alzheimer-related PS1 mutations. *Cell*. 141:1146-1158.

Lee, J.S., M.H. Zhang, E.K. Yun, D. Geum, K. Kim, T.H. Kim, Y.S. Lim, and J.S. Seo. 2005. Heat shock protein 27 interacts with vimentin and prevents insolubilization of vimentin subunits induced by cadmium. *Experimental & molecular medicine*. 37:427-435.

Lee, K.Y., and R.N. Johnston. 1997. Neurofilaments are part of the high molecular weight complex containing neuronal cdc2-like kinase (nclk). *Brain research*. 773:197-202.

Lee, S.M., J.A. Olzmann, L.S. Chin, and L. Li. 2011. Mutations associated with Charcot-Marie-Tooth disease cause SIMPLE protein mislocalization and degradation by the proteasome and aggresome-autophagy pathways. *Journal of cell science*. 124:3319-3331.

Lee, Y.J., S.Y. Jeong, M. Karbowski, C.L. Smith, and R.J. Youle. 2004. Roles of the mammalian mitochondrial fission and fusion mediators Fis1, Drp1, and Opa1 in apoptosis. *Molecular biology of the cell*. 15:5001-5011.

Leu, J.I., J. Pimkina, P. Pandey, M.E. Murphy, and D.L. George. 2011. HSP70 inhibition by the small-molecule 2-phenylethynesulfonamide impairs protein clearance pathways in tumor cells. *Molecular cancer research : MCR*. 9:936-947.

Leung, C.L., D. Sun, M. Zheng, D.R. Knowles, and R.K. Liem. 1999. Microtubule actin cross-linking factor (MACF): a hybrid of dystonin and dystrophin that can interact with the actin and microtubule cytoskeletons. *The Journal of cell biology*. 147:1275-1286.

Levy, J.R., C.J. Sumner, J.P. Caviston, M.K. Tokito, S. Ranganathan, L.A. Ligon, K.E. Wallace, B.H. LaMonte, G.G. Harmison, I. Puls, K.H. Fischbeck, and E.L. Holzbaur. 2006. A motor neuron disease-associated mutation in p150Glued perturbs dynactin function and induces protein aggregation. *The Journal of cell biology*. 172:733-745.

Li, J., Y.R. Han, M.R. Plummer, and K. Herrup. 2009. Cytoplasmic ATM in neurons modulates synaptic function. *Current biology : CB*. 19:2091-2096.

Li, S., S. Xu, B.A. Roelofs, L. Boyman, W.J. Lederer, H. Sesaki, and M. Karbowski. 2015a. Transient assembly of F-actin on the outer mitochondrial membrane contributes to mitochondrial fission. *The Journal of cell biology*. 208:109-123.

Li, X. 2013. Autosomal Recessive Spastic Ataxia of Charlevoix-Saguenay (ARSACS): a once obscure neurodegenerative disease with increasing significance for neurological research. *McGill Science Undergraduate Research Journal*. 8:69.

Li, X., M. Menade, G. Kozlov, Z. Hu, Z. Dai, P.S. McPherson, B. Brais, and K. Gehring. 2015b. High-Throughput Screening for Ligands of the HEPN Domain of Sacsin. *PloS one*. 10:e0137298.

Li, Z., K. Okamoto, Y. Hayashi, and M. Sheng. 2004. The importance of dendritic mitochondria in the morphogenesis and plasticity of spines and synapses. *Cell*. 119:873-887.

Liem, R.K., and A. Messing. 2009. Dysfunctions of neuronal and glial intermediate filaments in disease. *The Journal of clinical investigation*. 119:1814-1824.

Liesa, M., M. Palacin, and A. Zorzano. 2009. Mitochondrial dynamics in mammalian health and disease. *Physiol Rev*. 89:799-845.

Ligon, L.A., and O. Steward. 2000. Role of microtubules and actin filaments in the movement of mitochondria in the axons and dendrites of cultured hippocampal neurons. *J Comp Neurol*. 427:351-361.

Liu, H., P. Wang, W. Song, and X. Sun. 2009. Degradation of regulator of calcineurin 1 (RCAN1) is mediated by both chaperone-mediated autophagy and ubiquitin proteasome pathways. *FASEB journal : official publication of the Federation of American Societies for Experimental Biology*. 23:3383-3392.

Liu, L., X.B. Li, X.H. Zi, L. Shen, M. Hu Zh, X. Huang Sh, D.L. Yu, H.B. Li, K. Xia, B.S. Tang, and R.X. Zhang. 2016. A novel hemizygous SACS mutation identified by whole exome sequencing and SNP array analysis in a Chinese ARSACS patient. *Journal of the neurological sciences*. 362:111-114.

Liu, W., R. Acin-Perez, K.D. Geghman, G. Manfredi, B. Lu, and C. Li. 2011. Pink1 regulates the oxidative phosphorylation machinery via mitochondrial fission. *Proceedings of the National Academy of Sciences of the United States of America*. 108:12920-12924.

Lodi, R., J.M. Cooper, J.L. Bradley, D. Manners, P. Styles, D.J. Taylor, and A.H. Schapira. 1999. Deficit of in vivo mitochondrial ATP production in patients with Friedreich ataxia. *Proceedings of the National Academy of Sciences of the United States of America*. 96:11492-11495.

Long, J., T.R. Gallagher, J.R. Cavey, P.W. Sheppard, S.H. Ralston, R. Layfield, and M.S. Searle. 2008. Ubiquitin recognition by the ubiquitin-associated domain of p62 involves a novel conformational switch. *The Journal of biological chemistry*. 283:5427-5440.

Loson, O.C., Z. Song, H. Chen, and D.C. Chan. 2013. Fis1, Mff, MiD49, and MiD51 mediate Drp1 recruitment in mitochondrial fission. *Molecular biology of the cell*. 24:659-667.

Louis, E.D., H. Yi, C. Erickson-Davis, J.P. Vonsattel, and P.L. Faust. 2009. Structural study of Purkinje cell axonal torpedoes in essential tremor. *Neuroscience letters*. 450:287-291.

Lowe, J., A. Blanchard, K. Morrell, G. Lennox, L. Reynolds, M. Billett, M. Landon, and R.J. Mayer. 1988. Ubiquitin is a common factor in intermediate filament inclusion bodies of diverse type in man, including those of Parkinson's disease, Pick's disease, and Alzheimer's disease, as well as Rosenthal fibres in cerebellar astrocytomas, cytoplasmic bodies in muscle, and mallory bodies in alcoholic liver disease. *The Journal of pathology*. 155:9-15.

Lu, B. 2009. Mitochondrial dynamics and neurodegeneration. *Curr Neurol Neurosci Rep*. 9:212-219.

Lu, L., Q. Cai, J.H. Tian, and Z.H. Sheng. 2009. Snapin associates with late endocytic compartments and interacts with late endosomal SNAREs. *Bioscience reports*. 29:261-269.

Lynch-Day, M.A., K. Mao, K. Wang, M. Zhao, and D.J. Klionsky. 2012. The role of autophagy in Parkinson's disease. *Cold Spring Harbor perspectives in medicine*. 2:a009357.

Macaskill, A.F., J.E. Rinholm, A.E. Twelvetrees, I.L. Arancibia-Carcamo, J. Muir, A. Fransson, P. Aspenstrom, D. Attwell, and J.T. Kittler. 2009. Miro1 is a calcium sensor for glutamate receptor-dependent localization of mitochondria at synapses. *Neuron*. 61:541-555.

Macdonald, P.J., N. Stepanyants, N. Mehrotra, J.A. Mears, X. Qi, H. Sesaki, and R. Ramachandran. 2014. A dimeric equilibrium intermediate nucleates Drp1 reassembly on mitochondrial membranes for fission. *Molecular biology of the cell*. 25:1905-1915.

Magrane, J., R.C. Smith, K. Walsh, and H.W. Querfurth. 2004. Heat shock protein 70 participates in the neuroprotective response to intracellularly expressed beta-amyloid in neurons. *The Journal of neuroscience : the official journal of the Society for Neuroscience*. 24:1700-1706.

Mahloudji, M., G.H. Amirhakimi, P. Haghighi, and A.A. Khodadoust. 1972. Marinesco-Sjogren syndrome. Report of an autopsy. *Brain : a journal of neurology*. 95:675-680.

Malagelada, C., Z.H. Jin, V. Jackson-Lewis, S. Przedborski, and L.A. Greene. 2010. Rapamycin protects against neuron death in in vitro and in vivo models of Parkinson's disease. *The Journal of neuroscience : the official journal of the Society for Neuroscience*. 30:1166-1175.

Malone, A.M., C.T. Anderson, T. Stearns, and C.R. Jacobs. 2007. Primary cilia in bone. *Journal of musculoskeletal & neuronal interactions*. 7:301.

Maloyan, A., A. Sanbe, H. Osinska, M. Westfall, D. Robinson, K. Imahashi, E. Murphy, and J. Robbins. 2005. Mitochondrial dysfunction and apoptosis underlie the pathogenic process in alpha-B-crystallin desmin-related cardiomyopathy. *Circulation*. 112:3451-3461.

Manczak, M., M.J. Calkins, and P.H. Reddy. 2011. Impaired mitochondrial dynamics and abnormal interaction of amyloid beta with mitochondrial protein Drp1 in neurons from patients with Alzheimer's disease: implications for neuronal damage. *Human molecular genetics*. 20:2495-2509.

Manczak, M., and P.H. Reddy. 2012. Abnormal interaction between the mitochondrial fission protein Drp1 and hyperphosphorylated tau in Alzheimer's disease neurons: implications for mitochondrial dysfunction and neuronal damage. *Human molecular genetics*. 21:2538-2547.

Manetto, V., N.H. Sternberger, G. Perry, L.A. Sternberger, and P. Gambetti. 1988. Phosphorylation of neurofilaments is altered in amyotrophic lateral sclerosis. *Journal of neuropathology and experimental neurology*. 47:642-653.

Martin, M.H., J.P. Bouchard, M. Sylvain, O. St-Onge, and S. Truchon. 2007. Autosomal recessive spastic ataxia of Charlevoix-Saguenay: a report of MR imaging in 5 patients. *AJNR Am J Neuroradiol*. 28:1606-1608.

Martinez-Martinez, S., A. Rodriguez, M.D. Lopez-Maderuelo, I. Ortega-Perez, J. Vazquez, and J.M. Redondo. 2006. Blockade of NFAT activation by the second calcineurin binding site. *The Journal of biological chemistry*. 281:6227-6235.

Masciullo, M., A. Modoni, A. Tessa, F.M. Santorelli, V. Rizzo, G. D'Amico, F. Laschena, T. Tartaglione, and G. Silvestri. 2012. Novel SACS mutations in two unrelated Italian patients with spastic ataxia: clinico-diagnostic characterization and results of serial brain MRI studies. *Eur J Neurol*. 19:e77-78.

Massey, A., R. Kiffin, and A.M. Cuervo. 2004. Pathophysiology of chaperone-mediated autophagy. *The international journal of biochemistry & cell biology*. 36:2420-2434.

Matsuda, N., S. Sato, K. Shiba, K. Okatsu, K. Saisho, C.A. Gautier, Y.S. Sou, S. Saiki, S. Kawajiri, F. Sato, M. Kimura, M. Komatsu, N. Hattori, and K. Tanaka. 2010. PINK1 stabilized by mitochondrial depolarization recruits Parkin to damaged mitochondria and activates latent Parkin for mitophagy. *The Journal of cell biology*. 189:211-221.

Mavrou, A., G.T. Tsangaris, E. Roma, and A. Kolialexi. 2008. The ATM gene and ataxia telangiectasia. *Anticancer Res*. 28:401-405.

Mayer, R.J., J. Lowe, G. Lennox, F. Doherty, and M. Landon. 1989. Intermediate filaments and ubiquitin: a new thread in the understanding of chronic neurodegenerative diseases. *Progress in clinical and biological research*. 317:809-818.

McClellan, A.J., M.D. Scott, and J. Frydman. 2005. Folding and quality control of the VHL tumor suppressor proceed through distinct chaperone pathways. *Cell*. 121:739-748.

McKenzie, S.L., S. Henikoff, and M. Meselson. 1975. Localization of RNA from heat-induced polysomes at puff sites in Drosophila melanogaster. *Proceedings of the National Academy of Sciences of the United States of America*. 72:1117-1121.

McLaughlin, S.H., H.W. Smith, and S.E. Jackson. 2002. Stimulation of the weak ATPase activity of human hsp90 by a client protein. *J Mol Biol*. 315:787-798.

McLean, P.J., H. Kawamata, S. Shariff, J. Hewett, N. Sharma, K. Ueda, X.O. Breakefield, and B.T. Hyman. 2002. TorsinA and heat shock proteins act as molecular chaperones: suppression of alpha-synuclein aggregation. *Journal of neurochemistry*. 83:846-854.

McMurray, C.T. 2000. Neurodegeneration: diseases of the cytoskeleton? *Cell death and differentiation*. 7:861-865.

McNaught, K.S., C.W. Olanow, B. Halliwell, O. Isacson, and P. Jenner. 2001. Failure of the ubiquitin-proteasome system in Parkinson's disease. *Nature reviews. Neuroscience*. 2:589-594.

Mears, J.A., L.L. Lackner, S. Fang, E. Ingerman, J. Nunnari, and J.E. Hinshaw. 2011. Conformational changes in Dnm1 support a contractile mechanism for mitochondrial fission. *Nature structural & molecular biology*. 18:20-26.

Meeusen, S., R. DeVay, J. Block, A. Cassidy-Stone, S. Wayson, J.M. McCaffery, and J. Nunnari. 2006. Mitochondrial inner-membrane fusion and crista maintenance requires the dynamin-related GTPase Mgm1. *Cell*. 127:383-395.

Meimaridou, E., S.B. Gooljar, N. Ramnarace, L. Anthonypillai, A.J. Clark, and J.P. Chapple. 2011. The cytosolic chaperone Hsc70 promotes traffic to the cell surface of intracellular retained melanocortin-4 receptor mutants. *Mol Endocrinol*. 25:1650-1660.

Menzies, F.M., J. Huebener, M. Renna, M. Bonin, O. Riess, and D.C. Rubinsztein. 2010. Autophagy induction reduces mutant ataxin-3 levels and toxicity in a mouse model of spinocerebellar ataxia type 3. *Brain : a journal of neurology*. 133:93-104.

Mersiyanova, I.V., A.V. Perepelov, A.V. Polyakov, V.F. Sitnikov, E.L. Dadali, R.B. Oparin, A.N. Petrin, and O.V. Evgrafov. 2000. A new variant of Charcot-Marie-Tooth disease type 2 is probably the result of a mutation in the neurofilament-light gene. *American journal of human genetics*. 67:37-46.

Michiorri, S., V. Gelmetti, E. Giarda, F. Lombardi, F. Romano, R. Marongiu, S. Nerini-Molteni, P. Sale, R. Vago, G. Arena, L. Torosantucci, L. Cassina, M.A. Russo, B. Dallapiccola, E.M. Valente, and G. Casari. 2010. The Parkinson-associated protein PINK1 interacts with Beclin1 and promotes autophagy. *Cell death and differentiation*. 17:962-974.

Milner, D.J., M. Mavroidis, N. Weisleder, and Y. Capetanaki. 2000. Desmin cytoskeleton linked to muscle mitochondrial distribution and respiratory function. *The Journal of cell biology*. 150:1283-1298.

Minami, Y., Y. Kimura, H. Kawasaki, K. Suzuki, and I. Yahara. 1994. The carboxy-terminal region of mammalian HSP90 is required for its dimerization and function in vivo. *Molecular and cellular biology*. 14:1459-1464.

Mishra, R.K., S.S. Jatiani, A. Kumar, V.R. Simhadri, R.V. Hosur, and R. Mittal. 2004. Dynamin interacts with members of the sumoylation machinery. *The Journal of biological chemistry*. 279:31445-31454.

Mitra, K., and J. Lippincott-Schwartz. 2010. Analysis of mitochondrial dynamics and functions using imaging approaches. *Current protocols in cell biology / editorial board, Juan S. Bonifacino ... [et al.]*. Chapter 4:Unit 4 25 21-21.

Mitsuhashi, S., and P.B. Kang. 2012. Update on the genetics of limb girdle muscular dystrophy. *Seminars in pediatric neurology*. 19:211-218.

Mittal, S., and S. Ganesh. 2010. Protein quality control mechanisms and neurodegenerative disorders: Checks, balances and deadlocks. *Neuroscience research*. 68:159-166.

Miyatake, S., N. Miyake, H. Doi, H. Saitsu, K. Ogata, M. Kawai, and N. Matsumoto. 2012. A Novel SACS Mutation in an Atypical Case with Autosomal Recessive Spastic Ataxia of Charlevoix-Saguenay (ARSACS). *Intern Med*. 51:2221-2226.

Mizushima, N., B. Levine, A.M. Cuervo, and D.J. Klionsky. 2008. Autophagy fights disease through cellular self-digestion. *Nature*. 451:1069-1075.

Morimoto, R.I., and M.G. Santoro. 1998. Stress-inducible responses and heat shock proteins: new pharmacologic targets for cytoprotection. *Nat Biotechnol*. 16:833-838.

Morris, R.L., and P.J. Hollenbeck. 1995. Axonal transport of mitochondria along microtubules and F-actin in living vertebrate neurons. *The Journal of cell biology*. 131:1315-1326.

Mortiboys, H., K.J. Thomas, W.J. Koopman, S. Klaffke, P. Abou-Sleiman, S. Olpin, N.W. Wood, P.H. Willems, J.A. Smeitink, M.R. Cookson, and O. Bandmann. 2008. Mitochondrial function and morphology are impaired in parkin-mutant fibroblasts. *Annals of neurology*. 64:555-565.

Mose-Larsen, P., R. Bravo, S.J. Fey, J.V. Small, and J.E. Celis. 1982. Putative association of mitochondria with a subpopulation of intermediate-sized filaments in cultured human skin fibroblasts. *Cell*. 31:681-692.

Mosser, D.D., N.G. Theodorakis, and R.I. Morimoto. 1988. Coordinate changes in heat shock element-binding activity and HSP70 gene transcription rates in human cells. *Molecular and cellular biology*. 8:4736-4744.

Mozdy, A.D., J.M. McCaffery, and J.M. Shaw. 2000. Dnm1p GTPase-mediated mitochondrial fission is a multi-step process requiring the novel integral membrane component Fis1p. *The Journal of cell biology*. 151:367-380.

Muchowski, P.J., G. Schaffar, A. Sittler, E.E. Wanker, M.K. Hayer-Hartl, and F.U. Hartl. 2000. Hsp70 and hsp40 chaperones can inhibit self-assembly of polyglutamine proteins into amyloid-like fibrils. *Proceedings of the National Academy of Sciences of the United States of America*. 97:7841-7846.

Muchowski, P.J., and J.L. Wacker. 2005. Modulation of neurodegeneration by molecular chaperones. *Nature reviews. Neuroscience*. 6:11-22.

Mueller, T.D., and J. Feigon. 2002. Solution structures of UBA domains reveal a conserved hydrophobic surface for protein-protein interactions. *J Mol Biol*. 319:1243-1255.

Munch, C., R. Sedlmeier, T. Meyer, V. Homberg, A.D. Sperfeld, A. Kurt, J. Prudlo, G. Peraus, C.O. Hanemann, G. Stumm, and A.C. Ludolph. 2004. Point mutations of the p150 subunit of dynactin (DCTN1) gene in ALS. *Neurology*. 63:724-726.

Muqit, M.M., S.M. Davidson, M.D. Payne Smith, L.P. MacCormac, S. Kahns, P.H. Jensen, N.W. Wood, and D.S. Latchman. 2004. Parkin is recruited into aggresomes in a stress-specific manner: over-expression of parkin reduces aggresome formation but can be dissociated from parkin's effect on neuronal survival. *Human molecular genetics*. 13:117-135.

Murakami, T., M. Shoji, Y. Imai, H. Inoue, T. Kawarabayashi, E. Matsubara, Y. Harigaya, A. Sasaki, R. Takahashi, and K. Abe. 2004. Pael-R is accumulated in Lewy bodies of Parkinson's disease. *Annals of neurology*. 55:439-442.

Murdock, D.G., B.E. Boone, L.A. Esposito, and D.C. Wallace. 1999. Up-regulation of nuclear and mitochondrial genes in the skeletal muscle of mice lacking the heart/muscle isoform of the adenine nucleotide translocator. *The Journal of biological chemistry*. 274:14429-14433.

Nadeau, K., A. Das, and C.T. Walsh. 1993. Hsp90 chaperonins possess ATPase activity and bind heat shock transcription factors and peptidyl prolyl isomerases. *The Journal of biological chemistry*. 268:1479-1487.

Nagaoka, U., K. Kim, N.R. Jana, H. Doi, M. Maruyama, K. Mitsui, F. Oyama, and N. Nukina. 2004. Increased expression of p62 in expanded polyglutamine-expressing cells and its association with polyglutamine inclusions. *Journal of neurochemistry*. 91:57-68.

Nair, S.C., E.J. Toran, R.A. Rimerman, S. Hjermstad, T.E. Smithgall, and D.F. Smith. 1996. A pathway of multi-chaperone interactions common to diverse regulatory proteins: estrogen receptor, Fes tyrosine kinase, heat shock transcription factor Hsf1, and the aryl hydrocarbon receptor. *Cell Stress Chaperones*. 1:237-250.

Nakamura, N., Y. Kimura, M. Tokuda, S. Honda, and S. Hirose. 2006. MARCH-V is a novel mitofusin 2- and Drp1-binding protein able to change mitochondrial morphology. *EMBO reports*. 7:1019-1022.

Nakano, T., K. Nakaso, K. Nakashima, and E. Ohama. 2004. Expression of ubiquitin-binding protein p62 in ubiquitin-immunoreactive intraneuronal inclusions in

amyotrophic lateral sclerosis with dementia: analysis of five autopsy cases with broad clinicopathological spectrum. *Acta neuropathologica*. 107:359-364.

Nangaku, M., R. Sato-Yoshitake, Y. Okada, Y. Noda, R. Takemura, H. Yamazaki, and N. Hirokawa. 1994. KIF1B, a novel microtubule plus end-directed monomeric motor protein for transport of mitochondria. *Cell*. 79:1209-1220.

Narendra, D., A. Tanaka, D.F. Suen, and R.J. Youle. 2008. Parkin is recruited selectively to impaired mitochondria and promotes their autophagy. *The Journal of cell biology*. 183:795-803.

Narendra, D., A. Tanaka, D.F. Suen, and R.J. Youle. 2009. Parkin-induced mitophagy in the pathogenesis of Parkinson disease. *Autophagy*. 5:706-708.

Narendra, D.P., S.M. Jin, A. Tanaka, D.F. Suen, C.A. Gautier, J. Shen, M.R. Cookson, and R.J. Youle. 2010. PINK1 is selectively stabilized on impaired mitochondria to activate Parkin. *PLoS Biol*. 8:e1000298.

Navon, A., and A. Ciechanover. 2009. The 26 S proteasome: from basic mechanisms to drug targeting. *The Journal of biological chemistry*. 284:33713-33718.

Nekrasova, O.E., M.G. Mendez, I.S. Chernoivanenko, P.A. Tyurin-Kuzmin, E.R. Kuczmarski, V.I. Gelfand, R.D. Goldman, and A.A. Minin. 2011. Vimentin intermediate filaments modulate the motility of mitochondria. *Molecular biology of the cell*. 22:2282-2289.

Nethisinghe, S., L. Clayton, S. Vermeer, J.P. Chapple, M. Reilly, F. Bremner, and P. Giunti. 2011. Retinal Imaging in Autosomal Recessive Spastic Ataxia of Charlevoix-Saguenay. *Neuro-Ophthalmology*. 35:197-201.

Nixon, R.A., and T.B. Shea. 1992. Dynamics of neuronal intermediate filaments: a developmental perspective. *Cell motility and the cytoskeleton*. 22:81-91.

Nixon, R.A., J. Wegiel, A. Kumar, W.H. Yu, C. Peterhoff, A. Cataldo, and A.M. Cuervo. 2005. Extensive involvement of autophagy in Alzheimer disease: an immuno-electron microscopy study. *Journal of neuropathology and experimental neurology*. 64:113-122.

Nixon, R.A., D.S. Yang, and J.H. Lee. 2008. Neurodegenerative lysosomal disorders: a continuum from development to late age. *Autophagy*. 4:590-599.

Noskova, L., V. Stranecky, H. Hartmannova, A. Pristoupilova, V. Baresova, R. Ivanek, H. Hulkova, H. Jahnova, J. van der Zee, J.F. Staropoli, K.B. Sims, J. Tyynela, C. Van Broeckhoven, P.C. Nijssen, S.E. Mole, M. Elleder, and S. Kmoch. 2011. Mutations in DNAJC5, encoding cysteine-string protein alpha, cause autosomal-dominant adult-onset neuronal ceroid lipofuscinosis. *American journal of human genetics*. 89:241-252.

Novoselov, S.S., W.J. Mustill, A.L. Gray, J.R. Dick, N. Kanuga, B. Kalmar, L. Greensmith, and M.E. Cheetham. 2013. Molecular chaperone mediated late-stage neuroprotection in the SOD1(G93A) mouse model of amyotrophic lateral sclerosis. *PloS one*. 8:e73944.

Nunnari, J., W.F. Marshall, A. Straight, A. Murray, J.W. Sedat, and P. Walter. 1997. Mitochondrial transmission during mating in Saccharomyces cerevisiae is determined by mitochondrial fusion and fission and the intramitochondrial segregation of mitochondrial DNA. *Molecular biology of the cell*. 8:1233-1242.

Ogawa, T., Y. Takiyama, K. Sakoe, K. Mori, M. Namekawa, H. Shimazaki, I. Nakano, and M. Nishizawa. 2004. Identification of a SACS gene missense mutation in ARSACS. *Neurology*. 62:107-109.

Ojala, T., P. Polinati, T. Manninen, A. Hiippala, J. Rajantie, R. Karikoski, A. Suomalainen, and T. Tyni. 2012. New mutation of mitochondrial DNAJC19

causing dilated and noncompaction cardiomyopathy, anemia, ataxia, and male genital anomalies. *Pediatric research*. 72:432-437.

Okamoto, P.M., B. Tripet, J. Litowski, R.S. Hodges, and R.B. Vallee. 1999. Multiple distinct coiled-coils are involved in dynamin self-assembly. *The Journal of biological chemistry*. 274:10277-10286.

Okawa, S., M. Sugawara, S. Watanabe, T. Imota, and I. Toyoshima. 2006. A novel sacsin mutation in a Japanese woman showing clinical uniformity of autosomal recessive spastic ataxia of Charlevoix-Saguenay. *J Neurol Neurosurg Psychiatry*. 77:280-282.

Olichon, A., L. Baricault, N. Gas, E. Guillou, A. Valette, P. Belenguer, and G. Lenaers. 2003. Loss of OPA1 perturbates the mitochondrial inner membrane structure and integrity, leading to cytochrome c release and apoptosis. *The Journal of biological chemistry*. 278:7743-7746.

Olsson, J.E., J.W. Gordon, B.S. Pawlyk, D. Roof, A. Hayes, R.S. Molday, S. Mukai, G.S. Cowley, E.L. Berson, and T.P. Dryja. 1992. Transgenic mice with a rhodopsin mutation (Pro23His): a mouse model of autosomal dominant retinitis pigmentosa. *Neuron*. 9:815-830.

Otera, H., N. Ishihara, and K. Mihara. 2013. New insights into the function and regulation of mitochondrial fission. *Biochimica et biophysica acta*. 1833:1256-1268.

Otera, H., and K. Mihara. 2011. Discovery of the membrane receptor for mitochondrial fission GTPase Drp1. *Small GTPases*. 2:167-172.

Otera, H., C. Wang, M.M. Cleland, K. Setoguchi, S. Yokota, R.J. Youle, and K. Mihara. 2010. Mff is an essential factor for mitochondrial recruitment of Drp1 during mitochondrial fission in mammalian cells. *The Journal of cell biology*. 191:1141-1158.

Otey, C.A., and O. Carpen. 2004. Alpha-actinin revisited: a fresh look at an old player. *Cell motility and the cytoskeleton*. 58:104-111.

Otsuga, D., B.R. Keegan, E. Brisch, J.W. Thatcher, G.J. Hermann, W. Bleazard, and J.M. Shaw. 1998. The dynamin-related GTPase, Dnm1p, controls mitochondrial morphology in yeast. *The Journal of cell biology*. 143:333-349.

Ouyang, Y., Y. Takiyama, K. Sakoe, H. Shimazaki, T. Ogawa, S. Nagano, Y. Yamamoto, and I. Nakano. 2006. Sacsin-related ataxia (ARSACS): expanding the genotype upstream from the gigantic exon. *Neurology*. 66:1103-1104.

Pallanck, L.J. 2010. Culling sick mitochondria from the herd. *The Journal of cell biology*. 191:1225-1227.

Palmer, C.S., L.D. Osellame, D. Laine, O.S. Koutsopoulos, A.E. Frazier, and M.T. Ryan. 2011. MiD49 and MiD51, new components of the mitochondrial fission machinery. *EMBO reports*. 12:565-573.

Panaretou, B., G. Siligardi, P. Meyer, A. Maloney, J.K. Sullivan, S. Singh, S.H. Millson, P.A. Clarke, S. Naaby-Hansen, R. Stein, R. Cramer, M. Mollapour, P. Workman, P.W. Piper, L.H. Pearl, and C. Prodromou. 2002. Activation of the ATPase activity of hsp90 by the stress-regulated cochaperone aha1. *Mol Cell*. 10:1307-1318.

Pandolfo, M. 1999. Friedreich's ataxia: clinical aspects and pathogenesis. *Semin Neurol*. 19:311-321.

Pandolfo, M. 2001. Molecular basis of Friedreich ataxia. *Movement disorders : official journal of the Movement Disorder Society*. 16:815-821.

Pankiv, S., T.H. Clausen, T. Lamark, A. Brech, J.A. Bruun, H. Outzen, A. Overvatn, G. Bjorkoy, and T. Johansen. 2007. p62/SQSTM1 binds directly to Atg8/LC3 to

facilitate degradation of ubiquitinated protein aggregates by autophagy. *The Journal of biological chemistry*. 282:24131-24145.

Parfitt, D.A. 2011. The Ataxia Protein Sacsin: Localisation and Identification of Potential Interacting Partners.

Parfitt, D.A., G.J. Michael, E.G. Vermeulen, N.V. Prodromou, T.R. Webb, J.M. Gallo, M.E. Cheetham, W.S. Nicoll, G.L. Blatch, and J.P. Chapple. 2009. The ataxia protein sacsin is a functional co-chaperone that protects against polyglutamine-expanded ataxin-1. *Human molecular genetics*. 18:1556-1565.

Park, K.S., I. Jo, K. Pak, S.W. Bae, H. Rhim, S.H. Suh, J. Park, H. Zhu, I. So, and K.W. Kim. 2002. FCCP depolarizes plasma membrane potential by activating proton and Na+ currents in bovine aortic endothelial cells. *Pflugers Archiv : European journal of physiology*. 443:344-352.

Parone, P.A., S. Da Cruz, D. Tondera, Y. Mattenberger, D.I. James, P. Maechler, F. Barja, and J.C. Martinou. 2008. Preventing mitochondrial fission impairs mitochondrial function and leads to loss of mitochondrial DNA. *PloS one*. 3:e3257.

Parysek, L.M., and R.D. Goldman. 1987. Characterization of intermediate filaments in PC12 cells. *The Journal of neuroscience : the official journal of the Society for Neuroscience*. 7:781-791.

Paschal, B.M., E.L. Holzbaur, K.K. Pfister, S. Clark, D.I. Meyer, and R.B. Vallee. 1993. Characterization of a 50-kDa polypeptide in cytoplasmic dynein preparations reveals a complex with p150GLUED and a novel actin. *The Journal of biological chemistry*. 268:15318-15323.

Pearl, L.H., and C. Prodromou. 2006. Structure and mechanism of the Hsp90 molecular chaperone machinery. *Annual review of biochemistry*. 75:271-294.

Pedrotti, B., R. Colombo, and K. Islam. 1994. Microtubule associated protein MAP1A is an actin-binding and crosslinking protein. *Cell motility and the cytoskeleton*. 29:110-116.

Peiffer, J., W. Schlote, A. Bischoff, E. Boltshauser, and G. Muller. 1977. Generalized giant axonal neuropathy: a filament-forming disease of neuronal, endothelial, glial, and schwann cells in a patient without kinky hair. *Acta neuropathologica*. 40:213-218.

Pelletier, O., E. Pokidysheva, L.S. Hirst, N. Bouxsein, Y. Li, and C.R. Safinya. 2003. Structure of actin cross-linked with alpha-actinin: a network of bundles. *Physical review letters*. 91:148102.

Pendergrass, W., N. Wolf, and M. Poot. 2004. Efficacy of MitoTracker Green and CMXrosamine to measure changes in mitochondrial membrane potentials in living cells and tissues. *Cytometry. Part A : the journal of the International Society for Analytical Cytology*. 61:162-169.

Perez-Olle, R., M.A. Lopez-Toledano, D. Goryunov, N. Cabrera-Poch, L. Stefanis, K. Brown, and R.K. Liem. 2005. Mutations in the neurofilament light gene linked to Charcot-Marie-Tooth disease cause defects in transport. *Journal of neurochemistry*. 93:861-874.

Perez-Sala, D., C.L. Oeste, A.E. Martinez, M.J. Carrasco, B. Garzon, and F.J. Canada. 2015. Vimentin filament organization and stress sensing depend on its single cysteine residue and zinc binding. *Nature communications*. 6:7287.

Perlman, S.L. 2004. Symptomatic and disease-modifying therapy for the progressive ataxias. *Neurologist*. 10:275-289.

Perng, M.D., L. Cairns, I.P. van den, A. Prescott, A.M. Hutcheson, and R.A. Quinlan. 1999. Intermediate filament interactions can be altered by HSP27 and alphaB-crystallin. *Journal of cell science*. 112 (Pt 13):2099-2112.

Perrot, R., and J. Eyer. 2009. Neuronal intermediate filaments and neurodegenerative disorders. *Brain research bulletin*. 80:282-295.

Peters, C., M.J. Bayer, S. Buhler, J.S. Andersen, M. Mann, and A. Mayer. 2001. Trans-complex formation by proteolipid channels in the terminal phase of membrane fusion. *Nature*. 409:581-588.

Pikkarainen, M., P. Hartikainen, and I. Alafuzoff. 2008. Neuropathologic features of frontotemporal lobar degeneration with ubiquitin-positive inclusions visualized with ubiquitin-binding protein p62 immunohistochemistry. *Journal of neuropathology and experimental neurology*. 67:280-298.

Pikkarainen, M., P. Hartikainen, H. Soininen, and I. Alafuzoff. 2011. Distribution and pattern of pathology in subjects with familial or sporadic late-onset cerebellar ataxia as assessed by p62/sequestosome immunohistochemistry. *Cerebellum*. 10:720-731.

Pilliod, J., S. Moutton, J. Lavie, E. Maurat, C. Hubert, N. Bellance, M. Anheim, S. Forlani, F. Mochel, K. N'Guyen, C. Thauvin-Robinet, C. Verny, D. Milea, G. Lesca, M. Koenig, D. Rodriguez, N. Houcinat, J. Van-Gils, C.M. Durand, A. Guichet, M. Barth, D. Bonneau, P. Convers, E. Maillart, L. Guyant-Marechal, D. Hannequin, G. Fromager, A. Afenjar, S. Chantot-Bastaraud, S. Valence, P. Charles, P. Berquin, C. Rooryck, J. Bouron, A. Brice, D. Lacombe, R. Rossignol, G. Stevanin, G. Benard, L. Burglen, A. Durr, C. Goizet, and I. Coupry. 2015. New practical definitions for the diagnosis of autosomal recessive spastic ataxia of Charlevoix-Saguenay. *Annals of neurology*.

Piperno, G., M. Ledizet, and X.J. Chang. 1987. Microtubules Containing Acetylated Alpha-Tubulin in Mammalian-Cells in Culture. *Journal of Cell Biology*. 104:289-302.

Pitts, K.R., Y. Yoon, E.W. Krueger, and M.A. McNiven. 1999. The dynamin-like protein DLP1 is essential for normal distribution and morphology of the endoplasmic reticulum and mitochondria in mammalian cells. *Molecular biology of the cell*. 10:4403-4417.

Portier, M.M., B. de Nechaud, and F. Gros. 1983. Peripherin, a new member of the intermediate filament protein family. *Developmental neuroscience*. 6:335-344.

Praefcke, G.J., and H.T. McMahon. 2004. The dynamin superfamily: universal membrane tubulation and fission molecules? *Nature reviews. Molecular cell biology*. 5:133-147.

Presley, J.F., N.B. Cole, T.A. Schroer, K. Hirschberg, K.J. Zaal, and J. Lippincott-Schwartz. 1997. ER-to-Golgi transport visualized in living cells. *Nature*. 389:81-85.

Princiotta, M.F., D. Finzi, S.B. Qian, J. Gibbs, S. Schuchmann, F. Buttgereit, J.R. Bennink, and J.W. Yewdell. 2003. Quantitating protein synthesis, degradation, and endogenous antigen processing. *Immunity*. 18:343-354.

Prodi, E., M. Grisoli, M. Panzeri, L. Minati, F. Fattori, A. Erbetta, G. Uziel, S. D'Arrigo, A. Tessa, C. Ciano, F.M. Santorelli, M. Savoiardo, and C. Mariotti. 2012. Supratentorial and pontine MRI abnormalities characterize recessive spastic ataxia of Charlevoix-Saguenay. A comprehensive study of an Italian series. *Eur J Neurol*.

Prodromou, C., G. Siligardi, R. O'Brien, D.N. Woolfson, L. Regan, B. Panaretou, J.E. Ladbury, P.W. Piper, and L.H. Pearl. 1999. Regulation of Hsp90 ATPase

activity by tetratricopeptide repeat (TPR)-domain co-chaperones. *The EMBO journal*. 18:754-762.

Puccio, H., D. Simon, M. Cossee, P. Criqui-Filipe, F. Tiziano, J. Melki, C. Hindelang, R. Matyas, P. Rustin, and M. Koenig. 2001. Mouse models for Friedreich ataxia exhibit cardiomyopathy, sensory nerve defect and Fe-S enzyme deficiency followed by intramitochondrial iron deposits. *Nature genetics*. 27:181-186.

Puls, I., C. Jonnakuty, B.H. LaMonte, E.L. Holzbaur, M. Tokito, E. Mann, M.K. Floeter, K. Bidus, D. Drayna, S.J. Oh, R.H. Brown, Jr., C.L. Ludlow, and K.H. Fischbeck. 2003. Mutant dynactin in motor neuron disease. *Nature genetics*. 33:455-456.

Pyle, A., H. Griffin, J. Duff, S. Bennett, S. Zwolinski, T. Smertenko, P. Yu-Wai Man, M. Santibanez-Koref, R. Horvath, and P.F. Chinnery. 2013. Late-onset sacsinopathy diagnosed by exome sequencing and comparative genomic hybridization. *Journal of neurogenetics*. 27:176-182.

Pyle, A., H. Griffin, P. Yu-Wai-Man, J. Duff, G. Eglon, S. Pickering-Brown, M. Santibanez-Korev, R. Horvath, and P.F. Chinnery. 2012. Prominent sensorimotor neuropathy due to SACS mutations revealed by whole-exome sequencing. *Archives of neurology*. 69:1351-1354.

Qi, X., M.H. Disatnik, N. Shen, R.A. Sobel, and D. Mochly-Rosen. 2011. Aberrant mitochondrial fission in neurons induced by protein kinase C{delta} under oxidative stress conditions in vivo. *Molecular biology of the cell*. 22:256-265.

Qin, Z.H., Y. Wang, K.B. Kegel, A. Kazantsev, B.L. Apostol, L.M. Thompson, J. Yoder, N. Aronin, and M. DiFiglia. 2003. Autophagy regulates the processing of amino terminal huntingtin fragments. *Human molecular genetics*. 12:3231-3244.

Quintanilla, R.A., Y.N. Jin, R. von Bernhardi, and G.V. Johnson. 2013. Mitochondrial permeability transition pore induces mitochondria injury in Huntington disease. *Mol Neurodegener*. 8:45.

Ramos, A., N. Kazachkova, F. Silva, P. Maciel, A. Silva-Fernandes, S. Duarte-Silva, C. Santos, and M. Lima. 2015. Differential mtDNA damage patterns in a transgenic mouse model of Machado-Joseph disease (MJD/SCA3). *Journal of molecular neuroscience : MN*. 55:449-453.

Ramser, J., F.E. Abidi, C.A. Burckle, C. Lenski, H. Toriello, G. Wen, H.A. Lubs, S. Engert, R.E. Stevenson, A. Meindl, C.E. Schwartz, and G. Nguyen. 2005. A unique exonic splice enhancer mutation in a family with X-linked mental retardation and epilepsy points to a novel role of the renin receptor. *Human molecular genetics*. 14:1019-1027.

Rapaport, D., M. Brunner, W. Neupert, and B. Westermann. 1998. Fzo1p is a mitochondrial outer membrane protein essential for the biogenesis of functional mitochondria in Saccharomyces cerevisiae. *The Journal of biological chemistry*. 273:20150-20155.

Ravikumar, B., A. Acevedo-Arozena, S. Imarisio, Z. Berger, C. Vacher, C.J. O'Kane, S.D. Brown, and D.C. Rubinsztein. 2005. Dynein mutations impair autophagic clearance of aggregate-prone proteins. *Nature genetics*. 37:771-776.

Ravikumar, B., R. Duden, and D.C. Rubinsztein. 2002. Aggregate-prone proteins with polyglutamine and polyalanine expansions are degraded by autophagy. *Human molecular genetics*. 11:1107-1117.

Ravikumar, B., K. Moreau, and D.C. Rubinsztein. 2010. Plasma membrane helps autophagosomes grow. *Autophagy*. 6:1184-1186.

Ravikumar, B., C. Vacher, Z. Berger, J.E. Davies, S. Luo, L.G. Oroz, F. Scaravilli, D.F. Easton, R. Duden, C.J. O'Kane, and D.C. Rubinsztein. 2004. Inhibition of

mTOR induces autophagy and reduces toxicity of polyglutamine expansions in fly and mouse models of Huntington disease. *Nature genetics*. 36:585-595.

Reggiori, F., and D.J. Klionsky. 2002. Autophagy in the eukaryotic cell. *Eukaryotic cell*. 1:11-21.

Reipert, S., F. Steinbock, I. Fischer, R.E. Bittner, A. Zeold, and G. Wiche. 1999. Association of mitochondria with plectin and desmin intermediate filaments in striated muscle. *Experimental cell research*. 252:479-491.

Reis, K., A. Fransson, and P. Aspenstrom. 2009. The Miro GTPases: at the heart of the mitochondrial transport machinery. *FEBS letters*. 583:1391-1398.

Rezniczek, G.A., C. Abrahamsberg, P. Fuchs, D. Spazierer, and G. Wiche. 2003. Plectin 5'-transcript diversity: short alternative sequences determine stability of gene products, initiation of translation and subcellular localization of isoforms. *Human molecular genetics*. 12:3181-3194.

Richter, A., J.D. Rioux, J.P. Bouchard, J. Mercier, J. Mathieu, B. Ge, J. Poirier, D. Julien, G. Gyapay, J. Weissenbach, T.J. Hudson, S.B. Melancon, and K. Morgan. 1999. Location score and haplotype analyses of the locus for autosomal recessive spastic ataxia of Charlevoix-Saguenay, in chromosome region 13q11. *American journal of human genetics*. 64:768-775.

Richter, A.M., R.K. Ozgul, V.C. Poisson, and H. Topaloglu. 2004. Private SACS mutations in autosomal recessive spastic ataxia of Charlevoix-Saguenay (ARSACS) families from Turkey. *Neurogenetics*. 5:165-170.

Rideout, H.J., I. Lang-Rollin, and L. Stefanis. 2004. Involvement of macroautophagy in the dissolution of neuronal inclusions. *The international journal of biochemistry & cell biology*. 36:2551-2562.

Riehemann, K., and C. Sorg. 1993. Sequence homologies between four cytoskeleton-associated proteins. *Trends in biochemical sciences*. 18:82-83.

Rodrigues, A.J., M. do Carmo Costa, T.L. Silva, D. Ferreira, F. Bajanca, E. Logarinho, and P. Maciel. 2010. Absence of ataxin-3 leads to cytoskeletal disorganization and increased cell death. *Biochimica et biophysica acta*. 1803:1154-1163.

Rodriguez, A., J. Roy, S. Martinez-Martinez, M.D. Lopez-Maderuelo, P. Nino-Moreno, L. Orti, D. Pantoja-Uceda, A. Pineda-Lucena, M.S. Cyert, and J.M. Redondo. 2009. A conserved docking surface on calcineurin mediates interaction with substrates and immunosuppressants. *Mol Cell*. 33:616-626.

Rohatgi, R., L. Milenkovic, and M.P. Scott. 2007. Patched1 regulates hedgehog signaling at the primary cilium. *Science*. 317:372-376.

Romano, A., A. Tessa, A. Barca, F. Fattori, M.F. de Leva, A. Terracciano, C. Storelli, F.M. Santorelli, and T. Verri. 2013. Comparative analysis and functional mapping of SACS mutations reveal novel insights into sacsin repeated architecture. *Hum Mutat*. 34:525-537.

Roof, D.J., M. Adamian, and A. Hayes. 1994. Rhodopsin accumulation at abnormal sites in retinas of mice with a human P23H rhodopsin transgene. *Investigative ophthalmology & visual science*. 35:4049-4062.

Ross, C.A., and C.M. Pickart. 2004. The ubiquitin-proteasome pathway in Parkinson's disease and other neurodegenerative diseases. *Trends in cell biology*. 14:703-711.

Ross, C.A., and M.A. Poirier. 2004. Protein aggregation and neurodegenerative disease. *Nature medicine*. 10 Suppl:S10-17.

Roy, O.W., N.R. Cohen, and J.A. Nicoll. 2005. Pathophysiology of dementias and implications for therapy. *Indian J Pathol Microbiol*. 48:289-299.

Rubinsztein, D.C., A.M. Cuervo, B. Ravikumar, S. Sarkar, V. Korolchuk, S. Kaushik, and D.J. Klionsky. 2009. In search of an "autophagomometer". *Autophagy*. 5:585-589.

Rubinsztein, D.C., J.E. Gestwicki, L.O. Murphy, and D.J. Klionsky. 2007. Potential therapeutic applications of autophagy. *Nature reviews. Drug discovery*. 6:304-312.

Rubinsztein, D.C., B. Ravikumar, A. Acevedo-Arozena, S. Imarisio, C.J. O'Kane, and S.D. Brown. 2005. Dyneins, autophagy, aggregation and neurodegeneration. *Autophagy*. 1:177-178.

Rudrabhatla, P., H. Jaffe, and H.C. Pant. 2011. Direct evidence of phosphorylated neuronal intermediate filament proteins in neurofibrillary tangles (NFTs): phosphoproteomics of Alzheimer's NFTs. *FASEB journal : official publication of the Federation of American Societies for Experimental Biology*. 25:3896-3905.

Rusten, T.E., and H. Stenmark. 2010. p62, an autophagy hero or culprit? *Nature cell biology*. 12:207-209.

Saito, H., and H. Uchida. 1977. Initiation of the DNA replication of bacteriophage lambda in Escherichia coli K12. *J Mol Biol*. 113:1-25.

Saliba, R.S., P.M. Munro, P.J. Luthert, and M.E. Cheetham. 2002. The cellular fate of mutant rhodopsin: quality control, degradation and aggresome formation. *Journal of cell science*. 115:2907-2918.

Sanchez, M.G., J.E. Perez, M.R. Perez, and A.G. Redondo. 2015. Novel SACS mutation in autosomal recessive spastic ataxia of Charlevoix-Saguenay. *Journal of the neurological sciences*. 358:475-476.

Santel, A., S. Frank, B. Gaume, M. Herrler, R.J. Youle, and M.T. Fuller. 2003. Mitofusin-1 protein is a generally expressed mediator of mitochondrial fusion in mammalian cells. *Journal of cell science*. 116:2763-2774.

Santel, A., and M.T. Fuller. 2001. Control of mitochondrial morphology by a human mitofusin. *Journal of cell science*. 114:867-874.

Santos, D., and S.M. Cardoso. 2012. Mitochondrial dynamics and neuronal fate in Parkinson's disease. *Mitochondrion*. 12:428-437.

Saotome, M., D. Safiulina, G. Szabadkai, S. Das, A. Fransson, P. Aspenstrom, R. Rizzuto, and G. Hajnoczky. 2008. Bidirectional Ca2+-dependent control of mitochondrial dynamics by the Miro GTPase. *Proceedings of the National Academy of Sciences of the United States of America*. 105:20728-20733.

Sarparanta, J., P.H. Jonson, C. Golzio, S. Sandell, H. Luque, M. Screen, K. McDonald, J.M. Stajich, I. Mahjneh, A. Vihola, O. Raheem, S. Penttila, S. Lehtinen, S. Huovinen, J. Palmio, G. Tasca, E. Ricci, P. Hackman, M. Hauser, N. Katsanis, and B. Udd. 2012. Mutations affecting the cytoplasmic functions of the co-chaperone DNAJB6 cause limb-girdle muscular dystrophy. *Nature genetics*. 44:450-455, S451-452.

Sarria, A.J., S.R. Panini, and R.M. Evans. 1992. A functional role for vimentin intermediate filaments in the metabolism of lipoprotein-derived cholesterol in human SW-13 cells. *The Journal of biological chemistry*. 267:19455-19463.

Savitsky, K., A. Bar-Shira, S. Gilad, G. Rotman, Y. Ziv, L. Vanagaite, D.A. Tagle, S. Smith, T. Uziel, S. Sfez, M. Ashkenazi, I. Pecker, M. Frydman, R. Harnik, S.R. Patanjali, A. Simmons, G.A. Clines, A. Sartiel, R.A. Gatti, L. Chessa, O. Sanal, M.F. Lavin, N.G. Jaspers, A.M. Taylor, C.F. Arlett, T. Miki, S.M. Weissman, M. Lovett, F.S. Collins, and Y. Shiloh. 1995. A single ataxia telangiectasia gene with a product similar to PI-3 kinase. *Science*. 268:1749-1753.

Schafer, D.A., S.R. Gill, J.A. Cooper, J.E. Heuser, and T.A. Schroer. 1994. Ultrastructural analysis of the dynactin complex: an actin-related protein is a component of a filament that resembles F-actin. *The Journal of cell biology*. 126:403-412.

Schlossmacher, M.G., M.P. Frosch, W.P. Gai, M. Medina, N. Sharma, L. Forno, T. Ochiishi, H. Shimura, R. Sharon, N. Hattori, J.W. Langston, Y. Mizuno, B.T. Hyman, D.J. Selkoe, and K.S. Kosik. 2002. Parkin localizes to the Lewy bodies of Parkinson disease and dementia with Lewy bodies. *The American journal of pathology*. 160:1655-1667.

Schmidt, M.L., M.J. Carden, V.M. Lee, and J.Q. Trojanowski. 1987. Phosphate dependent and independent neurofilament epitopes in the axonal swellings of patients with motor neuron disease and controls. *Laboratory investigation; a journal of technical methods and pathology*. 56:282-294.

Schnapp, B.J., and T.S. Reese. 1989. Dynein is the motor for retrograde axonal transport of organelles. *Proceedings of the National Academy of Sciences of the United States of America*. 86:1548-1552.

Schols, L., G. Amoiridis, H. Przuntek, G. Frank, J.T. Epplen, and C. Epplen. 1997. Friedreich's ataxia. Revision of the phenotype according to molecular genetics. *Brain : a journal of neurology*. 120 (Pt 12):2131-2140.

Schon, E.A., and S. Przedborski. 2011. Mitochondria: the next (neurode)generation. *Neuron*. 70:1033-1053.

Schroder, R., W.S. Kunz, F. Rouan, E. Pfendner, K. Tolksdorf, K. Kappes-Horn, M. Altenschmidt-Mehring, R. Knoblich, P.F. van der Ven, J. Reimann, D.O. Furst, I. Blumcke, S. Vielhaber, D. Zillikens, S. Eming, T. Klockgether, J. Uitto, G. Wiche, and A. Rolfs. 2002. Disorganization of the desmin cytoskeleton and mitochondrial dysfunction in plectin-related epidermolysis bullosa simplex with muscular dystrophy. *Journal of neuropathology and experimental neurology*. 61:520-530.

Schroer, T.A. 2004. Dynactin. *Annual review of cell and developmental biology*. 20:759-779.

Schroer, T.A., and M.P. Sheetz. 1991. Two activators of microtubule-based vesicle transport. *The Journal of cell biology*. 115:1309-1318.

Schubert, U., L.C. Anton, J. Gibbs, C.C. Norbury, J.W. Yewdell, and J.R. Bennink. 2000. Rapid degradation of a large fraction of newly synthesized proteins by proteasomes. *Nature*. 404:770-774.

Schulz, K.L., A. Eckert, V. Rhein, S. Mai, W. Haase, A.S. Reichert, M. Jendrach, W.E. Muller, and K. Leuner. 2012. A new link to mitochondrial impairment in tauopathies. *Mol Neurobiol*. 46:205-216.

Sedgwick, R.P. 1991. Ataxia-telangiectasia. *In* Handbook of Clinical Neurology. Vol. 60. B.G. Vinken P, Klawans H, editor. Elsevier, New York, USA. 347-423.

Senderek, J., M. Krieger, C. Stendel, C. Bergmann, M. Moser, N. Breitbach-Faller, S. Rudnik-Schoneborn, A. Blaschek, N.I. Wolf, I. Harting, K. North, J. Smith, F. Muntoni, M. Brockington, S. Quijano-Roy, F. Renault, R. Herrmann, L.M. Hendershot, J.M. Schroder, H. Lochmuller, H. Topaloglu, T. Voit, J. Weis, F. Ebinger, and K. Zerres. 2005. Mutations in SIL1 cause Marinesco-Sjogren syndrome, a cerebellar ataxia with cataract and myopathy. *Nature genetics*. 37:1312-1314.

Seo, A.Y., A.M. Joseph, D. Dutta, J.C. Hwang, J.P. Aris, and C. Leeuwenburgh. 2010. New insights into the role of mitochondria in aging: mitochondrial dynamics and more. *Journal of cell science*. 123:2533-2542.

Settembre, C., A. Fraldi, L. Jahreiss, C. Spampanato, C. Venturi, D. Medina, R. de Pablo, C. Tacchetti, D.C. Rubinsztein, and A. Ballabio. 2008. A block of autophagy in lysosomal storage disorders. *Human molecular genetics*. 17:119-129.

Shajahan, A.N., B.K. Timblin, R. Sandoval, C. Tiruppathi, A.B. Malik, and R.D. Minshall. 2004. Role of Src-induced dynamin-2 phosphorylation in caveolae-mediated endocytosis in endothelial cells. *The Journal of biological chemistry*. 279:20392-20400.

Shapiro, B.E., E.L. Logigian, E.H. Kolodny, and G.M. Pastores. 2008. Late-onset Tay-Sachs disease: the spectrum of peripheral neuropathy in 30 affected patients. *Muscle & nerve*. 38:1012-1015.

Shaw, G., and K. Weber. 1982. Differential expression of neurofilament triplet proteins in brain development. *Nature*. 298:277-279.

Shaw, J.M., and J. Nunnari. 2002. Mitochondrial dynamics and division in budding yeast. *Trends in cell biology*. 12:178-184.

Sherman, M.Y., and A.L. Goldberg. 2001. Cellular defenses against unfolded proteins: a cell biologist thinks about neurodegenerative diseases. *Neuron*. 29:15-32.

Shiber, A., and T. Ravid. 2014. Chaperoning proteins for destruction: diverse roles of Hsp70 chaperones and their co-chaperones in targeting misfolded proteins to the proteasome. *Biomolecules*. 4:704-724.

Shimazaki, H., K. Sakoe, K. Niijima, I. Nakano, and Y. Takiyama. 2007. An unusual case of a spasticity-lacking phenotype with a novel SACS mutation. *Journal of the Neurological Sciences*. 255:87-89.

Shimazaki, H., Y. Takiyama, J. Honda, K. Sakoe, M. Namekawa, J. Tsugawa, Y. Tsuboi, C. Suzuki, M. Baba, and I. Nakano. 2012. Middle Cerebellar Peduncles and Pontine T2 Hypointensities in ARSACS. *J Neuroimaging*.

Shimazaki, H., Y. Takiyama, K. Sakoe, Y. Ando, and I. Nakano. 2005. A phenotype without spasticity in sacsin-related ataxia. *Neurology*. 64:2129-2131.

Shimura, H., N. Hattori, S. Kubo, Y. Mizuno, S. Asakawa, S. Minoshima, N. Shimizu, K. Iwai, T. Chiba, K. Tanaka, and T. Suzuki. 2000. Familial Parkinson disease gene product, parkin, is a ubiquitin-protein ligase. *Nature genetics*. 25:302-305.

Shimura, H., M.G. Schlossmacher, N. Hattori, M.P. Frosch, A. Trockenbacher, R. Schneider, Y. Mizuno, K.S. Kosik, and D.J. Selkoe. 2001. Ubiquitination of a new form of alpha-synuclein by parkin from human brain: implications for Parkinson's disease. *Science*. 293:263-269.

Shiomura, Y., and N. Hirokawa. 1987. Colocalization of microtubule-associated protein 1A and microtubule-associated protein 2 on neuronal microtubules in situ revealed with double-label immunoelectron microscopy. *The Journal of cell biology*. 104:1575-1578.

Shirendeb, U., A.P. Reddy, M. Manczak, M.J. Calkins, P. Mao, D.A. Tagle, and P.H. Reddy. 2011. Abnormal mitochondrial dynamics, mitochondrial loss and mutant huntingtin oligomers in Huntington's disease: implications for selective neuronal damage. *Human molecular genetics*. 20:1438-1455.

Sihag, R.K., M. Inagaki, T. Yamaguchi, T.B. Shea, and H.C. Pant. 2007. Role of phosphorylation on the structural dynamics and function of types III and IV intermediate filaments. *Experimental cell research*. 313:2098-2109.

Siligardi, G., B. Panaretou, P. Meyer, S. Singh, D.N. Woolfson, P.W. Piper, L.H. Pearl, and C. Prodromou. 2002. Regulation of Hsp90 ATPase activity by the co-chaperone Cdc37p/p50cdc37. *The Journal of biological chemistry*. 277:20151-20159.

Silvestri, L., V. Caputo, E. Bellacchio, L. Atorino, B. Dallapiccola, E.M. Valente, and G. Casari. 2005. Mitochondrial import and enzymatic activity of PINK1 mutants associated to recessive parkinsonism. *Human molecular genetics*. 14:3477-3492.

Sjogren, T. 1950. Hereditary congenital spinocerebellar ataxia accompanied by congenital cataract and oligophrenia; a genetic and clinical investigation. *Confin Neurol*. 10:293-308.

Skulachev, V.P. 2001. Mitochondrial filaments and clusters as intracellular power-transmitting cables. *Trends in biochemical sciences*. 26:23-29.

Slupe, A.M., R.A. Merrill, K.H. Flippo, M.A. Lobas, J.C. Houtman, and S. Strack. 2013. A calcineurin docking motif (LXVP) in dynamin-related protein 1 contributes to mitochondrial fragmentation and ischemic neuronal injury. *The Journal of biological chemistry*. 288:12353-12365.

Smirnova, E., L. Griparic, D.L. Shurland, and A.M. van der Bliek. 2001. Dynamin-related protein Drp1 is required for mitochondrial division in mammalian cells. *Molecular biology of the cell*. 12:2245-2256.

Smirnova, E., D.L. Shurland, S.N. Ryazantsev, and A.M. van der Bliek. 1998. A human dynamin-related protein controls the distribution of mitochondria. *The Journal of cell biology*. 143:351-358.

Song, W., J. Chen, A. Petrilli, G. Liot, E. Klinglmayr, Y. Zhou, P. Poquiz, J. Tjong, M.A. Pouladi, M.R. Hayden, E. Masliah, M. Ellisman, I. Rouiller, R. Schwarzenbacher, B. Bossy, G. Perkins, and E. Bossy-Wetzel. 2011. Mutant huntingtin binds the mitochondrial fission GTPase dynamin-related protein-1 and increases its enzymatic activity. *Nature medicine*. 17:377-382.

Soto, C., and L.D. Estrada. 2008. Protein misfolding and neurodegeneration. *Archives of neurology*. 65:184-189.

Spada, M., S. Pagliardini, M. Yasuda, T. Tukel, G. Thiagarajan, H. Sakuraba, A. Ponzone, and R.J. Desnick. 2006. High incidence of later-onset fabry disease revealed by newborn screening. *American journal of human genetics*. 79:31-40.

Spillantini, M.G., M.L. Schmidt, V.M. Lee, J.Q. Trojanowski, R. Jakes, and M. Goedert. 1997. Alpha-synuclein in Lewy bodies. *Nature*. 388:839-840.

Stefanis, L., K.E. Larsen, H.J. Rideout, D. Sulzer, and L.A. Greene. 2001. Expression of A53T mutant but not wild-type alpha-synuclein in PC12 cells induces alterations of the ubiquitin-dependent degradation system, loss of dopamine release, and autophagic cell death. *Journal of Neuroscience*. 21:9549-9560.

Stevens, J.C., S.M. Murphy, I. Davagnanam, R. Phadke, G. Anderson, S. Nethisinghe, F. Bremner, P. Giunti, and M.M. Reilly. 2013. The ARSACS phenotype can include supranuclear gaze palsy and skin lipofuscin deposits. *J Neurol Neurosurg Psychiatry*. 84:114-116.

Stojanovski, D., O.S. Koutsopoulos, K. Okamoto, and M.T. Ryan. 2004. Levels of human Fis1 at the mitochondrial outer membrane regulate mitochondrial morphology. *Journal of cell science*. 117:1201-1210.

Stone, M.R., A. O'Neill, R.M. Lovering, J. Strong, W.G. Resneck, P.W. Reed, D.M. Toivola, J.A. Ursitti, M.B. Omary, and R.J. Bloch. 2007. Absence of keratin 19 in mice causes skeletal myopathy with mitochondrial and sarcolemmal reorganization. *Journal of cell science*. 120:3999-4008.

Strack, S., and J.T. Cribbs. 2012. Allosteric modulation of Drp1 mechanoenzyme assembly and mitochondrial fission by the variable domain. *The Journal of biological chemistry*. 287:10990-11001.

Strack, S., T.J. Wilson, and J.T. Cribbs. 2013. Cyclin-dependent kinases regulate splice-specific targeting of dynamin-related protein 1 to microtubules. *The Journal of cell biology*. 201:1037-1051.

Straube-West, K., P.A. Loomis, P. Opal, and R.D. Goldman. 1996. Alterations in neural intermediate filament organization: functional implications and the induction of pathological changes related to motor neuron disease. *Journal of cell science*. 109 (Pt 9):2319-2329.

Styers, M.L., A.P. Kowalczyk, and V. Faundez. 2005. Intermediate filaments and vesicular membrane traffic: the odd couple's first dance? *Traffic*. 6:359-365.

Styers, M.L., G. Salazar, R. Love, A.A. Peden, A.P. Kowalczyk, and V. Faundez. 2004. The endo-lysosomal sorting machinery interacts with the intermediate filament cytoskeleton. *Molecular biology of the cell*. 15:5369-5382.

Su, H.B., J. Li, S. Menon, J.B. Liu, A.R. Kumarapeli, N. Wei, and X.J. Wang. 2011. Perturbation of Cullin Deneddylation via Conditional Csn8 Ablation Impairs the Ubiquitin-Proteasome System and Causes Cardiomyocyte Necrosis and Dilated Cardiomyopathy in Mice. *Circulation research*. 108:40-U87.

Su, V., and A.F. Lau. 2009. Ubiquitin-like and ubiquitin-associated domain proteins: significance in proteasomal degradation. *Cellular and molecular life sciences : CMLS*. 66:2819-2833.

Summerhayes, I.C., D. Wong, and L.B. Chen. 1983. Effect of microtubules and intermediate filaments on mitochondrial distribution. *Journal of cell science*. 61:87-105.

Sun, Y., and G.A. Grabowski. 2010. Impaired autophagosomes and lysosomes in neuronopathic Gaucher disease. *Autophagy*. 6:648-649.

Sundborger, A.C., and J.E. Hinshaw. 2014. Regulating dynamin dynamics during endocytosis. *F1000prime reports*. 6:85.

Suzuki, M., Y. Sugimoto, Y. Ohsaki, M. Ueno, S. Kato, Y. Kitamura, H. Hosokawa, J.P. Davies, Y.A. Ioannou, M.T. Vanier, K. Ohno, and H. Ninomiya. 2007. Endosomal accumulation of Toll-like receptor 4 causes constitutive secretion of cytokines and activation of signal transducers and activators of transcription in Niemann-Pick disease type C (NPC) fibroblasts: a potential basis for glial cell activation in the NPC brain. *The Journal of neuroscience : the official journal of the Society for Neuroscience*. 27:1879-1891.

Swift, M., D. Morrell, E. Cromartie, A.R. Chamberlin, M.H. Skolnick, and D.T. Bishop. 1986. The incidence and gene frequency of ataxia-telangiectasia in the United States. *American journal of human genetics*. 39:573-583.

Synofzik, M., A.S. Soehn, J. Gburek-Augustat, J. Schicks, K.N. Karle, R. Schule, T.B. Haack, M. Schoning, S. Biskup, S. Rudnik-Schoneborn, J. Senderek, K.T. Hoffmann, P. MacLeod, J. Schwarz, B. Bender, S. Kruger, F. Kreuz, P. Bauer, and L. Schols. 2013. Autosomal recessive spastic ataxia of Charlevoix Saguenay (ARSACS): expanding the genetic, clinical and imaging spectrum. *Orphanet J Rare Dis*. 8:41.

Taguchi, N., N. Ishihara, A. Jofuku, T. Oka, and K. Mihara. 2007. Mitotic phosphorylation of dynamin-related GTPase Drp1 participates in mitochondrial fission. *The Journal of biological chemistry*. 282:11521-11529.

Taipale, M., D.F. Jarosz, and S. Lindquist. 2010. HSP90 at the hub of protein homeostasis: emerging mechanistic insights. *Nature reviews. Molecular cell biology*. 11:515-528.

Takado, Y., K. Hara, T. Shimohata, S. Tokiguchi, O. Onodera, and M. Nishizawa. 2007. New mutation in the non-gigantic exon of SACS in Japanese siblings.

Movement disorders : official journal of the Movement Disorder Society. 22:748-749.

Takamura, A., K. Higaki, K. Kajimaki, S. Otsuka, H. Ninomiya, J. Matsuda, K. Ohno, Y. Suzuki, and E. Nanba. 2008. Enhanced autophagy and mitochondrial aberrations in murine G(M1)-gangliosidosis. *Biochemical and biophysical research communications*. 367:616-622.

Takao, N., Y. Li, and K. Yamamoto. 2000. Protective roles for ATM in cellular response to oxidative stress. *FEBS letters*. 472:133-136.

Tan, J.M., E.S. Wong, D.S. Kirkpatrick, O. Pletnikova, H.S. Ko, S.P. Tay, M.W. Ho, J. Troncoso, S.P. Gygi, M.K. Lee, V.L. Dawson, T.M. Dawson, and K.L. Lim. 2008. Lysine 63-linked ubiquitination promotes the formation and autophagic clearance of protein inclusions associated with neurodegenerative diseases. *Human molecular genetics*. 17:431-439.

Tanaka, A. 2010. Parkin-mediated selective mitochondrial autophagy, mitophagy: Parkin purges damaged organelles from the vital mitochondrial network. *FEBS letters*. 584:1386-1392.

Tanaka, A., M.M. Cleland, S. Xu, D.P. Narendra, D.F. Suen, M. Karbowski, and R.J. Youle. 2010. Proteasome and p97 mediate mitophagy and degradation of mitofusins induced by Parkin. *The Journal of cell biology*. 191:1367-1380.

Tanaka, M., Y.M. Kim, G. Lee, E. Junn, T. Iwatsubo, and M.M. Mouradian. 2004. Aggresomes formed by alpha-synuclein and synphilin-1 are cytoprotective. *The Journal of biological chemistry*. 279:4625-4631.

Tanaka, Y., Y. Kanai, Y. Okada, S. Nonaka, S. Takeda, A. Harada, and N. Hirokawa. 1998. Targeted disruption of mouse conventional kinesin heavy chain, kif5B, results in abnormal perinuclear clustering of mitochondria. *Cell*. 93:1147-1158.

Tang, H.L., H.L. Lung, K.C. Wu, A.H. Le, H.M. Tang, and M.C. Fung. 2008. Vimentin supports mitochondrial morphology and organization. *The Biochemical journal*. 410:141-146.

Tao, G.Z., K.S. Looi, D.M. Toivola, P. Strnad, Q. Zhou, J. Liao, Y. Wei, A. Habtezion, and M.B. Omary. 2009. Keratins modulate the shape and function of hepatocyte mitochondria: a mechanism for protection from apoptosis. *Journal of cell science*. 122:3851-3855.

Taylor, J.P., F. Tanaka, J. Robitschek, C.M. Sandoval, A. Taye, S. Markovic-Plese, and K.H. Fischbeck. 2003. Aggresomes protect cells by enhancing the degradation of toxic polyglutamine-containing protein. *Human molecular genetics*. 12:749-757.

Terracciano, A., C. Casali, G.S. Grieco, D. Orteschi, S. Di Giandomenico, L. Seminara, R. Di Fabio, R. Carrozzo, A. Simonati, G. Stevanin, M. Zollino, and F.M. Santorelli. 2009. An inherited large-scale rearrangement in SACS associated with spastic ataxia and hearing loss. *Neurogenetics*. 10:151-155.

Terracciano, A., N.C. Foulds, A. Ditchfield, D.J. Bunyan, J.A. Crolla, S. Huang, F.M. Santorelli, and S.R. Hammans. 2010. Pseudodominant inheritance of spastic ataxia of Charlevoix-Saguenay. *Neurology*. 74:1152-1154.

Tessitore, A., M. Pirozzi, and A. Auricchio. 2009. Abnormal autophagy, ubiquitination, inflammation and apoptosis are dependent upon lysosomal storage and are useful biomarkers of mucopolysaccharidosis VI. *PathoGenetics*. 2:4.

Thiffault, I., M.J. Dicaire, M. Tetreault, K.N. Huang, J. Demers-Lamarche, G. Bernard, A. Duquette, R. Lariviere, K. Gehring, A. Montpetit, P.S. McPherson, A. Richter, L. Montermini, J. Mercier, G.A. Mitchell, N. Dupre, C. Prevost, J.P.

Bouchard, J. Mathieu, and B. Brais. 2013. Diversity of ARSACS mutations in French-Canadians. *Can J Neurol Sci*. 40:61-66.

Tieu, Q., and J. Nunnari. 2000. Mdv1p is a WD repeat protein that interacts with the dynamin-related GTPase, Dnm1p, to trigger mitochondrial division. *The Journal of cell biology*. 151:353-366.

Tobaben, S., P. Thakur, R. Fernandez-Chacon, T.C. Sudhof, J. Rettig, and B. Stahl. 2001. A trimeric protein complex functions as a synaptic chaperone machine. *Neuron*. 31:987-999.

Todorov, A. 1965. [Marinesco-Sjogren syndrome. 1st anatomo-clinical study]. *J Genet Hum*. 14:197-233.

Toei, M., R. Saum, and M. Forgac. 2010. Regulation and isoform function of the V-ATPases. *Biochemistry*. 49:4715-4723.

Toivola, D.M., G.Z. Tao, A. Habtezion, J. Liao, and M.B. Omary. 2005. Cellular integrity plus: organelle-related and protein-targeting functions of intermediate filaments. *Trends in cell biology*. 15:608-617.

Tolstonog, G.V., I.V. Belichenko-Weitzmann, J.P. Lu, R. Hartig, R.L. Shoeman, U. Traub, and P. Traub. 2005. Spontaneously immortalized mouse embryo fibroblasts: growth behavior of wild-type and vimentin-deficient cells in relation to mitochondrial structure and activity. *DNA and cell biology*. 24:680-709.

Tolstonog, G.V., R.L. Shoeman, U. Traub, and P. Traub. 2001. Role of the intermediate filament protein vimentin in delaying senescence and in the spontaneous immortalization of mouse embryo fibroblasts. *DNA and cell biology*. 20:509-529.

Tomkins, J., P. Usher, J.Y. Slade, P.G. Ince, A. Curtis, K. Bushby, and P.J. Shaw. 1998. Novel insertion in the KSP region of the neurofilament heavy gene in amyotrophic lateral sclerosis (ALS). *Neuroreport*. 9:3967-3970.

Tooze, S.A., and G. Schiavo. 2008. Liaisons dangereuses: autophagy, neuronal survival and neurodegeneration. *Current opinion in neurobiology*. 18:504-515.

Tran, P.B., and R.J. Miller. 1999. Aggregates in neurodegenerative disease: crowds and power? *Trends in neurosciences*. 22:194-197.

Trottier, Y., Y. Lutz, G. Stevanin, G. Imbert, D. Devys, G. Cancel, F. Saudou, C. Weber, G. David, L. Tora, and et al. 1995. Polyglutamine expansion as a pathological epitope in Huntington's disease and four dominant cerebellar ataxias. *Nature*. 378:403-406.

Trushina, E., R.B. Dyer, J.D. Badger, 2nd, D. Ure, L. Eide, D.D. Tran, B.T. Vrieze, V. Legendre-Guillemin, P.S. McPherson, B.S. Mandavilli, B. Van Houten, S. Zeitlin, M. McNiven, R. Aebersold, M. Hayden, J.E. Parisi, E. Seeberg, I. Dragatsis, K. Doyle, A. Bender, C. Chacko, and C.T. McMurray. 2004. Mutant huntingtin impairs axonal trafficking in mammalian neurons in vivo and in vitro. *Molecular and cellular biology*. 24:8195-8209.

Tsai, H.F., C.S. Liu, G.D. Chen, M.L. Lin, C. Li, Y.Y. Chen, B.T. Wang, and M. Hsieh. 2003. Prenatal diagnosis of Machado-Joseph disease/Spinocerebellar Ataxia Type 3 in Taiwan: early detection of expanded ataxin-3. *Journal of clinical laboratory analysis*. 17:195-200.

Tsai, J., and M.G. Douglas. 1996. A conserved HPD sequence of the J-domain is necessary for YDJ1 stimulation of Hsp70 ATPase activity at a site distinct from substrate binding. *The Journal of biological chemistry*. 271:9347-9354.

Tsutsumi, S., M. Mollapour, C. Graf, C.T. Lee, B.T. Scroggins, W. Xu, L. Haslerova, M. Hessling, A.A. Konstantinova, J.B. Trepel, B. Panaretou, J. Buchner, M.P. Mayer, C. Prodromou, and L. Neckers. 2009. Hsp90 charged-linker truncation

reverses the functional consequences of weakened hydrophobic contacts in the N domain. *Nature structural & molecular biology*. 16:1141-1147.

Turturici, G., G. Sconzo, and F. Geraci. 2011. Hsp70 and its molecular role in nervous system diseases. *Biochem Res Int*. 2011:618127.

Twig, G., A. Elorza, A.J. Molina, H. Mohamed, J.D. Wikstrom, G. Walzer, L. Stiles, S.E. Haigh, S. Katz, G. Las, J. Alroy, M. Wu, B.F. Py, J. Yuan, J.T. Deeney, B.E. Corkey, and O.S. Shirihai. 2008. Fission and selective fusion govern mitochondrial segregation and elimination by autophagy. *The EMBO journal*. 27:433-446.

Tyson, J.R., and C.J. Stirling. 2000. LHS1 and SIL1 provide a lumenal function that is essential for protein translocation into the endoplasmic reticulum. *The EMBO journal*. 19:6440-6452.

Tzoulis, C., S. Johansson, B.I. Haukanes, H. Boman, P.M. Knappskog, and L.A. Bindoff. 2013. Novel SACS mutations identified by whole exome sequencing in a norwegian family with autosomal recessive spastic ataxia of Charlevoix-Saguenay. *PloS one*. 8:e66145.

Uchihara, T., H. Fujigasaki, S. Koyano, A. Nakamura, S. Yagishita, and K. Iwabuchi. 2001. Non-expanded polyglutamine proteins in intranuclear inclusions of hereditary ataxias--triple-labeling immunofluorescence study. *Acta neuropathologica*. 102:149-152.

Uryu, K., C. Richter-Landsberg, W. Welch, E. Sun, O. Goldbaum, E.H. Norris, C.T. Pham, I. Yazawa, K. Hilburger, M. Micsenyi, B.I. Giasson, N.M. Bonini, V.M. Lee, and J.Q. Trojanowski. 2006. Convergence of heat shock protein 90 with ubiquitin in filamentous alpha-synuclein inclusions of alpha-synucleinopathies. *The American journal of pathology*. 168:947-961.

Vabulas, R.M., S. Raychaudhuri, M. Hayer-Hartl, and F.U. Hartl. 2010. Protein folding in the cytoplasm and the heat shock response. *Cold Spring Harb Perspect Biol*. 2:a004390.

Valente, E.M., P.M. Abou-Sleiman, V. Caputo, M.M. Muqit, K. Harvey, S. Gispert, Z. Ali, D. Del Turco, A.R. Bentivoglio, D.G. Healy, A. Albanese, R. Nussbaum, R. Gonzalez-Maldonado, T. Deller, S. Salvi, P. Cortelli, W.P. Gilks, D.S. Latchman, R.J. Harvey, B. Dallapiccola, G. Auburger, and N.W. Wood. 2004. Hereditary early-onset Parkinson's disease caused by mutations in PINK1. *Science*. 304:1158-1160.

Valentin-Vega, Y.A., K.H. Maclean, J. Tait-Mulder, S. Milasta, M. Steeves, F.C. Dorsey, J.L. Cleveland, D.R. Green, and M.B. Kastan. 2012. Mitochondrial dysfunction in ataxia-telangiectasia. *Blood*. 119:1490-1500.

Valetti, C., D.M. Wetzel, M. Schrader, M.J. Hasbani, S.R. Gill, T.E. Kreis, and T.A. Schroer. 1999. Role of dynactin in endocytic traffic: effects of dynamitin overexpression and colocalization with CLIP-170. *Molecular biology of the cell*. 10:4107-4120.

van de Warrenburg, B.P., N.V. Knoers, and H.P. Kremer. 2002. [Friedrich's ataxia: clinical difficulties and genetic possibilities]. *Ned Tijdschr Geneeskd*. 146:1669-1672.

van der Vaart, A., and F. Reggiori. 2010. The Golgi complex as a source for yeast autophagosomal membranes. *Autophagy*. 6:800-801.

Van Laar, V.S., and S.B. Berman. 2013. The interplay of neuronal mitochondrial dynamics and bioenergetics: implications for Parkinson's disease. *Neurobiology of disease*. 51:43-55.

Varadi, A., L.I. Johnson-Cadwell, V. Cirulli, Y. Yoon, V.J. Allan, and G.A. Rutter. 2004. Cytoplasmic dynein regulates the subcellular distribution of mitochondria by controlling the recruitment of the fission factor dynamin-related protein-1. *Journal of cell science*. 117:4389-4400.

Verhagen, M.M., J.J. Martin, M. van Deuren, C. Ceuterick-de Groote, C.M. Weemaes, B.H. Kremer, M.A. Taylor, M.A. Willemsen, and M. Lammens. 2012. Neuropathology in classical and variant ataxia-telangiectasia. *Neuropathology*. 32:234-244.

Verhoef, L.G., K. Lindsten, M.G. Masucci, and N.P. Dantuma. 2002. Aggregate formation inhibits proteasomal degradation of polyglutamine proteins. *Human molecular genetics*. 11:2689-2700.

Verhoeven, K., K.G. Claeys, S. Zuchner, J.M. Schroder, J. Weis, C. Ceuterick, A. Jordanova, E. Nelis, E. De Vriendt, M. Van Hul, P. Seeman, R. Mazanec, G.M. Saifi, K. Szigeti, P. Mancias, I.J. Butler, A. Kochanski, B. Ryniewicz, J. De Bleecker, P. Van den Bergh, C. Verellen, R. Van Coster, N. Goemans, M. Auer-Grumbach, W. Robberecht, V. Milic Rasic, Y. Nevo, I. Tournev, V. Guergueltcheva, F. Roelens, P. Vieregge, P. Vinci, M.T. Moreno, H.J. Christen, M.E. Shy, J.R. Lupski, J.M. Vance, P. De Jonghe, and V. Timmerman. 2006. MFN2 mutation distribution and genotype/phenotype correlation in Charcot-Marie-Tooth type 2. *Brain : a journal of neurology*. 129:2093-2102.

Vermeer, S., R.P. Meijer, B.J. Pijl, J. Timmermans, J.R. Cruysberg, M.M. Bos, H.J. Schelhaas, B.P. van de Warrenburg, N.V. Knoers, H. Scheffer, and B. Kremer. 2008. ARSACS in the Dutch population: a frequent cause of early-onset cerebellar ataxia. *Neurogenetics*. 9:207-214.

Vicart, P., A. Caron, P. Guicheney, Z. Li, M.C. Prevost, A. Faure, D. Chateau, F. Chapon, F. Tome, J.M. Dupret, D. Paulin, and M. Fardeau. 1998. A missense mutation in the alphaB-crystallin chaperone gene causes a desmin-related myopathy. *Nature genetics*. 20:92-95.

Vikstrom, K.L., S.S. Lim, R.D. Goldman, and G.G. Borisy. 1992. Steady state dynamics of intermediate filament networks. *The Journal of cell biology*. 118:121-129.

Vilarino-Guell, C., A. Rajput, A.J. Milnerwood, B. Shah, C. Szu-Tu, J. Trinh, I. Yu, M. Encarnacion, L.N. Munsie, L. Tapia, E.K. Gustavsson, P. Chou, I. Tatarnikov, D.M. Evans, F.T. Pishotta, M. Volta, D. Beccano-Kelly, C. Thompson, M.K. Lin, H.E. Sherman, H.J. Han, B.L. Guenther, W.W. Wasserman, V. Bernard, C.J. Ross, S. Appel-Cresswell, A.J. Stoessl, C.A. Robinson, D.W. Dickson, O.A. Ross, Z.K. Wszolek, J.O. Aasly, R.M. Wu, F. Hentati, R.A. Gibson, P.S. McPherson, M. Girard, M. Rajput, A.H. Rajput, and M.J. Farrer. 2014. DNAJC13 mutations in Parkinson disease. *Human molecular genetics*. 23:1794-1801.

Vives-Bauza, C., C. Zhou, Y. Huang, M. Cui, R.L. de Vries, J. Kim, J. May, M.A. Tocilescu, W. Liu, H.S. Ko, J. Magrane, D.J. Moore, V.L. Dawson, R. Grailhe, T.M. Dawson, C. Li, K. Tieu, and S. Przedborski. 2010. PINK1-dependent recruitment of Parkin to mitochondria in mitophagy. *Proceedings of the National Academy of Sciences of the United States of America*. 107:378-383.

Wachsstock, D.H., W.H. Schwartz, and T.D. Pollard. 1993. Affinity of alpha-actinin for actin determines the structure and mechanical properties of actin filament gels. *Biophysical journal*. 65:205-214.

Waelter, S., A. Boeddrich, R. Lurz, E. Scherzinger, G. Lueder, H. Lehrach, and E.E. Wanker. 2001. Accumulation of mutant huntingtin fragments in aggresome-like

inclusion bodies as a result of insufficient protein degradation. *Molecular biology of the cell*. 12:1393-1407.

Wagner, O.I., J. Lifshitz, P.A. Janmey, M. Linden, T.K. McIntosh, and J.F. Leterrier. 2003. Mechanisms of mitochondria-neurofilament interactions. *The Journal of neuroscience : the official journal of the Society for Neuroscience*. 23:9046-9058.

Wakabayashi, J., Z. Zhang, N. Wakabayashi, Y. Tamura, M. Fukaya, T.W. Kensler, M. Iijima, and H. Sesaki. 2009. The dynamin-related GTPase Drp1 is required for embryonic and brain development in mice. *The Journal of cell biology*. 186:805-816.

Walsh, P., D. Bursac, Y.C. Law, D. Cyr, and T. Lithgow. 2004. The J-protein family: modulating protein assembly, disassembly and translocation. *EMBO reports*. 5:567-571.

Wang, G., N.H. Moniri, K. Ozawa, J.S. Stamler, and Y. Daaka. 2006. Nitric oxide regulates endocytosis by S-nitrosylation of dynamin. *Proceedings of the National Academy of Sciences of the United States of America*. 103:1295-1300.

Wang, H., P.J. Lim, M. Karbowski, and M.J. Monteiro. 2009a. Effects of overexpression of huntingtin proteins on mitochondrial integrity. *Human molecular genetics*. 18:737-752.

Wang, H., P. Song, L. Du, W. Tian, W. Yue, M. Liu, D. Li, B. Wang, Y. Zhu, C. Cao, J. Zhou, and Q. Chen. 2011. Parkin ubiquitinates Drp1 for proteasome-dependent degradation: implication of dysregulated mitochondrial dynamics in Parkinson disease. *The Journal of biological chemistry*. 286:11649-11658.

Wang, L., T.V. Nguyen, R.W. McLaughlin, L.A. Sikkink, M. Ramirez-Alvarado, and R.M. Weinshilboum. 2005a. Human thiopurine S-methyltransferase pharmacogenetics: variant allozyme misfolding and aggresome formation. *Proceedings of the National Academy of Sciences of the United States of America*. 102:9394-9399.

Wang, W., J. Ding, E. Allen, P. Zhu, L. Zhang, H. Vogel, and Y. Yang. 2005b. Gigaxonin interacts with tubulin folding cofactor B and controls its degradation through the ubiquitin-proteasome pathway. *Current biology : CB*. 15:2050-2055.

Wang, X., and T.L. Schwarz. 2009. The mechanism of Ca2+ -dependent regulation of kinesin-mediated mitochondrial motility. *Cell*. 136:163-174.

Wang, X., B. Su, H.G. Lee, X. Li, G. Perry, M.A. Smith, and X. Zhu. 2009b. Impaired balance of mitochondrial fission and fusion in Alzheimer's disease. *The Journal of neuroscience : the official journal of the Society for Neuroscience*. 29:9090-9103.

Wang, X., B. Su, S.L. Siedlak, P.I. Moreira, H. Fujioka, Y. Wang, G. Casadesus, and X. Zhu. 2008. Amyloid-beta overproduction causes abnormal mitochondrial dynamics via differential modulation of mitochondrial fission/fusion proteins. *Proceedings of the National Academy of Sciences of the United States of America*. 105:19318-19323.

Wann, A.K., N. Zuo, C.J. Haycraft, C.G. Jensen, C.A. Poole, S.R. McGlashan, and M.M. Knight. 2012. Primary cilia mediate mechanotransduction through control of ATP-induced Ca2+ signaling in compressed chondrocytes. *FASEB journal : official publication of the Federation of American Societies for Experimental Biology*. 26:1663-1671.

Waterham, H.R., J. Koster, C.W. van Roermund, P.A. Mooyer, R.J. Wanders, and J.V. Leonard. 2007. A lethal defect of mitochondrial and peroxisomal fission. *The New England journal of medicine*. 356:1736-1741.

Webb, J.L., B. Ravikumar, J. Atkins, J.N. Skepper, and D.C. Rubinsztein. 2003. Alpha-Synuclein is degraded by both autophagy and the proteasome. *The Journal of biological chemistry*. 278:25009-25013.

Wei, N., G. Serino, and X.W. Deng. 2008. The COP9 signalosome: more than a protease. *Trends in biochemical sciences*. 33:592-600.

Weihofen, A., K.J. Thomas, B.L. Ostaszewski, M.R. Cookson, and D.J. Selkoe. 2009. Pink1 forms a multiprotein complex with Miro and Milton, linking Pink1 function to mitochondrial trafficking. *Biochemistry*. 48:2045-2052.

Westermann, B. 2010a. Mitochondrial dynamics in model organisms: what yeasts, worms and flies have taught us about fusion and fission of mitochondria. *Seminars in cell & developmental biology*. 21:542-549.

Westermann, B. 2010b. Mitochondrial fusion and fission in cell life and death. *Nature reviews. Molecular cell biology*. 11:872-884.

Westhoff, B., J.P. Chapple, J. van der Spuy, J. Hohfeld, and M.E. Cheetham. 2005. HSJ1 is a neuronal shuttling factor for the sorting of chaperone clients to the proteasome. *Current biology : CB*. 15:1058-1064.

Wetzel, R. 1994. Mutations and off-pathway aggregation of proteins. *Trends in biotechnology*. 12:193-198.

Wiche, G., S. Osmanagic-Myers, and M.J. Castanon. 2015. Networking and anchoring through plectin: a key to IF functionality and mechanotransduction. *Current opinion in cell biology*. 32:21-29.

Wigley, W.C., R.P. Fabunmi, M.G. Lee, C.R. Marino, S. Muallem, G.N. DeMartino, and P.J. Thomas. 1999. Dynamic association of proteasomal machinery with the centrosome. *The Journal of cell biology*. 145:481-490.

Wilkinson, K.A., and J.M. Henley. 2010. Mechanisms, regulation and consequences of protein SUMOylation. *The Biochemical journal*. 428:133-145.

Wilson, T.J., A.M. Slupe, and S. Strack. 2013. Cell signaling and mitochondrial dynamics: Implications for neuronal function and neurodegenerative disease. *Neurobiology of disease*. 51:13-26.

Windoffer, R., M. Beil, T.M. Magin, and R.E. Leube. 2011. Cytoskeleton in motion: the dynamics of keratin intermediate filaments in epithelia. *The Journal of cell biology*. 194:669-678.

Wing, S.S., H.L. Chiang, A.L. Goldberg, and J.F. Dice. 1991. Proteins containing peptide sequences related to Lys-Phe-Glu-Arg-Gln are selectively depleted in liver and heart, but not skeletal muscle, of fasted rats. *The Biochemical journal*. 275 (Pt 1):165-169.

Winslow, A.R., and D.C. Rubinsztein. 2008. Autophagy in neurodegeneration and development. *Biochimica et biophysica acta*. 1782:723-729.

Winter, L., C. Abrahamsberg, and G. Wiche. 2008. Plectin isoform 1b mediates mitochondrion-intermediate filament network linkage and controls organelle shape. *The Journal of cell biology*. 181:903-911.

Winter, L., I. Staszewska, E. Mihailovska, I. Fischer, W.H. Goldmann, R. Schroder, and G. Wiche. 2014. Chemical chaperone ameliorates pathological protein aggregation in plectin-deficient muscle. *The Journal of clinical investigation*. 124:1144-1157.

Wisniewski, T., and J.E. Goldman. 1998. Alpha B-crystallin is associated with intermediate filaments in astrocytoma cells. *Neurochemical research*. 23:385-392.

Wraith, J.E. 2002. Lysosomal disorders. *Seminars in neonatology : SN*. 7:75-83.

Wu, G., L. Liu, J. Huang, S. Pang, G. Wei, Y. Cui, and B. Yan. 2011. Alterations of autophagic-lysosomal system in the peripheral leukocytes of patients with myocardial infarction. *Clinica chimica acta; international journal of clinical chemistry*. 412:1567-1571.

Wullschleger, S., R. Loewith, and M.N. Hall. 2006. TOR signaling in growth and metabolism. *Cell*. 124:471-484.

Wyttenbach, A., J. Carmichael, J. Swartz, R.A. Furlong, Y. Narain, J. Rankin, and D.C. Rubinsztein. 2000. Effects of heat shock, heat shock protein 40 (HDJ-2), and proteasome inhibition on protein aggregation in cellular models of Huntington's disease. *Proceedings of the National Academy of Sciences of the United States of America*. 97:2898-2903.

Xie, R., S. Nguyen, W.L. McKeehan, and L. Liu. 2010. Acetylated microtubules are required for fusion of autophagosomes with lysosomes. *BMC cell biology*. 11:89.

Xiong, N., M. Jia, C. Chen, J. Xiong, Z. Zhang, J. Huang, L. Hou, H. Yang, X. Cao, Z. Liang, S. Sun, Z. Lin, and T. Wang. 2011. Potential autophagy enhancers attenuate rotenone-induced toxicity in SH-SY5Y. *Neuroscience*. 199:292-302.

Xu, W., M. Marcu, X. Yuan, E. Mimnaugh, C. Patterson, and L. Neckers. 2002. Chaperone-dependent E3 ubiquitin ligase CHIP mediates a degradative pathway for c-ErbB2/Neu. *Proceedings of the National Academy of Sciences of the United States of America*. 99:12847-12852.

Yamamoto, A., M.L. Cremona, and J.E. Rothman. 2006. Autophagy-mediated clearance of huntingtin aggregates triggered by the insulin-signaling pathway. *The Journal of cell biology*. 172:719-731.

Yamamoto, Y., K. Hiraoka, M. Araki, S. Nagano, H. Shimazaki, Y. Takiyama, and S. Sakoda. 2005. Novel compound heterozygous mutations in sacsin-related ataxia. *J Neurol Sci*. 239:101-104.

Yang, Y., K. Fukui, T. Koike, and X. Zheng. 2007. Induction of autophagy in neurite degeneration of mouse superior cervical ganglion neurons. *The European journal of neuroscience*. 26:2979-2988.

Yeh, T.Y., A.K. Kowalska, B.R. Scipioni, F.K. Cheong, M. Zheng, U. Derewenda, Z.S. Derewenda, and T.A. Schroer. 2013. Dynactin helps target Polo-like kinase 1 to kinetochores via its left-handed beta-helical p27 subunit. *The EMBO journal*. 32:1023-1035.

Yeh, T.Y., N.J. Quintyne, B.R. Scipioni, D.M. Eckley, and T.A. Schroer. 2012. Dynactin's pointed-end complex is a cargo-targeting module. *Molecular biology of the cell*. 23:3827-3837.

Yen, W.L., T. Shintani, U. Nair, Y. Cao, B.C. Richardson, Z. Li, F.M. Hughson, M. Baba, and D.J. Klionsky. 2010. The conserved oligomeric Golgi complex is involved in double-membrane vesicle formation during autophagy. *The Journal of cell biology*. 188:101-114.

Yla-Anttila, P., H. Vihinen, E. Jokitalo, and E.L. Eskelinen. 2009. 3D tomography reveals connections between the phagophore and endoplasmic reticulum. *Autophagy*. 5:1180-1185.

Yokoyama, K., and H. Imamura. 2005. Rotation, structure, and classification of prokaryotic V-ATPase. *Journal of bioenergetics and biomembranes*. 37:405-410.

Yonashiro, R., S. Ishido, S. Kyo, T. Fukuda, E. Goto, Y. Matsuki, M. Ohmura-Hoshino, K. Sada, H. Hotta, H. Yamamura, R. Inatome, and S. Yanagi. 2006. A novel mitochondrial ubiquitin ligase plays a critical role in mitochondrial dynamics. *The EMBO journal*. 25:3618-3626.

Yoon, K.H., M. Yoon, R.D. Moir, S. Khuon, F.W. Flitney, and R.D. Goldman. 2001a. Insights into the dynamic properties of keratin intermediate filaments in living epithelial cells. *The Journal of cell biology*. 153:503-516.

Yoon, M., R.D. Moir, V. Prahlad, and R.D. Goldman. 1998. Motile properties of vimentin intermediate filament networks in living cells. *The Journal of cell biology*. 143:147-157.

Yoon, Y., K.R. Pitts, and M.A. McNiven. 2001b. Mammalian dynamin-like protein DLP1 tubulates membranes. *Molecular biology of the cell*. 12:2894-2905.

Yorimitsu, T., and D.J. Klionsky. 2005. Autophagy: molecular machinery for self-eating. *Cell death and differentiation*. 12 Suppl 2:1542-1552.

Youle, R.J., and D.P. Narendra. 2011. Mechanisms of mitophagy. *Nature reviews. Molecular cell biology*. 12:9-14.

Young, J.C., W.M. Obermann, and F.U. Hartl. 1998. Specific binding of tetratricopeptide repeat proteins to the C-terminal 12-kDa domain of hsp90. *The Journal of biological chemistry*. 273:18007-18010.

Yu, T., R.J. Fox, L.S. Burwell, and Y. Yoon. 2005. Regulation of mitochondrial fission and apoptosis by the mitochondrial outer membrane protein hFis1. *Journal of cell science*. 118:4141-4151.

Yu, T., B.S. Jhun, and Y. Yoon. 2011. High-glucose stimulation increases reactive oxygen species production through the calcium and mitogen-activated protein kinase-mediated activation of mitochondrial fission. *Antioxid Redox Signal*. 14:425-437.

Zaarur, N., A.B. Meriin, E. Bejarano, X. Xu, V.L. Gabai, A.M. Cuervo, and M.Y. Sherman. 2014. Proteasome failure promotes positioning of lysosomes around the aggresome via local block of microtubule-dependent transport. *Molecular and cellular biology*. 34:1336-1348.

Zaglia, T., G. Milan, A. Ruhs, M. Franzoso, E. Bertaggia, N. Pianca, A. Carpi, P. Carullo, P. Pesce, D. Sacerdoti, C. Sarais, D. Catalucci, M. Kruger, M. Mongillo, and M. Sandri. 2014. Atrogin-1 deficiency promotes cardiomyopathy and premature death via impaired autophagy. *The Journal of clinical investigation*. 124:2410-2424.

Zanna, C., A. Ghelli, A.M. Porcelli, M. Karbowski, R.J. Youle, S. Schimpf, B. Wissinger, M. Pinti, A. Cossarizza, S. Vidoni, M.L. Valentino, M. Rugolo, and V. Carelli. 2008. OPA1 mutations associated with dominant optic atrophy impair oxidative phosphorylation and mitochondrial fusion. *Brain : a journal of neurology*. 131:352-367.

Zatloukal, K., C. Stumptner, A. Fuchsbichler, H. Heid, M. Schnoelzer, L. Kenner, R. Kleinert, M. Prinz, A. Aguzzi, and H. Denk. 2002. p62 Is a common component of cytoplasmic inclusions in protein aggregation diseases. *The American journal of pathology*. 160:255-263.

Zhang, J., X. Yao, L. Fischer, J.F. Abenza, M.A. Penalva, and X. Xiang. 2011. The p25 subunit of the dynactin complex is required for dynein-early endosome interaction. *The Journal of cell biology*. 193:1245-1255.

Zhang, M.H., J.S. Lee, H.J. Kim, D.I. Jin, J.I. Kim, K.J. Lee, and J.S. Seo. 2006. HSP90 protects apoptotic cleavage of vimentin in geldanamycin-induced apoptosis. *Molecular and cellular biochemistry*. 281:111-121.

Zhang, Y., S. Kwon, T. Yamaguchi, F. Cubizolles, S. Rousseaux, M. Kneissel, C. Cao, N. Li, H.L. Cheng, K. Chua, D. Lombard, A. Mizeracki, G. Matthias, F.W. Alt, S. Khochbin, and P. Matthias. 2008. Mice lacking histone deacetylase 6 have hyperacetylated tubulin but are viable and develop normally. *Molecular and cellular biology*. 28:1688-1701.

Zhang, Y.Q., M.X. Henderson, C.M. Colangelo, S.D. Ginsberg, C. Bruce, T. Wu, and S.S. Chandra. 2012. Identification of CSPalpha clients reveals a role in dynamin 1 regulation. *Neuron*. 74:136-150.

Zhao, J., T. Liu, S. Jin, X. Wang, M. Qu, P. Uhlen, N. Tomilin, O. Shupliakov, U. Lendahl, and M. Nister. 2011. Human MIEF1 recruits Drp1 to mitochondrial outer membranes and promotes mitochondrial fusion rather than fission. *The EMBO journal*. 30:2762-2778.

Zhao, J., Y. Ren, Q. Jiang, and J. Feng. 2003. Parkin is recruited to the centrosome in response to inhibition of proteasomes. *Journal of cell science*. 116:4011-4019.

Zhou, B., Y.B. Zhu, L. Lin, Q. Cai, and Z.H. Sheng. 2011. Snapin deficiency is associated with developmental defects of the central nervous system. *Bioscience reports*. 31:151-158.

Zhou, C., Y. Huang, Y. Shao, J. May, D. Prou, C. Perier, W. Dauer, E.A. Schon, and S. Przedborski. 2008a. The kinase domain of mitochondrial PINK1 faces the cytoplasm. *Proceedings of the National Academy of Sciences of the United States of America*. 105:12022-12027.

Zhou, H.X., G. Rivas, and A.P. Minton. 2008b. Macromolecular crowding and confinement: biochemical, biophysical, and potential physiological consequences. *Annu Rev Biophys*. 37:375-397.

Zhu, D., S. Shi, H. Wang, and K. Liao. 2009. Growth arrest induces primary-cilium formation and sensitizes IGF-1-receptor signaling during differentiation induction of 3T3-L1 preadipocytes. *Journal of cell science*. 122:2760-2768.

Zhu, Q., S. Couillard-Despres, and J.P. Julien. 1997. Delayed maturation of regenerating myelinated axons in mice lacking neurofilaments. *Experimental neurology*. 148:299-316.

Zoncu, R., A. Efeyan, and D.M. Sabatini. 2011. mTOR: from growth signal integration to cancer, diabetes and ageing. *Nature reviews. Molecular cell biology*. 12:21-35.

Zuchner, S., I.V. Mersiyanova, M. Muglia, N. Bissar-Tadmouri, J. Rochelle, E.L. Dadali, M. Zappia, E. Nelis, A. Patitucci, J. Senderek, Y. Parman, O. Evgrafov, P.D. Jonghe, Y. Takahashi, S. Tsuji, M.A. Pericak-Vance, A. Quattrone, E. Battaloglu, A.V. Polyakov, V. Timmerman, J.M. Schroder, and J.M. Vance. 2004. Mutations in the mitochondrial GTPase mitofusin 2 cause Charcot-Marie-Tooth neuropathy type 2A. *Nature genetics*. 36:449-451.

Zuchner, S., and J.M. Vance. 2005. Emerging pathways for hereditary axonopathies. *J Mol Med (Berl)*. 83:935-943.

Zunino, R., A. Schauss, P. Rippstein, M. Andrade-Navarro, and H.M. McBride. 2007. The SUMO protease SENP5 is required to maintain mitochondrial morphology and function. *Journal of cell science*. 120:1178-1188.

APPENDICES

Appendix 1. TMRM treated cell images.

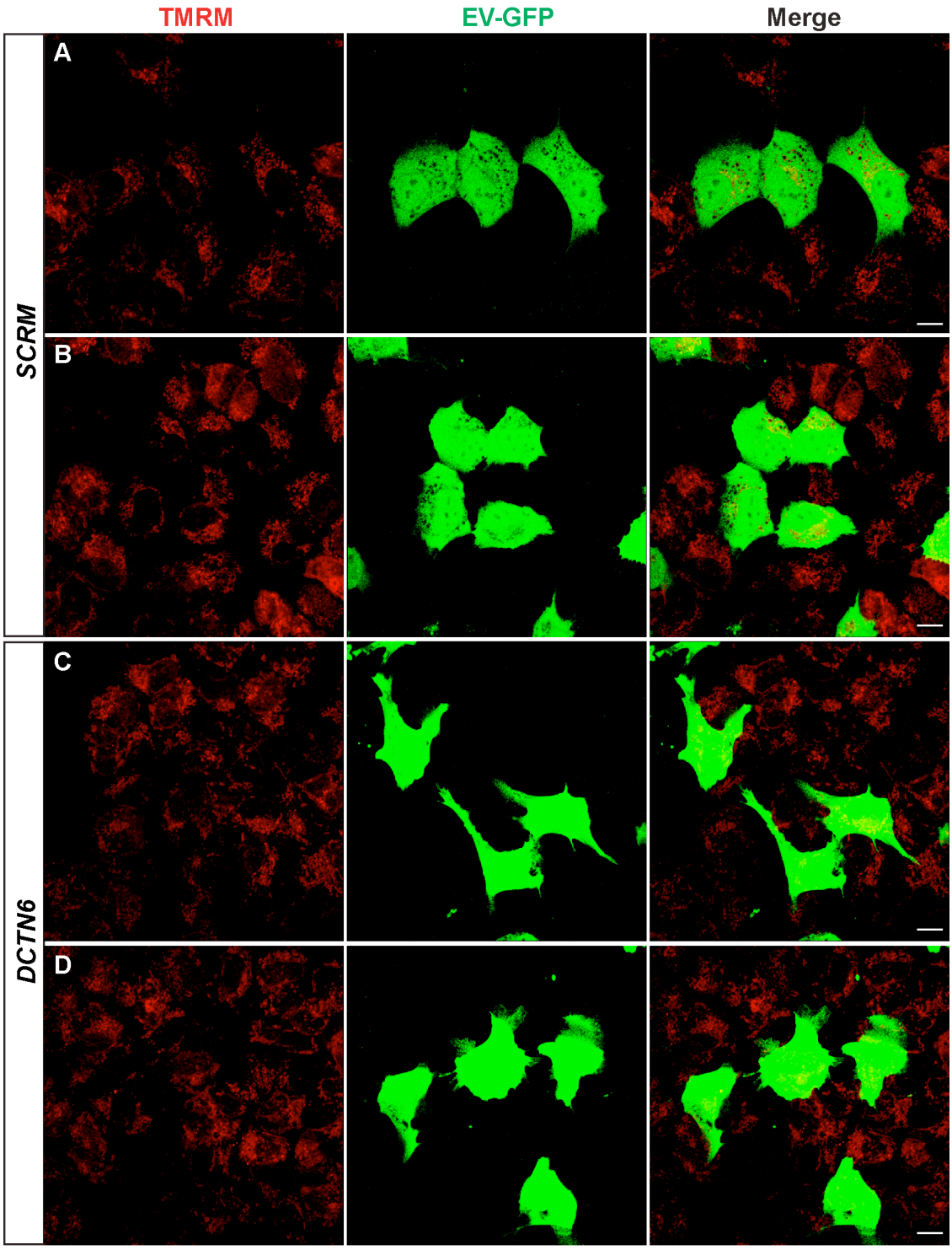

Appendix 2. Wild-type control HDFs used in this thesis.

WT control	Age (yrs)	Gender (M/F)
1	55	F
2	NA	NA
3	NA	NA
4	54	M
5	NA	NA

These were purchased from PromoCell or were kindly provided by Dr. Tristan McKay (St George's, University of London), or Dr. Sascha Vermeer (Radboud University, Nijmegen). WT controls were not age and gender matched with ARSACS HDF lines. WT numbers correspond with figure 4.6. NA: not available.

Appendix 3. Collapsed vimentin network in ARSACS patient HDFs.

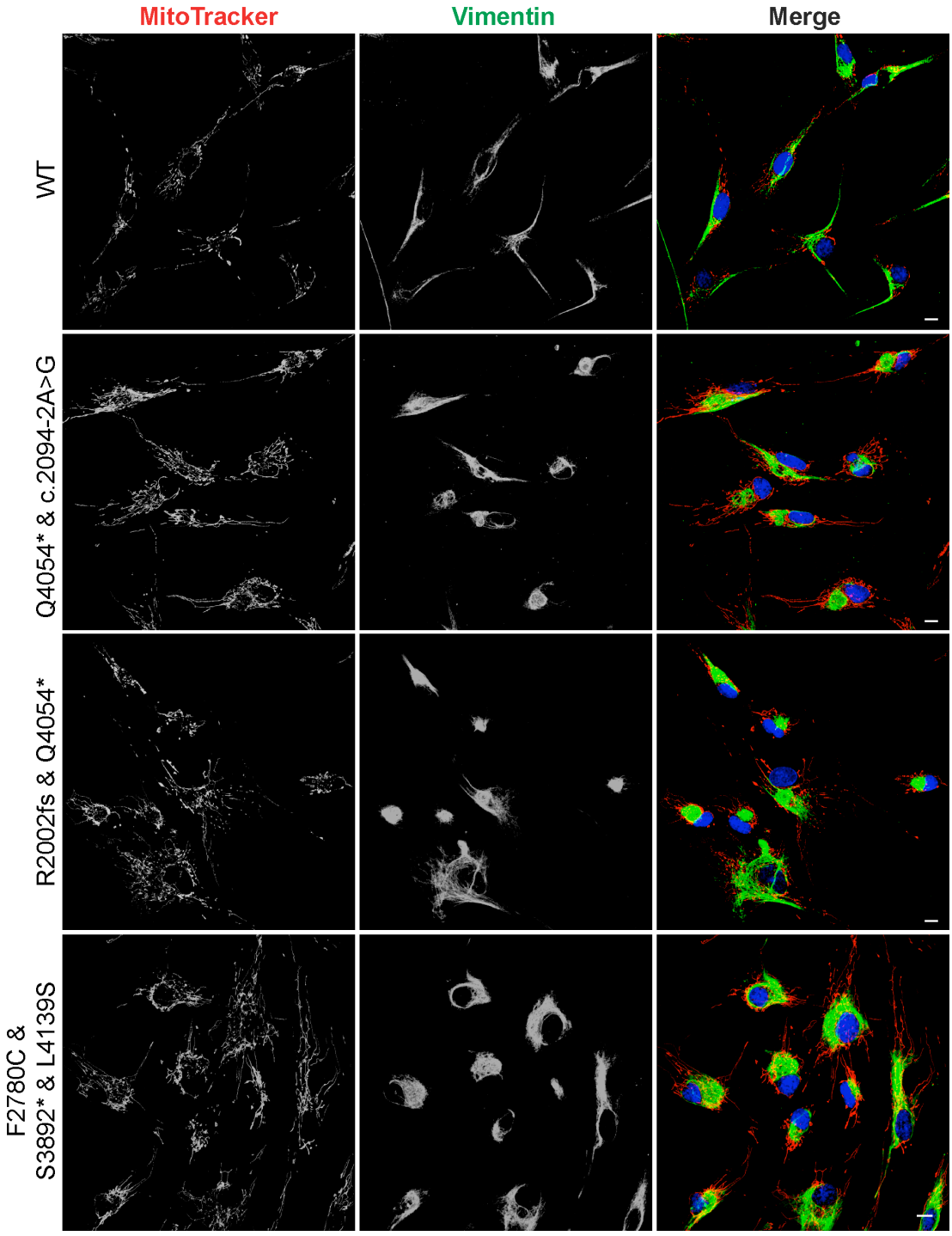

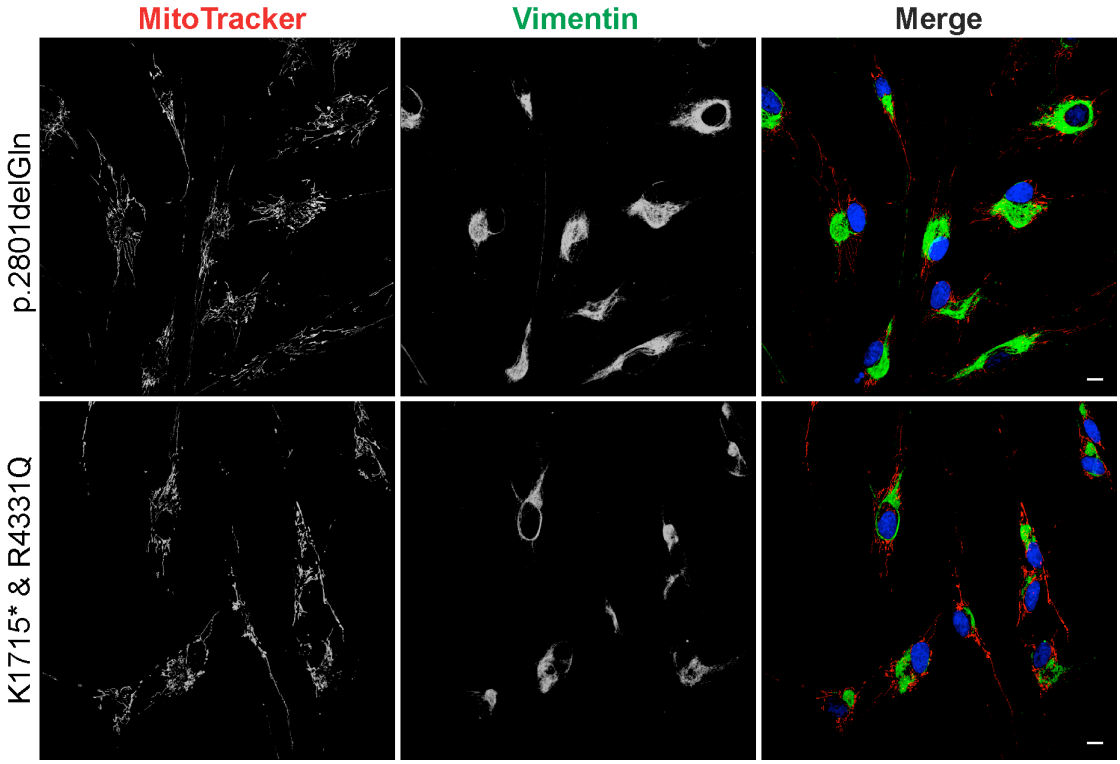
MitoTracker
Vimentin
Merge
p.2801delGln
K1715* & R4331Q

Appendix 4. Cilia incidence and length are reduced in ARSACS HDFs.